



Thèse présentée pour obtenir le grade de
Docteur de l'Université de Strasbourg

Discipline : Sciences Chimiques
par Dmitry Pogochev

**Sequential construction of crystalline heterometallic
architectures based on 7-azaindole and dipyrin ligands**

Soutenue publiquement le 13 Juillet 2010 devant la commission d'examen:

Prof. Claude Gros (Université de Bourgogne)	Rapporteur externe
Prof. Nicolas Mercier (Université d'Angers)	Rapporteur externe
Prof. Nicolas Giuseppone (Université de Strasbourg)	Examineur
Prof. Annie Powell (Karlsruhe Universität)	Examineur
Prof. Mir Wais Hosseini (Université de Strasbourg, IUF)	Codirecteur de thèse
Dr. Stéphane Baudron (CNRS-Université de Strasbourg)	Codirecteur de thèse



Thèse présentée pour obtenir le grade de
Docteur de l'Université de Strasbourg

Discipline : Sciences Chimiques
par Dmitry Pogozev

Sequential construction of crystalline heterometallic architectures based on 7-azaindole and dipyrin ligands

Soutenue publiquement le 13 Juillet 2010 devant la commission d'examen:

Prof. Claude Gros (Université de Bourgogne)	Rapporteur externe
Prof. Nicolas Mercier (Université d'Angers)	Rapporteur externe
Prof. Nicolas Giuseppone (Université de Strasbourg)	Examineur
Prof. Annie Powell (Karlsruhe Universität)	Examineur
Prof. Mir Wais Hosseini (Université de Strasbourg, IUF)	Codirecteur de thèse
Dr. Stéphane Baudron (CNRS-Université de Strasbourg)	Codirecteur de thèse

Résumé en français

Construction séquentielle d'architectures hétérométalliques cristallines basée sur des ligands dérivés du 7-azaindole et des dipyrroles

I. Introduction

Les architectures cristallines métallo-organiques revêtent un très grand intérêt pour leur propriétés catalytiques, magnétiques, optiques ou de porosité.¹ Cependant, l'élaboration de tels systèmes s'avère ardue lorsqu'ils incorporent plus d'un type de centre métallique. Pour la préparation de telles architectures hétérométalliques, l'une des approches possibles repose sur une stratégie séquentielle basée sur l'utilisation de ligands organiques possédant deux pôles de coordination, l'un primaire, l'autre secondaire (Figure 1).² Ces ligands forment, par coordination du pôle primaire à un centre métallique, des complexes présentant des groupements coordinants à leur périphérie que l'on peut qualifier de pôles secondaires. Ainsi, ces complexes peuvent être par la suite utilisés à leur tour comme ligands pour générer des assemblages discrets polymétalliques, ou en tant que métallatectons pour la formation de réseaux de coordination.

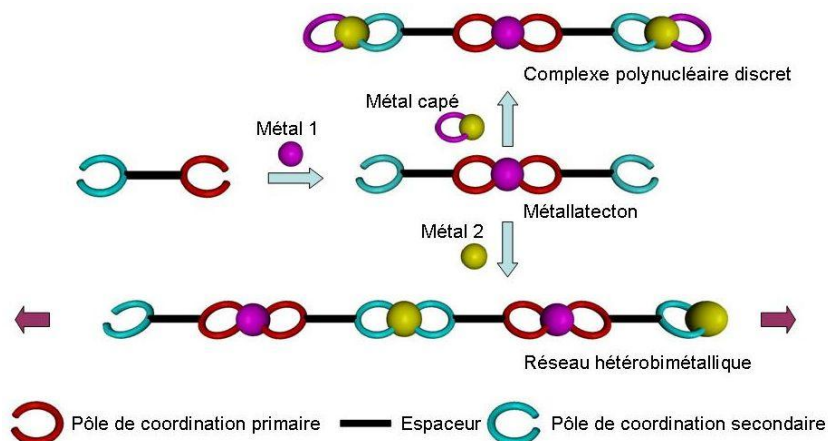


Figure 1. Stratégie d'élaboration d'assemblages supramoléculaires hétérométalliques finis et infinis.

Au cours de ce travail, cette stratégie a été déclinée à partir de ligands fonctionnalisés dérivés du 7-azaindole³ et de la dipyrriine⁴ (Figure 2). Ainsi, de nouveaux dérivés associant ces fonctions et un groupement coordonnant périphérique (pôle secondaire) ont été synthétisés puis employés pour la préparation de complexes métalliques coordinants. L'assemblage de ces derniers avec d'autres centres métalliques a ensuite été étudié.

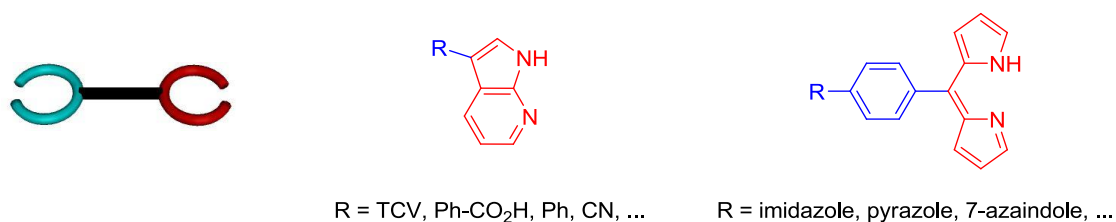


Figure 2. Ligands dérivés du 7-azaindole (à gauche) et de la dipyrriine (à droite) développés au cours de ce travail

II. Systèmes homométalliques basés sur les deux modes de coordination du 7-azaindole.

Le 7-azaindole est un dérivé hétérocyclique azoté largement exploité en chimie médicinale.³ Cependant, relativement peu d'exemples où il est employé comme ligand au sein de complexes métalliques ont été rapportés.⁵ Ceci est assez surprenant au regard des divers modes de coordination qui sont envisageables, d'une part, pour le 7-azaindole et, d'autre part, pour sa base conjuguée, le 7-azaindolate. Cette diversité de modes de coordination à partir du 3-tricyanovinylène-7-azaindole (azaH-TCV), nouveau dérivé dont la synthèse a été mise au point au cours de ce travail, est illustrée ici. Ainsi, ce dérivé forme un complexe par réaction avec le dimère $\text{Rh}_2(\text{OAc})_4$, au sein duquel le ligand est coordonné par l'azote pyridinique alors que le N-H pyrrolique forme une liaison hydrogène avec un atome d'oxygène du pont acétate (Figure 3b). Une série de complexes de formule $[(\text{azaH-R})_2\text{Rh}_2(\text{OAc})_4]$ ($\text{R} = \text{PhCN}, m\text{-Ph-CO}_2\text{H}, p\text{-PhCO}_2\text{H}, \dots$) a été synthétisée et caractérisée par diffraction des rayons et révèle la récurrence de ce motif. La base conjuguée, aza-TCV⁻, forme quant à elle par réaction avec des sels de Cu(II), un dimère de type roue à aube $\text{Cu}_2(\text{aza-TCV})_4$ analogue au complexe $\text{Cu}_2(\text{OAc})_4$ (Figure 3c). Les composés présentés sur la Figure 3 possèdent des groupements nitriles périphériques disponibles pour la réaction avec d'autres centres métalliques. Cependant à ce jour, aucune architecture cristalline hétérométallique n'a malheureusement pu être isolée.

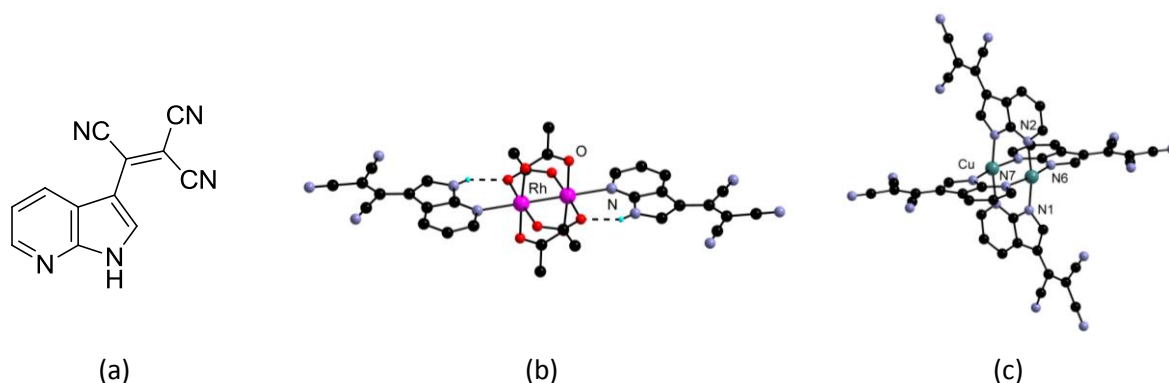


Figure 3. Le ligand azaH-TCV (a), structures cristallines du complexe $[(\text{azaH-TCV})_2\text{Rh}_2(\text{OAc})_4]$ (b) et du complexe $[\text{Cu}_2(\text{aza-TCV})_4(\text{DMF})_2]$ (c).

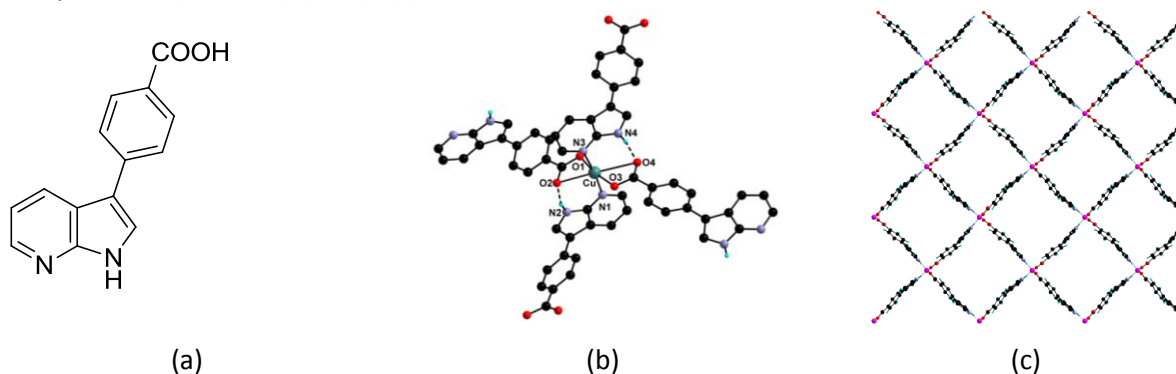


Figure 4. Le ligand azaH-Ph-CO₂H (a), le nœud de construction (b) et une vue du réseau $[\text{Cu}(\text{azaH-PhCO}_2)_2]_\infty$ (c).

Afin de tirer parti de l'analogie des modes de coordination du 7-azaindolate et du carboxylate, des ligands de type azaH-Ph-CO₂H ont été développés et associés à des sels métalliques. Plusieurs réseaux de coordination ont pu ainsi être obtenus. L'exemple du réseau [Cu(azaH-PhCO₂)₂]_∞ est présenté sur la Figure 4. Ce réseau est stable jusqu'à 270 °C et conserve sa cristallinité à 100 °C sous vide. Notons cependant que pour ce type de composés, la fonction azaindole reste protonée et forme à nouveau une liaison hydrogène avec un atome d'oxygène de la fonction carboxylate.

Des dérivés comportant plusieurs groupements 7-azaindole ont également été préparés. Cependant, la faible solubilité de ces composés a limité leur emploi pour la préparation d'architectures étendues. Seules des poudres non cristallines ont été obtenues à partir de ces ligands. Ceci est sans doute dû à l'auto-complémentarité pour la liaison hydrogène qui limite la solubilité de ces espèces. Afin de pallier ce problème, un pôle de coordination primaire alternatif a été envisagé. Ainsi, de nouveaux ligands dipyrriines portant un groupement périphérique non auto-complémentaire ont été préparés.

III. Réseaux hétérométalliques construits à partir d'un ligand incorporant une dipyrriine et un groupement imidazole.

Plusieurs dérivés de ce type ont pu être synthétisés parmi lesquels le dpm-imid et le dpm-pz qui incorporent une fonction imidazole et pyrazole respectivement. Une série de complexes homo- et hétéroleptiques du Co(III) et du Cu(II) a été préparée et caractérisée.⁶ Les structures cristallines des complexes hétéroleptiques [(acacCN)Cu(dpm-imid)] et [(acacCN)Cu(dpm-pz)] sont présentées sur la Figure 7. A l'état solide, ces deux complexes s'organisent en réseaux 1D, basés sur des motifs d'assemblage différents. Alors qu'au sein de la structure de [(acacCN)Cu(dpm-imid)], la fonction imidazole est coordonnée à l'ion Cu(II) d'un complexe voisin (Figure 5a), dans le cas de [(acacCN)Cu(dpm-pz)], une interaction Cu...NC avec le groupement nitrile périphérique de la fonction acétylacétonate (acacCN), permet la formation de chaînes (Figure 5b).

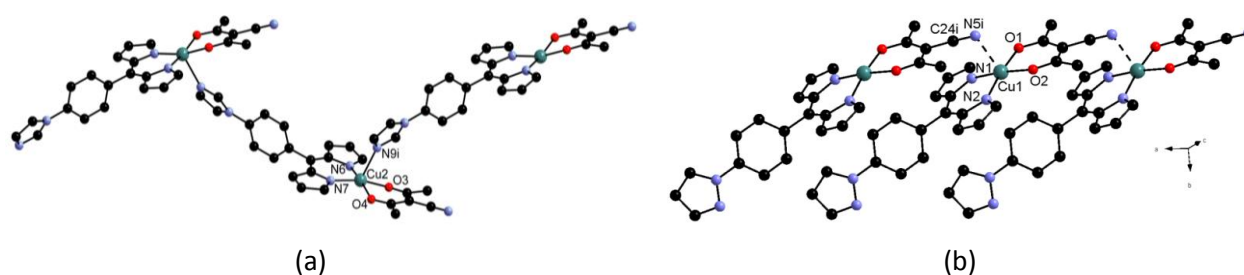


Figure 5. Structure cristalline des complexes [(acacCN)Cu(dpm-imid)] (a) et [(acacCN)Cu(dpm-pz)] (b).

L'effet du groupement nitrile périphérique sur l'arrangement cristallin a alors été étudié par association de ces complexes avec des sels d'argent (Figure 6). La réaction du complexe parent $[(\text{acac})\text{Cu}(\text{dpm-imid})]$ avec le sel AgSbF_6 permet la formation d'une espèce trinuécléaire discrète $[(\text{acac})\text{Cu}(\text{dpm-imid})]_2\text{Ag}(\text{SbF}_6)$ (Figure 6a). La même réaction avec le complexe $[(\text{acacCN})\text{Cu}(\text{dpm-imid})]$ aboutit également à la formation d'espèces trinuécléaires $\{[(\text{acac})\text{Cu}(\text{dpm-imid})]_2\text{Ag}\}^+$. Cependant, en fonction du sel d'argent employé, ces espèces s'organisent soit par coordination du groupement nitrile périphérique à l'ion $\text{Ag}(\text{I})$ (dans le cas de l'anion OTf^-) soit par interaction $\text{Cu}\cdots\text{NC}$ (dans le cas des anions BF_4^- et PF_6^-) (Figure 6b et c).

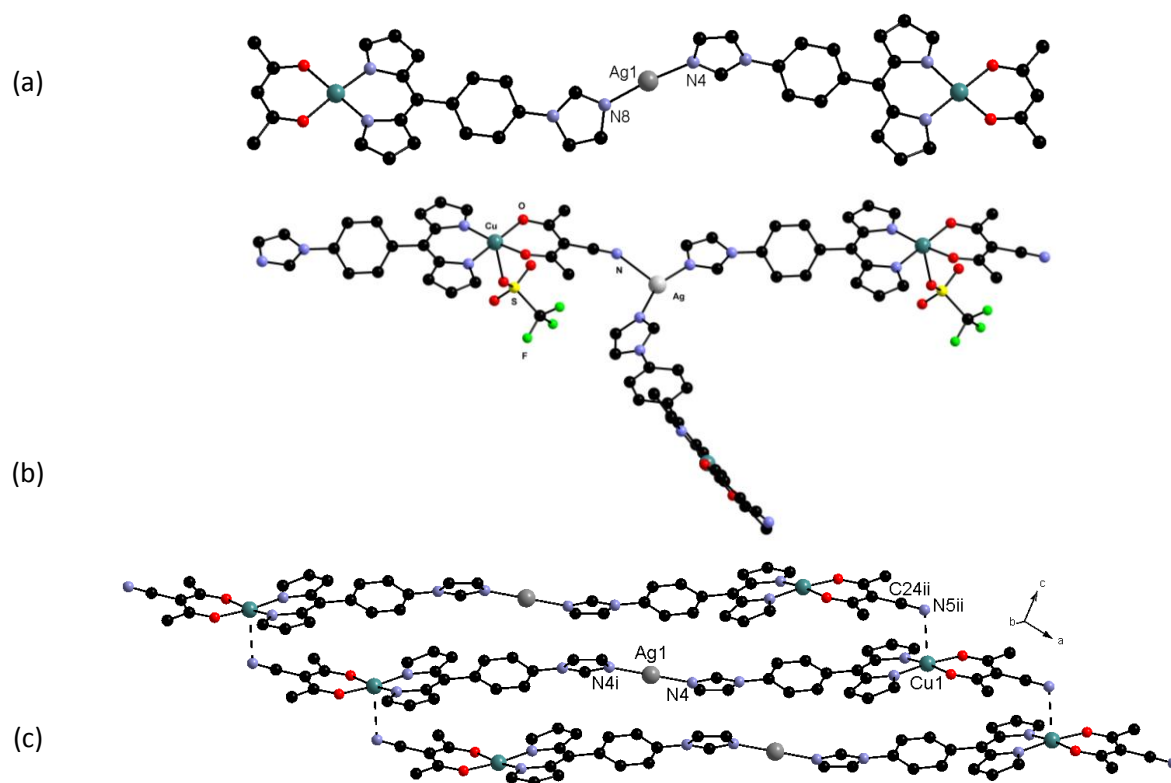


Figure 6. Structure cristalline de $\{[(\text{acac})\text{Cu}(\text{dpm-imid})]_2\text{Ag}\}(\text{SbF}_6)$ (a), $\{[(\text{acacCN})\text{Cu}(\text{dpm-imid})]_2\text{Ag}\}(\text{OTf})$ (b) et $\{[(\text{acacCN})\text{Cu}(\text{dpm-imid})]_2\text{Ag}\}(\text{BF}_4)$ (c). Les anions ont été omis par souci de clarté.

Cette approche permet donc la formation d'architectures hétérométalliques discrètes ou infinies en fonction de la présence du nitrile périphérique. Cependant, les architectures formées sont majoritairement unidimensionnelles. Afin d'augmenter la dimensionnalité, de nouveaux complexes de $\text{Co}(\text{III})$ ont été préparés et associés à des sels d'argent. Ainsi, le complexe $(\text{acacCN})\text{Co}(\text{dpm-4py})_2$ portant deux dipyrines fonctionnalisées par un groupement pyridyl forme, par auto-assemblage avec le sel AgBF_4 , un réseau bidimensionnel (Figure 7). Cette structure consiste en une alternance $\Delta\Delta\Delta\Delta\dots$ de couches homochirales. On note de plus l'analogie entre ce composé et celui obtenu avec le complexe homoleptique de $\text{Co}(\text{III})$ analogue.⁷

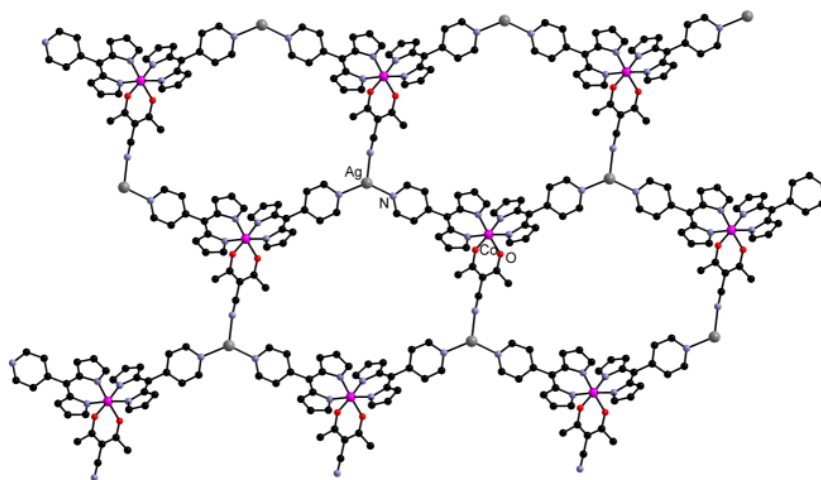


Figure 7. Structure bidimensionnelle $\{[(\text{acacCN})\text{Co}(\text{dpm-4py})_2]_2\text{Ag}\}_\infty(\text{BF}_4)(\text{C}_6\text{H}_6)_{0.5}(\text{CH}_3\text{CN})_3$. Les anions ont été omis par souci de clarté.

Il est intéressant de noter que ces complexes hétéroléptiques comme ceux du type $[(\text{acacCN})\text{Cu}(\text{dpm-imid})]$ portent à leur périphérie deux groupements coordinants différenciés. Selon la stratégie présentée sur la Figure 1, il est dès lors envisageable de préparer de façon séquentielle des architectures hétéotrimétalliques. Un premier pas dans cette approche est illustré par la préparation d'un complexe discret tétranucléaire $[(\text{acacCN})\text{Cu}(\text{dpm-imid})]_2\text{Rh}_2(\text{OAc})_4$ (Figure 8).



Figure 8. Structure cristalline du complexe tétranucléaire $[(\text{acacCN})\text{Cu}(\text{dpm-imid})]_2\text{Rh}_2(\text{OAc})_4$.

IV. Un ligand combinant le 7-azaindole et la dipyrriane.

Au cours de l'étude de l'association des dérivés du 7-azaindole avec le dimère $\text{Rh}_2(\text{OAc})_4$, la robustesse d'un motif combinant liaisons de coordination et hydrogène a pu être mise en avant. Dès lors, une stratégie envisagée pour la préparation d'architectures hétérométalliques repose sur l'utilisation de complexes métalliques portant des groupements azaindole à leur périphérie et leur association avec le dimère $\text{Rh}_2(\text{OAc})_4$. Dans ce but, le dérivé azaH-dpm (Figure 9) incorporant une fonction dipyrriane a été préparé.⁸ Plusieurs complexes incorporant ce ligand ont été synthétisés et la structure cristalline des complexes $[\text{M}(\text{azaH-dpm})_2]$ ($\text{M} = \text{Ni}, \text{Cu}, \text{Zn}$) est présentée sur la Figure 9. Ces complexes s'organisent en réseaux uni-dimensionnels grâce à l'auto-complémentarité du point de vue de la liaison hydrogène des fonctions 7-azaindole périphériques.

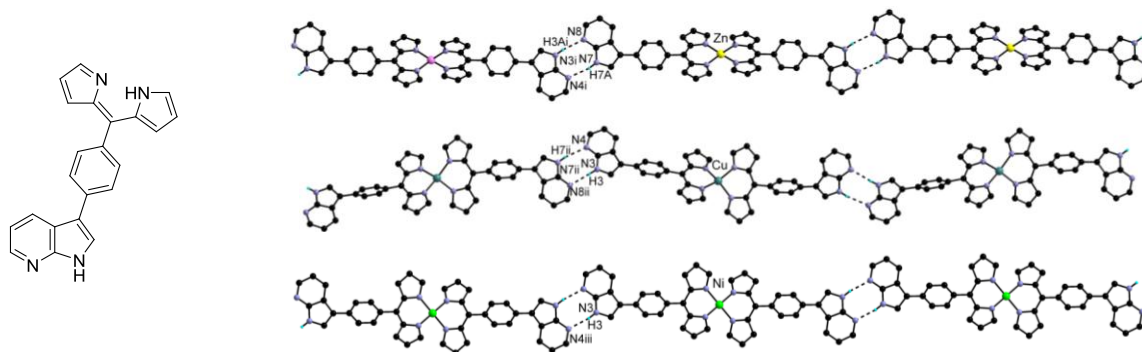


Figure 9. Ligand azaH-dpm (à gauche) et structure cristalline des réseaux 1D $[M(\text{azaH-dpm})_2]$ ($M = \text{Ni}, \text{Cu}, \text{Zn}$) (à droite).

De plus, notons que le ligand azaH-dpm forme bien, par réaction avec le dimère $\text{Rh}_2(\text{OAc})_4$, le motif attendu (Figure 10).

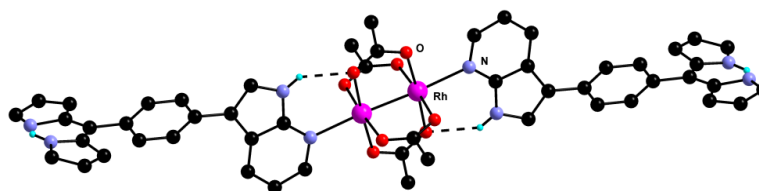


Figure 10. Structure cristalline du dimère $[(\text{azaH-dpm})_2\text{Rh}_2(\text{OAc})_4]$.

V. Conclusion

Au cours de ce travail, une approche novatrice pour la construction séquentielle d'architectures hétérométalliques a été développée. A cette fin, de nouveaux ligands organiques basés sur des dérivés du 7-azaindole et de la dipyrroline ont été préparés. A partir de ces ligands, des complexes homo- et hétéroleptiques ont été synthétisés et caractérisés par diffraction des rayons X. Ces composés portent à leur périphérie des groupements coordinants permettant leur association avec d'autres centres métalliques. Alors que dans les cas des dérivés du 7-azaindole, des problèmes de solubilité ont limité la mise en œuvre de la stratégie présentée sur la Figure 1, dans le cas des dérivés de la dipyrroline, des architectures hétérométalliques cristallines ont pu être préparées et caractérisées avec succès. Enfin, en perspective à ce travail, la différenciation des pôles de coordination au niveau des complexes métalliques permet d'envisager la formation d'architectures hétérotrimétalliques.

Références:

1. (a) Robson, R. *Dalton Trans.*, **2008**, 5113. (b) *Chem. Soc. Rev.*, **2009**, 38, themed issue on Metal-Organic Frameworks.
2. (a) Kahn, O. *Acc. Chem. Res.* **2000**, 33, 647. (b) Baudron, S. A., Hosseini, M. W. *Inorg. Chem.* **2006**, 45, 5260. (c) Andruh, M. *Chem. Commun.* **2007**, 2565. (d) Baudron, S. A., Hosseini, M. W., Kyritsakas,

- N., Kurmoo, M. *Dalton Trans.* **2007**, 1129. (e) Pardo, E.; Ruiz-Garcia, R.; Cano, J.; Ottenwaelde, X.; Lescouëzec, R.; Journaux, Y.; Lloret, F.; Julve, M. *Dalton Trans.* **2008**, 2780. (f) Constable, E. C. *Coord. Chem. Rev.* **2008**, 252, 842. (g) Goldberg, I. *CrystEngComm.* **2008**, 10, 637.
3. (a) Mérour, J. –Y.; Joseph, B. *Curr. Org. Chem.* **2001**, 5, 471. (b) Popowycz, F.; Routier, S. ; Joseph B.; Mérour, J. –Y. *Tetrahedron* **2007**, 63, 1031.
4. Wood, T. E., Thompson, A., *Chem. Rev.*, **2007**, 107, 1831.
5. (a) Lee, C. F.; Chin, K. F.; Peng, S. M.; Che, C. M. *J. Chem Soc. Dalton Trans.* **1993**, 467. (b) Wang, S. *Coord. Chem. Rev.* **2001**, 215, 79.
6. Pogochev, D.; Baudron, S. A.; Hosseini, M. W. *Inorg. Chem.*, **2010**, 49, 331.
7. Halper, S. R.; Do, L.; Stork, J. R.; Cohen, S. M. *J. Am. Chem. Soc.*, **2006**, 128, 15255.
8. Pogochev, D.; Baudron, S. A.; Hosseini, M. W. *CrystEngComm*, **2010**, DOI: 10.1039/b927348d.

Communications à des congrès / workshops:

1. 1st **FuMaSSeC** meeting (Barcelone, Espagne, 29 Juin 2007)

Communication orale: *"Synthesis of novel metal-organic frameworks based on 7-azaindole derivatives."* Dmitry Pogozhev, Stéphane Baudron, Mir Wais Hosseini.

2. 2nd **FuMaSSeC** meeting (Strasbourg, 26-27 Novembre 2007)

Communication orale: *"Novel 7-azaindole ligands for the synthesis of metal-organic frameworks"* Dmitry Pogozhev, Stéphane Baudron, Mir Wais Hosseini.

3. 3rd **FuMaSSeC** meeting (Nottingham, UK, 30 Juin - 1er Juillet 2008)

Communication orale: *"Metal-organic complexes and frameworks based on novel 7-azaindole ligands"* Dmitry Pogozhev, Stéphane Baudron, Mir Wais Hosseini.

4. 4th **FuMaSSeC** meeting (Barcelone, Espagne, 19-20 Avril 2008)

Communication orale: *"Metal-organic complexes and frameworks based on novel 7-azaindole and dipyrin ligands"* Dmitry Pogozhev, Stéphane Baudron, Mir Wais Hosseini.

5. 2nd **"Karlsruhe-Strasbourg bilateral meetings on progress in Supramolecular Chemistry"** (Karlsruhe, Allemagne, 5 Décembre 2008)

Communication orale: *"Metal-organic complexes and frameworks based on novel 7-azaindole ligands"* Dmitry Pogozhev, Stéphane Baudron, Mir Wais Hosseini.

6. 1st **International conference on Metal-Organic Framework and Open Frameworks Compounds, MOF 2008** (Augsburg, Allemagne, 8-10 Octobre 2008)

Communication par affiche: *"Coordination networks and complexes based on 7-azaindole derivatives and their conjugated base"* Dmitry Pogozhev, Stéphane Baudron, Mir Wais Hosseini.

Publications:

1) *Combination of hydrogen and coordination bonding for the construction of one-dimensional networks based on a 7-azaindole appended dipyrin*

Pogozhev, D.; Baudron, S. A.; Hosseini, M. W. *CrystEngComm*, **2010**, 12, 2238-2244.

2) *Assembly of heteroleptic copper complexes with silver ions: from discrete trinuclear complexes to infinite networks*

Pogozhev, D.; Baudron, S. A.; Hosseini, M. W. *Inorg. Chem.*, **2010**, 49, 331-338.

Acknowledgements

I would like to thank Prof. Mir. Wais Hosseini for giving me the opportunity to work in his laboratory in Strasbourg and his help during these three years.

I would like to thank Dr. Stéphane Baudron for being a brilliant supervisor, excellent scientist, a tactful person with perpetual patience and excellent sense of humor. During all the time of my Ph.D thesis he helped me with all scientific and non-scientific problems, he motivated me in difficult periods of battles with French administration and sometimes with myself. I would like to thank Dr. Stéphane Baudron because he is great!

I would like to thank my Swiss colleague Dr. Fabrice Eckes, who helped in all my language and computer troubles and was very intelligent and competent person in everything, from the scientific till political subjects. I would like to thank Thomas Lang, as a very harmonious person who never says “no” and helps me with all my permanent troubles. A special thanks to my German and Italian colleagues Dr. Elisabeth Kühn and Cristina Carpanese, who all the time were a little bit early and a little bit late, who I share the same office with and were my first comrades in all stories for a three years.

All my lab colleagues, past and present: a brilliant student Brandon Kilduff, Prof. Jean-Marc Planeix, Prof. Véronique Bulach, Dr. Ernest Graf, Dr. Sylvie Ferlay-Charitat, Dr. Mohamedally Kurmoo, Dr. Abdelaziz Jouaiti, Nathalie Kyritsakas-Gruber, Dr. Domingo Salazar, Dr. Aurélie Guenet, Dr. Marina Kozlova, Dr. Pierre Dechambenoit, Dr. Jérôme Ehrhart, Dr. Yusuke Yoshida, Catherine Bronner, Nicolas Delcey, Nicolas Zigon, Alexandre Gehin, Alexandre Ovsyannikov, Patrick Larpent, Claude Wolter, Fabien Sguerra, Mei-Jin Lin, Valérie Rey, Françoise Rothhut and all the others.

To my parents

Table of Content

I.	GENERAL INTRODUCTION	3
I.1.	Supramolecular chemistry	5
I.2.	Molecular self-assembly	5
I.3.	Molecular tectonics.....	6
I.4.	Intermolecular Interactions.....	7
I.4.1.	<i>van der Waals interactions</i>	8
I.4.2.	<i>π-π stackings</i>	8
I.4.3.	<i>Ag-Ag interactions</i>	9
I.4.4.	<i>Ag- π interactions</i>	9
I.4.5.	<i>Hydrogen bonds</i>	10
I.4.6.	<i>Coordination bonds</i>	11
I.5.	Coordination networks	12
I.5.1.	<i>Dimensionality and geometry</i>	12
I.5.1.1.	One dimensional networks.....	12
I.5.1.2.	Two dimensional networks	14
I.5.1.3.	Three dimensional networks	16
I.5.1.4.	Network topology.....	17
I.5.2.	<i>Metal-organic frameworks</i>	18
I.5.2.1.	Terminology.....	18
I.5.2.2.	Porosity and interpenetrations of the networks	19
I.5.2.3.	MOF's engineering	21
I.5.2.4.	Heterometallic architectures.....	22
I.6.	Aim of the work.....	25
I.7.	References	26
II.	CHAPTER 1	29
II.1.	Introduction.....	31
II.1.1.	<i>Generalities regarding 7-Azaindole</i>	31
II.1.2.	<i>Coordination chemistry of 7-azaindole</i>	32
II.1.2.1.	Metal complexes incorporating 7-azaindole	33
II.1.2.2.	Metal complexes incorporating 7-azaindolate ligands.....	35
II.2.	Ligands	38
II.3.	Complexes and networks.....	41
II.3.1.	<i>Rhodium complexes</i>	41
II.3.2.	<i>Networks based on the benzoic acid appended ligands 8 and 9</i>	43
II.3.3.	<i>Complexes and networks based on the 3-tricyanovinylene-7-azaindole ligand</i>	51
II.4.	Conclusion	55
II.5.	References	56

III.	CHAPTER 2	57
III.1.	Introduction	59
III.1.1.	<i>Dipyrrens</i>	59
III.1.2.	<i>Two modes of coordination</i>	60
III.1.2.1.	Coordination chemistry of dipyrrens.....	61
III.1.2.2.	Coordination chemistry of dipyrriate	61
III.1.3.	<i>Networks</i>	64
III.1.3.1.	Homonuclear networks	64
III.1.3.2.	Heteronuclear networks.....	65
III.1.3.2.1.	<i>Coordination to a second metal centre at the peripheral group</i>	65
III.1.3.2.2.	<i>Assistance of Ag-π interactions</i>	67
III.2.	Preparation of the ligand	68
III.3.	Preparation of complexes and networks	70
III.3.1.	<i>Neutral dipyrrens as ligands for the preparation of [2+2] macrocycles with silver ions</i>	70
III.3.1.1.	Behavior in solution.....	76
III.3.2.	<i>Coordination chemistry of dipyrriate</i>	78
III.3.2.1.	Homoleptic discrete complexes	78
III.3.2.2.	Heteroleptic complexes and networks.....	81
III.3.2.2.1.	<i>Heteroleptic complexes and networks with copper (II)</i>	82
III.3.2.2.2.	<i>Heteroleptic complexes with cobalt (III)</i>	87
III.3.2.3.	Heterometallic architectures.....	90
III.4.	Conclusion	99
III.5.	References	101
IV.	CHAPTER 3	103
IV.1.	Introduction.....	105
IV.1.1.	<i>Strategy towards homometallic networks</i>	105
IV.1.2.	<i>Strategy towards heterometallic architectures</i>	108
IV.2.	Ligand	109
IV.3.	Preparation of complexes and H-bond networks upon coordination of the dipyrren pole.....	110
IV.4.	Towards heterometallic architectures.....	113
IV.5.	Conclusion	116
IV.6.	Reference.....	117
V.	GENERAL CONCLUSION AND PERSPECTIVE.....	119
VI.	EXPERIMENTAL SECTION	125
VI.1.	General remarks.....	127
VI.2.	Compounds reported in Chapter 1	129
VI.3.	Compounds reported in Chapter 2	143
VI.4.	Compounds reported in Chapter 3	172
VII.	APPENDIX	181

I. General introduction

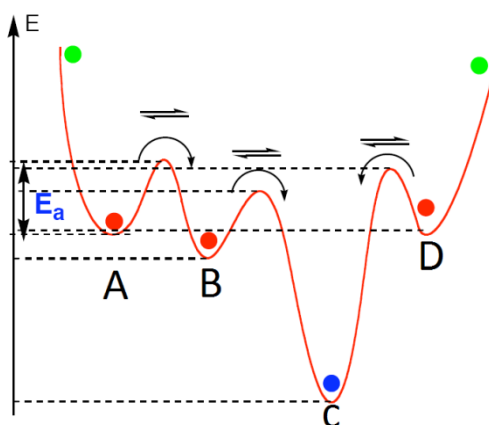
I.1. Supramolecular chemistry

Supramolecular chemistry is one of the most intensively developing and promising areas of chemistry today. This field combines the interests of various scientific fields, from inorganic chemistry and crystallography to biochemistry. The term supramolecular chemistry was defined by Professor Jean-Marie Lehn in 1978 as a "beyond the field of molecular chemistry based on the covalent bond, there is a field of supramolecular chemistry, the chemistry of molecular assemblies and of the intermolecular bond"¹. Contrary to classical chemistry, which is based on covalent intramolecular interaction, supramolecular chemistry focuses on weak interactions between molecules, such as van der Waals, hydrogen bonding, π - π interactions, metal coordination etc...

I.2. Molecular self-assembly

The basic concepts of supramolecular chemistry can be emphasized as *molecular recognitions* between complementary molecules, self-assembly and self-organization processes which lead to the formation of supramolecular entities.

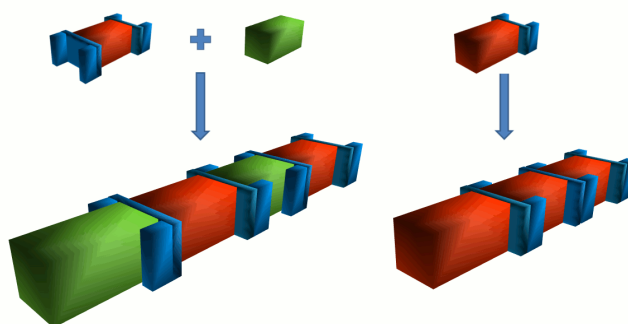
Molecular self-assembly is a spontaneous thermodynamic process based on the assembly of pre-organized substances leading to aggregates *via* weak non-covalent intermolecular interactions. Contrary to assemblies organized by covalent interactions, self-assembled architectures are obtained by reversible processes allowing self-repairing. This reversibility is related to the low activation energy barrier of the non-covalent interactions. As a consequence of this, the system may get out of the local minima and reach the final most stable thermodynamic state (**Scheme 1**).



Scheme 1: Schematic representation of the activation energy barrier for molecular self-assembly process.

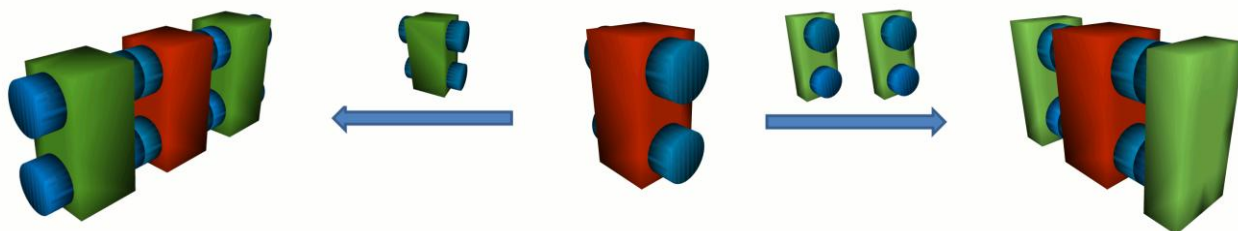
I.3. Molecular tectonics

The term “molecular tectonics” was firstly defined by S. Mann² in 1993. This approach is based on the use of active building blocks (“tectons”), which are able to recognize each other *via* specific non-covalent interactions and to form supramolecular architectures through “controlled” self-assembly processes³ in the crystalline state. Molecular recognition is a selective association process and requires the coexistence of two complementary interaction sites, able to form a recognition pattern. Depending on the nature and number of interaction sites, these tectons can be divided in self-complementary and complementary tectons (**Scheme 2**). In the case of self-complementary tecton, the system contains a single component bearing complementary recognition sites. In contrast, for the second case, at least two complementary tectons are required.



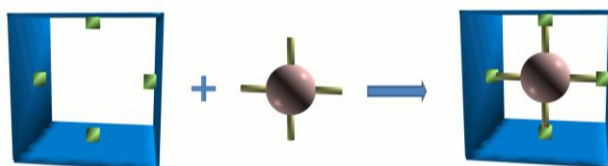
Scheme 2: Self-assembly of complementary (left) and self-complementary (right) tectons.

Depending on the relative positions of the recognition sites, tectons can be classified into *exo* (**Scheme 3**) and *endo* categories (**Scheme 4**). In the first case, the recognition sites are arranged in a divergent mode and such tectons can form either infinite networks or discrete complexes.



Scheme 3: Representation of Exo receptors: infinite networks (left) and discrete complexes (right).

In the second *endo* type receptors, the interaction sites are arranged in a convergent fashion which prevent the iteration of the assembling processes and thus leads to the formation of discrete inclusion architectures.



Scheme 4: Representation of Endo receptors.

For example, the crystal structure of the *meso*-5,15-di(4-pyridyl)-10,20-di(4-trifluoromethylphenyl)porphyrinato zinc (II) complex⁴, which was synthesized in our laboratory, reveals a 3-D network formed by the self-complementary tectons. The zinc (II) centre, adopting a distorted octahedral environment, is coordinated to four nitrogen atoms of the macrocyclic core of the porphyrin (*Endo* arrangement of the coordinating sites) and to two pyridyl fragments arranged in a divergent fashion belonging to neighbouring molecules.

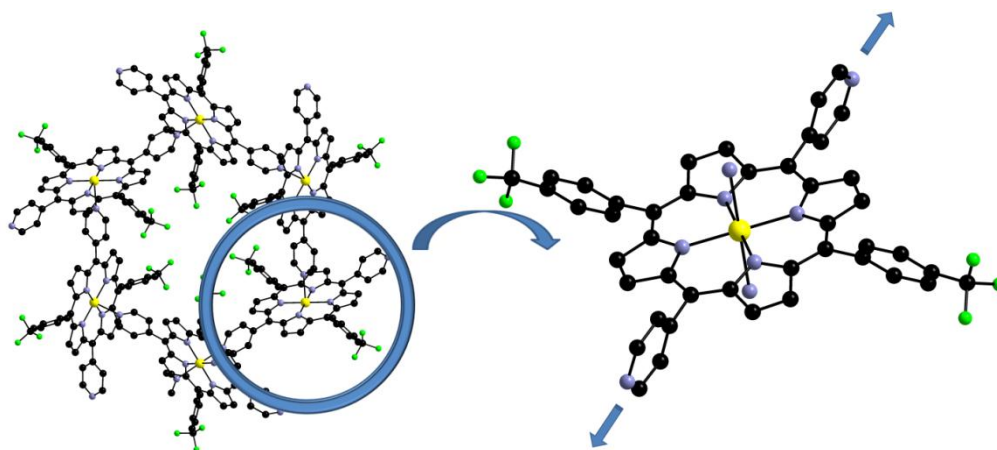
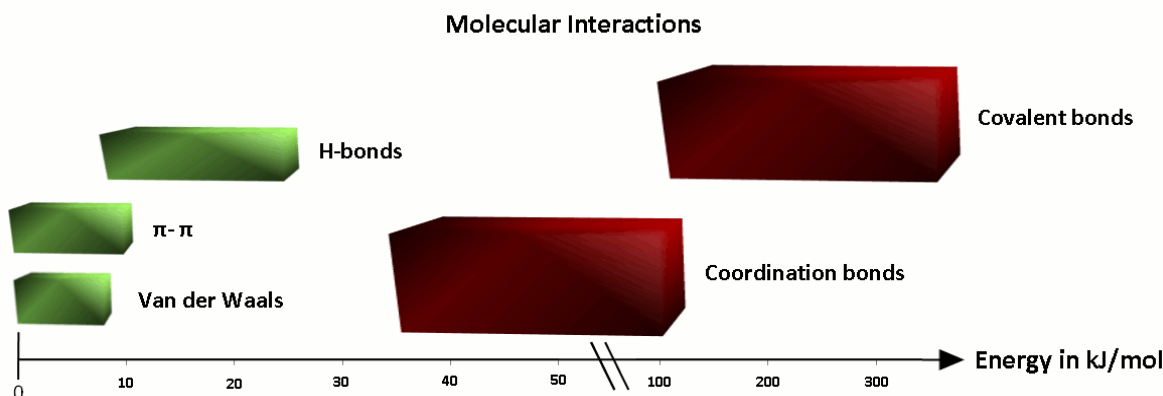


Fig. 1: Example of a self complementary network with ligand appended pyridine as secondary coordination pole.

I.4. Intermolecular Interactions

A molecular crystal may be regarded as a supramolecular architecture composed of molecular networks or periodic assemblies. Its formation may then be described as self assembly processes based on repetition of molecular recognition events resulting from non covalent interactions between molecular components composing the crystal. The interaction energy associated with the recognition processes may range from weak to strong (**Scheme 5**). Chemists usually chop the energy axis which ranges between zero and *ca* 100 Kcal/ mol (≈ 418 kJ/ mol) into categories (van der Waals and π - π interactions, hydrogen and coordination bonding, electrostatic charge-charge interactions etc.). The formation of networks and their packing leading to the crystalline material usually combines several types of interactions. Some of the intermolecular interactions and their specificity are discussed and illustrated below.



Scheme 5: Strong (red) and weak (green) molecular interactions.

1.4.1. van der Waals interactions

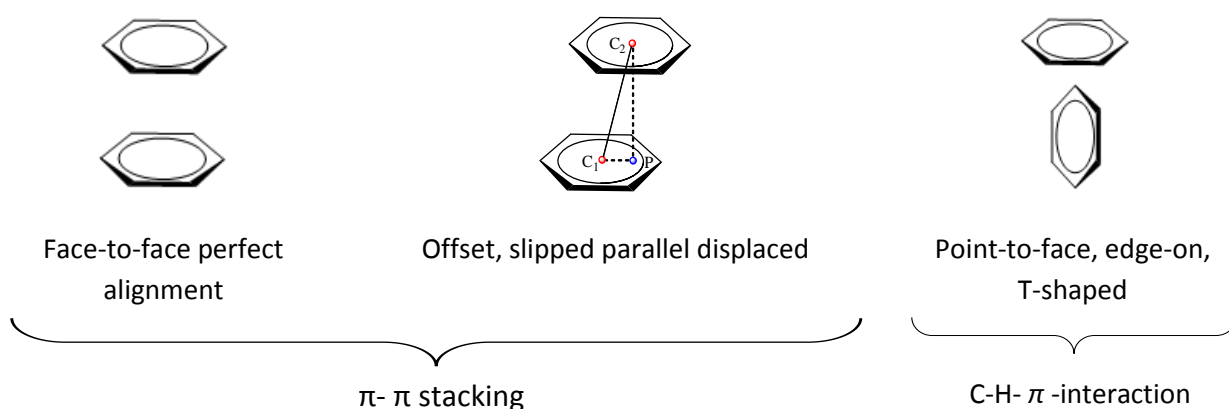
van der Waals interactions are relatively weak electrostatic intermolecular interactions (0.8-8 kJ/mole) appearing between permanent or induced dipoles. These interactions, effective only at very short distance, are not directional and non selective. Depending on their nature, these forces can be divided into three groups:

- Orientation interactions appearing between permanent dipoles.
- Dispersion (London) interactions: taking place between induced dipoles.
- Induction interaction: engaging permanent and induced dipoles.

In spite of the weak energy of these interactions, they play an important role in chemistry as a one of the forces governing chemical properties of compounds and exert considerable influence on the formation of crystal materials.

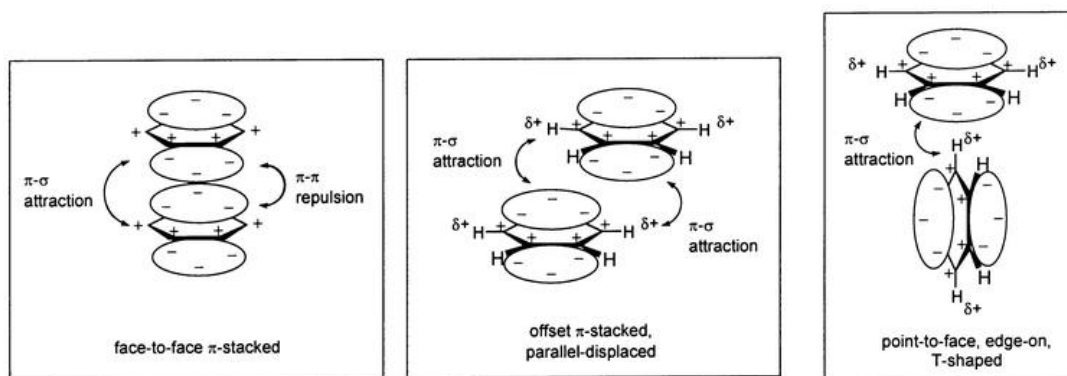
1.4.2. π - π stackings

Aromatic-aromatic π - π interactions (π - π stacking) are important non-covalent intermolecular attractive complexes. As the above-mentioned hydrogen-bonding, these interactions might participate in the self-assembly of tectons and thus play an important role in controlling the packing and/or interpenetration of network in the crystalline phase. The arrangement of aromatic rings can be considered in two limiting forms, as a perfect face-to-face and as point-to-face T-shaped edge-on (C-H- π -interaction) alignment. The slipped parallel displaced alignment can be seen as an intermediate case (**Scheme 6**). The stacked aromatic rings are approximately parallel with distances between centroids of the rings in the 3.3-3.8 Å range (**Scheme 6**, C₁-C₂ distance), and offset distance (distance between centroid and projection of the second centroid in the plane of the first ring, C₁-P length on **Scheme 6**) less than 1.3 Å.



Scheme 6: Different arrangement of aromatic-aromatic π - π and C-H- π -interactions.

The nature of this type of interaction is still a matter of debate⁵. There are several models for the stabilization of π - π interactions based on electrostatic or van der Waals forces for the such as dipole-dipole, dipole-induced dipole or induced dipole- induced dipole interactions. Other models are based on solvophobic effects and charge transfer processes. Hunter and Sanders⁶ suggested an electrostatic model based on the attraction of aromatic π -electrons of one molecule with a positively charged σ -frame of an adjacent molecule (**Scheme 7**). These π - σ attractions overcome the π - π repulsion between two negatively charged π -systems. In the case of offset or π -stacking or point-to-face geometry, π - σ attractions are dominating forces.



Scheme 7: Attractive electrostatic interactions between the σ -frame and π -electrons density. (This figure was taken from Janiak's review article⁷).

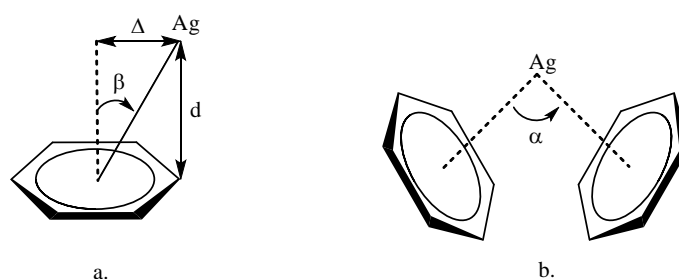
From the energetic point of view, these interactions depend from the nature of the substances and the polarity of the solvent (from 1 kJ/mole in solution^{8a} to 10 kJ/mole in the gas phase^{8b}).

1.4.3. Ag-Ag interactions

The silver-silver interaction is a particular case of metal-metal d^{10} - d^{10} interactions which are often observed in systems based on transition metal cations (*i.e.* Au (I), Cu (I), Ag (I))⁹. Regarding the nature of these interactions, different models were suggested¹⁰. Some models attribute the metal-metal attraction to hybridization, while others consider the attraction as a correlation effect. The silver-silver d^{10} - d^{10} interactions are weak with an energy strongly dependent on the ligand type, roughly estimated around 5(7)-13(2)⁹ kJ mol⁻¹. The range of typical Ag-Ag distances is 2.4-3.6 Å.¹¹ This interaction, when present, may be pertinent since it may influence the organization in the crystalline state.¹²

1.4.4. Ag- π interactions

Silver (I), as many transition metal cations, can accept π -electrons from aromatic systems and form stable organometallic complexes. Although Ag- π interactions are comparatively weaker, they play an important role as directive forces in crystal engineering. The widely accepted descriptive model of this interaction is the Dewar-Chatt-Duncanson model¹³ which predicts that the η^2 bonding of silver (I) is the preferred one. Nevertheless, examples with η^1 , η^6 and other types of bonding are known too. By an analysis of the CCD (Cambridge Crystallographic Database), Kochi, Lindeman and Rathore¹⁴ emphasized the critical structural features inherent to all analyzed silver/arene complexes and the absence of preference toward either η^1 or η^2 coordination. The distance between the silver atom and the plane of coordinated benzene lies in the range $d = 2.41 \pm 0.05 \text{ \AA}$ ($\beta = 32 \pm 3^\circ$, $\Delta = 1.53 \pm 0.2 \text{ \AA}$, **Scheme 8a**).



Scheme 8: Ag- π interactions.

Three groups of silver/bis(monoarene) complexes were distinguished with octahedral, tetrahedral and linear hybridization of silver and accordingly with three regions of angles between the planes of coordinated benzene ($\alpha = 95, 130$ and $155 \pm 3^\circ$, **Scheme 8b**).

Regarding the examples of Ag- η^6 interactions, the reported range of Ag-centroid distances is 2.89-3.37 Å¹⁵, which denotes the weakness of this interaction compared with the η^1 or η^2 modes of complexation.

1.4.5. Hydrogen bonds

L. Pauling gave one of the most operative definition of hydrogen bond¹⁶.

A hydrogen bond is an interaction that directs the association of a covalently bound hydrogen atom with one or more other atoms, groups of atoms, or molecules into an aggregate structure that is sufficiently stable to make it convenient for the chemist to consider it as an independent chemical species.

The formation of hydrogen bonding interactions implicates the coexistence in the system of proton donor (A-H) and proton acceptor (B) sites. Accordingly, a proton donor is a group containing an electronegative atom with covalently bonded hydrogen atom (for example -OH, -NH) and a proton acceptor as an electronegative centre (for example -C=O, -N=). The number and nature of the hydrogen bonding donor/acceptor can obviously vary from systems to systems providing a wide landscape of possibilities such as linear and bifurcated (**Fig. 2b**).

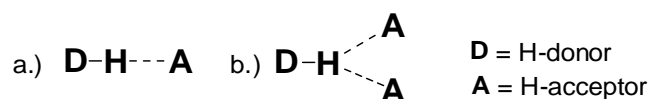


Fig. 2: H-bond interactions.

Based on the graph-set concept, Etter developed a system of assignments for hydrogen bonding motifs¹⁷. In this frame, numerous different types of hydrogen bonds (depending on the nature of the donors and acceptors involved) were identified. In the case of intermolecular hydrogen bonds, three designators were used (**Table 1**): **C** (chain), **R** (ring), and **D** (dimer or other finite set), while **S** denotes an intramolecular hydrogen bond. The number of donors (**d**) and acceptors (**a**) used in each motif are assigned as subscripts and superscripts, respectively, and the number of atoms in the unit is indicated in parentheses.

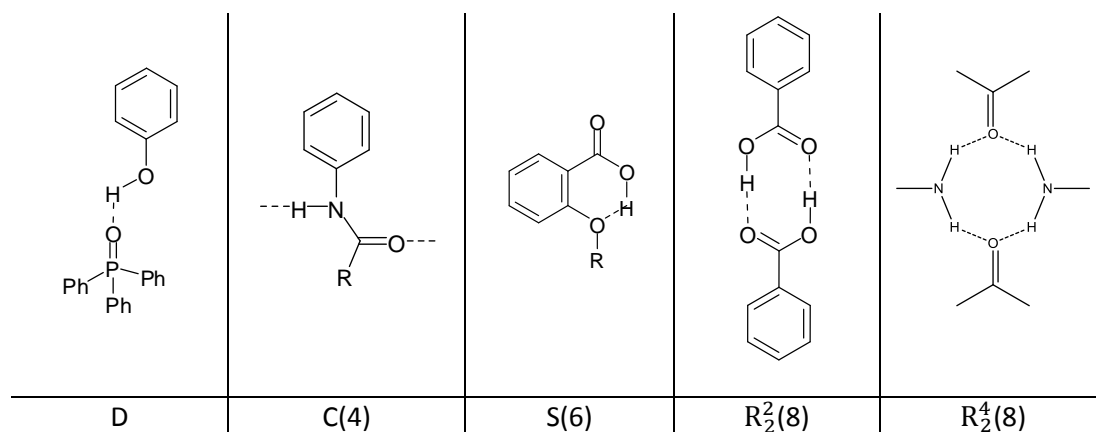
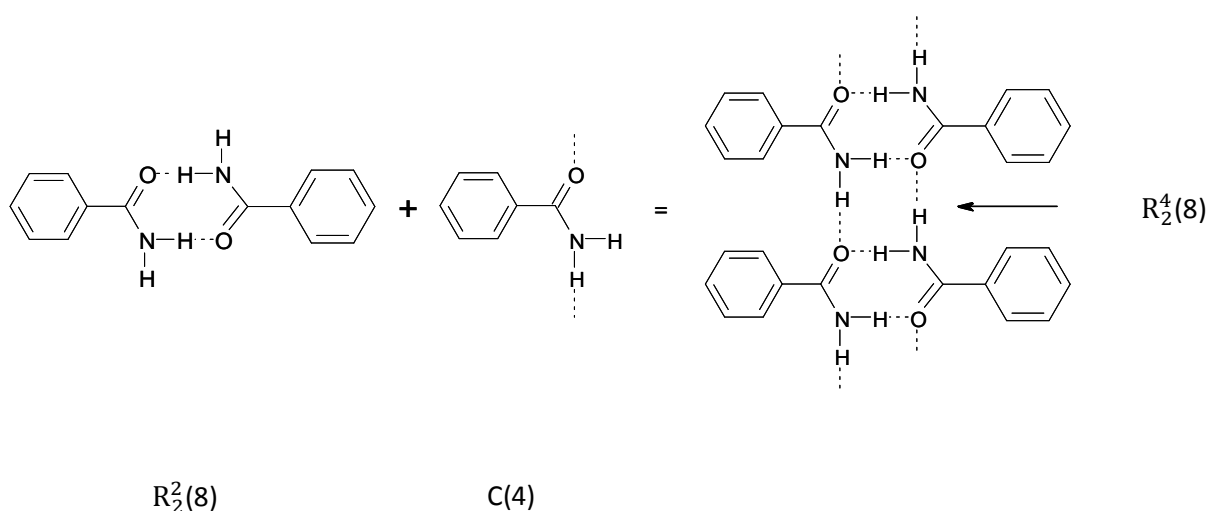


Table 1: Different designators for hydrogen bond interactions.

In the case of a more complex situation, when a compound contains two or more types of hydrogen bonds, the combination of these motifs can form additional pattern. For example, the combination of two different types of hydrogen bonds in primary amides (**Scheme 9**), such as chain C(4) and cyclic dimer, $R_2^2(8)$ can be observed. In turn, these two motifs form the third, $R_2^4(8)$ pattern.



Scheme 9: Example of coexisting different H-bond motifs in the same system.

Hydrogen bonding can be described as a directional electrostatic dipole-dipole interaction. Unlike van der Waals interactions, hydrogen bond ranges from weak to rather strong. Typical bond distance (2-3.5 Å) and energy (2-70 kJ/mol) associated with this interaction can vary within a wide range depending on the nature of donors and acceptors.

1.4.6. Coordination bonds

In a simplistic representation, coordination bond may be regarded as a donor-acceptor type interaction between a ligand (Lewis base) offering electron pairs and a metal centre (Lewis acid) accepting an electron pair in an unoccupied orbital. The coordination bond is by nature directional and its average energy ranges from *ca* 40 to 120 kJ/mol.

I.5. Coordination networks

I.5.1. Dimensionality and geometry

From the geometrical point of view, networks can be distinguished by their dimensionality as 1-D, 2-D and 3-D nets (**Fig. 3**). Contrary to single molecules, molecular networks present translation symmetry. The dimensionality of the network depends on the number of translations operating at the level of the assembling nodes.^{18,17} The formation of 1-D network is observed in the case of a single translation, accordingly 2-D and 3-D networks are based on two or three translations respectively.

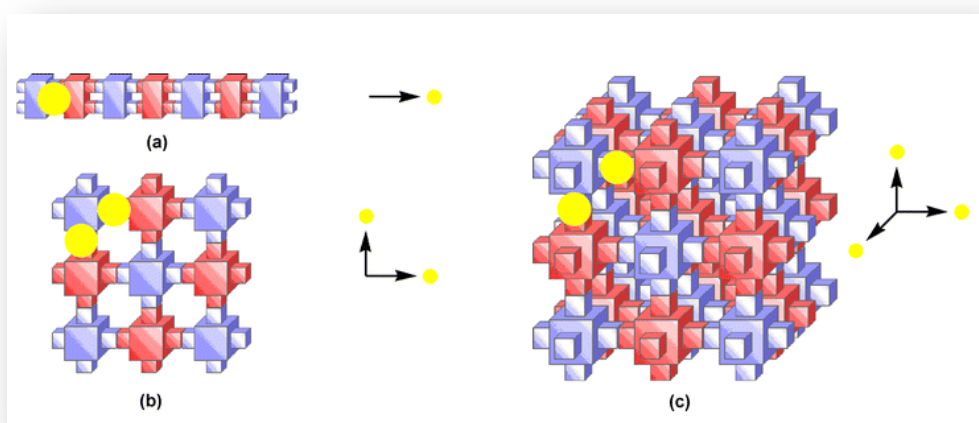


Fig. 3: Schematic representation of 1-D (a), 2-D (b) and 3-D (c) networks.

I.5.1.1. One dimensional networks

The formation of 1-D networks requires the use of tectons bearing at least two interaction sites arranged in a divergent fashion.^{18a} These networks may be designed using either a self-complementary tecton (single component system) (**Fig. 4a**) or a combination of complementary tectons (poly-component systems). In the latter category, the architecture may be organized by a single recognition pattern (**Fig. 4b**) or several different assembling nodes (**Fig. 4c-f**).

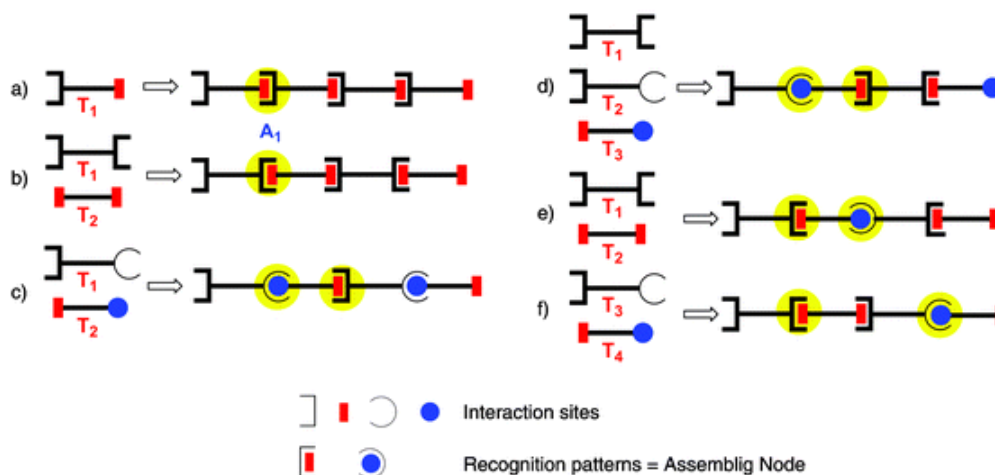


Fig. 4: Formation of 1-D networks.

With respect to their geometry, one dimensional networks can be classified into linear, stair, helical and zigzag types (**Fig. 5**). In terms of shape, cylinder, ladder, ring ribbon, ring-rod chain or even tubular architectures may be obtained (**Fig. 6**).

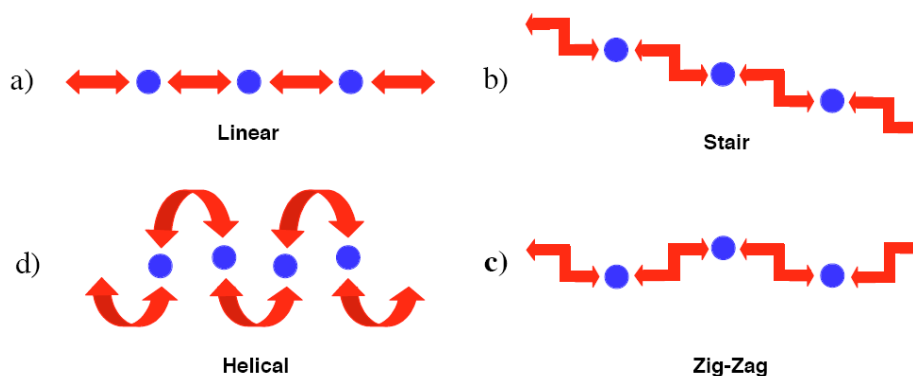


Fig. 5: Four geometrical types of 1-D networks: linear (a), stair (b), helical (c), zig-zag (d).

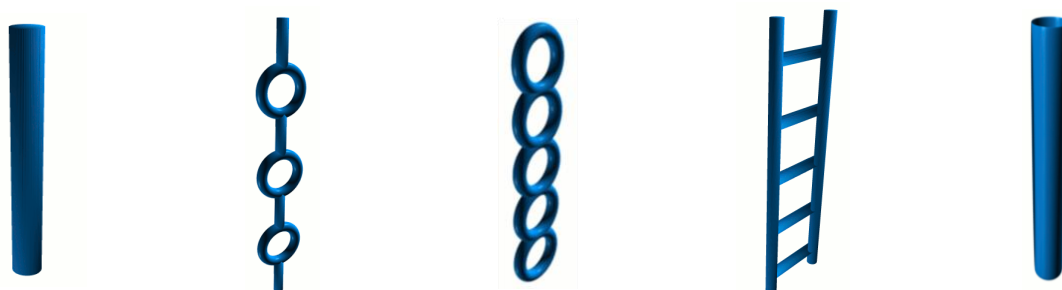


Fig. 6: Different shapes of 1-D linear networks.

Both the geometry and the shape of the 1-D networks depend on the nature and localization of the recognition sites within the structure of tectons. For example, two isomeric ligands 4,4'-pybut (1,4-bis(4-pyridyl)buta-1,3-diyne) and 2,2'-pybut with linear and "off-axis rod" functionality respectively and their 1-D networks with AgNO_3 have been reported. As a result of the ligand geometry, the linear 4,4'-pybut ligand leads to the formation of the linear 1-D chain $\{[\text{Ag}(4,4'\text{-pybut})]\text{NO}_3(\text{CH}_3\text{CN})_2\}^{19}$ (**Fig. 7a**), whereas the "off-axis rod" ligand 2,2'-pybut tends to form the zigzag shaped 1-D chain $\{[\text{Ag}(2,2'\text{-pybut})]\text{NO}_3\}^{20}$ (**Fig. 7b**) under the same conditions. Of course not only the nature and geometry of the tecton and metal define the structure and properties of the net, but solvent molecules and anions are also important and sometimes can play a determining role.²¹

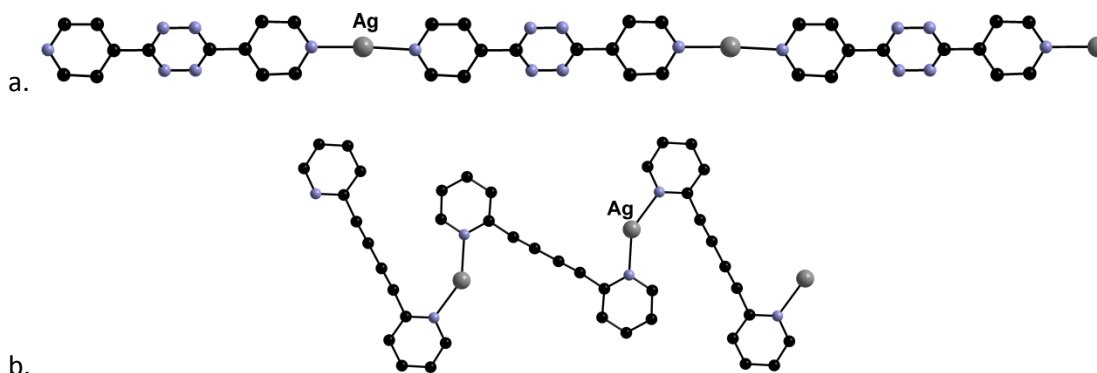


Fig. 7: Examples of the influence of the relative arrangement of recognition sites on the geometry of 1-D networks.

I.5.1.2. Two dimensional networks

By analogy with 1-D networks, the formation of 2-D architectures requires tectons bearing at least three divergently orientated recognition sites. Two examples of a single component system based on self-complementary tectons is depicted in **Fig. 8 a and b**. Example of combinations of complementary tectons leading to 2-D networks are given in **Fig. 8 c-e**. Depending on the nature of the recognition sites and the number of tectons, the formation of networks with one assembling node or with several different recognition patterns is possible.

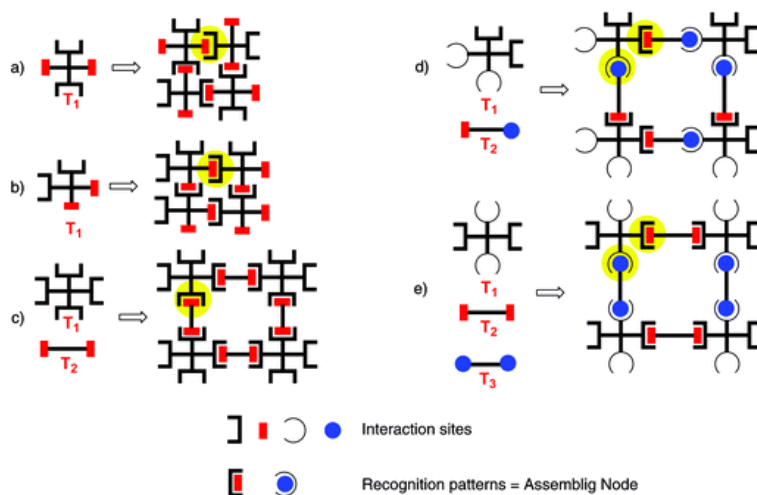


Fig. 8: Formation of 2-D networks.

Two dimensional networks, as 1-D nets, may be of different shapes, from the simple planar to zigzag or slot form (**Fig. 9**). Regarding the geometrical arrangement in the plane, several motifs can also be distinguished. The grid arrangement is one of the common geometrical types. It can assume different shapes depending on the angle of the grid and can be classified into square, honeycomb, rectangular, chevron grid type and others.

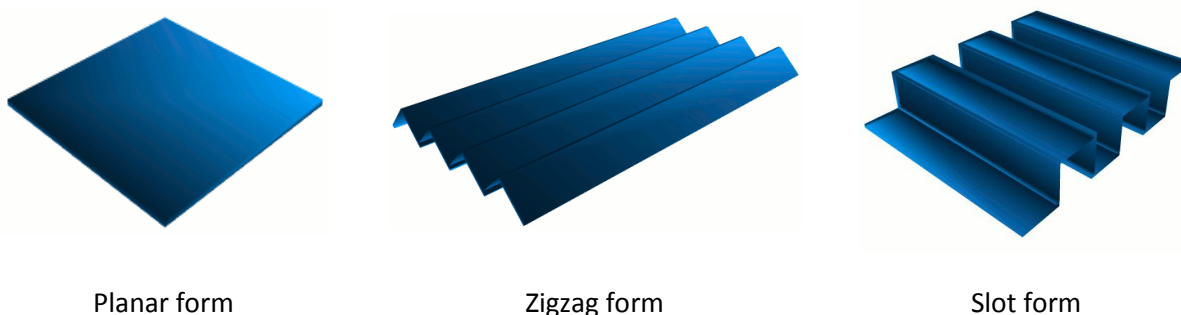


Fig. 9: Different shapes of 2-D networks

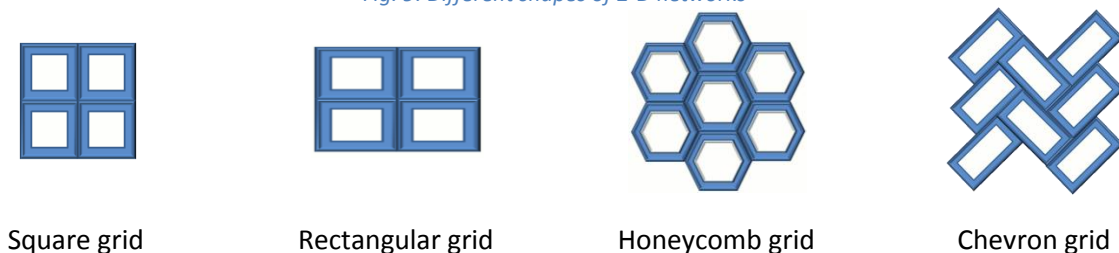


Fig. 10: Examples of grid arrangement of the 2-D network plane.

For example, the network $\{[\text{Ni}(\text{1,4-(4-Py)-benzene})_2(\text{H}_2\text{O})_2](\text{Benzene})(\text{MeOH})_5(\text{NO}_3)_2\}_\infty$ ²² (**Fig. 11**) illustrates the square grid arrangement with 15.63x15.56 Å cavity. The Ni center is in an octahedral environment with four pyridine moieties occupying the equatorial positions and two water molecules in the apical positions. In the case of this network, the ligand appended with two interaction sites plays the role of linear spacer between two nickel atoms (**Fig. 8c**). These coordination geometry around the metal centres defines the network structure and dimensionality.

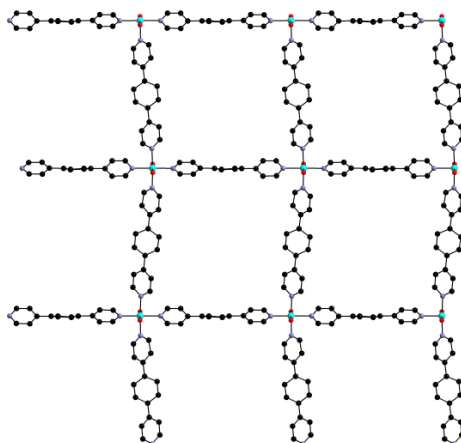


Fig. 11: Structure of the $\{[\text{Ni}(\text{1,4-(4-Py)-benzene})_2(\text{H}_2\text{O})_2](\text{Benzene})(\text{MeOH})_5(\text{NO}_3)_2\}_\infty$ square grid 2-D network.

In contrast, the $\{[\text{Cu}(\text{C}_{10}\text{H}_{26}\text{N}_6)]_3[\text{BTC}]_2(\text{H}_2\text{O})_{18}\}_\infty$ ⁱ network²³ adopts a 2-D honeycomb organization (**Fig. 12**). The copper center, which is in a square planar coordination geometry in the starting metallatecton, adopts an octahedral environment (**Fig. 12 right**) in the network via coordination of two carboxylates in the axial positions and plays the role of linear connector between two BTC fragments, which in turn, bearing three divergently orientated recognition sites (carboxylates), define the network structure and dimensionality.

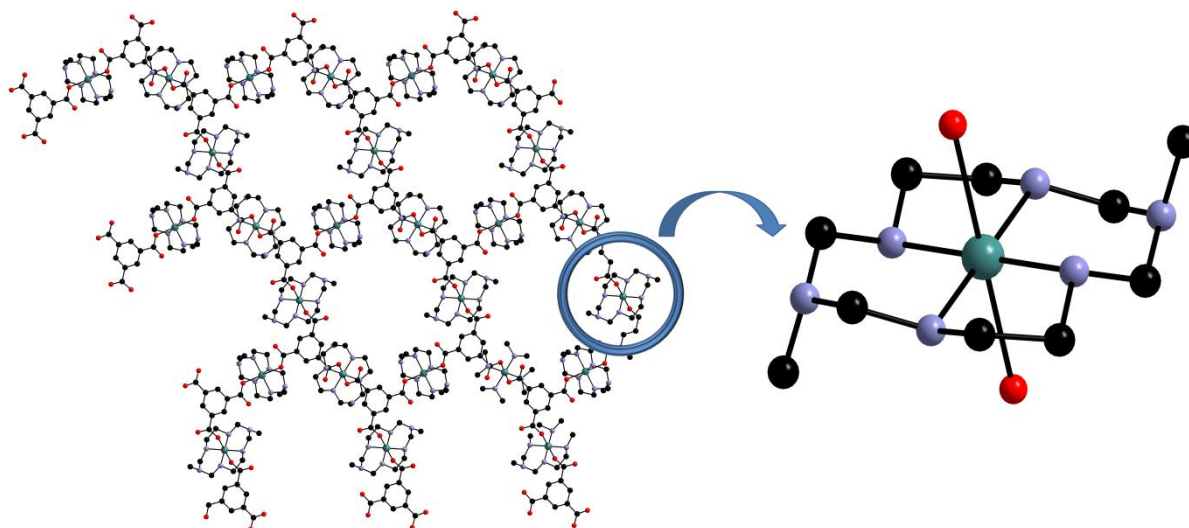


Fig. 12: Structure of the $\{[\text{Cu}(\text{C}_{10}\text{H}_{26}\text{N}_6)]_3[\text{BTC}]_2(\text{H}_2\text{O})_{18}\}_\infty$ 2-D honeycomb grid network²³.

ⁱ $\text{C}_{10}\text{H}_{26}\text{N}_6 \equiv$ 1,8-dimethyl-1,3,6,8,10,13-hexaazacyclotetradecane; BTC \equiv benzene-1,3,5-tricarboxylate

I.5.1.3. Three dimensional networks

Unlike 1-D and 2-D nets, in the case of the 3-D networks, the dimensionality of the architectures coincides with the dimensionality of the crystal. The formation of 3-D system requires the use of at least four non coplanar recognition sites. As in the former cases, the number of recognition patterns in the system depends on the nature of the recognition sites and number of tectons. Regarding the arrangement of 3-D networks, variation of the types is much more complicated than in the previous cases. For instance, the cubic net type (**Fig. 13**) is a typical representative for this group.

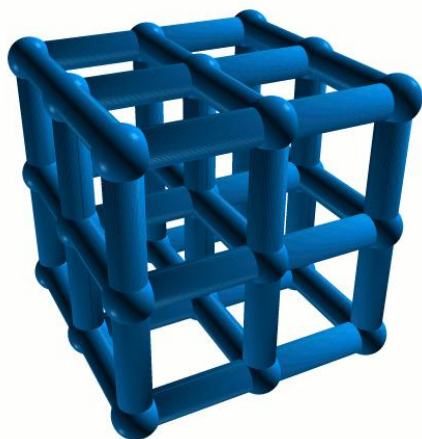


Fig. 13: Cubic grid 3-D network.

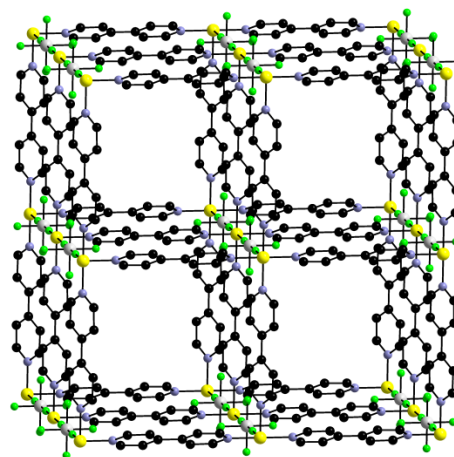


Fig. 14: Structure of distorted cubic grid 3-D network $\{[\text{Zn}(4,4'\text{-bpy})_2]\text{SiF}_6\}_\infty$.²⁴

For example, the structure of the 3-D network $\{[\text{Zn}(4,4'\text{-bpy})_2]\text{SiF}_6\}_\infty$ ⁱ was described²⁴. This network adopts a 3-D distorted cubic grid arrangement (**Fig. 14**) and yields channel with dimensions about $11.3 \times 11.3 \text{ \AA}$ along its c axis and $7.7 \times 11.3 \text{ \AA}$ along the a and b axes. The zinc centre adopts an octahedral environment by coordination of four pyridyl moieties in a square planar fashion and two SiF_6^- anions which are bound perpendicularly to the zinc-pyridyl plane. Other examples of 3-D networks will be discussed in the following “Metal-organic frameworks” part.

ⁱ 4,4'-bpy \equiv 4,4'-bipyridine

I.5.1.4. Network topology

In an attempt to classify the topology of a chemical network, Wells proposed in 1977 a model for network description²⁵. Looking at the problem from a mathematical point of view, any chemical network can be considered as a series of connection points and connectors. The notation of Wells consists in describing a net by (n,p) -net where p is number of connections to neighbouring nodes that radiate from any of the node and n is the number of nodes in the smallest closed circuits in the net²⁶. It is worth noting that nets with different geometry can be topologically identical (**Fig. 15 a and b**). For example, the infinite honeycomb 2-D type network **Fig. 15a** and the net **Fig. 15b** can be both considered as (6,3)-nets.

- a. (6,3)-net in Wells topology b. (6,3) -net in Wells topology c. 4.8^2 -net in Shl6fli topology
 (6^3 -net in Shl6fli topology) (6^3 -net in Shl6fli topology)

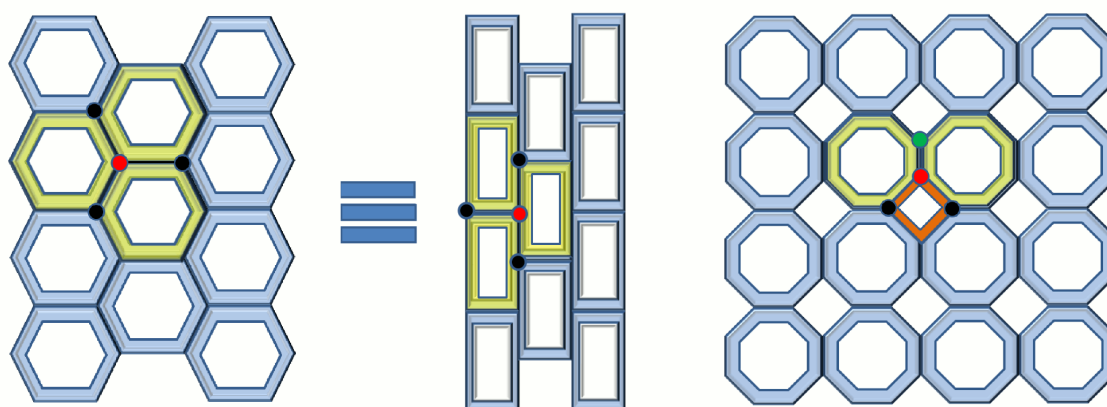


Fig. 15: Two geometrically different forms of (6,3) nets (a and b in Wells topology) and a 4.8^2 net (in Shl6fli topology).

The Wells notation can be applied only for nets in which all shortest circuits outgoing from any unconditioned nodes are identical, otherwise the Shl6fli notation should be applied. Shl6fli symbols are presented in the form of an n^p combination where n is a number of nodes on the route from one node to itself based on each pair of connections at the node²⁷ and p is the number of equivalent pairs. For example, in the cases of nets **Fig. 15a** and **Fig. 15b** all three pairs of nodes (black dots on the picture) connected to the same node (red dot on the picture) are equivalent. The shortest routes from one node to itself through any two neighbouring nodes consist of six nodes, meaning that the Shl6fli symbol for this net is 6^3 . The former examples can be described the same way in both notations, but in more complex cases, as **Fig. 15c**, only Shl6fli symbols can be applied. There are two different types of node pairs surrounding any of the nodes. The shortest circuit back to a three-connected node (red dot on the picture) is a 4-gone between one pair of connections and two 8-gons between the other two pairs (one green and one black dot on the picture). Hence this net can be described as 4.8^2 -net.

I.5.2. Metal-organic frameworks

I.5.2.1. Terminology

The term coordination polymer was first used by Bailar in 1967²⁸ in comparing organic polymers with inorganic compounds which can be considered as polymeric species²⁹. Later, in 1990, Robson³⁰ reported porous coordination polymers capable of anion exchange and, in 1995, the groups of Yaghi³¹ and Moore³² described investigations in the field of guest molecule adsorption.

Metal organic frameworks (MOF) are hybrid organic–inorganic infinite architectures composed of an inorganic complex or cluster and an organic linker acting as a bridge. The term “metal–organic framework” implies geometrically well-defined structures. While strong bonding provides robustness, the linking units can be modified by organic synthesis³³.

Some of the most famous and representative examples of MOFs have been described by the group of Yaghi^{34,33} in 1999. These compounds were based on 1,4-dicarboxylic acid appended ligands linked by tetrahedral Zn_4O units and forming 3-D extended cuboid type networks with 3-D intersecting channel. Depending on the spacer between the two carboxylates, MOFs with different void space (**Fig. 16**, yellow spheres) were obtained. The first example in this group, MOF-5³⁴ (**Fig. 16**), is based on the $Zn_4O(BDC)_3$ cluster (BDC=benzenedicarboxylate) with 12.94 Å spacing between the centres of adjacent clusters and large cavity, indicated by a yellow sphere of 18.5 Å diameter and a free volume of 80 %. Expansion of the spacer increases the internal void space and in the case of the longest terphenyl-4,4'-dicarboxylate linker, the calculated pore sizes is up to 28.8 Å, and the free volumes up to 91 %.

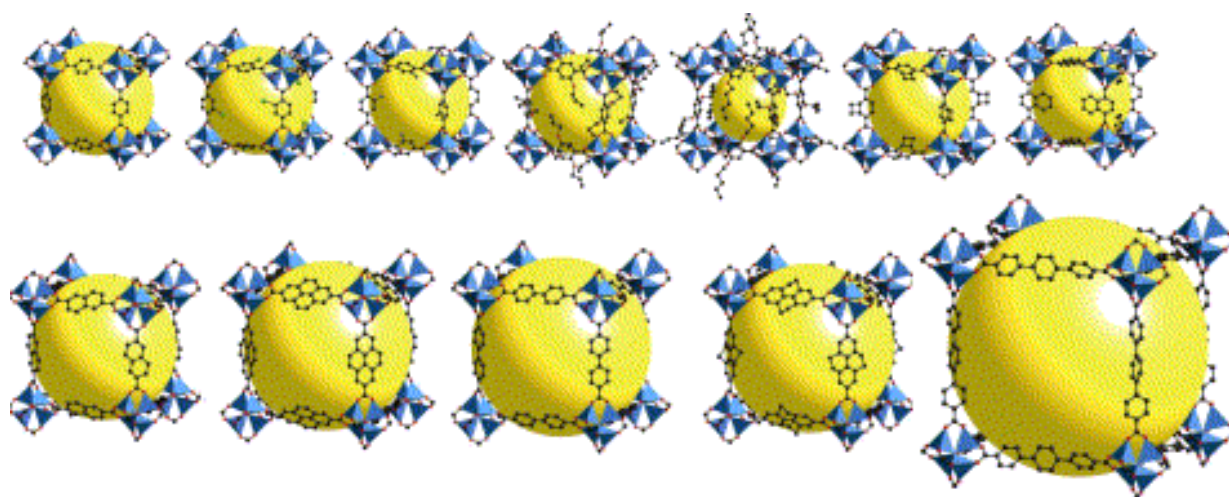


Fig. 16: Family of MOFs based on 1,4-dicarboxylic acid appended ligands and Zn_4O clusters (This figure was taken from of Rowsell, J. L. C., Yaghi, O. M. article³³).

I.5.2.2. Porosity and interpenetrations of the networks

These porous networks attracted considerable attention as architectures featuring nanometer-size space, which can be of interest in different fields of chemistry spanning from storage and separation of compounds to heterogeneous catalysis. Considering the size of the pores, these networks can be classified either as microporous ($d < 2.0$ nm), mesoporous ($2.0 \leq d \leq 50$ nm) and macroporous ($d > 50$ nm) materials³⁵. Since nature disliking vacuum, the vacant space in the pores is always occupied by the guest solvent molecules, template molecules or through interpenetration of the networks.⁴² With respect to the stability of the framework upon evacuation of guest solvent molecules, porous materials can be classified in three categories (**Fig. 17**). The 1st generation of porous materials is stable only in the presence of guest solvent molecules and the removal of guest molecules lead to collapse of the entire architecture. The 2nd generation implicates stable and robust porous frameworks with permanent porosity with and without guest molecules. For the 3rd generation, frameworks are flexible and evacuation of solvents from the pores or other external actions leads to reversible changes in channels or pores.

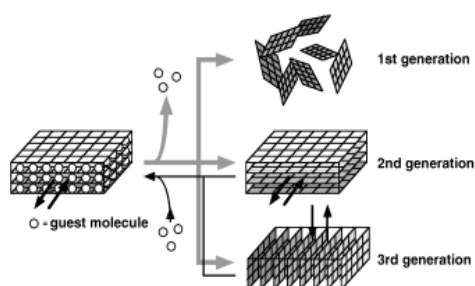


Fig. 17: Classification of porous materials by stability to evacuation of guest solvents. (This figure was taken from Kitagawa's article⁴²).

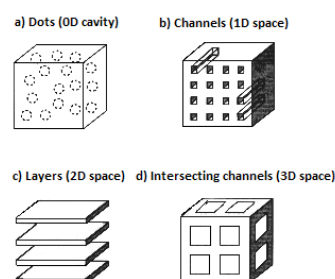


Fig. 18: Dimensional classification of porous materials (This figure was taken from Kitagawa's article⁴²).

From the point of view of the dimension, four groups of porous materials can be distinguished (**Fig. 18**). Cavities which are completely surrounded by the walls of the framework can be classified as 0D cavities. Accordingly, evacuation of guest molecules from the system is problematic. In contrast, materials with 1-D channels, 2-D layers or 3-D intersecting channels are often used to accommodate or exchange guest molecules.

When voids, cavities and channels size account for more than half the volume of the crystal, interpenetration is commonly observed for systems with large grid.³⁶ Network interpenetration is the entanglement of polymeric assemblies without any direct connections between them, but nevertheless, for topological reasons, separation requires a total collapse of the system (**Fig. 19**). The voids constructed by one network are occupied by one or few independent identical networks. Commonly, interpenetration is stabilized by different weak interactions between networks, such as van der Waals interactions or π - π stacking. It is worth noting that, in spite of partial occupation of porous space, interpenetration brings additional solidity to the system and allows the generation of stable architectures.



Fig. 19: Schematic representation of interpenetration for 3-D cubic (left) and 1-D ladder shape (right) networks.

Regarding the gas storage properties, the ability of MOFs to retain gas molecules depends not only on the cavity size, but also on the nature of the internal surface and the presence of potential fragments capable of interacting with gas molecules. Many computational studies have been conducted in this area, specifically in attempts to modulate³⁷ the H₂ adsorption properties of the MOFs. In most of the cases, these studies indicate the presence of only van der Waals type interactions between H₂ molecules and MOFs³⁸. Nevertheless, the presence of partial charges on the MOF's surface can provide dipole-induced dipole interaction with gas molecules^{37a,39} and thus enhance the binding of H₂. On the other hand, the presence transition metal with free coordination sites in frameworks can also enhance the binding of H₂ through interaction between gas molecules and with open-shell metal ions.

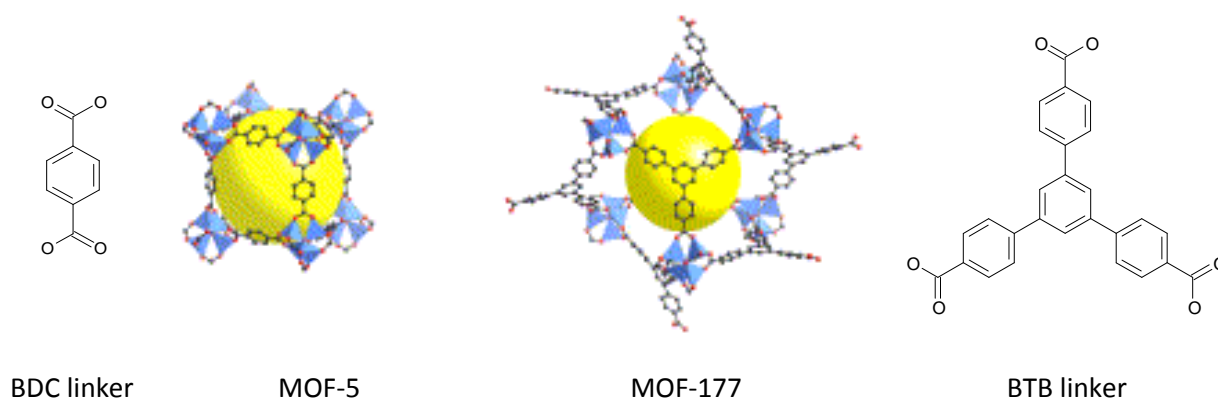


Fig. 20: MOF-5 and MOF-177 and corresponding linkers.

For example, the MOF with the highest BET surface area (MOF-177⁴⁰) of 4500 m²/g, reported so far (**Fig. 20**), exhibits a hydrogen adsorption of 7.1 wt % (at 77 K, 66bar). In comparison, MOF-5 has a BET surface area of 2900m²/g and a maximum excess adsorption of 4.951 wt % (at 77 K, 45.4 bar). Both MOFs contain the same Zn₄O cluster, but in the case of MOF-177, the BDC linkers are substituted by BTB (1,2,5-benzenetricarboxylate) units. The same BDC linker was used in the case of the MOF with the highest hydrogen storage capacity reported so far, NOTT-112⁴¹. The maximum hydrogen adsorption of 10 wt % (at 77 K, 77 bar) was observed with a corresponding BET surface area of 3800 m²/g. Contrary to MOF-177 and MOF-5, network NOTT-112 is based on copper paddlewheels and form three type of cages with different cavity size (**Fig. 21**). The cage A has an inner sphere diameter of approximately 13.0 Å, cage B 13.9 Å and the biggest one, cage C, shows a 20.0 Å diameter.

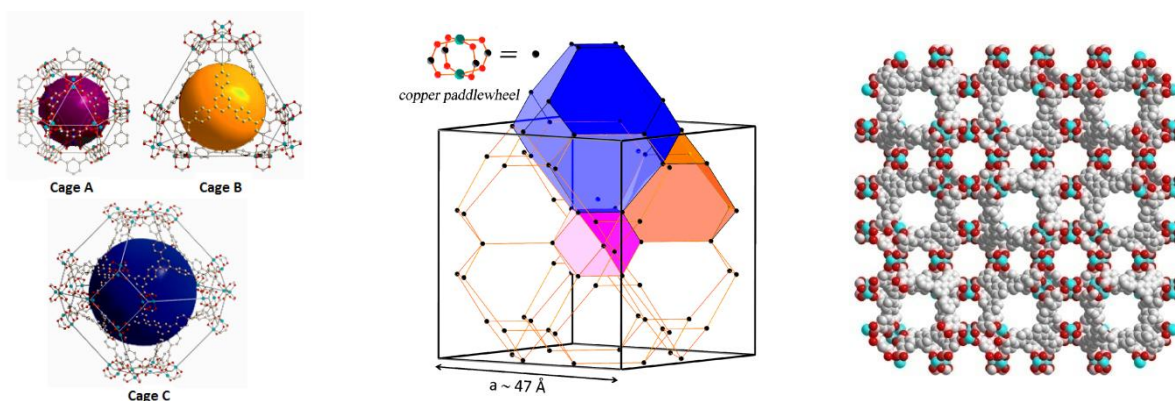


Fig. 21: Different cages in NOTT-112.

I.5.2.3. MOF's engineering

From the point of view of MOF's engineering, the metal organic frameworks can be considered in terms of connectors and linkers. The nature of these species incorporated with other auxiliary components, such as blocking ligands, counter anions or solvent guest molecules, define the structure and properties of the networks. The important characteristics of these connector and linkers are the number and orientation of interaction sites. Transition-metal ions, as typical components of MOFs, usually can be considered as connectors and ligands as linkers. Depending on the nature of the metal centre and its oxidation state, the number of coordination sites can vary from 2 to 7 (for lanthanides even higher numbers up to 10 may be reached). Accordingly, metal centers may adopt different coordination geometry, such as linear, square-planar, tetrahedral and others (**Fig. 22**), including distorted forms⁴².

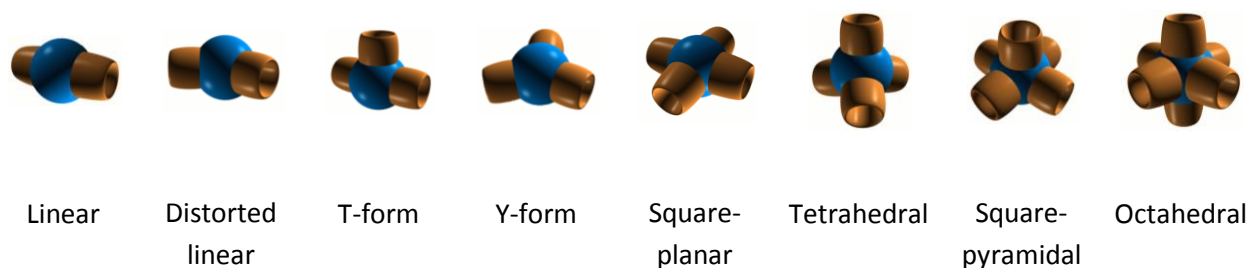


Fig. 22: Examples of metal coordination geometry.

Instead of using a naked metal centre (metal surrounded by labile ligands), one may use metal complexes as connectors. In the latter case, some of the coordination sites are occupied by auxiliary ligands (**Fig. 23**). Depending on the geometrical requirements of the metal used and number and denticity of auxiliary ligand, the construction of the architecture takes place using only the available coordination sites.

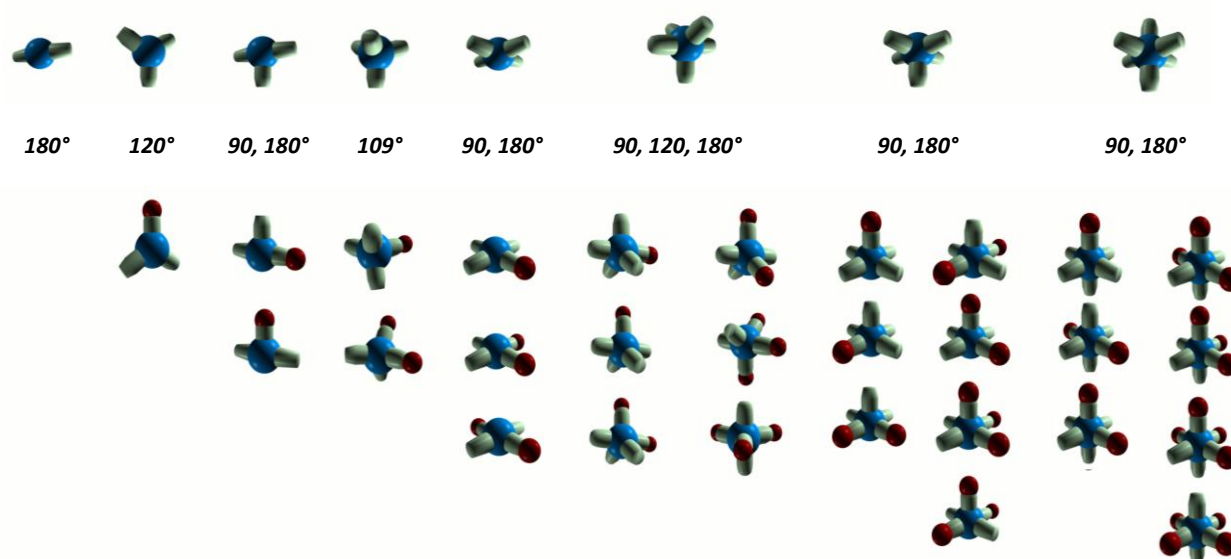


Fig. 23: Representation of capped metal complexes and angles introduced by the metal centre to the system. Red spheres and light green cylinders are capped and available sites for coordination respectively.

For example, the formation of the 3-D network $\{[\text{Ni}(\text{C}_{12}\text{H}_{30}\text{N}_6\text{O}_2)(\text{BDC})]^{+}(\text{H}_2\text{O})_4\}_{\infty}$ results from hydrogen bonding between self complementary 1-D coordination chains, which pack in a plywood motif (**Fig. 24**).⁴³ The nickel (II) center is in a distorted octahedral environment and surrounded by four nitrogen atoms belonging to the metallatecton in a square planar motif and two carboxylates which occupy the axial positions. In result, this starting metal complexes acts as a connector able to bring only linear geometry to the system. The BDC moiety acts as a linker with linear geometry. The combination of linear linkers and connectors forms the 1-D linear chain. However, the starting metal complexes are appended with secondary coordination poles, which act as hydrogen bonding donor (N-H) and acceptor (OH). As a result, these H-bond interactions between linear chains increase the dimensionality of the system leading to a 3-D MOF.

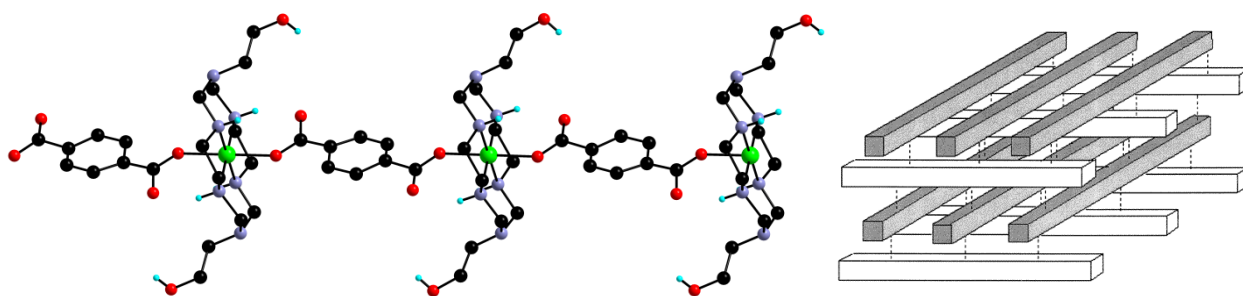
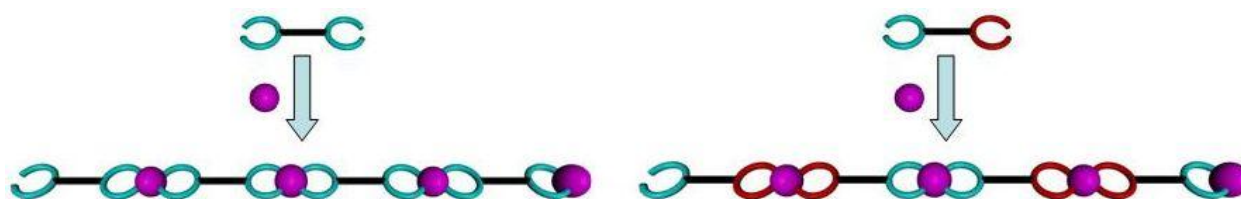


Fig. 24: Fragment of structure: 1-D chain within the 3-D network $\{[\text{Ni}(\text{C}_{12}\text{H}_{30}\text{N}_6\text{O}_2)(\text{BDC})]^{+}(\text{H}_2\text{O})_4\}_{\infty}$.

As mentioned above, from the crystal engineering point of view, the influence of the anion molecules on the architecture of the MOFs can also be important. Depending on the nature of these species, they can play different roles, such as H-bond acceptor (for example OTf^- , NO_3^-) and bridging units between metal centers. In the case of rather non-coordinating anions, such as PF_6^- and BF_4^- , they reduce, through charge neutralization, significant Coulombic repulsion between neighbouring positively charged polymeric assemblies.

1.5.2.4. Heterometallic architectures

As seen in this brief introduction, the field of coordination polymer and MOFs is particularly interesting from the point of view of both their synthesis and their resulting physical properties. However, it is interesting to note that the vast majority of these architectures are homometallic. Preparation of these homometallic frameworks implies the use of single metal source and of a ditopic ligand appended by one or similar types of coordination poles (**Scheme 10**).



Scheme 10: Strategy for the preparation of homometallic network.

ⁱ $\text{C}_{12}\text{H}_{30}\text{N}_6\text{O}_2 \equiv$ 1,8-di(2-hydroxyethyl)-1,3,6,8,10,13-hexaazacyclotetradecane;
BDC \equiv benzene-1,4-dicarboxylate

Following a synthetic approach analogous to the one employed for the homometallic systems, the combination of a ditopic ligand with metal ions, concurrently and in the absence of any differentiation at both the organic and metallic levels, can lead to a mixture of systems among which the homometallic architectures and a variety of heterometallic ones resulting from a statistical distribution of the metal centres (**Fig. 25**)⁴⁴.

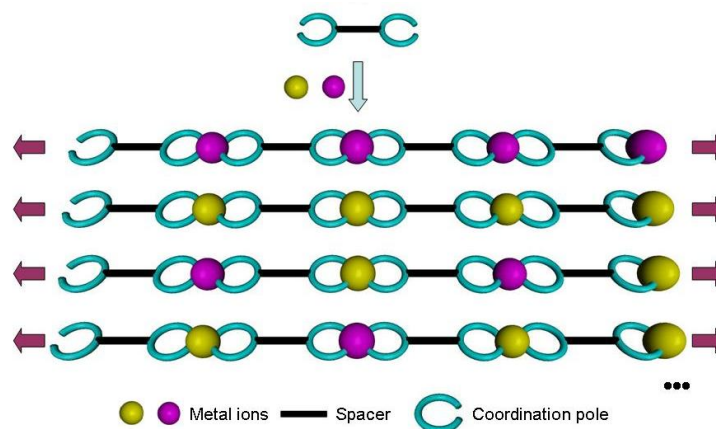
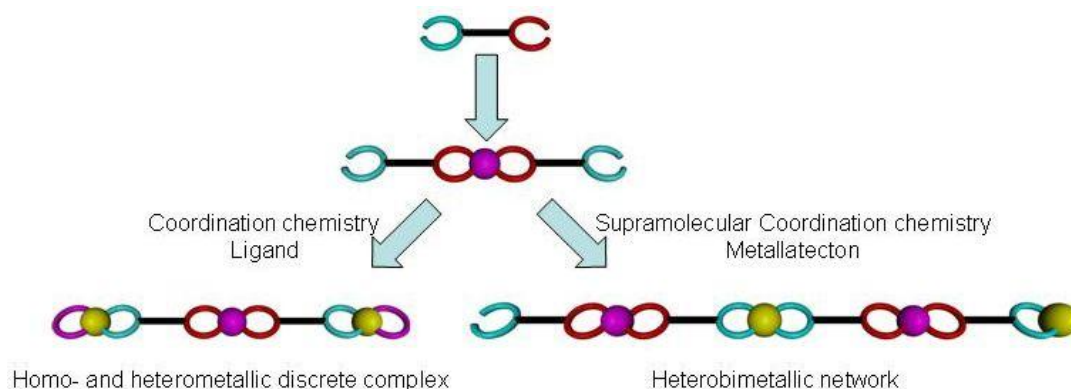


Fig. 25: Application of the synthetic approach to homometallic architectures to the heterometallic case.

A possible alternative for the controlled preparation of heterobimetallic coordination networks may be a sequential approach. This strategy is based on the sequential construction of heterobimetallic architectures in the crystalline state relying on an organic ligand bearing differentiated coordination poles which may be referred to as primary and secondary. This differentiation results from the difference in the nature of the elements and/or the charge of the poles and induces a coordination sequence. Upon reaction with a first metal centre, M1, a discrete complex is formed that may be isolated and characterized (**Scheme 11**). The latter offers secondary coordination poles at its periphery. Therefore, upon assembly with another metal centre, M2, heterometallic architecture can be formed. We shall note here that two complementary views of the intermediate complex can be given. Indeed, considering it as a ligand, one can envision the formation of discrete complexes upon reaction with a second metal centre by classical coordination chemistry. However, upon repetition of the coordination event, it can be regarded as a metallatecton or a building unit for the elaboration of infinite periodic architectures or networks. With the first approach, homo- and hetero-metallic complexes of tuneable nuclearity can be prepared, while, with the second one, the emphasis is put on the preparation of heterobimetallic extended architectures of controlled dimensionality.



Scheme 11: Strategy of the preparation of discrete complexes and heterobimetallic coordination networks.

To demonstrate the first strategy illustrated in **Scheme 11** (*left*) the complex $[\text{Pd}(\text{L}^{\text{i}})_2]^{2-}$ appended by two peripheral 4,5-diazafluorene coordination poles was reacted with two equivalents of the second metalloligand $\{[(\text{cyclen}^{\text{ii}})\text{Ni}](\text{BF}_4)_2\}$. In this case, the *cyclen* moiety was employed as a capping ligand for the Ni(II) cations, thus blocking four coordination sites. The resulting self-assembled species consists in the heterobimetallic trinuclear complex $\{[(\text{Pd}(\text{L}^{\text{i}})_2)(\text{Ni}(\text{cyclen}^{\text{ii}}))_2](\text{BF}_4)_2(\text{DMF})_6\}$ (**Fig. 26**).⁴⁵

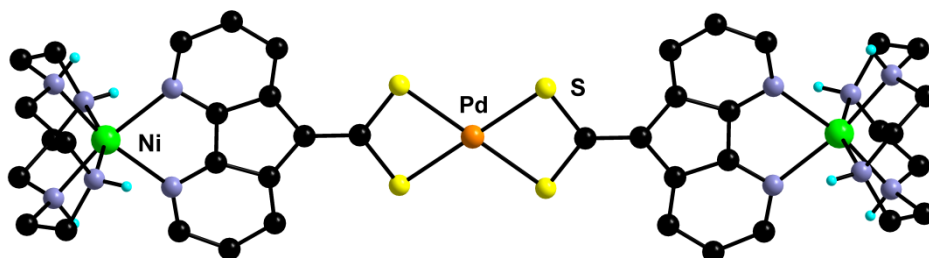


Fig. 26: Structure of the heterobimetallic complex $[(\text{cyclen})\text{Ni}(\text{Pd}(\text{L}^{\text{i}})_2)\text{Ni}(\text{cyclen})]^{2+}$.

To demonstrate the second strategy illustrated in **Scheme 11** (*right*), the 4-pyridyl appended ligand $\text{Pytyp}^{\text{iii}}$, comprising a tridentate and a monodentate coordination pole, was used to form the metallatecton $[\text{Ru}(\text{Pytyp})_2]^{2+}$.⁴⁶ The latter bears at its periphery two available pyridine groups. Upon reaction with a silver salt and coordination to peripheral pyridyl groups, a one-dimensional heterobimetallic network, $\{[\text{Ru}(\text{tpypy})_2\text{Ag}(\text{NO}_3)(\text{MeCN})](\text{NO}_3)_2(\text{H}_2\text{O})(\text{MeCN})\}_\infty$, was obtained (**Fig. 27**).⁴⁷

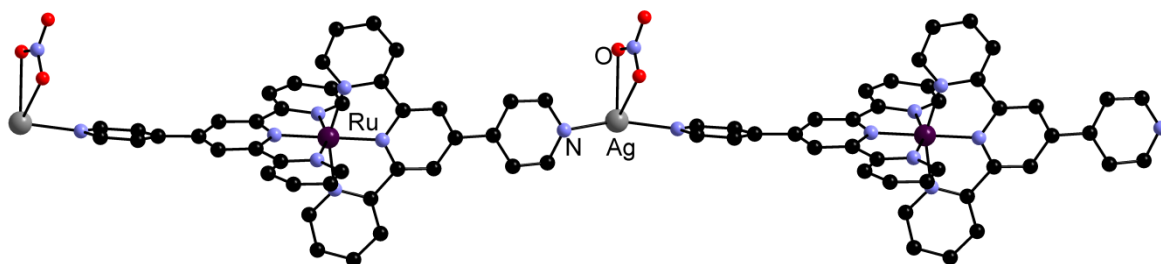


Fig. 27: Structure of the heterobimetallic network $\{[\text{Ru}(\text{tpypy})_2\text{Ag}(\text{NO}_3)(\text{MeCN})](\text{NO}_3)_2(\text{H}_2\text{O})(\text{MeCN})\}_\infty$.⁴⁶

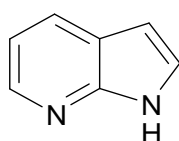
ⁱ L = μ_2 -4,5-diazafluoren-9-ylidene-methanedithiolato-N,N',S,S'

ⁱⁱ Cyclen = 1,4,7,10-tetraazacyclododecane

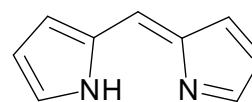
ⁱⁱⁱ Pytyp = 4'-(4-pyridyl)-2,2':6', 2''-terpyridine

I.6. Aim of the work

The aim of this work is the preparation of homo- and heterometallic architectures. Functionalized 7-azaindole and/or dipyririn (DPM) derivatives (**Scheme 12**), acting as coordination poles, were chosen as the key organic bridging ligands. Both moieties are nitrogen based heterocycles. The 7-azaindole fragment is a fused heterocyclic system consisting of a pyridine and a pyrrole moieties offering two nitrogen atoms forming a 1,3 N-C-N sequence and convergently oriented. In the case of DPM, a higher degree of freedom is present between the two nitrogen atoms which can point in the same direction as for 7-azaindole, or at any direction owing to the non-rigid connection between the two pyrrolic rings. These differences lead to different coordination chemistry for these two species.



7-azaindole



Dipyririn (DPM)

Scheme 12: 7-azaindole and dipyririn molecule.

In the first chapter of this work, we will illustrate the coordination chemistry of the ligands appended by a 7-azaindole moiety acting as a primary coordination pole and other groups as secondary poles (**Fig. 28**). The second chapter will be focusing on the elaboration of homo- and hetero-metallic architectures based on the ligands with a dipyririn as a primary coordination pole and finally, in the third chapter, the coordination chemistry of the ligand appended with both 7-azaindole and DPM coordination poles will be discussed.

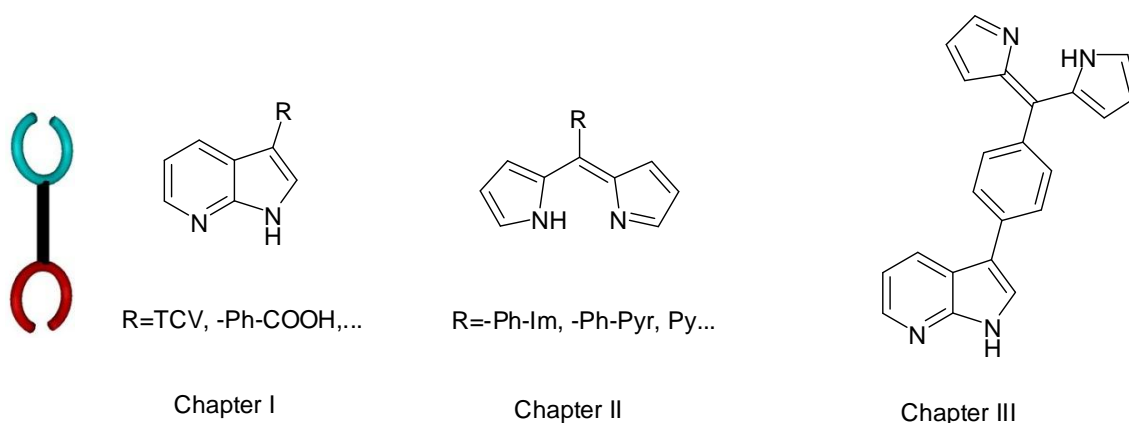


Fig. 28: Families of ligands used in this work.

I.7. References

- ¹ (a) Lehn, J. M., *Pure Appl. Chem.* **1978**, *50*, 871; (b) Lehn, J. M., *Supramolecular Chemistry: Concepts and Perspectives*, Wiley-VCH, **1995**; (c) Lehn, J. M., *Angew. Chem. Int. Ed. Engl.* **1988**, *27*, 89; (d) Lehn, J. M., *Angew. Chem. Int. Ed. Engl.* **1990**, *29*, 1304.
- ² Mann, S., *Nature* **1993**, *365*, 499.
- ³ Hosseini, M. W., *Acc. Chem. Res.* **2005**, *38*, 313.
- ⁴ Kuhn, E., Bulach, V., Hosseini, M. W., *Chem. Commun.* **2008**, 5104.
- ⁵ (a) Lightfoot, M. P., Mair, F. S., Pritchard, R. G., Warren, J. W., *Chem. Commun.* **1999**, 1945; (b) Ning, G. L., Wu, L. P., Sugimoto, K., Munakata, M., Kuroda-Sowa, T. Maekawa, M., *J. Chem. Soc., Dalton Trans.* **1999**, 2529; (c) Brown, S. P., Schnell, I., Brand, J. D., Müllen, K., Spiess, H. W., *J. Am. Chem. Soc.* **1999**, *121*, 6712; (d) Lämsä, M., Huuskonen, J., Rissanen, K., Pursiainen, J., *Chem. Eur. -J.* **1998**, *4*, 84; (e) Dance, I., Scudder, M., *Chem. Eur. -J.* **1996**, *2*, 481; (f) Hunter, C. A., *Chem. Soc. Rev.* **1994**, *23*, 101; (g) Hunter, C. A., *Angew. Chem. Int. Ed. Engl.* **1993**, *32*, 1653; (h) Guckian, K. M., Schweitzer, B. A., Ren, R. X. F., Sheils, C. J., Tahmassebi, D. C., Kool, E. T., *J. Am. Chem. Soc.* **2000**, *122*, 2213.
- ⁶ Hunter, C. A., Sanders, J. K. M., *J. Am. Chem. Soc.* **1990**, *112*, 5525.
- ⁷ Janiak, C., *J. Chem. Soc., Dalton Trans.* **2000**, 3885.
- ⁸ (a) Adams, H., Carrer, F. J., Hunter, C. A., Morales, J. S., Seward, E. M., *Angew. Chem. Int. Ed. Engl.* **1996**, *35*, 1542; (b) Grover, J. R., Walters, E. A., Hui, E. T., *J. Phys. Chem.* **1987**, *91*, 3233.
- ⁹ Pyykko, P., *Chem. Rev.* **1997**, *97*, 597.
- ¹⁰ (a) Orgel, L. E., *J. Chem. Soc.* **1958**, 4186; (b) Rogers, D. B., Shannon, R. D., Prewitt, C. T., Gillson, J. L., *Inorg. Chem.* **1971**, *10*, 723; (c) Kleppmann, N., G., Bilz, H., *Commun. Phys.* **1976**, 105; (d) Mehrotra, P. K., Hoffmann, R., *Inorg. Chem.* **1978**, *17*, 2187; (e) Jiang, Y., Alvarez, R., Hoffmann, R., *Inorg. Chem.* **1985**, *24*, 749; (f) Jansen, M., *Angew. Chem. Int. Ed. Engl.* **1987**, *26*, 1098.
- ¹¹ Harvey, P. D., *Coord. Chem. Rev.* **1996**, *153*, 175.
- ¹² Khlobystov, A. N., Blake A. J., Champness, N. R., Lemenovskii, D. A., Majouga, A. G., Zyk, N. V., Schröder, M., *Coord. Chem. Rev.* **2001**, *222*, 155.
- ¹³ Shelly, K., Finster, D. C., Lee, Y. J., Scheidt, W. R., Reed, C. A., *J. Am. Chem.* **1985**, *107*, 1985.
- ¹⁴ Kochi, K., Lindeman, S. V., Rathore, R., *Inorg. Chem.* **2000**, *39*, 5707.
- ¹⁵ Mascal, M., Kerdelhue, J. L., Blake, A. J., Cooke, P. A., Mortimer, R. J., Teat, S. J., *Eur. J. Inorg. Chem.* **2000**, 485.
- ¹⁶ Pauling, L., *The Nature of the Chemical Bond 3rd ed.*, Cornell University Press, New York, **1960**.
- ¹⁷ Etter, M. C., *Acc. Chem. Res.* **1990**, *23*, 120.
- ¹⁸ (a) Hosseini, M. W., *CrystEngComm.* **2004**, *6*, 318; (b) Fowler, F. W., Lauher, J. W., *J. Am. Chem. Soc.* **1993**, *115*, 5991.
- ¹⁹ Blake, A. J., Baum, G., Champness, N. R., Chung, S. S. M., Cooke, P. A., Fenske, D., Khlobystov, A. N., Lemenovskii, D. A., Li, W. S., Schröder, M., *J. Chem. Soc. Dalton Trans.* **2000**, 4285.
- ²⁰ Richardson, C., Steel, P. J., *Inorg. Chem. Commun.* **1998**, *1*, 260.
- ²¹ (a) Blake, A. J., Champness, N. R., Khlobystov, A. N., Lemenovskii, D. A., Li, W. S., Schröder, M., *Chem. Commun.* **1997**, 1339; (b) Vranka, R. G., Amma, E. L., *Inorg. Chem.* **1966**, *5*, 1020; (c) Blake, A. J., Champness, N. R., Crew, M., Parsons, S., *New J. Chem.* **1999**, *23*, 13; (d.) Venkataraman, D., Lee, S., Moore, J. S., Zhang, P., Hirsch, K. A., Gardner, G. B., Covey, A. C., Prentice, C. L., *J. Chem. Mater.* **1996**, *8*, 2030.
- ²² Biradha, K., Fujita, M., *J. Chem. Soc., Dalton Trans.* **2000**, 3805.
- ²³ Ko, J. W., Min, K. S., Suh, M. P., *Inorg. Chem.* **2002**, *41*, 2151.
- ²⁴ Lin, M. J., Jouaiti, A., Kyritsakas, N., Hosseini, M. W., *CrystEngComm.* **2008**, *11*, 189.
- ²⁵ Wells, A. F., *Three-dimensional Nets and Polyhedra*, Wiley-Interscience, New York, **1977**.
- ²⁶ Batten, S. R., Robson, R., *Angew. Chem. Int. Ed.* **1998**, *37*, 1460.
- ²⁷ Steed, J. W., Atwood, J.L., *Supramolecular Chemistry, Second edition*, Wiley. **2009**.
- ²⁸ Bailar, J. C., *Prep. Inorg. React.* **1964**, *1*.
- ²⁹ Robin, A. Y., Fromm, K. M., *Coord.Chem.Rev.* **2006**, *250*, 2127.
- ³⁰ Hoskins, B. F., Robson, R., *J. Am. Chem. Soc.* **1990**, *112*, 1221.

- ³¹ Yaghi, O. M., Li, G., Li, H., *Nature* **1995**, *378*, 703.
- ³² Venkataraman, D., Gardner, G. B., Lee, S., Moore, J. S., *J. Am. Chem. Soc.* **1995**, *117*, 11601.
- ³³ Rowsell, J. L. C., Yaghi, O. M., *Micropor. Mesopor. Mater.* **2004**, *73*, 3.
- ³⁴ Yaghi, O. M., Eddaoudi, M., O'Keeffe, M., Li, H., *Nature* **1999**, *402*, 276.
- ³⁵ Corma, A., *Chem. Rev.* **1997**, *97*, 2373.
- ³⁶ (a) Batten, S. R., Robson, R., *Angew. Chem.* **1998**, *110*, 1558; (b) Batten, S. R., Robson, R., *Angew. Chem.Int. Ed.* **1998**, *37*, 1460; (c) Batten, S. R., *CrystEngComm.* **2001**, *3*, 67; (d) Carlucci, L., Ciani, G., Proserpio, D. M., *CrystEngComm.* **2003**, *5*, 269; (e) Blatov, V. A., Carlucci, L., Proserpio, D. M., *CrystEngComm.* **2004**, *6*, 377; (f) Carlucci, L., Ciani, G., Proserpio, D. M., *Coord. Chem. Rev.* **2003**, *246*, 247; (g) Carlucci, L., Ciani, G., Proserpio, D. M., Rizzato, S., *Chem. Eur. -J.* **2002**, *8*, 1520.
- ³⁷ (a) Lochan, R. C., Head-Gordon, M., *Phys. Chem. Chem. Phys.* **2006**, *8*, 1357; (b) Düren, T., Snurr, R. Q., *J. Phys. Chem. B.* **2004**, *108*, 15703; (c) Han, S. S., Furukawa, H., Yaghi, O. M., Goddard, I. W. A., *J. Am. Chem. Soc.* **2008**, *130*, 11580.
- ³⁸ Murray, L. J., Dincă, M., Long, J. R., *Chem. Soc. Rev.* **2009**, *38*, 1294.
- ³⁹ Lochan, R. C., Khaliullin, R. Z., Head-Gordon, M., *Inorg. Chem.* **2008**, *47*, 4032.
- ⁴⁰ Wong-Foy, A. G., Matzger, A. J., Yaghi, O. M., *J. Am. Chem. Soc.* **2006**, *128*, 3494.
- ⁴¹ Yan, Y., Lin, X., Yang, S., Blake, A. J., Dailly, A., Champness, N. R., Hubberstey, P., Schröder, M., *Chem. Commun.* **2009**, 1025.
- ⁴² Kitaura, R., Noro, S., Kitagawa, S., *Angew. Chem. Int. Ed.* **2004**, *43*, 2334.
- ⁴³ Choi H. J., Suh, M. O., *Inorg. Chem.* **1999**, *38*, 6309.
- ⁴⁴ Baudron, S. A., *Ideas in Chemistry and Molecular sciences; Advances in Synthetic Chemistry*, **2010**, pp263-282, Wiley VCH, Weinheim, B. Pignataro (ed.).
- ⁴⁵ Baudron, S. A., Hosseini, M. W., Kyritsakas, N., Kurmoo, M., *Dalton Trans.* **2007**, 1129.
- ⁴⁶ Constable, E. C., Cargill Thompson, A. M. W., *J. Chem. Soc., Dalton Trans.* **1994**, **1409**.
- ⁴⁷ Beeves, J. E., Constable, E. C., Housecroft, C. E., Kepert, C. J., Price, D. J., *CrystEngComm.* **2007**, *9*, 456.

II. Chapter 1

II.1. Introduction

II.1.1. Generalities regarding 7-Azaindole

7-azaindole (1H-pyrrolo[2,3-b]pyridine) is a nitrogen based heterocyclic compound consisting in a pyridine fused with a pyrrolic 5-membered ring (**Fig. 29**). Substitution of the C-7 position of indole by a sp^2 -hybridized nitrogen atom provides a skeleton containing two different nitrogen atoms. A theoretical study on 7-azaindole showed that the nitrogen atom of the pyridine ring behaves as a π and σ acceptor whereas the one of the pyrrolic ring acts as a π donor and σ acceptor¹. The lower negative charge density is located on the pyrrolic nitrogen atom. The two N based centers may behave as a hydrogen-bond donor and acceptor set in a rigid three-atom arrangement². Regarding carbon atoms, the highest electron density³ is observed at the 3-position (**Fig. 29**). Although, commonly 7-azaindole and other pyrrolopyridines derivatives are compared to indole, however the presence of the additional nitrogen atom in 7-azaindole brings a series of differences in chemical and physical properties. For example, 7-azaindole is a stronger base (pK_a of 4.59 in H_2O at 20 °C) than indole ($pK_a < 1$ in H_2O at 20 °C).⁴

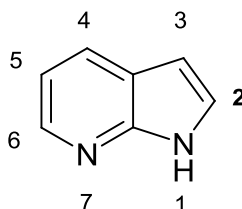


Fig. 29: 7-azaindole.

The optical properties of 7-azaindole derivatives have been investigated by fluorescence spectroscopy. At room temperature, the proton transfer process leading to tautomers of 7-azaindole is very fast and no dimeric form emission can be observed. At lower temperature, the emission from the dimer is observed⁵. The energy barrier associated with the tautomerism has been determined in different solvent (*i.e.* $E_{ACT} = 4.8$ kcal/mole in ethanol)⁶.

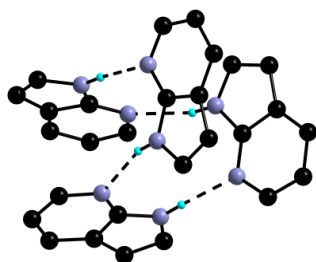


Fig. 30: Structure of 7-azaindole.

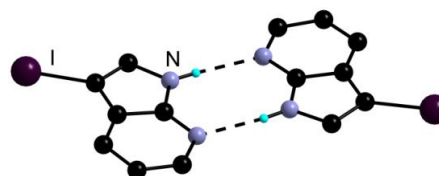


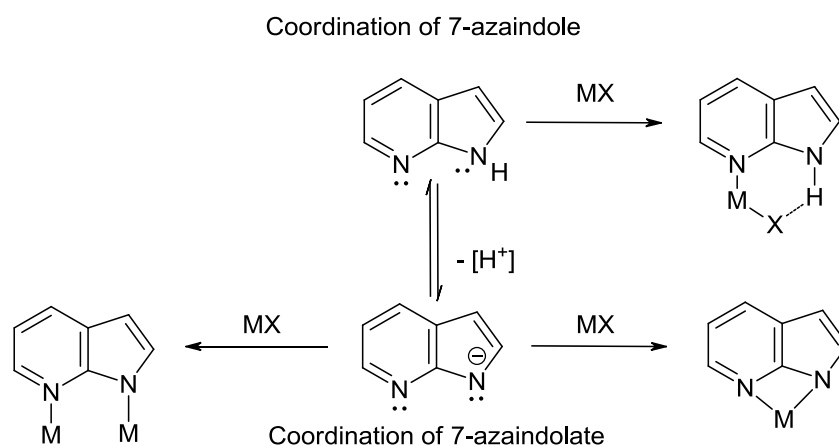
Fig. 31: Structure of 3-iodo-7-azaindole.

The self-complementary 7-azaindole unit might, as for carboxylic acid derivatives, display two modes of H-bonding, mainly the dimeric and the catemer motifs. Crystals of 7-azaindole were obtained by slow evaporation of a benzene solution and the crystal structure has been solved by X-ray diffraction on single-crystal (**Fig. 30**). The structural study revealed that in the solid state, molecules are arranged into tetrameric units, which may be regarded as a finite catemer, via four complementary N-H...N interactions. These tetramers interact by van der Waals forces⁷. In marked contrast, the structural investigation on 3-iodo-7-azaindole revealed the presence of two crystallographically independent molecules, forming a dimer $R_2^2(8)$ via dual N-H...N hydrogen bonds (**Fig. 31**). The latter arrangement is observed for all reported structures of functionalized derivatives at the 3 position as well as for compounds prepared and studied in the course of our investigations. In both cases of organization mentioned above (dimeric and catemeric modes of interaction), the hydrogen bonded interaction between 7-azaindoles is rather strong ($d(N-H...N) = 2.90$ Å, $\alpha(N-H...N) = 168.1^\circ$ for the iodo derivative).

In solution at room temperature, the unfunctionalized 7-azaindole shows no emission in the visible. However, at 77 K, it phosphoresces at 480 nm. In the solid state⁸, the emission band is very weak at 350 nm. In contrast, the 3-iodo derivative forming dimers in the crystalline state exhibits a unique, large Stokes-shifted fluorescence band centered at 500 nm throughout 298 - 10 K temperature range⁹; in addition, it phosphoresces at *ca* 600 nm at room-temperature. Upon deprotonation, a bright blue emission is observed both in solution and in the solid state. However, unfortunately, the 7-azaindolate anion is air and moisture sensitive. A possible way to stabilize the anionic form may be its coordination to a metal centre. Several such metal complexes incorporating either 7-azaindolate have been reported. A brief overview of the coordination chemistry of these derivatives is given in the following.

II.1.2. Coordination chemistry of 7-azaindole

Both 7-azaindole and its conjugate base can be employed as ligands (**Scheme 13**). In the case of the former, coordination takes place at the pyridyl ring with conservation of the pyrrolic proton. In turn, this hydrogen atom can be involved in hydrogen bonding with coordinated anions or solvent molecules.



Scheme 13: Coordination chemistry of 7-azaindole and its conjugate base.

In the case of 7-azaindolate, both nitrogen atoms are potentially coordinating. Owing to the 1,3 arrangement of these atoms, the anion might either behave as a bridging or a chelating ligand, although the first mode is expected to be favored. Indeed, the vast majority of reported complexes features a bridging mode of coordination (see below). Only one example of a metal complex where 7-azaindolate acts as a chelate has been described. In the ytterbium (II) complex, $[\text{Yb}(\text{aza})_2(\text{DME})_2]$ ¹⁰, two nitrogen atoms of 7-azaindolate bind in a nearly symmetrical fashion to the metal centre with the ytterbium ion lying in the ligand plane (**Fig. 32**).

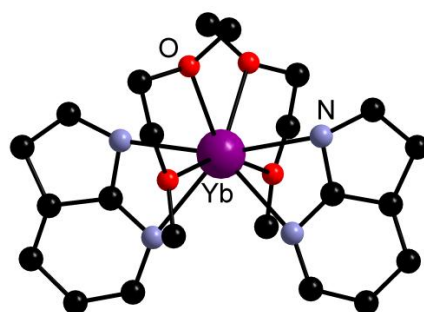
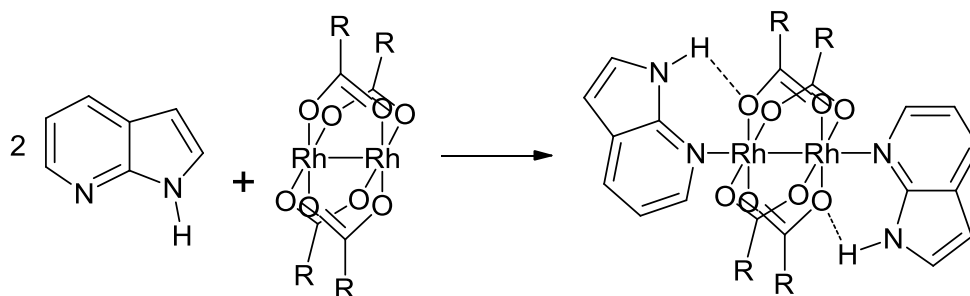


Fig. 32: Structure of $[\text{Yb}(\text{aza})_2(\text{DME})_2]$.

II.1.2.1. Metal complexes incorporating 7-azaindole

As stated above, assistance to coordination by a hydrogen bond through the pyrrolic NH acting as a donor is expected for 7-azaindole. This is actually observed in the majority of metal complexes. A brief overview of such complexes is given below with an emphasis on compounds relevant to our investigation. In particular, coordination of 7-azaindole to rhodium (II) carboxylate complexes, such as acetate ($[\text{Rh}_2(\text{OAc})_4]^{11}$) and propionate ($[\text{Rh}_2(\text{C}_2\text{H}_5\text{COO})_4]^{12}$), is worth being mentioned. These complexes exhibit a “paddlewheel” type structure leaving the axial position on each rhodium ion available for further ligation (**Scheme 14**).



Scheme 14: Rhodium (II) acetate as a bridging unit.

The crystal structure of $[\text{Rh}_2(\text{C}_2\text{H}_5\text{COO})_4(\text{H-aza})_2]$ has been reported. The molecular units, shown in **Fig. 33a**, consist of the dirhodium(II) tetrapropionate paddlewheel core with a Rh-Rh distance of 2.403(1) Å and two axially bound 7-azaindole molecules with Rh-N distances of 2.284(6) Å and 2.266(6) Å. Each 7-azaindole molecule coordinates through the pyridine nitrogen atom. The two 7-azaindole molecules do not lie in the same plane but form an angle of 68.4°. ¹²

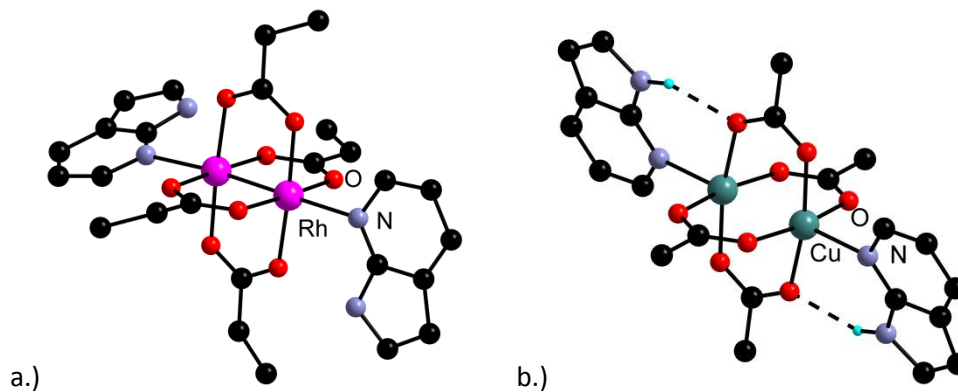


Fig. 33: Structures of $[\text{Rh}_2(\text{C}_2\text{H}_5\text{COO})_4(\text{H-aza})_2]$ (a) and $[\text{Cu}_2(\text{OAc})_4(\text{H-aza})_2]$ (b).

Interestingly, in the crystal structure of the copper analogue, $[\text{Cu}_2(\text{OAc})_4(\text{H-aza})_2]$ (**Fig. 33b**), the two coordinated 7-azaindole molecules lie in the same plane. ¹³ In both cases, intramolecular H-bond interactions between pyrrolic NH of the 7-azaindole fragment and the acetate oxygen atoms with N-H...O distances of 2.721 and 2.822 Å are observed.

Complexes with various metal halides have also been reported. We will mention here complexes with ZnCl_2^{14} and Cu(II) halides. The general feature in these compounds is the coordination of the pyridyl nitrogen atom to the metal center and hydrogen bonding interaction between the pyrrolic NH and the halides.

The structure of the complex with zinc (II) chloride consists of $[\text{ZnCl}_2(\text{H-aza})_2]$ units (**Fig. 34**) with a tetrahedral Zn_2Cl_2 core ($d_{\text{Zn-N}} = 2.063(2)$ - $2.035(3)$ Å). Weak intra-molecular hydrogen bonds between the Cl^- anions and the 7-azaindole pyrrolic hydrogen atoms are observed with N-Cl distances of 3.268(2) Å and 3.285(3) Å.

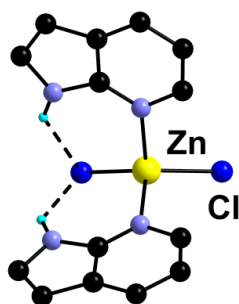


Fig. 34: Structure of $[Zn(H-aza)_2Cl_2]$.

Upon reaction of 7-azaindole with Cu(II) salts, depending on the reaction conditions and the anion, a variety of complexes have been obtained. For example, compounds with two or four 7-azaindole molecules coordinated to the copper center, $[Cu-\mu-Cl_2(H-aza)_2]_n$ and $[Cu(Haza)_4F](BF_4)^{17,15}$, or combining two units with different formulae (1+4 and 1+2) as in $[Cu_2Cl_4(H-aza)_6]^{15,17}$ have been described.

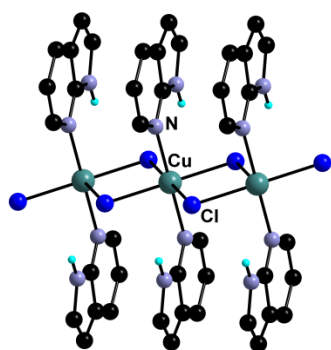


Fig. 35: Structure of $[Cu-\mu-Cl_2(H-aza)_2]_n$.

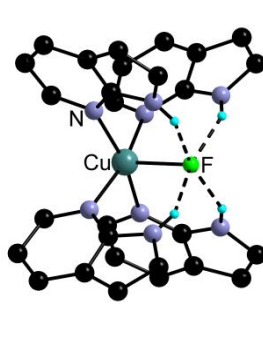


Fig. 36: Structure of $[Cu(H-aza)_4F](BF_4)$.

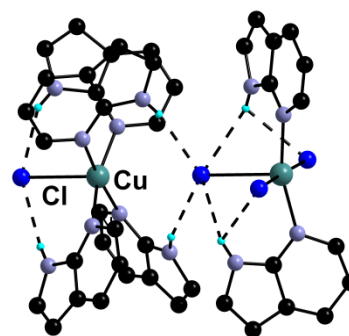


Fig. 37: Structure of $[CuCl(H-aza)_4][CuCl_3(H-aza)]$.

In $[Cu-\mu-Cl_2(H-aza)_2]_n^{16}$, the copper center is in an octahedral environment with four bridging chloride anions in the plane and two 7-azaindole molecules. These units organize into 1-D chains (**Fig. 35**). The bond distance between copper and chloride of the neighboring unit is 3.143(2) Å.

Complex $[Cu(H-aza)_4F](BF_4)$ was obtained by reaction of 7-azaindole with $Cu(BF_4)_2$. The copper(II) cation is in a square-pyramidal environment and coordinated to four nitrogen atoms of four ligands and one fluoride anion, generated by decomposition of the BF_4^- anion, at the apical position (**Fig. 36**). As in $[Rh_2(C_2H_5COO)_4(aza)_2]$, an intra molecular H-bond is observed; in this case between the hydrogen atom of the uncoordinated pyrrolic nitrogen and the F^- ion with an N—F distance of 2.692(1) Å. To our knowledge, no analogue with another halide anion has been reported. However, a similar unit is combined with $[CuCl_2(H-aza)_2]$ to form $[CuCl(H-aza)_4][CuCl_3(H-aza)]$. This comprises two different Cu(II) sites (**Fig. 37**): $[Cu(Haza)_2Cl_3]^+$ and $[Cu(Haza)_3Cl]^-$ units. In both moieties, the Cu(II) ions have a square-pyramidal geometry with axial position of copper occupied by a chloride atoms at distances of 2.888(2) and 2.720(3) Å. The basal plane in the first unit, $[Cu(Haza)_2Cl_3]^+$ consists of two nitrogen atoms of two ligands and three chloride ions. Regarding the Cu(II) ion in the second unit $[Cu(Haza)_4Cl]^-$, the basal plane consists of four nitrogen atoms of four ligands.

Intramolecular H-bond interactions are present in both units between pyrrolic hydrogen atoms and the Cl^- ions with N—Cl distances 3.133(7) and 3.362(7) Å and an intermolecular H-bond is observed between the hydrogen of a non-coordinating nitrogen atom and a neighboring Cl^- atom with a N—Cl distance of 3.198(5) Å. Cu—N bond distances range from 2.03 to 2.07 Å.

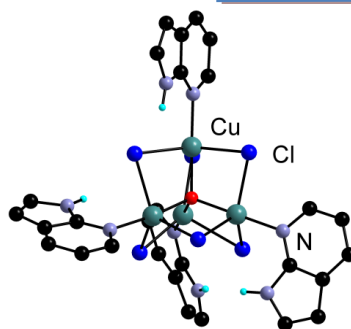
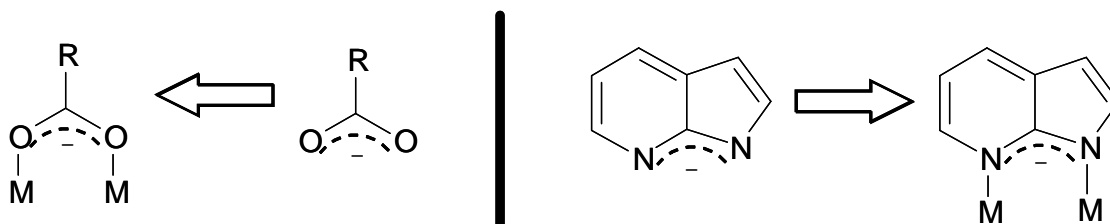


Fig. 38: Structure of $[\text{Cu}_4\text{OCl}_6(\text{Haza})_4]$.

Finally, the rather unusual tetranuclear complex $[\text{Cu}_4\text{OCl}_6(\text{Haza})_4]$ ¹⁷ has been also described (Fig. 38). The complex contains the Cu_4OCl_6 core with a μ_4 -oxygen atom tetrahedrally surrounded by four copper atoms. In turn, all copper atoms are bridged by chlorine atoms and four 7-azaindole moieties are bonded to the copper centers *via* the pyridine nitrogen atoms. The pyrrolic NHs are involved in intramolecular hydrogen bonding interactions with the chlorides of the core.

II.1.2.2. Metal complexes incorporating 7-azaindolate ligands

The 7-azaindolate anion is a ligand similar to carboxylates (Scheme 15) and can be expected to act as a versatile binucleating ligand for a number of transition metals. Indeed, dimeric complexes of the type $\text{M}_2(\text{aza})_4$ ($\text{M} = \text{Cu}(\text{II}), \text{Ni}(\text{II})$)^{18,19} have been reported as well as complexes with a tetrahedral core of the $\text{M}_4\text{O}(\text{aza})_6$ type ($\text{M} = \text{Zn}(\text{II}), \text{Co}(\text{II})$)^{20, 21}.



Scheme 15: Comparison of 7-azaindolate and carboxylate.

The dimeric “paddlewheel” type structure of $[\text{Cu}_2(\text{aza})_4(\text{DMF})_2]$ (Fig. 40), which is similar to that of carboxylates, (for example $[\text{Cu}_2(\text{OAc})_4(\text{H}_2\text{O})_2]$, Fig. 39), contains four 7-azaindolate bridging two $\text{Cu}(\text{II})$ ions and two coordinated DMF molecules, with a Cu-N bond length of 2.003(4) Å and a Cu-Cu distance of 2.782(4) Å. This latter distance is longer than in the copper acetate case (2.64 Å).²¹

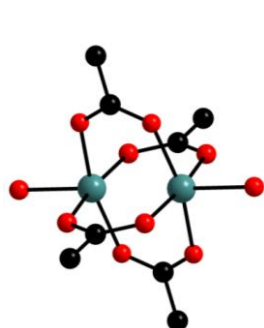


Fig. 39: Structure of $[\text{Cu}_2(\text{OAc})_4(\text{H}_2\text{O})_2]$.²²

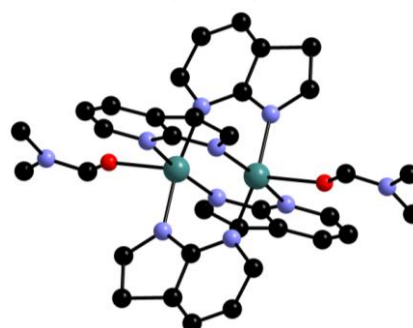


Fig. 40: Structure of $[\text{Cu}_2(\text{aza})_4(\text{DMF})_2]$.

Analysis of the temperature-dependent magnetic susceptibility data on $[\text{Cu}_2(\text{aza})_4(\text{DMSO})_2] \cdot 2\text{-DMSO}$ indicated a strong antiferromagnetic coupling between the copper atoms ($J = -389 \text{ cm}^{-1}$, $g = 2.11$).¹⁸ This value of the J coupling is similar to what has been determined for copper(II) acetate ($J = -296 \text{ cm}^{-1}$, $g = 2.09$).²³

Depending on the reaction conditions, only a partial substitution (**Fig. 41**) of the acetate in the “paddlewheel” unit is possible such as in $[\text{Cu}_2(\text{CH}_3\text{COO})_2(\text{aza})_2(\text{H-aza})_2]$, with two bridging coplanar 7-azaindolates and two acetate ligands.²⁴ The axial positions of the copper ions are occupied by the pyridyl nitrogen atom of two non-deprotonated 7-azaindole molecules, in an arrangement similar to the one observed in $[\text{Cu}_2(\text{CH}_3\text{COO})_4(\text{H-aza})_2]$ (**Fig. 33b**). It is interesting to note that this compound features both 7-azaindole and 7-azaindolate as ligands.

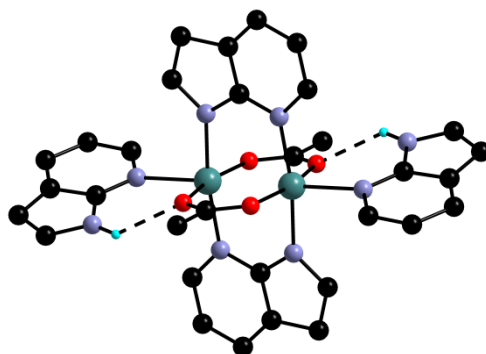


Fig. 41: Structure of $[\text{Cu}_2(\text{CH}_3\text{COO})_2(\text{aza})_2(\text{H-aza})_2]$.

Reaction of Zn(II) with 7-azaindole in methanol, in the presence of triethylamine, gave a tetrameric complex $[\text{Zn}_4\text{O}(\text{aza})_6]$ (**Fig. 43**). The Zn···Zn and Zn–O distances range from 3.147(2) to 3.209(2) and 1.903(8)–1.975(8) Å respectively. The structure of the core in this complex is identical to the one observed with carboxylates, such as $[\text{Zn}_4\text{O}(\text{CH}_3\text{COO})_6]$ ²⁵ and $[\text{Zn}_4\text{O}(\text{BDC})_3]$ (MOF-5)²⁶ (**Fig. 42**).



Fig. 42: Structure of the tetrahedral core in $[\text{Zn}_4\text{O}(\text{BDC})_3]$ (MOF-5).

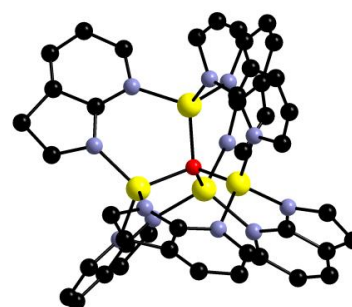


Fig. 43: Structure of $[\text{Zn}_4\text{O}(\text{aza})_6]$.

The zinc complex is especially interesting for its blue luminescence. At room temperature, the cluster displays intense photoluminescence at 448 nm in the solid state and at 425 nm in acetonitrile. The lifetime and quantum yield of the emission are 0.1 μs and 0.17 respectively. This complex has an electronic excited-state lifetime 10 times longer than that for zinc (II) acetate.

7-azaindolate complexes of aluminium and boron were investigated by Wang²⁷ and illustrate both modes of coordination. Regarding the aluminium complexes, depending on the reaction conditions, mono-, di-, tri- or tetra-nuclear complexes have been synthesized. Reaction of 7-azaindole with an excess of $\text{Al}(\text{CH}_3)_3$ led to the isolation of two mononuclear complexes²⁸ $[\text{Al}(\text{aza})_2(\text{H-aza})\text{CH}_3]$ (**Fig. 44**) and $[\text{Al}(\text{aza})_3(\text{H-aza})]$. The 7-azaindole in these two complexes acts as a terminal ligand and is bonded to the aluminium by the indole nitrogen atom in the solid state. There is an intermolecular hydrogen bond between the 7-azaindole and 7-azaindolate ligands in this case. The 7-azaindole fragment presented in the structure is in a tautomeric form as the hydrogen atom is bonded to the pyridyl nitrogen centre.

Dinuclear complexes $[Al_2(aza)_2(CH_3)_4]$ and $[Al_2(aza)_4(CH_3)_2]$ (**Fig. 45**) were prepared upon reaction with $Al(CH_3)_3$ in a 1:1 and 1:2 ratio.²⁹ The 7-azaindole in these two complexes acts as a bridging ligand. Both compounds are bright blue emitters in solution and in the solid state with $\lambda_{max} = 430$ and 442 nm, respectively.

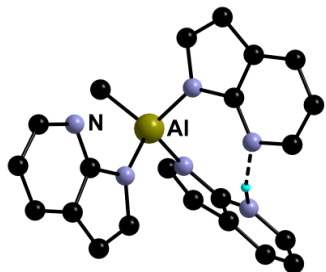


Fig. 44: Structures of mononuclear aluminium complex $[Al(aza)_2(H-aza)CH_3]$.

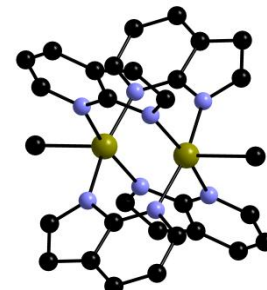
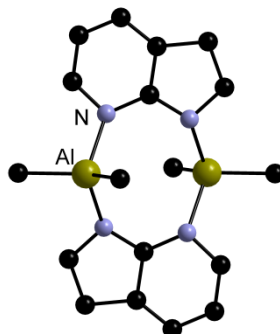


Fig. 45: Structures of dinuclear aluminium complexes $[Al_2(aza)_2(CH_3)_4]$ (left) and $[Al_2(aza)_4(CH_3)_2]$ (right).

In both cases, mono- and dinuclear complexes are rather unstable and air-sensitive. The remarkably stable trinuclear compound $[Al_3(\mu_3-O)(CH_3)(7-aza)_4(OCH(CF_3)_2)_2]$ and a tetranuclear compound $[Al_4(\mu_3-O)_2(7-aza)_6(OCH(CF_3)_2)_2]$ with oxo ligands have been obtained (**Fig. 46**). In the first case one oxo ligand is bonded to three Al(III) ions while in the case of the tetranuclear compound, there are two triply bridging oxo ligands. These compounds exhibit a bright blue emission similar to the one of the mono- and dinuclear species.

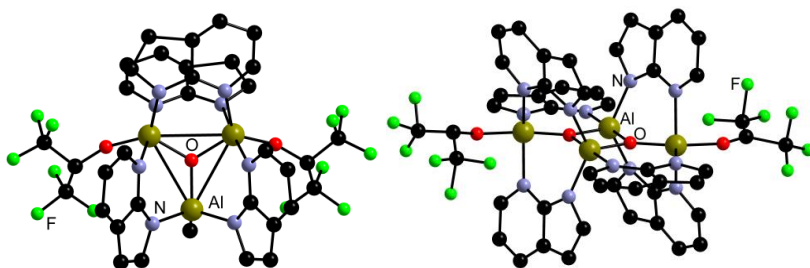


Fig. 46: Structures of tri- and tetranuclear aluminium complexes $[Al_3(\mu_3-O)(CH_3)(7-aza)_4(OCH(CF_3)_2)_2]$ and $[Al_4(\mu_3-O)_2(7-aza)_6(OCH(CF_3)_2)_2]$.

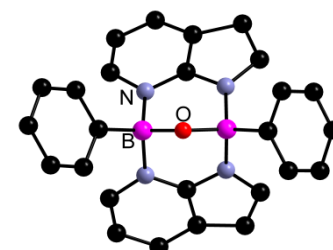


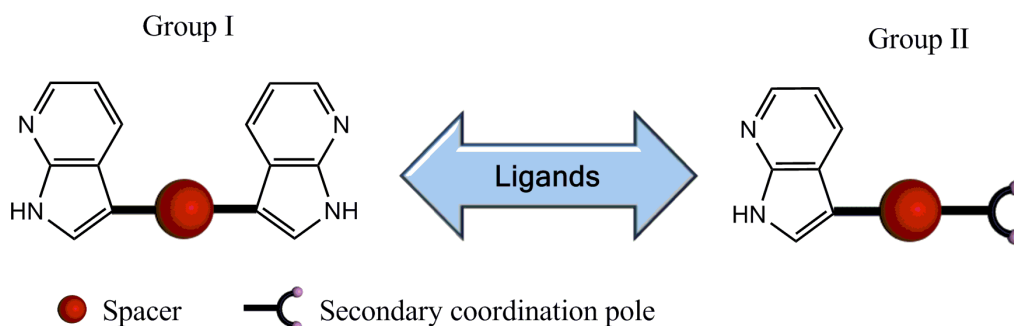
Fig. 47: Structures of $B_2(O)(7-aza)_2Ph_2$.

The instability of aluminum 7-aza complexes originates mostly from the ionic character of Al–C and Al–N bonds. On the other hand, B–C and B–N bonds are fairly covalent, hence much more stable than Al–C and Al–N bonds. Two dinuclear boron complexes $B_2(O)(7-aza)_2(C_2H_5)_2$ and $B_2(O)(7-aza)_2Ph_2$ (**Fig. 47**) with similar architecture were synthesized.^{30,31} They are emitters at 450 and 430 nm, respectively.³²

In light of these results, it appears that both 7-azaindole and 7-azaindolate derivatives can act as ligands forming diverse metal complexes with interesting physical properties such as luminescence. It is worth noting however that most of the reported complexes comprise unfunctionalized and commercially available 7-azaindole. This is surprising given the extensive body of research on functionalization of such derivatives, in particular at the so-called 3-position³³. Such molecules bearing an additional coordinating group could be promising ligands for the development of the construction strategy elaborated in the previous chapter.

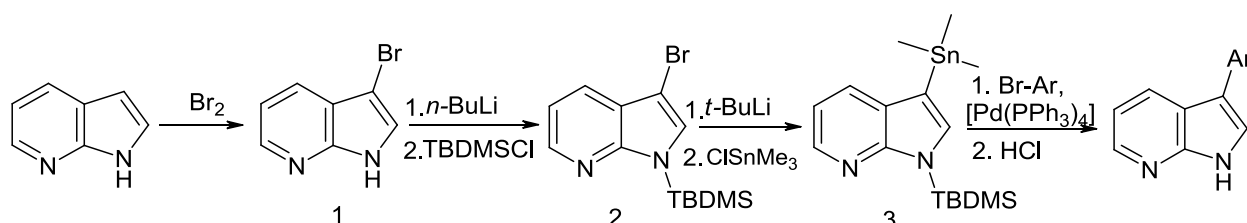
II.2. Ligands

Two families of ligands can be considered. The first one (Group I) consists of molecules incorporating several 7-azaindole moieties linked by either an aliphatic or an aromatic spacer (**Scheme 16 left**). The second series (Group II), comprises 7-azaindole derivatives functionalized at the 3 position by a secondary coordinating group (**Scheme 16 right**). The nature of the group attached at the 3 position determines the synthetic route followed.



Scheme 16: Two groups of ligands based on 7-azaindole.

The general procedure for the preparation of ligands (**Scheme 17**) with an aromatic functional group or spacer relies on the Pd-catalyzed Stille coupling of 1-protected-3-methylstannyl-7-azaindole with aryl and heteroaryl halides. This synthetic route for the functionalization of 7-azaindole by an aromatic group has been described in the literature.³⁴ Only few examples of alternative synthetic schemes based on Suzuki coupling with the corresponding boronic acids have been reported.³⁵



Scheme 17: General synthetic scheme for the preparation of derivatives with an aromatic functional group.

In the first step, commercial 7-azaindole is converted into 3-bromo-7-azaindole (**1**). The pyrrolic nitrogen atom is then protected by a -TBDMS (*tert-butyl(dimethyl)silyl*) group (**2**). Conversion to the 3-methylstannyl functionalized derivative (**3**) was performed upon deprotonation using *t*-BuLi and subsequent reaction with Cl-SnMe₃ in THF. The -TBDMS group was chosen as a protecting group owing to better reported results with respect to others groups such as -Boc, -MEM or -Ts in the Pd-catalyzed coupling reactions engaging 5-bromopyrimidine and 2-bromopyrimidine.^{34a} Ligands and intermediates were characterized by ¹H-NMR, ¹³C-NMR, IR and either elemental analysis or HRMS. Detailed reaction yields as well as characterization data are given in the experimental section.

This synthetic scheme (**Scheme 17**) was followed to prepare ligands based on two 7-azaindoles bridged by an aromatic spacer, namely phenyl (**4**) and fluorenyl (**5**). Unfortunately, probably owing to strong intermolecular interactions through hydrogen bonding, these derivatives are poorly soluble in common organic solvents, making their use as ligands for the formation of metal complexes rather difficult (**Table 2**).

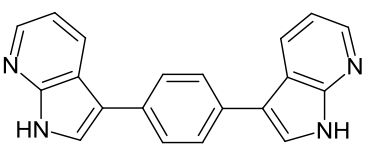
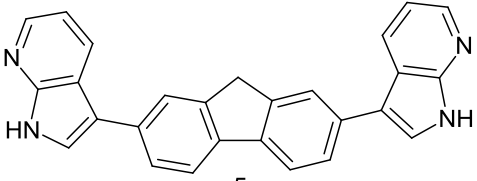
Ligands		
Yields:	28%	12%

Table 2: Ligands from the Group I with an aromatic spacer.

Four ligands (**6-9**) belonging to Group II appended by a pyrimidine^{34a}, benzonitrile or benzoic acid groups have been prepared. Unlike the symmetrical ligands, these derivatives (**Table 3**) are more soluble and most of them have been successfully used for the preparation of metal organic complexes and networks.

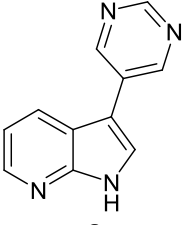
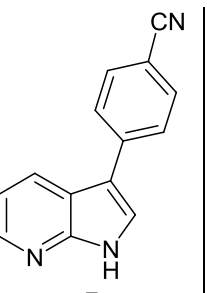
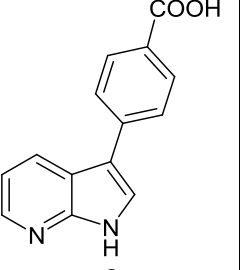
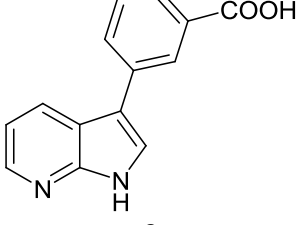
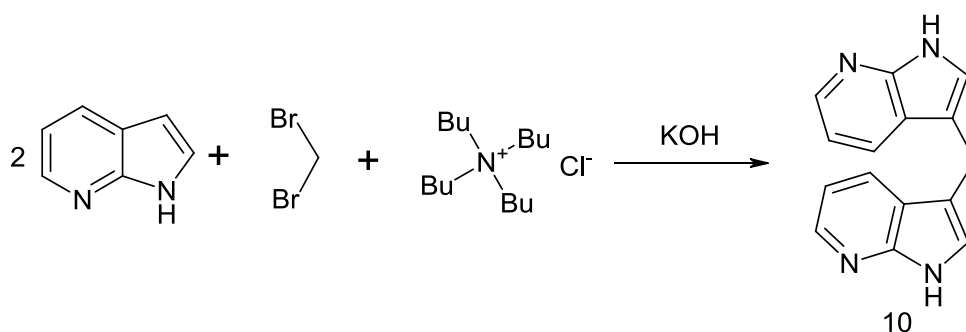
Ligands				
Yields:	51 % (74 % ^{34a})	17 %	29 %	48 %

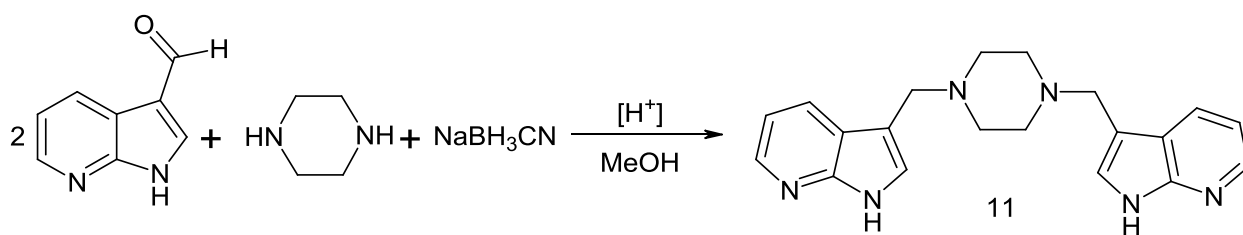
Table 3: Ligands from the Group II with an aromatic functional group appended.

Ligands with an aliphatic spacer were also prepared following different methods depending on the spacer itself. For example, in the case of ligand (**10**) based on a methylene spacer (**Scheme 18**), the compound was prepared, as described, by reaction of 7-azaindole with dibromomethane (17 %) under basic conditions in the presence of Bu₄NCl (**Scheme 18**).³⁶ The isolated compound is just one of the three possible alkylated isomers, the other two being alkylated derivatives at the pyridine or pyrrole nitrogen atoms.



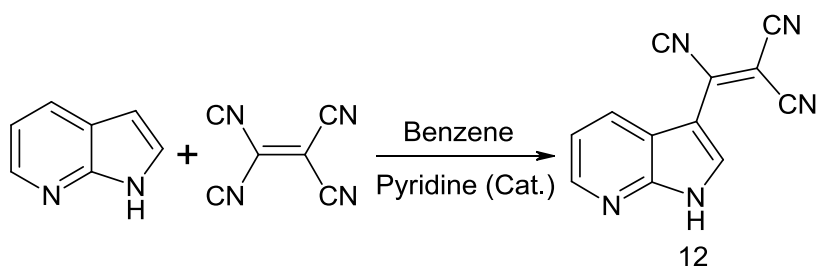
Scheme 18: Preparation of bis(7-azaindol-3-yl)methane (**10**).³⁶

The *N,N'*-bis((7-azaindol-3-yl)methyl)piperazine ligand (**11**) was prepared in 78 % yield (**Scheme 19**) by a reductive amination of the reaction product between 7-azaindole-3-carboxaldehyde and piperazine, in analogy with compounds described in the literature.³⁷



Scheme 19: Preparation of the *N,N'*-Bis((7-azaindol-3-yl)methyl)piperazine ligand **11**.

The 7-azaindole and indole exhibit similar reactivity. By analogy with the reported synthesis of the indole analogue³⁸, 3-tricyanovinylene-7-azaindole ligand (**12**) (Scheme 20) was prepared in good yield (93 %) upon reaction of 7-azaindole with TCNE in the presence of pyridine.



Scheme 20: Preparation of the 3-tricyanovinylene-7-azaindole ligand. **12**.

These compounds have been characterized by the classic analytical methods as well as by X-ray diffraction on single-crystal for two cases. Note that the crystal structure of ligand **10** has been reported.³⁶ Both 3-(4-benzonitrilyl)-7-azaindole (**7**) and 3-tricyanovinylene-7-azaindole (**12**) crystallized in the monoclinic space group $P2_1/c$ with one molecule in general position (Fig. 48).

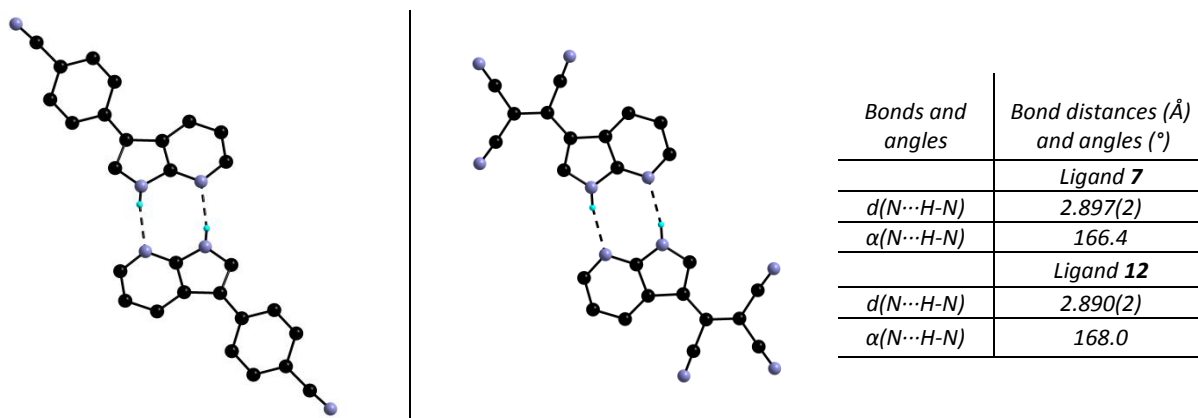


Fig. 48: Hydrogen-bonded dimers in the crystal structure of ligands **7** (right) and **12** (left). Table 4: Bond distances and angles

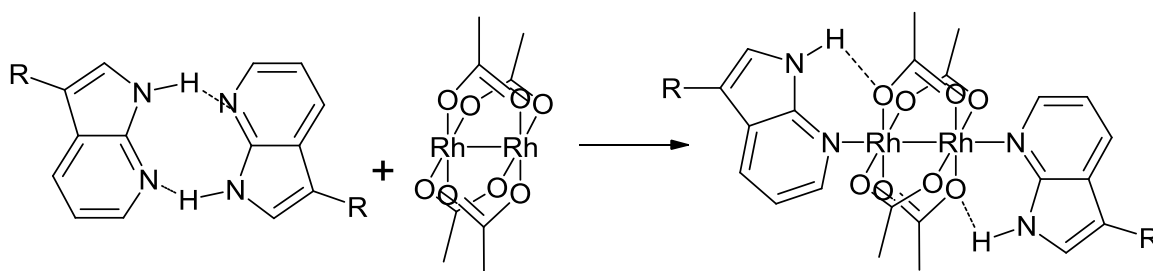
As reported in the literature, functionalized derivatives arrange in dimers^{9,36} unlike 7-azaindole which organizes in tetrameric units.⁷ A similar arrangement is observed here with molecules organized into hydrogen-bonded dimers *via* complementary N-H...N bonds (Table 4), as observed for 3-iodo-7-azaindole. In **12**, the tricyanovinylene and 7-azaindole moieties are coplanar (3.05 °), while in the case of **7**, the benzonitrile group and the bicyclic core form an angle of 24.52 °.

Having synthesized and characterized these ligands, we have then used them as ligands either as azaindole or its conjugate base for the formation of metal complexes and networks.

II.3. Complexes and networks

II.3.1. Rhodium complexes

As seen in **Fig. 31** and **Fig. 48**, functionalized derivatives organize into hydrogen-bonded dimers. Interestingly, the crystal structure of the $[\text{Rh}_2(\text{OAc})_4(7\text{-aza})_2]$ (**Fig. 33a**) shows a combination of coordination and hydrogen bonding and led us to see this compound as an expansion of the purely organic dimer by the paddlewheel binuclear complex. It therefore appeared appealing to prepare analogues with ligands of Group II as it should afford complexes with peripheral coordinating groups (**Scheme 21**). A series of four such complexes, obtained by reaction of two equivalents of ligands (**7-9**, **12**) with one equivalent of $[\text{Rh}_2(\text{OAc})_4]$ at room temperature, has been synthesized and characterized by X-ray single crystal diffraction, IR and either elemental analysis or HRMS.



Scheme 21: Preparation of complexes based on rhodium acetate.

Complexes $[\text{Rh}_2(\mathbf{7})_2(\text{OAc})_4](\text{DMF})_2$ (**13**) (**Fig. 49**) was obtained in crystalline form in 16.6 % yield while the tricyanovinylene analogue, $[\text{Rh}_2(\mathbf{12})_2(\text{OAc})_4](\text{DiOX})_4$ (**14**) (**Fig. 50**), was isolated in 33.5 % yield.

Both compounds crystallize in the triclinic space group *P*-1 (from DMF and DiOX respectively) with one paddlewheel complex on an inversion centre and an azaindole derivative in general position.

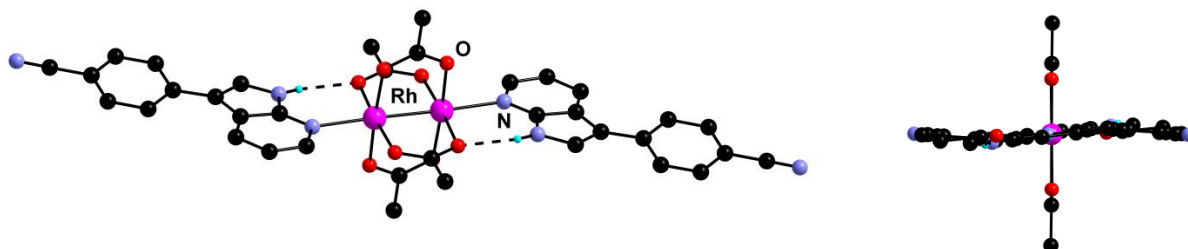


*Fig. 49: Structure of the $[\text{Rh}_2(\text{C}_{14}\text{H}_9\text{N}_3)_2(\text{OAc})_4](\text{DMF})$ complex (**13**).*

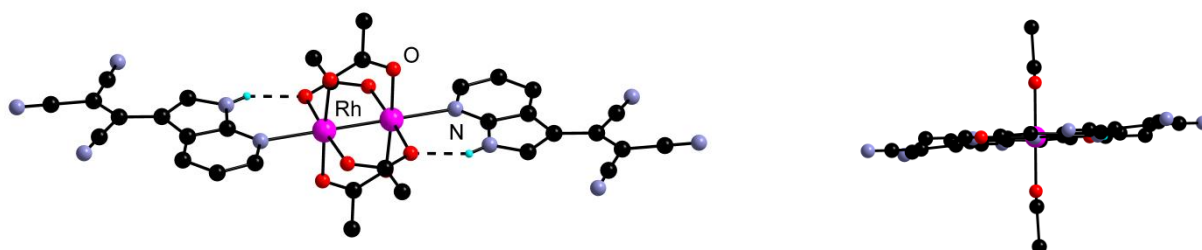


*Fig. 50: Structure of the $[\text{Rh}_2(\text{C}_{12}\text{H}_5\text{N}_5)_2(\text{OAc})_4](\text{DiOX})_4$ complex (**14**).*

As expected, the pyridyl nitrogen atom is coordinated to the Rh centre with Rh-Rh and Rh-N distances similar to what has been reported for $[\text{Rh}_2(\text{C}_2\text{H}_5\text{COO})_4(\text{H-aza})_2]$ (**Table 5**).¹² A hydrogen bonding interaction is observed between the pyrrolic NH and an oxygen atom of the acetate ligand. As a result of the symmetry, both 7-azaindole molecules are coplanar and lie in the same plane as the hydrogen

bonded acetates. It is particularly interesting to note that the benzonitrile and 7-azaindole moieties are coplanar in **14** while there are not in the structure of the free ligand **7** (see **Fig. 20**).

	$[\text{Rh}_2(\text{C}_{14}\text{H}_9\text{N}_3)_2(\text{OAc})_4](\text{DMF})$ 13	$[\text{Rh}_2(\text{C}_{12}\text{H}_5\text{N}_5)_2(\text{OAc})_4](\text{DiOX})_4$ 14	$[\text{Rh}_2(\text{C}_2\text{H}_5\text{COO})_4(\text{H-aza})_2]$ ¹²
d(Rh-Rh)	2.4076(4) Å	2.4031(4) Å	2.403(1) Å
d(Rh-N)	2.279(2) Å	2.290(2) Å	2.266(6) Å
d(N-H-O)	2.795(3) Å	2.720(4) Å	2.721 Å
$\alpha(\text{N-H-O})$	146.6°	147.5°	

Table 5: Bond distances in $[\text{Rh}_2(\text{C}_{14}\text{H}_9\text{N}_3)_2(\text{OAc})_4](\text{DMF})$, $[\text{Rh}_2(\text{C}_{12}\text{H}_5\text{N}_5)_2(\text{OAc})_4](\text{DiOX})_4$ and $[\text{Rh}_2(\text{C}_2\text{H}_5\text{COO})_4(\text{H-aza})_2]$ complexes.

Owing to a better solubility, the behavior in solution of only complex **14** was investigated by ¹H-NMR (300 MHz) in acetone-d₆. Compared to the free ligand, all the signals in the aromatic region in the spectrum of the complex are deshielded (**Fig. 51**). The hydrogen atoms of the rhodium acetate fragment appear as a singlet in the aliphatic region. These observations suggest that the complex is stable in acetone solution. The shift of signals of the pyridine moiety, corresponding to the signals of protons which are the closest to the coordinated pyridyl nitrogen, is in the 0.4 to 0.6 ppm range. On the contrary, signals of the protons in the second position of 7-azaindole fragments, being the farthest protons to coordinated pyridyl nitrogen, are shifted only by 0.1 ppm compared to the corresponding peak in the spectrum of the free ligand.

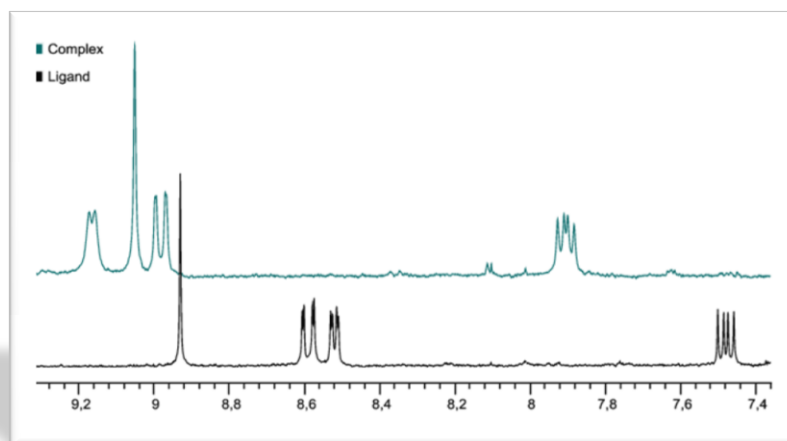


Fig. 51: Comparison of complex **14** and starting ligand **12** spectra.

The former two complexes are discrete species. The analogues obtained with ligands **8** and **9** bearing peripheral self-complementary carboxylic acid groups can assemble *via* hydrogen bonding. Complexes $[\text{Rh}_2(\mathbf{8})_2(\text{OAc})_4](\text{DEF})_2$ (**15**) (**Fig. 52**) and $[\text{Rh}_2(\mathbf{9})_2(\text{OAc})_4]$ (**16**) (**Fig. 53**) were synthesized and crystallized from DEF/EtOH/H₂O (3/2/2) mixture or 1-propanol solution in 62.3 % and 81.9 % yields respectively. Both compounds **13** and **14** crystallize in the triclinic *P*-1 space group with the organic ligands in general position and the rhodium acetate fragment on an inversion center.

The organization of the $[(\text{Rh}_2(\text{OAc})_4)(\text{H-aza})_2]$ core is similar to the one described above for **13** and **14** (**Table 6**). In the case of **15**, the carboxylic acid groups are hydrogen bonded to the DEF solvent molecules forming the $R_4^4(14)$ motif³⁹, leading to a one-dimensional arrangement.

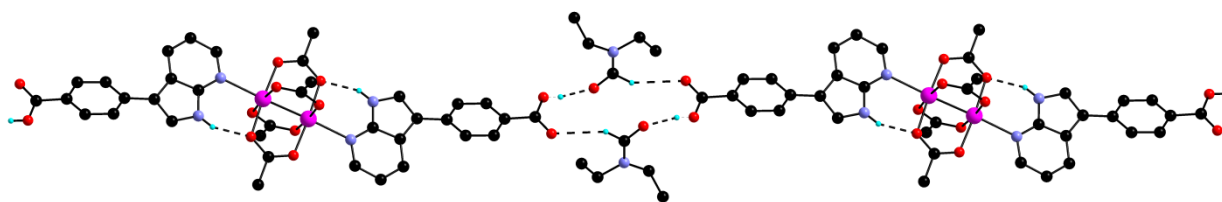


Fig. 52: Structure of H-bond network in the crystal structure of **15**.

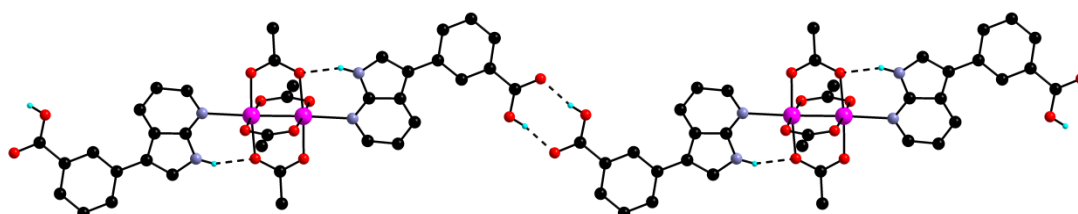


Fig. 53: H-bond network in **16**.

Zig-zag chains are observed in the crystal structure of **16** (Fig. 24), but with $R_2^2(8)$ motifs between self-complementary carboxylic acid groups.

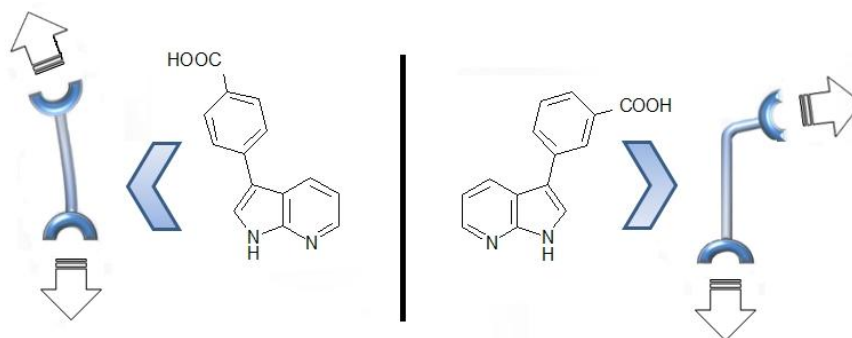
Compound 15		Compound 16	
Distances (Å) and angles(°)		Distances (Å) and angles(°)	
d(Rh-Rh)	2.4055(4)	d(Rh-Rh)	2.407(1)
d(Rh-N)	2.274(2)	d(Rh-N)	2.266(4)
d(N-H...O) _{acetate}	2.781(3)	d(N-H...O) _{acetate}	2.834(5)
α (N-H...O) _{acetate}	145.8	α (N-H...O) _{acetate}	142.4
d(O-H...O) _{DEF}	2.554(5)	d(O-H...O)	2.625(5)
α (O-H...O) _{DEF}	155.0	α (O-H...O)	169.1
d(C-H...O) _{DEF}	3.536(5)		
α (C-H...O) _{DEF}	144.1		

Table 6: Bond distances and angles in rhodium acetate complexes **15** and **16**.

In order to prepare heterometallic architectures, all the former rhodium acetate complexes were reacted with a variety of metals. However, owing to the low solubility of these species, only solvents such as DMF, DEF and DMSO could be used and only pink polycrystalline or amorphous materials were obtained. Therefore, no single crystal structure determination by X-Ray diffraction could be performed leaving the organization of these heterometallic architectures undetermined.

II.3.2. Networks based on the benzoic acid appended ligands **8** and **9**

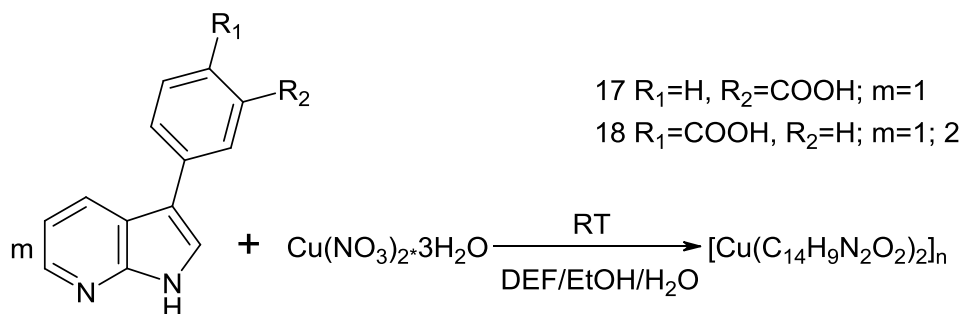
As emphasized in the introduction, 7-azaindole and carboxylic acid display analogous coordination propensity. In this respect, ligands **8** and **9** are particularly interesting as they incorporate both functional groups. They are positional isomers, as **8** bears a benzoic acid in *para* position while **9** features this group in *meta* position (Scheme 22). This geometrical difference should have a strong influence on the organization of coordination networks obtained with these ligands. Another interesting aspect of these ligands is the variable degree of deprotonation as they contain two types of acidic groups.



Scheme 22: Bent and L-form ligands.

Many attempts to prepare coordination networks were made using a variety of metal salts. Unfortunately, crystalline materials could only be obtained with copper(II) and cobalt(II) salts. In these compounds, derivatives **8** and **9** are present in the 7-azaindole/carboxylate form, acting thus as monoanionic ligands. We will describe first the two networks obtained with copper salts and then the cobalt containing compound.

Two networks with copper (II) were obtained by reaction of the ligands with copper nitrate (**Scheme 23**) at room temperature in DEF/EtOH/H₂O mixtures (in different proportions: 3/1/3 and 3/2/2 respectively).



Scheme 23: Preparation of the copper (II) networks based on ligands **8** and **9**.

Both reactions take place over a two weeks period and afford the compounds as green crystals. In the case of the *meta*-functionalized ligand **9**, a 2-D network [Cu(**9**)₂]_∞ (**17**) was prepared and crystallized from a DEF/EtOH/H₂O (3/1/3) mixture in 63.8 % yield (**Fig. 54**). This compound crystallizes in the monoclinic *C2/c* space group with one copper ion on a twofold screw axis and two organic ligands in general position. This compound does not contain any solvent and shows a rather dense packing. The packing generates no cavity.

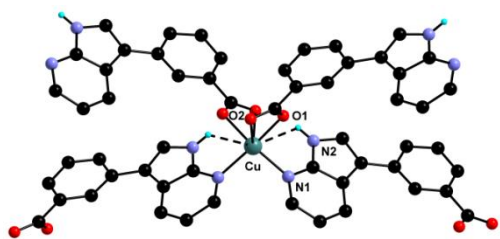


Fig. 54 Coordination sphere around the Cu centre in **17**.

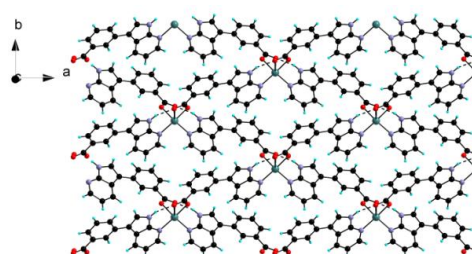


Fig. 55: View of the 2-D network along the *c* axis.

Bonds and distances	
$d(\text{N1-Cu})$	1.995(2) (Å)
$d(\text{O1-Cu})$	1.953(19) (Å)
$d(\text{O2-Cu})$	2.711(2) (Å)

Table 7: Bonds and distances.

The copper center is in a CuN₂O₄ distorted octahedral environment, coordinated to two carboxylate groups and the nitrogen atoms of two 7-azaindole groups. As the carboxylate is not

coordinated in a symmetrical fashion, the two Cu-O bonds vary (**Table 7**). As in the case of the rhodium complexes described above, the pyrrolic NH is hydrogen bonded to an oxygen atom with a N-H-O of 2.807(4) Å ($\alpha(\text{N-H-O}) = 100.88^\circ$). As seen **Fig. 55**, the overall organization is a 2-D network.

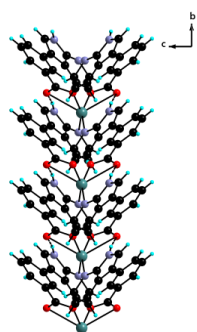


Fig. 56: View along the *a* axis.

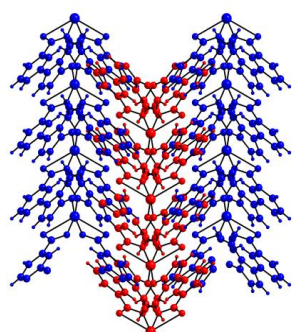


Fig. 57: View along axes *a*, with addition of surrounded layers.

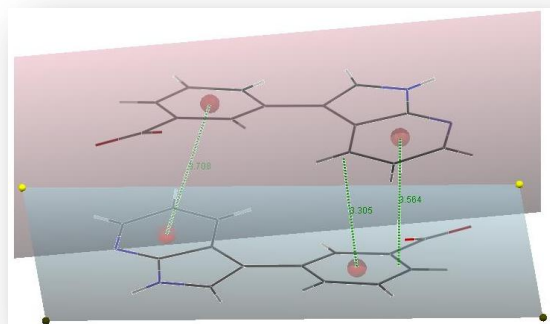


Fig. 58: π - π stacking between aromatic systems.

As shown in **Fig. 56**, along the *a* axis, the networks have a chevron type arrangement. As seen in **Fig. 57**, these chevrons interdigit along the *b* axis via π - π stacking. This stacking takes place between one ligand and its symmetry equivalent generated by an inversion centre with an interaction between the pyridyl and the phenyl rings (**Fig. 58**). The aromatic rings are not parallel owing to the twist angle between the 7-azaindole and the phenyl ring of 11.92° . These aromatic systems are not perfectly eclipsed as observed usually in π - π stacking interactions. The distance between centroids of the corresponding aromatic rings is 3.708 Å while the distances between the centroid of one ring and the plane of the interacting ring are 3.303 Å and 3.522 Å.

In the case of the *para*-functionalized ligand **8**, a 3-D network $[\text{Cu}(\text{C}_{14}\text{H}_9\text{N}_2\text{O}_2)_2](\text{solvent})_\infty$ (**18**) was prepared and crystallized from a DEF/EtOH/H₂O (3/2/2) mixture in 62% yield. The same network was obtained in crystalline form when the reaction was performed using other stoichiometry of the reagents (2/1 and 1/1). This compound crystallizes in the monoclinic space group $P2_1/n$ with copper atom and two ligand fragments in general positions. Here again, the copper centre is in a CuN_2O_4 distorted octahedral environment (**Fig. 59a**, **Table 8**) similar to what has been observed for **17**. A hydrogen bonding is also observed as in **17** with $d(\text{N-H-O}) = 2.790(4)$ Å ($\alpha(\text{N-H-O}) = 170.5^\circ$).

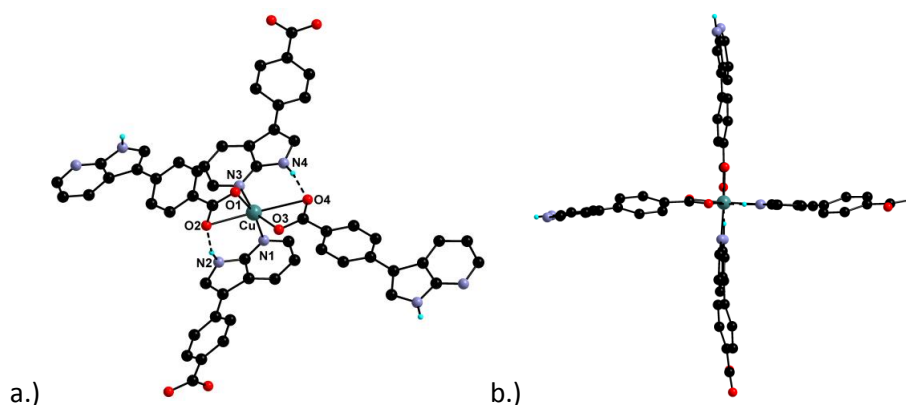


Fig. 59: Structure of the core in network **18**.

Bond distances	Bond distance	Angles
$d(\text{N1-Cu})=2.012(3)\text{Å}$	$d(\text{Cu-N3})=1.999(3)\text{Å}$	$\alpha(\text{N1-Cu-N3})=91.37(10)^\circ$
$d(\text{O1-Cu})=2.504(4)\text{Å}$	$d(\text{Cu-O3})=1.952(3)\text{Å}$	$\alpha(\text{O1-Cu-O3})=103.78(9)^\circ$
$d(\text{O2-Cu})=2.674(3)\text{Å}$	$d(\text{Cu-O4})=1.956(2)\text{Å}$	$\alpha(\text{O2-Cu-O4})=104.13(9)^\circ$

Table 8: Bond distances and angles (**18**).

From the view along the *a* axis (**Fig. 59b**), the core of this network can be described almost as a cross. Each ligand fragments, coordinated to the copper by 7-azaindole moiety, are practically in a same plane with ligand coordinated by carboxylate (angles between the planes of the ligands less than 6 °). These planes are intersecting with practically right angle (deviation less than 3 °).

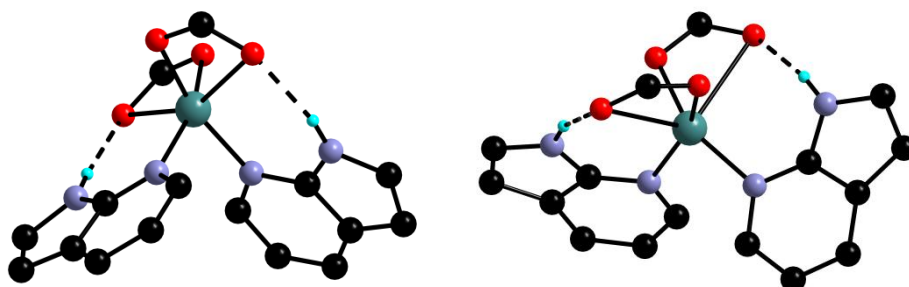


Fig. 60: Cores of the networks in the cases of 17 (right) and 18 (left).

The two metallic nodes are similar in **17** and **18**. In both cases, the planes of carboxylate groups are almost perpendicular (82.32 ° and 89.93 ° respectively). The difference lies in the angle between the two 7-azaindole groups. In **17**, they form an angle of 67.85 °, while it is 86.93 ° in **18** (**Fig. 60**).

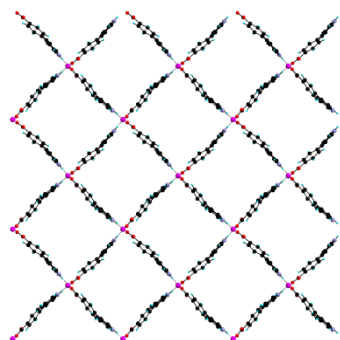


Fig. 61: View along the a axis.

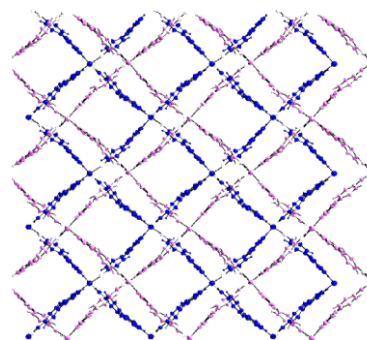


Fig. 62: Two interpenetrated networks.

In spite of the similarity of the metallic nodes, the difference in the position of the functional groups provides overall strikingly different networks. Indeed, in **18**, a 3-D network with cavities is observed (**Fig. 61**). In the crystal, two 3-D networks are interpenetrated *via* weak π - π stacking between aromatic rings (**Fig. 62**). This interpenetration hinders the presence of the 3-D porous channels and no cavities are observed along the *c* axis (**Fig. 63**). The latter are not empty but filled with a mixture of disordered EtOH, H₂O and DEF molecules. The corresponding electronic density was removed from the structural refinement using the SQUEEZE command and will therefore not be described in the following.

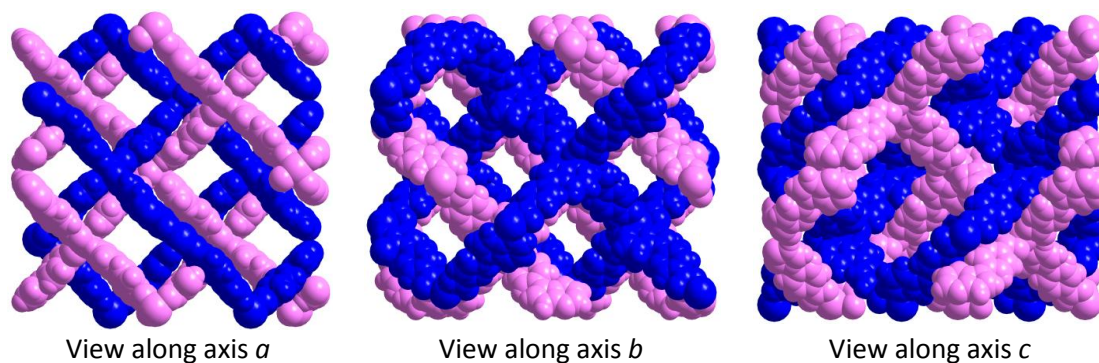


Fig. 63: Influence of interpenetration in dimensionality of the canals, view along the different axis.

Regarding the π - π stacking, in the case of this network, the interactions take place between 7-azaindole rings of two neighboring ligands. These ligands are symmetry related by an inversion centre and are offset. The angle between planes of the 7-azaindole fragments is 9.52° and distance between the centroids of the two pyridine groups is 3.675 \AA while the corresponding distances between the centroids of pyrrolic rings is 3.683 \AA (**Fig. 64**). This latter distance is shorter than in the case of the interaction in former network. These distances are in agreement with the ones usually reported in the literature for π - π stacking interactions (3.3 - 3.8 \AA).⁴⁰

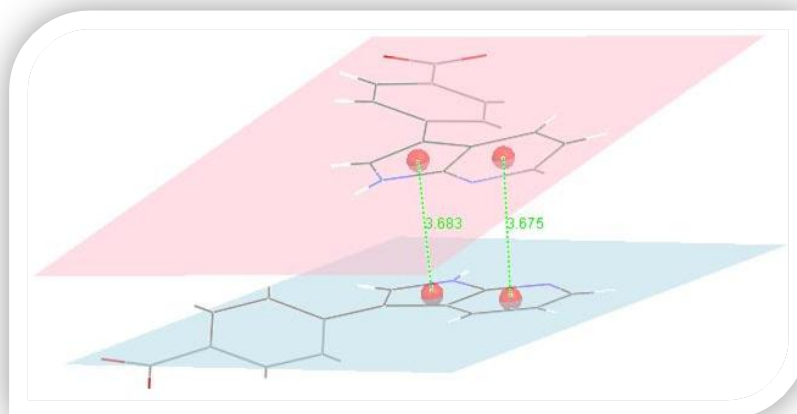


Fig. 64: π - π stacking of the aromatic rings.

The pores are occupied by disordered solvent molecules (DEF or/and H_2O , or/and EtOH). The potential free volume was calculated using the Platon program and estimated to be 47 % of the total volume of the cell. The stability of the network was studied by TGA analysis under a stream of nitrogen (under a N_2 flux of $20.0 \text{ mL}\cdot\text{min}^{-1}$).

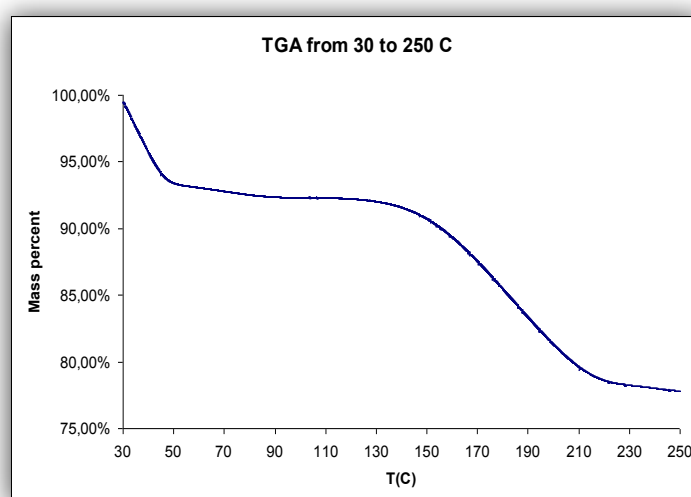


Fig. 65: TGA analysis of network 19.

Several steps of weight loss can be observed (**Fig. 65**). Between room temperature and 50°C , a first weight loss of about 7.8 % is observed. Then, up to 130°C , a plateau is observed and, in a second stage, between 130 and 230°C , 14.2 % of weight loss is measured. These steps correspond to desolvation of the compound. Above 270°C , the network decomposes.

Crystallinity of the compound was examined by powder X-ray diffraction analyses (data collected under ambient conditions) after desolvation of samples under vacuum at RT and at 100°C (24 h). After both treatments, crystallinity is retained (**Fig. 66**). However, while the sample evacuated at room temperature retains the original structure, the one evacuated at 100°C for 24 h displays a structure different from the one observed for **18**.



*Fig. 66: Powder X-ray diffraction analyses of **18** after the desolvation in different conditions.*

In order to investigate the sorption properties of network **18**, the BET (Brunauer-Emmett-Teller) measurements were performed. The sorption of nitrogen was studied at 77 K. The solvent molecules were evacuated from the sample by degassing at 150 °C (13.3 Pa, 200 min). The sample displayed a **Type IV** adsorption isotherm and hysteresis loop type H3, typical for a crystalline mesoporous material⁴¹ (**Fig. 67 left**). The BET surface area was 242 m²/g. As mentioned before, evacuation of guest solvent molecules at temperature over 100 °C leads to a crystalline phase different from the original structure of **18**. The residue after the BET measurement was analyzed by powder X-ray diffraction analyses. The sample retained its crystallinity, however with a change in the structure with respect to the one of **18** (**Fig. 67 right**) and to the one observed for the sample evacuated at 100°C for 24 h.

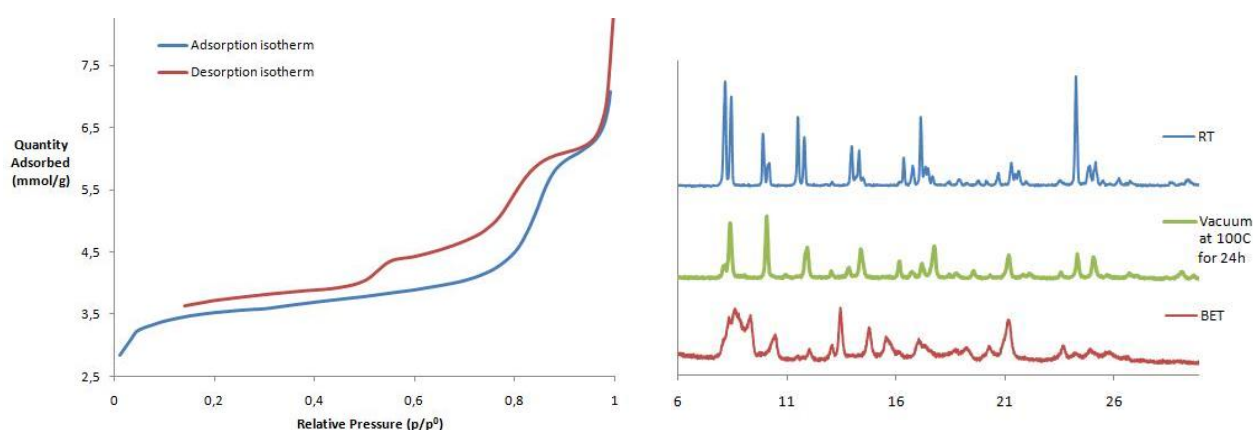
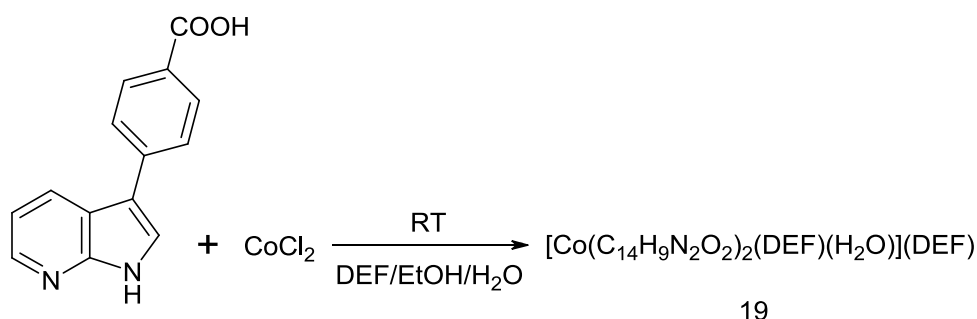


*Fig. 67: BET measurement (sorption and desorption of N₂) of network **18** (left) and powder X-ray diffraction analyses of samples before and after BET measurement (right).*

Reaction of ligand **8** with CoCl_2 in a DEF/EtOH/ H_2O (3/2/2) mixture led after six months to the formation of pink crystals of the 2-D network $[\text{Co}(\text{C}_{14}\text{H}_9\text{N}_2\text{O}_2)_2(\text{H}_2\text{O})(\text{DEF})](\text{DEF})$ (**19**) (**Scheme 24**). We should note here that, in spite of numerous attempts, the synthesis of this MOF was not reproducible. However, it will be described in the next few lines owing to its interesting structure.



*Scheme 24: Preparation of the $[\text{Co}(\text{C}_{14}\text{H}_9\text{N}_2\text{O}_2)_2(\text{H}_2\text{O})(\text{DEF})](\text{DEF})$ network (**19**).*

This compound crystallizes in the monoclinic $P2_1/c$ space group with a cobalt atom, two ligands and solvents molecules in general positions. As in the previous examples with copper, the 7-azaindole group is not deprotonated and coordinates the metal centre *via* the pyridyl nitrogen atom. Compound **19** consists of $[\text{Co}(\text{COO})_2(\text{H-aza})_2(\text{H}_2\text{O})(\text{DEF})]$ core (**Fig. 68**, **Table 9**) in which the Co(II) center has a slightly distorted octahedral coordination and is coordinated to two 7-azaindole and two carboxylate groups of the ligands and one water and one DEF solvent molecules. A second DEF molecule lies outside of the cobalt coordination sphere. The water molecule coordinated to the cobalt center is involved in bifurcated intramolecular hydrogen bonding interaction with oxygen atoms of the two neighboring carboxylate groups. These O-H-O bond distances are 2.594 and 2.623 Å with the O-H-O angle is 160.3°.

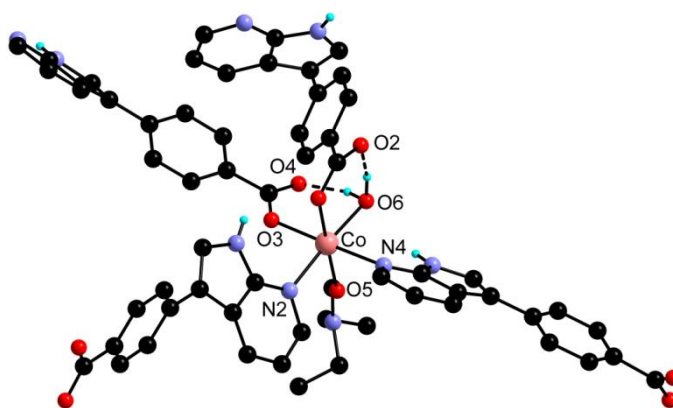


Fig. 68: Structure of the core in the case of $[\text{Co}(\text{COO})_2(\text{H-aza})_2(\text{H}_2\text{O})(\text{DEF})]$ network.

Bond distances	Bond distance	Angles
$d(\text{O3-Co})=2.076(2)\text{Å}$	$d(\text{Co-N4})=2.169(3)\text{Å}$	$\alpha(\text{O3-Co-N4})=176.29(9)^\circ$
$d(\text{O1-Co})=2.087(2)\text{Å}$	$d(\text{Co-O5})=2.115(2)\text{Å}$	$\alpha(\text{O1-Co-O5})=177.72(8)^\circ$
$d(\text{N2-Co})=2.150(3)\text{Å}$	$d(\text{Co-O6})=2.139(2)\text{Å}$	$\alpha(\text{N2-Co-O6})=174.75(9)^\circ$

Table 9: Bond distances and angles.

2-D zigzag grid type networks are formed and stack with the coordinated DEF molecules protruding (**Fig. 69**). Along the b axis (**Fig. 70**), a side view of the free space within the grid is apparent. However, no channels are formed along this direction owing to the stacking of the neighboring layers.

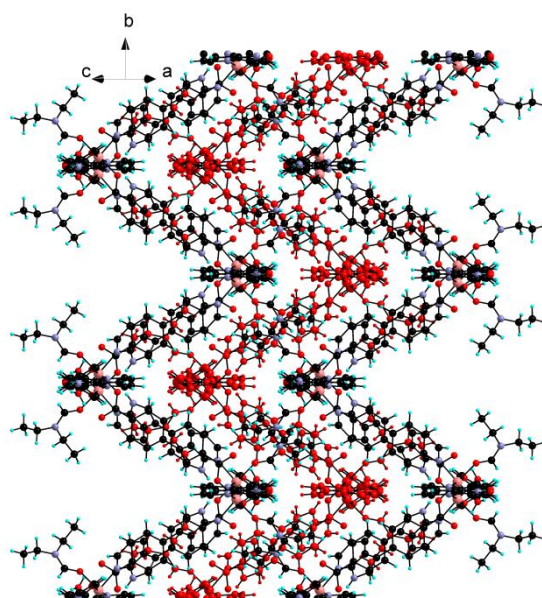


Fig. 69: 2-D zigzag type network.

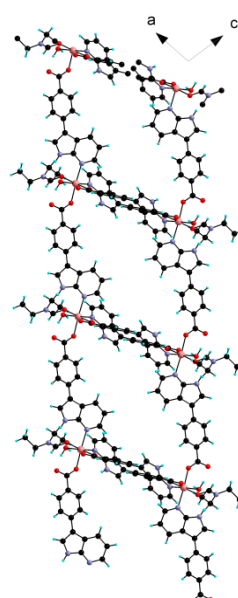


Fig. 70: View along the b axis.

Viewed along the *a* axis, the network appears as a checkerboard with every other rhombic cavity ($13.758(3) \text{ \AA} \times 13.643(8) \text{ \AA}$ (Co-Co distances), 103.86° (Co-Co-Co angle)) occupied by the coordinated DEF molecules (**Fig. 71**). A second DMF molecule, which is not included in the cobalt coordination sphere, occupies the free space within this network. No void is therefore actually observed in this system. This DEF molecule is hydrogen bonded to the coordinated water molecule with O-H-O bond distance of 3.097 \AA ($\alpha(\text{C-H-O}) = 112.1^\circ$), and the pyrrolic nitrogen atom of 7-azaindole with O-H-N distance of 2.951 \AA ($\alpha(\text{N-H-O}) = 129.9^\circ$).

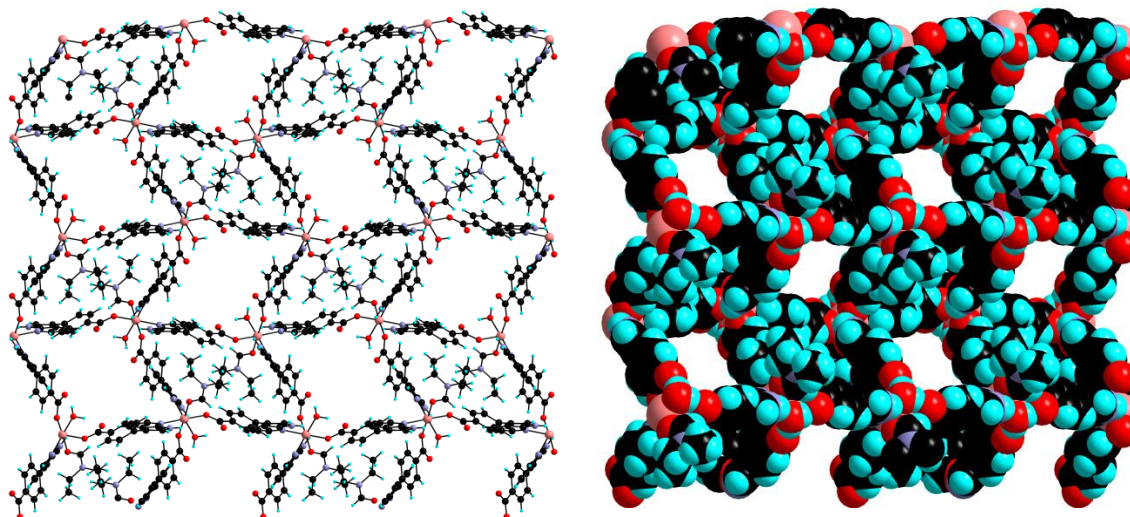
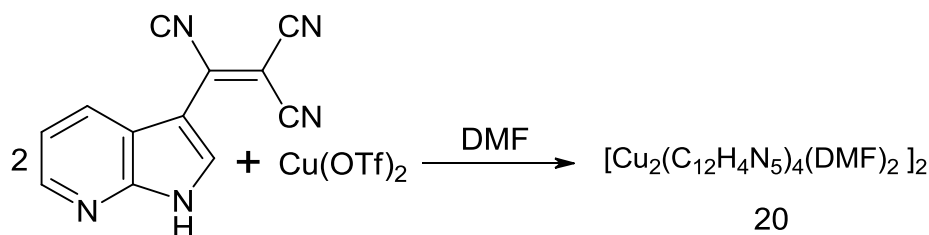


Fig. 71: View along axes *a*.

Unfortunately, all attempts to remove the solvent under vacuum or to exchange it by immersing the crystals in another solvent resulted in the collapse of the system and loss of crystallinity.

II.3.3. Complexes and networks based on the 3-tricyanovinylene-7-azaindole ligand.

The 3-tricyanovinylene-7-azaindole has been used as a ligand to form complexes with Cu(II) salts. Depending on the salt employed, either a discrete complex or a one-dimensional chain was obtained. Compounds were synthesized by reaction of the ligand with corresponding Cu(II) salt in DMF at room temperature in a stoichiometric ratio of 1:2 and 1:1 respectively. In the first case, upon reaction with $\text{Cu}(\text{OTf})_2$, a discrete paddlewheel complex, $[\text{Cu}_2(\text{C}_{12}\text{H}_4\text{N}_6)(\text{DMF})_2]$ (**20**), was obtained as green-blue crystals in 58.8 % yield (**Scheme 25**). This compound crystallizes in the triclinic *P*-1 space group with the paddlewheel core on an inversion centre.



Scheme 25: Preparation of the $[\text{Cu}_2(\text{C}_{12}\text{H}_4\text{N}_6)(\text{DMF})_2]$ complex (20).

This dimeric complex incorporates four ligands as 7-azaindolates acting as bridges to form a paddlewheel as observed with copper acetate. Two DMF molecules are coordinated in the axial positions of the metallic core (Cu-O distance 2.232(3) Å). As seen in **Fig. 72**, along the Cu-Cu axis, the two ligands and copper ions lie in the same plane. Furthermore, the angle between tricyanovinylene and 7-azaindole groups is only 3.75 °.

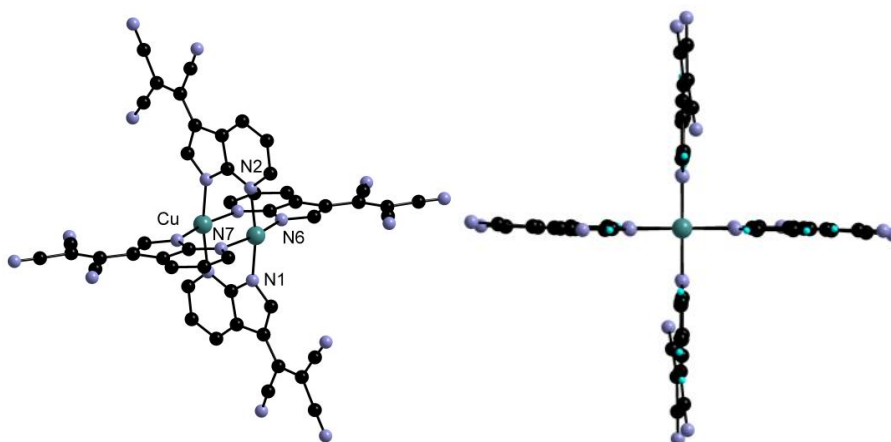


Fig. 72: Structure of the of the $[\text{Cu}_2(\text{C}_{12}\text{H}_4\text{N}_6)(\text{DMF})_2]$ complex (20).

This complex is analogous to the one reported with unfunctionalized 7-azaindole. While this paddlewheel is similar to the ones obtained with carboxylate ions or dpt (1,3-diphenyltriazene) for example, the ligand is not symmetrical and therefore four different isomers can be envisaged (**Fig. 73**). One isomer contains a copper ion coordinated to four (*isomer a*) pyridine groups, the second features three pyridine groups coordinated to the same ions (*isomer b*), the last two isomers contain metal ions with a mixed pyridine and pyrrolic coordination sphere in *trans* or *cis* (*isomers c and d*).

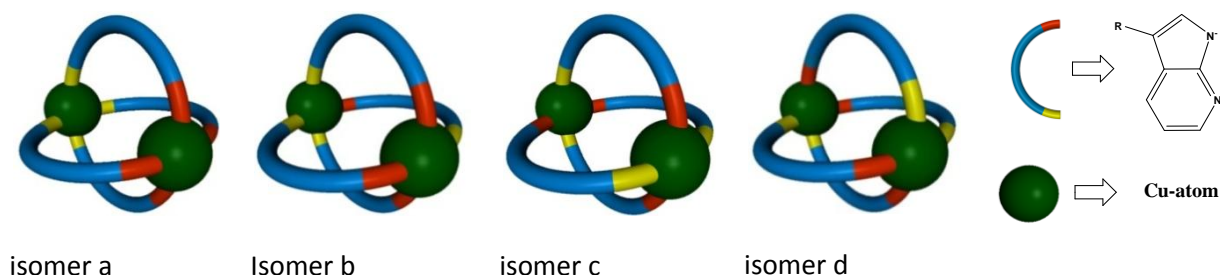
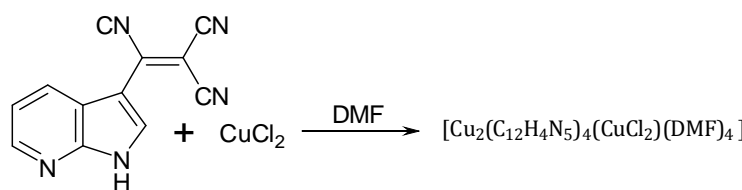


Fig. 73: Possible isomers of core in the $[\text{Cu}_2(\text{C}_{12}\text{H}_4\text{N}_6)(\text{DMF})_2]$ (**20**).

Isomers *a* and *b* are probably less favored owing to charge unbalance within the complex (**Fig. 73**). In compound **20**, as in the reported $[\text{Cu}_2(7\text{-aza})_4(\text{DMF})_2]$ complex, isomer *d* is observed. The Cu-Cu distance (**Table 10**) is longer than in the $[\text{Cu}_2(\text{aza})_4(\text{DMF})_2]$ complex (2.782(2) Å), $[\text{Cu}_2(\text{OAc})_4]$ (2.64 Å) and $[\text{Cu}_2(\text{dpt})_4]$ (2.40 Å).²¹

Upon reaction of ligand **12** with CuCl_2 , a 1-D chain $[(\text{Cu}_2(\text{C}_{12}\text{H}_4\text{N}_6)_4)(\text{CuCl}_2)(\text{DMF})_4]_\infty$ (**21**) was obtained in crystalline form in 28.2 % yield (**Scheme 26**). This compound crystallizes in the triclinic *P*-1 space group with the copper atom of the CuCl_2 unit and the paddlewheel lying on inversion centers.



Scheme 26: Preparation of the $[(\text{Cu}_2(\text{azaTCV})_4)(\text{CuCl}_2)(\text{DMF})_4]_n$ (**21**).

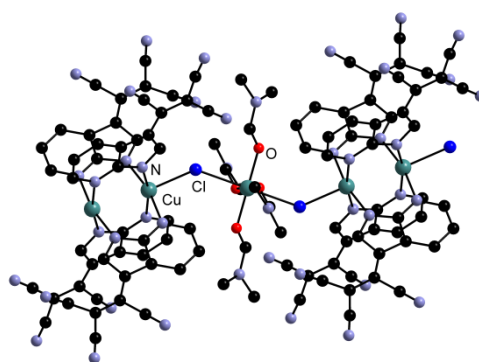


Fig. 74: Structure of the $[(\text{Cu}_2(\text{azaTCV})_4)(\text{CuCl}_2)(\text{DMF})_4]_n$.

This network consists of $[\text{Cu}_2(\text{C}_{12}\text{H}_4\text{N}_6)_4]$ paddlewheels, identical to the core of the previous complex, bridged by $[\text{CuCl}_2(\text{DMF})_2]$ units *via* the chloride anions coordinated to the axial positions. The Cu-Cl-Cu angle is 138.1°. The Cu-Cl bond distance within the bridging $[\text{CuCl}_2(\text{DMF})_2]$ unit (2.752(2) Å) is longer than the one involving the copper ion belonging to the paddlewheel (2.465(1) Å). The former distance is probably longer owing to the Jahn-Teller effect. Regarding the paddlewheel core, the bond distances are similar in **20** and **21** (**Table 10**).

Bond distances/ Complexes	$[\text{Cu}_2(\text{azaTCV})_4(\text{DMF})_2]$	$[(\text{Cu}_2(\text{azaTCV})_4)(\text{CuCl}_2)(\text{DMF})_4]$
d(Cu-Cu)	2.8247(8) Å	2.8813(10) Å
d(Cu-N1) _{pyrrole}	1.991(3) Å	2.019(4) Å
d(Cu-N6) _{pyrrole}	1.996(3) Å	2.014(4) Å
d(Cu-N2) _{pyridine}	2.018(3) Å	2.039(4) Å
d(Cu-N7) _{pyridine}	2.024(4) Å	2.037(4) Å

Table 10: Bond distances in copper/3-tricyanovinylene-7-azaindole complexes **20** and **21**.

The magnetic properties of both compounds were studied in collaboration with Dr. Guillaume Rogez at the Institut de Physique et Chimie des Matériaux de Strasbourg (UMR CNRS-Uds 7504) using a Quantum Design MPMS-XL SQUID magnetometer. The static susceptibility measurement was performed in the 300 - 1.8 K temperature range with an applied field of 50 kOe in the case of the discrete complex

and 5 kOe in the case of the network. Magnetization measurements at different fields at a given temperature confirm the absence of ferromagnetic impurities. Data were corrected for the sample holder and diamagnetism was estimated from Pascal constants.

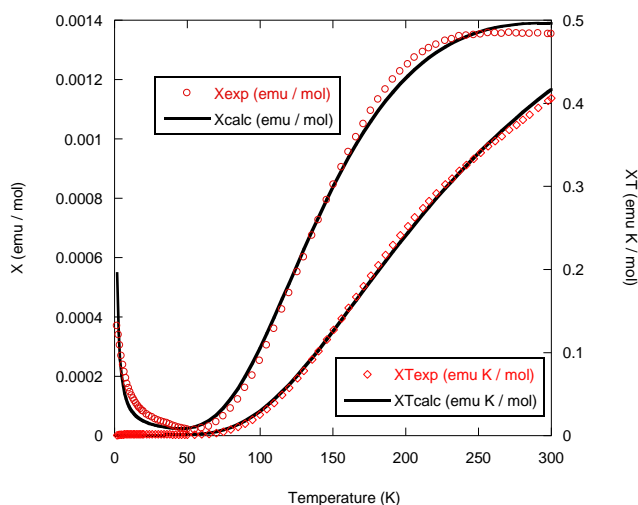


Fig. 75: Temperature dependence of the magnetic susceptibility of **20** (red circles) and fit using the expression shown below.

In the first case (**20**), the data were fitted using the following spin Hamiltonian where the spin operator \mathbf{S} is defined as $\mathbf{S} = \mathbf{S}_{\text{Cu1}} + \mathbf{S}_{\text{Cu2}}$:

$$\mathbf{H} = -J \mathbf{S}_{\text{Cu1}} \mathbf{S}_{\text{Cu2}} + g \beta \mathbf{H} \mathbf{S}$$

A certain amount ρ of paramagnetic impurity ($\mathbf{S}_{\text{impur}} = \frac{1}{2}$) was considered. The fit leads to the following values: $J = -327(5) \text{ cm}^{-1}$, $g = 2.08(5)$ and $\rho = 0.12(8) \%$ with an agreement factor $R^i = 2 \times 10^{-3}$.

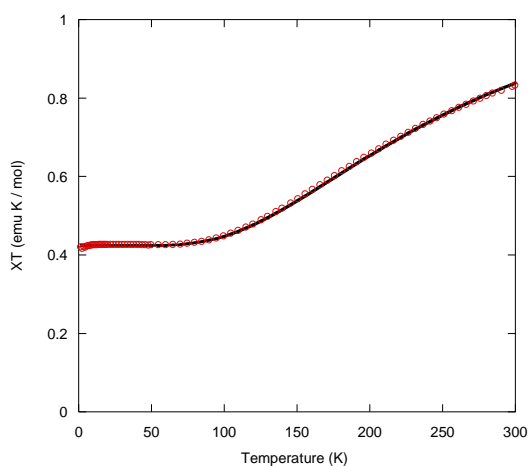


Fig. 76: $\chi T = f(T)$ (open circles : experimental points, full line: best fit) per formula unit.

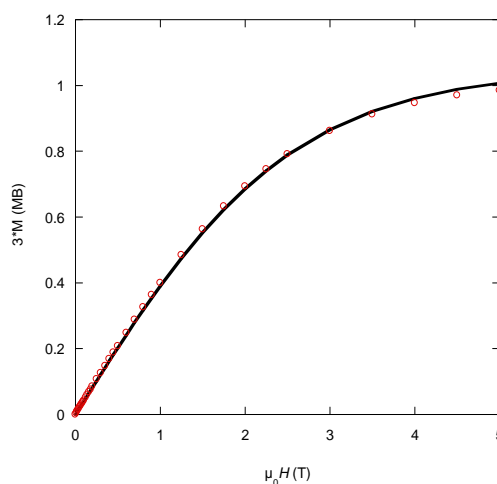


Fig. 77: $M = f(H)$ (open circles : experimental points, full line: best fit).

$$R^i \text{ is defined as } R = \frac{\sum (\chi_{\text{exp}} - \chi_{\text{calc}})^2}{\sum \chi_{\text{exp}}^2}$$

Regarding network **21**, at 300 K, the χT product is well below the expected value for three Cu(II) ions (experimental value: $0.83 \text{ emu}\cdot\text{K}\cdot\text{mol}^{-1}$, expected value for three uncoupled Cu(II) ions : $1.24 \text{ emu}\cdot\text{K}\cdot\text{mol}^{-1}$ assuming $g = 2.1$). Upon decreasing the temperature, the χT product decreases regularly down to a plateau reached at around 70 K ($0.43 \text{ emu}\cdot\text{K}\cdot\text{mol}^{-1}$). This value corresponds to the one expected for a single isolated Cu (II) ion. Then the χT product remains almost constant down to very low temperature, where it starts to decrease slightly.

Considering the nature of the bridging ligands and the $\chi T = f(T)$ curve (**Fig. 76**), it seemed reasonable to consider only an intradimer interaction, with a negligible interaction between Cu(1) and Cu(2) *via* the chloride bridges to model the experimental data.

With this approximation, and considering an equal g factor for all Cu(II), $J = -342.9 \text{ cm}^{-1}$ (with respect to an Heisenberg Hamiltonian of the form $\hat{H} = -J_{ij} \hat{S}_i \hat{S}_j$) and $g = 2.13$ were obtained. The excellent quality of the fit ($R^i = 2.2 \times 10^{-5}$) validates the approximation.

Moreover the $M = f(H)$ measurements at very low temperature (**Fig. 77**), can be fitted by a Brillouin function for an isotropic spin $S = 1/2$ (with $g = 2.10$, $R = 2.6 \times 10^{-4}$). This confirms that one Cu(II) remains uncoupled with the other two, and therefore that the interaction between Cu(1) and Cu(2) is indeed negligible with respect to the intradimer interaction.

Finally the small decrease of the χT product **21** is likely due to very weak antiferromagnetic interaction between Cu(2) which cannot be modelled with this approximation.

These results are well correlated with literature data for corresponding 7-azaindole copper complex $[\text{Cu}_2(\text{aza})_4(\text{DMSO})_2] \cdot 2\text{-DMSO}$ ¹⁸ (**Table 11**).

Data/Complexes	$[\text{Cu}_2(\text{aza-TCV})_4(\text{DMF})_2]$	$[(\text{Cu}_2(\text{aza-TCV})_4)(\text{CuCl}_2)(\text{DMF})_4]$	$[\text{Cu}_2(\text{aza})_4(\text{DMSO})_2] \cdot 2\text{-DMSO}$
$J (\text{cm}^{-1})$	-327(5)	-342.9	-389
g	2.08(5)	2.13	2.11

Table 11: Comparison of magnetic properties of compounds **20-21** and literature data for $[\text{Cu}_2(\text{aza})_4(\text{DMSO})_2] \cdot 2\text{-DMSO}$.¹⁸

II.4. Conclusion

Novel 7-azaindole appended ligands were synthesized and used for the preparation of discrete complexes and extended architectures. Owing to the ability of 7-azaindole group to coordinate metal centres without deprotonation or as 7-azaindolate, two modes of coordination were defined. In the frame of the first mode, a series of compounds, based on $[\text{Rh}_2(\text{OAc})_4]$, was obtained. However, as a result of the poor solubility of these discrete complexes, their use as metallatectons for the elaboration of heterometallic architectures was problematic. In the case of the rhodium acetate complexes based on the ligands appended by peripheral carboxylic acid groups two H-bond 1-D networks were obtained *via* the $R_4^4(14)$ (with DEF solvent molecule) and the $R_2^2(8)$ motifs. Two extended 3-D networks **17** and **18** were obtained by reactions with copper(II) and one **19** with cobalt(II) salts. Depending on the position of the carboxylic acid groups of the starting ligand, porous (**18**) and non-porous (**17**) architectures, with similar organization in the core, were obtained in the copper case. In the case of compound **18** interpenetration of networks and partial blocking of the pore was observed. Network **18** was analyzed by TGA and BET measurements, showing different steps of desolvation and collapse of the network above 270°C and a BET surface area 242 m²/g.

One way to circumvent the problems of solubility of the discrete rhodium acetate complexes for the elaboration of heterometallic architectures could be to use ligands without a spacer between the two coordination poles (**Fig. 78**). One approach to solve the issue of interpenetration, in the case of network **18**, could be substitution of the aromatic spacer by a non-aromatic one.

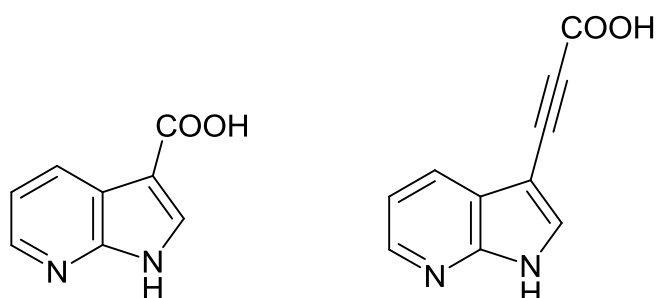


Fig. 78: Potential alternative ligands.

Both modes of coordination were illustrated with ligand **12** appended by a TCV moiety. The formation of discrete complex **20** based on $[\text{Rh}_2(\text{OAc})_4]$ occurs without deprotonation of the 7-azaindole pole. Upon reactions with $\text{Cu}(\text{OTf})_2$ and CuCl_2 , the formation of a discrete paddlewheel type copper (II) complex **20**, and a heteronuclear homometallic 1-D network **21** were observed. Network **21** contains binuclear species identical to the one observed for **20** however bridged by CuCl_2 fragments, coordinated in the copper axial positions of the paddlewheel core. These compounds illustrate the coordination of 7-azaindolate, similar to the one observed in the literature for 7-azaindole copper (II) complex¹⁸. The magnetic properties of discrete complex **20** ($J = -327(5) \text{ cm}^{-1}$, $g = 2.08(5)$) and network **21** ($J = -342.9 \text{ cm}^{-1}$, $g = 2.13$) were also measured.

II.5. References

- ¹ Ciureanu, M., *Rev. Roum. Chim.* **1976**, *21*, 1007.
- ² Popowycz, F., Routier, S., Joseph, B., Mérour, J., *Tetrahedron* **2007**, *63*, 1031.
- ³ Catalan, J., Mo, O., Perez, P., Yanez, M., *Tetrahedron* **1983**, *39*, 2851.
- ⁴ Adler, T. K., Alber, A., *J. Chem. Soc.* **1960**, 1794.
- ⁵ Hetherington, W. M., Micheels, R. H., Eisenthal, K. L., *Chem. Phys. Lett.* **1979**, *66*, 230.
- ⁶ (a) J. Herbich, J., Sepio, J., Waluk, J., *J. Mol. Struct.* **1984**, *114*, 329; (b) Chen, Y., Gai, F., Petrich, J. W., *J. Am. Chem. Soc.* **1993**, *115*, 10158; (c) Schowen, R. L. *Angew. Chem., Int. Ed. Engl.* **1997**, *36*, 1434.
- ⁷ Dufour, P., Dufour, N., Dartiguenave, Y., Dartiguenave, M., Beauchamp, A., Lebus, A., Bélanger-Gariépy, F., *Can. J. Chem.* **1990**, *68*, 193.
- ⁸ Wang, S. *Coord. Chem. Rev.*, **2001**, *215*, 79.
- ⁹ Chou, P. T., Liao, J. H., Wei, C. Y., Yang, C. Y., Yu, W. S., Chou, Y. H., *J. Am. Chem. Soc.* **2000**, *122*, 986.
- ¹⁰ Deacon, G. B., Delbridge, E. E., Skelton, B. W., White, A. H., *Eur. J. Inorg. Chem.* **1999**, 751.
- ¹¹ Rempel, G. A., Legzdins, P., Smith, H., Wilkinson, G., *Inorg. Synth.* **1972**, *13*, 90.
- ¹² Cotton, F. A., Felthouse, T. R., *Inorg. Chem.* **1981**, *20*, 600.
- ¹³ Kani, Y., Tsuchimoto, M., Ohba, S., *Acta Cryst.* **2000**, *C56*, e193.
- ¹⁴ Sheldrick, W. S., *Z. Naturforschung B* **1982**, *37*, 653.
- ¹⁵ Albada, G. A., Nur, S., Horst, M. G., Mutikainen, I., Turpeinen, U., Reedijk, J., *J. Mol. Str.* **2008**, *874*, 41.
- ¹⁶ Albada, G. A., Tanase, S., Mutikainen, I., Turpeinen, U., Reedijk, J., *Inorg. Chim. Acta* **2008**, *361*, 1463.
- ¹⁷ Poitras, J., Beauchamp, A. L., *Can. J. Chem.* **1992**, *70*, 2846.
- ¹⁸ Brookes, R. W., Martin, R. L., *Inorg. Chem.* **1975**, *14*, 528.
- ¹⁹ Brookes, R. W., Martin, R. L., *Aust. J. Chem.* **1974**, *27*, 1569.
- ²⁰ Lee, C. F., Chin, K. F., Peng, S. M., Che, C. M., *J. Chem. Soc. Dalton Trans.* **1993**, 467.
- ²¹ Peng, S. M., Lin, Y. N., *Acta Cryst. Sect. C* **1986**, *42*, 1725.
- ²² Harris, C. M., Martin, R. L., *Proc. Chem. Soc.* **1958**, 259.
- ²³ (a) Guha, B. C., *Proc. Roy. Soc. A*, **1951**, *206*, 353. (b) Kahn, O. in *Molecular Magnetism*, **1993**, Wiley-VCH, 107.
- ²⁴ Peng, B., Ming, S., Hsien, C., *J. Chin. Chem. Soc.* **1988**, *35*, 325.
- ²⁵ Koyama, H., Saito, Y. *Bull. Chem. Soc. Jpn.* **1954**, *27*, 112.
- ²⁶ Li, H., Eddaoudi, M., O'Keeffe, M., Yaghi, O. M., *Nature*, **1999**, *402*, 276.
- ²⁷ Wang, S. *Coord. Chem. Rev.* **2001**, *215*, 79.
- ²⁸ Ashenurst, J., Wu, G., Wang, S. *J. Am. Chem. Soc.* **2000**, *122*, 2541.
- ²⁹ Ashenurst, J., Wu, G., Wang, S. *J. Am. Chem. Soc.* **2000**, *122*, 3528.
- ³⁰ Hassan, A., Wang, S., *J. Chem. Soc. Chem. Commun.* **1998**, 339.
- ³¹ Wu, Q., Esteghamatian, M., Hu, N. X., Popovic, Z. G., Enright, S., Breeze, R., Wang, S., *Angew. Chem. Int. Ed. Engl.* **1999**, *38*, 985.
- ³² Sham, H. T., Kwok, C., Che, C., Zhu, N. *Chem. Commun.* **2005**, 3547.
- ³³ Popowicz, S., Routier, B., Joseph, J., Mérour, Y., *Tetrahedron* **2007**, *63*, 1031.
- ³⁴ (a) Alvarez, M., Fernandez, D., Joule, A., *Synthesis* **1999**, *4*, 615; (b) Shen, L., Prouty, C., Conway, B. R., Westover, L., Xu, J. X., Look, R. A., Chen, X., Beavers, M. P., Roberts, J., Murray, W. V., Demarest, K. T., Kuo, G. H., *Bioorg. Med. Chem.* **2004**, *12*, 1239; (c) Kelly, T. A., McNeil, D. W., Rose, J. M., David, E., Shih, C. K., Grob, P. M., *J. Med. Chem.* **1997**, *40*, 2430.
- ³⁵ Huang, S., Li, R., Connolly, P. J., Emanuel, S., Middleton, S. A., *Bioorg. Med. Chem. Lett.* **2006**, *16*, 4818.
- ³⁶ Song, D., Schmider, H., Wang, S., *Org. Lett.* **2002**, *4*, 4049.
- ³⁷ Kim, B. T., *Bioorg. Med. Chem.* **2004**, *12*, 5505.
- ³⁸ Noland, W. E., Kuryla, W. C., Lange, R. F., *J. Am. Chem. Soc.* **1959**, *81*, 6010.
- ³⁹ Etter, M. C., *Acc. Chem. Res.* **1990**, *23*, 120.
- ⁴⁰ Janiak C., *J. Chem. Soc. Dalton Trans.* **2000**, 3885.
- ⁴¹ (a) Kitagawa, S., Kitaura, R., Noro, S., *Angew. Chem. Int. Ed.* **2004**, *43*, 2334; (b) Sing, K. S. W., Everett, D. H., Haul, R. A. W., Pierotti, R. A., Moscou, L., Rouquerol, J., Siemieniowska, T., *Pure Appl. Chem.* **1985**, *57*, 603.

III. Chapter 2

III.1. Introduction

III.1.1. Dipyrrens

Dipyrromethenes or 4,6-Dipyrrens (DPMs) form a group of ligands containing two conjugated pyrrolic rings connected by a methene moiety. By analogy with porphyrin chemistry, the positions 1 and 9 are referred as α -positions, 2,3,7,8 as β -positions and position 5 as the *meso* position (**Fig. 79**). The derivatives of 4,6-dipyrin have attracted much attention due to their propensity to strongly chelate transition metals. In particular, luminescent¹ as well as porous¹³ materials based on DPM have been reported.

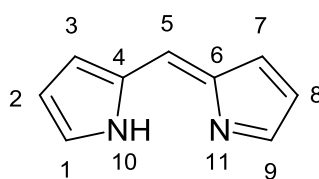
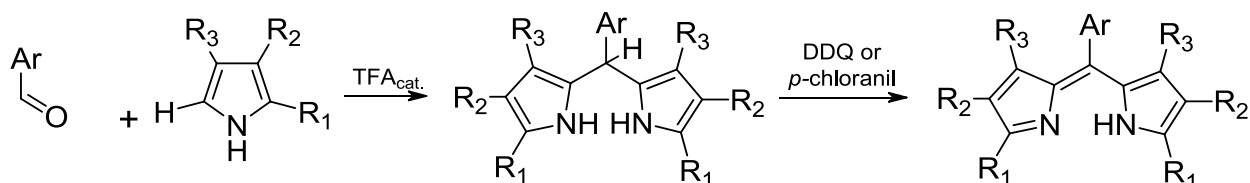


Fig. 79: Structure of 4,6-Dipyrrens.

MacDonald² has developed a method for the preparation α - and β -substituted DPM derivatives, based on the coupling between 2-formyl pyrrole and an α -unsubstituted pyrrole in the presence of an acid. J.S. Lindsey³ reported another synthetic procedure applicable in large scale, which allows the preparation of the α -, β - (un)substituted and *meso*- substituted derivatives. This synthetic route (**Scheme 27**) based on the preparation of intermediate dipyrromethanes and subsequent oxidation by DDQ or *p*-chloranil is particularly suitable for 5-aryl dipyrrens owing to the enhanced stability of the corresponding dipyrromethane precursor.



Scheme 27: Preparation of DPMs by Lindsey's method.³

Regarding the organization of the ligands in the solid state (**Fig. 80**), depending on the nature of the secondary coordination pole, compounds are organized as isolated molecules or as hydrogen bonded networks. For example, the formation of a 1-D hydrogen bonded chain is observed in the case of ligand DPM-Py¹⁴ in which the pyridyl nitrogen atom forms a hydrogen bond with the pyrrolic hydrogen atom.

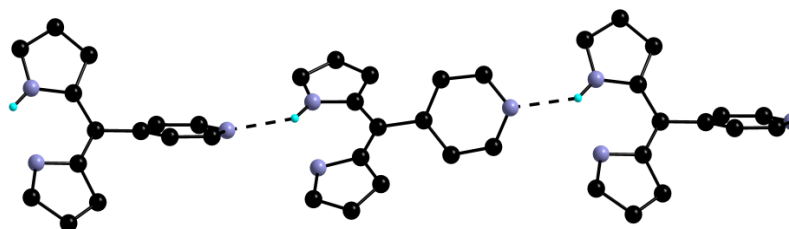


Fig. 80: Structure of the DPM-Py.¹⁴

Intermediate 5-aryl dipyrromethanes are stable enough to allow their purification. Crystal structures on some of the compounds have been reported.^{14,4} Such derivatives contain two H-donor centers offering the possibility of self-assembly by hydrogen bonding with solvent molecules or with secondary interaction sites. For example, the formation of a hydrogen bonded 1-D network is observed in the case of 5-(4-benzamide)-dipyrromethane by interaction between the pyrrolic protons and the amide moieties (**Fig. 81**).^{4b}

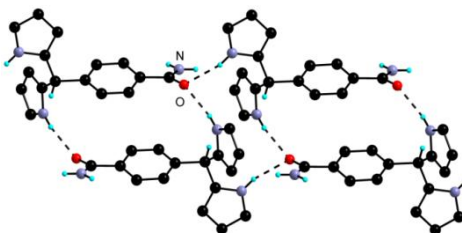
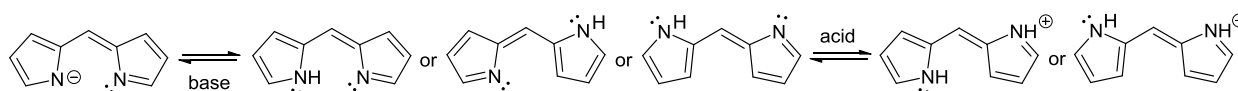


Fig. 81: Structure of 5-(4-benzamide)-dipyrromethane.^{4b}

Owing to the coexistence of both conjugated imine and amine functionalities, the DPM core presents an amphoteric character and may undergo two acid-base equilibria, leading to three distinct states: neutral⁶, cationic^{5,6}, and anionic. It's worth to note, that DPM exhibit rotation of the pyrrolyl group around the central methine linkage and may exist in different conformations.⁵



Scheme 28: Dipyrins acid-base equilibria.

For example upon reaction of *DPM-Ph-CN* with trifluoromethanesulfonic acid, the 1-D H-bond network $\{DPM-Ph-CN \cdot HOTf\}_\infty$ has been reported⁶ (**Fig. 82**).

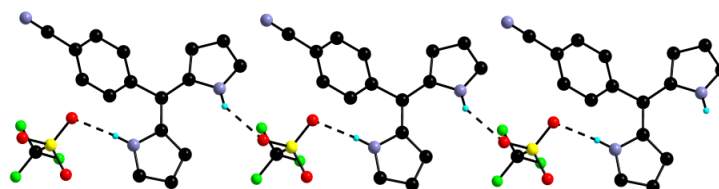
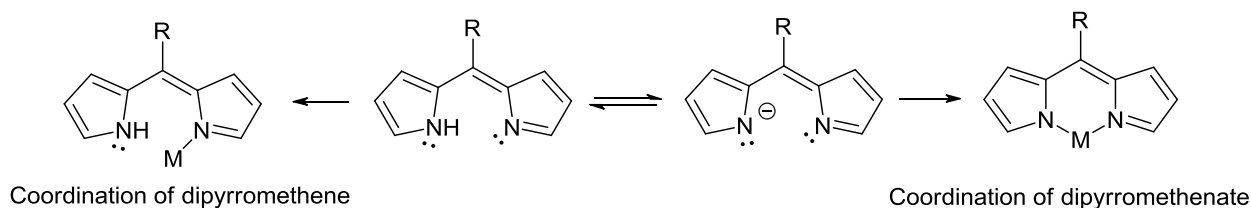


Fig. 82: Structure of protonated $\{DPM-Ph-CN \cdot HOTf\}_\infty$.

III.1.2. Two modes of coordination

As for 7-azaindole derivatives (see Chapter 1), the acid-base equilibrium provides two types of ligands, either neutral DPMs or their anionic conjugate base (**Scheme 29**). In the former case, these derivatives are monodentate ligands, while, in the latter case, chelate type coordination can occur. This mode of coordination is actually the one commonly observed for complexes incorporating DPMs.



Scheme 29: Two modes of coordination of DPMs.

III.1.2.1. Coordination chemistry of dipyrrens

Examples of complexes incorporating a DPM in its neutral state are scarce. To our knowledge, only one such compound synthesized in our laboratory by Domingo Salazar-Mendoza⁶ has been actually reported in the literature. The neutral ligand was obtained upon reaction of a benzonitrile appended DPM, DPM-Ph-CN, with $\text{Ag}(\text{BF}_4)$ affording homonuclear [2+2] metallamacrocycles.

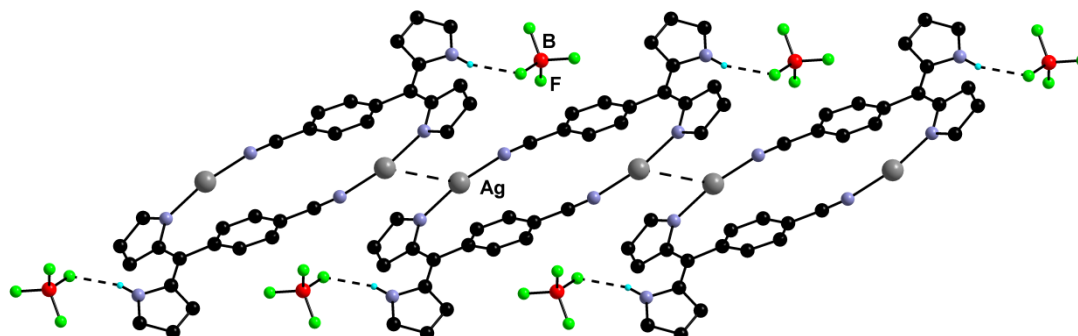


Fig. 83: Structure of $[\text{Ag}_2(\text{DPM-Ph-CN})_2](\text{BF}_4)_2$ complex.⁶

In these dicationic 2+2 metallamacrocycles (**Fig. 83**), two ligands bridge two Ag^+ cations. The silver atoms are linearly coordinated to one nitrile group and the non-protonated pyrrole nitrogen atom of the DPM moiety of a second ligand. These macrocycles in turn organize into 1-D network *via* d^{10} - d^{10} interactions⁷ between silver atoms ($d\text{Ag-Ag} = 3.396\text{\AA}$). The BF_4^- anions are hydrogen bonded to the NH of the uncoordinated pyrrole ring.

III.1.2.2. Coordination chemistry of dipyrinate

In comparison, homoleptic metal complexes of the conjugate base of *meso* substituted dipyrrens are well described and abundant in the literature. In these compounds, the ligand acts as a monoanionic chelate. As expected, depending on the coordination preference of the metal centers, different geometries of the complexes are observed. In the case of complexes of the $\text{M}(\text{DPM})_2$ type with divalent metal ions, the coordination geometry varies from square planar as in the case of palladium(II)⁸, *via* distorted tetrahedral for nickel(II)^{9,10} and copper(II)¹¹ ions, to tetrahedral for zinc(II) species¹² (**Fig. 84**). The square planar geometry in this type of species is nonetheless disfavored owing to steric repulsion of the α -CHs, explaining the distorted environment around the nickel ion in the reported structures of $\text{Ni}(\text{DPM})_2$ complexes.

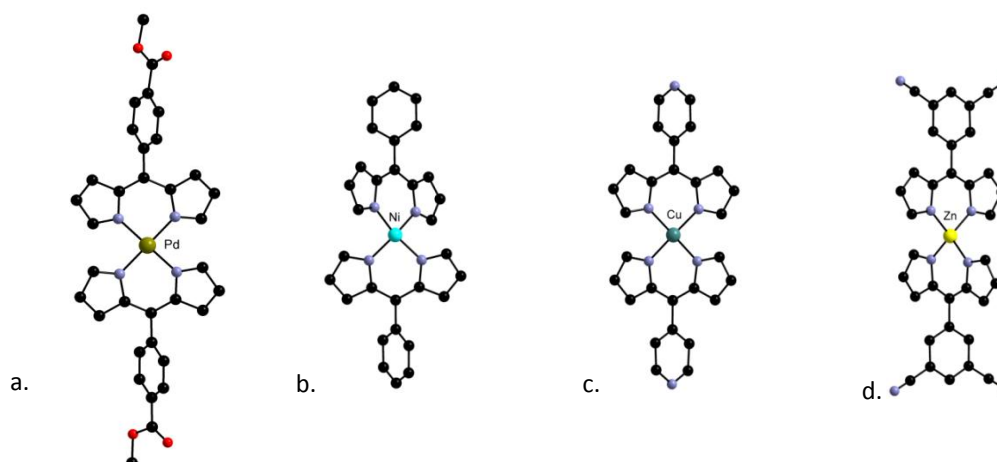
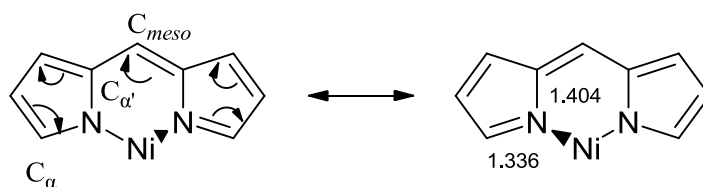


Fig. 84: Examples of homoleptic discrete complexes with Pd^{II} (a), Ni^{II} (b), Cu^{II} (c) and Zn^{II} (d).

In their report of the crystal structure of the $[\text{Ni}(\text{DPM-Ph})_2]$ complex, Brückner et al.⁹ described the influence of the resonance effect in the dipyrinyl moiety on bond organization in the core. Two bond types, short and long, were defined based on resonance description of the π -electrons in the ligand molecule. Considering two resonance structures on **Scheme 30** as limiting forms, the C_α -N bond would receive partial π -contribution, the $\text{C}_{\alpha'}$ -N bond would not. The difference in double bond character of these bonds explains the observed bond length differences in a qualitative way.



Scheme 30: Organization in the core of $[\text{Ni}(\text{DPM-Ph})_2]$ complex.

Regarding the N-M bond distances, for nickel ($[\text{Ni}(\text{DPM-Ph})_2]$) and copper ($[\text{Cu}(\text{DPM-4-Py})]$) complexes, all four Ni(Cu)-N distances are equal (1.879 Å and 1.951 Å). In the case of Zn(DPM-3,5-dicyanophenyl) complex, the Zn-M distances are around 1.97 Å.

Building on the first report by Dolphin¹⁵ of the synthesis and crystal structure of a $\text{Co}(\text{DPM-Ph})_3$ complex, Cohen and coworkers¹³ have developed a family of homoleptic complexes $\text{M}(\text{DPM})_3$, of trivalent metals with 4-pyridine moieties in the *meso* position of the DPM. Complexes with cobalt, iron¹³, indium and gallium¹⁴ were obtained and show an octahedral coordination environment (**Fig. 85**) and a pseudo-3-fold symmetry of the compound. The average N-M bond distances are 1.94 Å for $\text{M} = \text{Co}$, 1.96 Å for $\text{M} = \text{Fe}$, 2.20-2.25 Å for $\text{M} = \text{In}$ and 2.06 Å for $\text{M} = \text{Ga}$. Contrary to the cobalt and iron species, the indium complex is less symmetrical and two of the 4-pyridine-DPM ligands are canted from their associated N-In-N coordination planes.

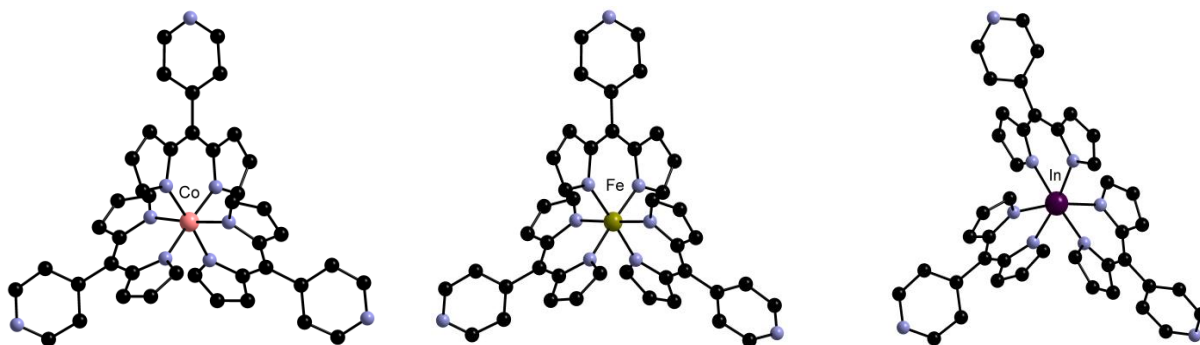


Fig. 85: Examples of DPM complexes with trivalent metals.

It is worth noting that the $[\text{Co}^{\text{II}}(\text{Ph-DPM})_2]$ ¹⁵ analogue has been reported, but this compound was air-sensitive and converts into the cobalt(III) tris-dipyrinato derivative. A series of stable homoleptic cobalt(II)/DPM complexes^{16,17} was prepared by introduction of methyl groups at the α position of the DPM (**Fig. 86**), probably inhibiting oxidation process for steric reasons, and preventing the formation of a tris chelate complex.

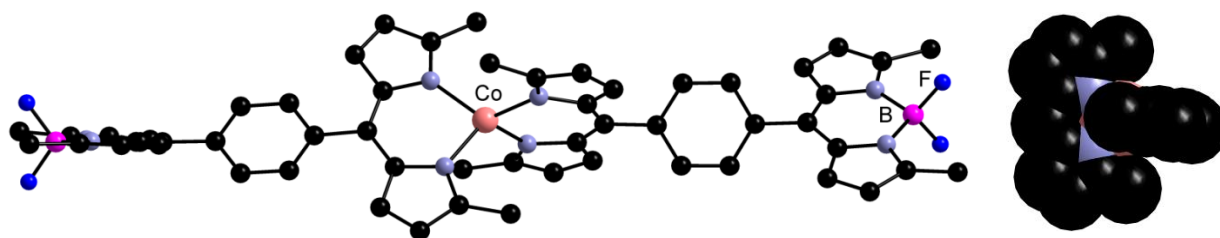


Fig. 86: Example of a homoleptic cobalt (II)/DPM complex.¹⁶

Heteroleptic complexes incorporating DPM have also been described. During the reaction of $\text{Co}^{\text{II}}(\text{salen})$ (N,N' -bis(salicylidene)ethylenediamine) complex with the DPM-PH-CN ligand, the oxidation from Co^{II} to Co^{III} and formation of the heteroleptic complex $[\text{Co}(\text{DPM-Ph-CN})(\text{salen})]$ are observed.⁶ In this compound (**Fig. 87**), the $\text{Co}(\text{III})$ center adopts an octahedral coordination geometry and is surrounded by the salen and the deprotonated DPM moieties as dianionic tetradentate and monoanionic chelate-type ligands, respectively. The salen moiety adopts a twisted conformation.

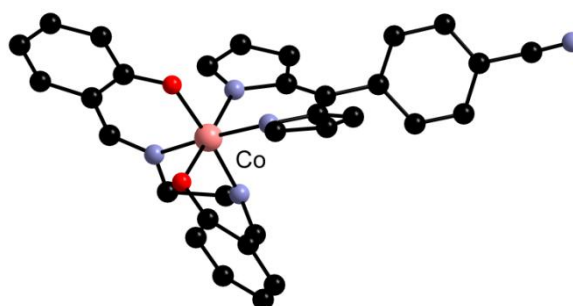


Fig. 87: Structure of $[\text{Co}(\text{DPM-Ph-CN})\text{SALEN}]$ complex.⁶

Several heteroleptic discrete complexes with copper have been reported.¹¹ Thus, the $(\text{acac})\text{Cu}(\text{DPM-}p\text{-PhCN})$ and $(\text{acac})\text{Cu}(\text{DPM-}o\text{-py})$, complexes crystallize as isolated molecules with square planar $\text{Cu}(\text{II})$ ions^{11,21} (**Fig. 88**) with the same Cu-N distances (1.95 Å) in both cases. Regarding the Cu-O distances, the bond lengths are 1.93-1.94 and 1.91 Å respectively. Other heteroleptic copper complexes of the $(\text{acac})\text{Cu}(\text{DPM})$ and $(\text{hfac})\text{Cu}(\text{DPM})$ types have been also reported as described in the following section.

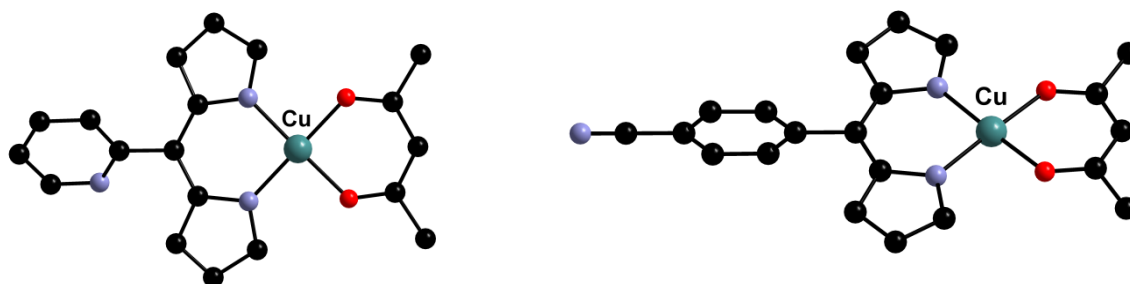


Fig. 88: Structure of heteroleptic discrete complexes $(\text{acac})\text{Cu}(\text{DPM-}p\text{-PhCN})$ and $(\text{acac})\text{Cu}(\text{DPM-}o\text{-py})$.¹¹

III.1.3. Networks

The above mentioned complexes crystallize as discrete species, they can however organize into infinite architectures. Indeed, complexes incorporating a dipyrin bearing a secondary peripheral coordinating group can self-assemble when the metal center features at least one site available for further coordination leading to homonuclear networks, while upon reaction with a second metal centre, heteronuclear architectures can be obtained. Work along both approaches have been reported, a brief overview is given here.

III.1.3.1. Homonuclear networks

Complexes of the $(\text{hfac})_2\text{Cu}$ type (hfac = hexafluoroacetylacetonate) are known to form coordination polymers upon association with polypyridyl ligands.¹⁸ Taking advantage of this observation, Cohen and coworkers have developed a family of heteroleptic copper complexes, $(\text{hfac})\text{Cu}(\text{DPM})$ and $(\text{acac})\text{Cu}(\text{DPM})$, with DPMs bearing a peripheral coordinating group in order to promote self-assembly of these species.^{11,19,20,21}

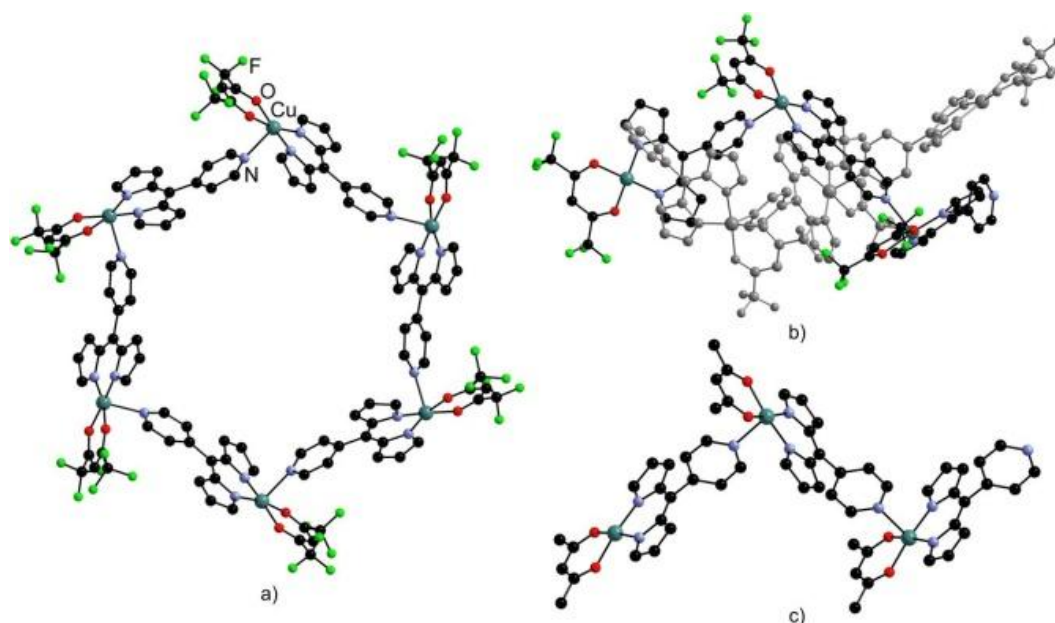


Fig. 89: Hexagonal arrangement (a) and supramolecular helix (one strand is shown in faded gray) (b) coexist in the crystal structure of $(\text{hfac})\text{Cu}(\text{DPM-}p\text{-py})$ while 1-D zig-zag chains are observed in the case of $(\text{acac})\text{Cu}(\text{DPM-}p\text{-py})$ (c)^{19,11}. Hydrogen atoms have been omitted for clarity.

The crystal structure of $(\text{hfac})\text{Cu}(\text{DPM-}p\text{-py})$ revealed a beautiful example of a coexistence of two supramolecular arrangements, a discrete hexagon and a double helix both resulting from the coordination of the pyridyl group to the copper centre of a neighboring complex leading to penta-coordinated Cu(II) ions (**Fig. 89a** and **b**).¹⁹ This unique organization appears to be promoted by the presence of the fluorine atoms on the hfac capping ligand. Indeed, the $(\text{acac})\text{Cu}(\text{DPM-}p\text{-py})$ analogue (**Fig. 89c**) organizes into zigzag chains.¹¹ Furthermore, no steric effect of the peripheral pyridyl group could be observed, since the $(\text{hfac})\text{Cu}(\text{DPM-}p\text{-quin})$ also forms hexagons, although solely this organization is present in the crystal structure with the absence of double helices.²¹ The zigzag chain arrangement is the most encountered one as it is observed in the crystal structure of a series of complexes: $(\text{hfac})\text{Cu}(\text{DPM-}m\text{-py})$, $(\text{acac})\text{Cu}(\text{DPM-}m\text{-py})$, $(\text{hfac})\text{Cu}(\text{DPM-}m\text{-quin})$, $(\text{hfac})\text{Cu}(\text{DPM-}p\text{-PhSMe})$.^{11,20,21} As expected, the self-assembly of these heteroleptic species is dependent on the position of the peripheral coordinating group and its nature.

III.1.3.2. Heteronuclear networks

III.1.3.2.1. Coordination to a second metal centre at the peripheral group

The use of homoleptic $M(\text{DPM-}p\text{-py})_3$ complexes ($M = \text{Co(III)}, \text{Fe(III)}, \text{In(III)}, \text{Ga(III)}$) as metallatectons for the formation of heterometallic MOFs upon association with Ag^+ salts has been thoroughly investigated by the group of Cohen.¹³ In a seminal paper, both $\text{Fe}(\text{DPM-}p\text{-py})_3$ and $\text{Co}(\text{DPM-}p\text{-py})_3$ were shown to form MOFs (**Fig. 90a** and **b**) upon association with $\text{Ag}(\text{OTf})$ and $\text{Ag}(\text{BF}_4)$. The Ag^+ ions are coordinated to three pyridyl groups and interact with the anion, while the metalloligands retain their octahedral coordination geometry. These 3-D networks with (10,3) topology were shown to be doubly interpenetrated in the crystal. Interestingly, upon reaction with $\text{Ag}(\text{XF}_6)$ ($X = \text{P}, \text{Sb}$), 2-D honeycomb networks were obtained resulting again from the coordination of three pyridyl groups to the Ag^+ ion (**Fig. 90c**).²² The directing effect of the anion remains unclear given that a pseudo-polymorph of the $\{[\text{Co}(\text{DPM-}p\text{-py})_3]\text{Ag}\}_\infty(\text{PF}_6)$ network was also obtained featuring a 3-D structure with (10,3) topology. Furthermore, the study of the association of $\text{In}(\text{DPM-}p\text{-py})_3$ and $\text{Ga}(\text{DPM-}p\text{-py})_3$ with silver salts also demonstrated that both 3-D and 2-D organizations could be obtained with PF_6^- .¹⁴ It nonetheless appears that with the OTf^- and BF_4^- salts, 3-D structures are favored, while 2-D arrangements are favored in the presence of SbF_6^- anions.

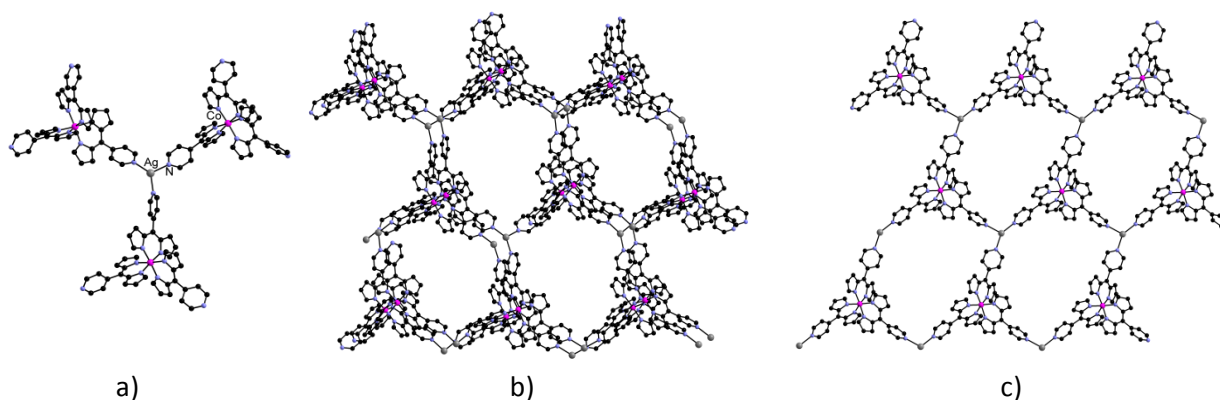


Fig. 90: Coordination around the silver atom (**a**) and view of the 3-D network (**b**) in $\{[\text{Co}(\text{DPM-}p\text{-py})_3]\text{Ag}\}_\infty(\text{OTf})(\text{CH}_3\text{CN})_2$; view of the 2-D network (**c**) in $\{[\text{Co}(\text{DPM-}p\text{-py})_3]\text{Ag}\}_\infty(\text{PF}_6)(\text{C}_6\text{H}_6)_{0.5}$.^{21,22} Hydrogen atoms, solvent molecules and anions are not shown for clarity.

This series of MOFs highlights the soundness of the approach given that isomorphous networks can be obtained with four different metal centers, namely $\text{Co(III)}, \text{Fe(III)}, \text{In(III)}, \text{Ga(III)}$. Moreover, crystals of mixed metal frameworks $\{[\text{Co/Fe}(\text{DPM-}p\text{-py})_3]\text{Ag}\}_\infty(\text{BF}_4)$ could also be obtained upon using a mixture of the starting metallatectons. The robustness of these frameworks was in addition exemplified in two ways. First, immersions of crystals of $\{[\text{Co}(\text{DPM-}p\text{-py})_3]\text{Ag}\}_\infty(\text{OTf})$ in solutions of ammonium salts of either BF_4^- or PF_6^- allowed complete displacement of the triflates and anion exchange in a single-crystal to single-crystal fashion. The absence of conversion from one network topology to the other depending on the anion introduced is also noteworthy. Secondly, the structure of the DPM was altered to probe its influence on the formation of the MOFs. Upon reaction of the modified $\text{Fe}(\text{DPM-}p\text{-quin})_3$ complex with $\text{Ag}(\text{OTf})$, crystals of a $\{[\text{Fe}(\text{DPM-}p\text{-quin})_3]\text{Ag}\}_\infty(\text{OTf})$ MOF with a (10,3) network topology were obtained.²² Another ligand modification validated even more the construction approach since the extended $\text{Co}(\text{DPM-}p\text{-PhCCpy})_3$ afforded also a MOF with (6,3) network topology upon association with $\text{Ag}(\text{PF}_6)$ (**Fig. 91**). The analogy between this framework and the parent one (**Fig. 90c**) is striking in spite of the doubling of the length of the DPM. These frameworks showed good thermal stability with a maximum weight loss of 5% below 260 °C. Larger weight losses were observed above 400 °C.

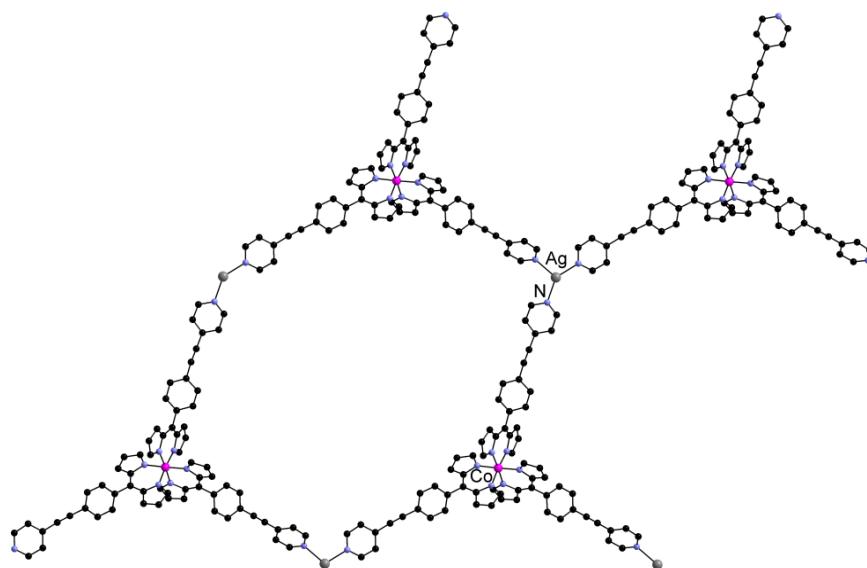


Fig. 91: A fraction of the expanded 2-D network with (6,3) topology in the structure of $\{[\text{Co}(\text{DPM-}p\text{-PhCCpy})_3]\text{Ag}\}_x(\text{PF}_6)(\text{C}_6\text{H}_6)_4$.²² Hydrogen atoms, solvent molecules and anions are not shown for clarity.

These heterometallic networks obtained with homoleptic $\text{M}(\text{DPM})_3$ complexes with a pyridine appended dipyrin do not feature any chirality given that both Λ and Δ enantiomers of the tris chelate species are present in the structure. Rather interestingly, an analogous reaction combining $\text{Co}(\text{DPM-}p\text{-PhCN})_3$ and $\text{Ag}(\text{OTf})$ afforded a chiral MOF with (10,3) topology where the silver ion are coordinated to three CN groups.²³ Only one enantiomer of the Co(III) complex is present within a crystal while the crystal batch as a whole is a racemate. This MOF features eight fold interpenetrations. This compound has been demonstrated to be stable up to 350 °C. While crystals of this MOF contain benzene molecules, they can be exchanged for toluene, *p*-xylene and ethylbenzene. Furthermore, evacuated crystals were shown to uptake toluene, ethylbenzene, nitrobenzene and *m*-nitrotoluene with better uptakes for the latter two solvents.²³

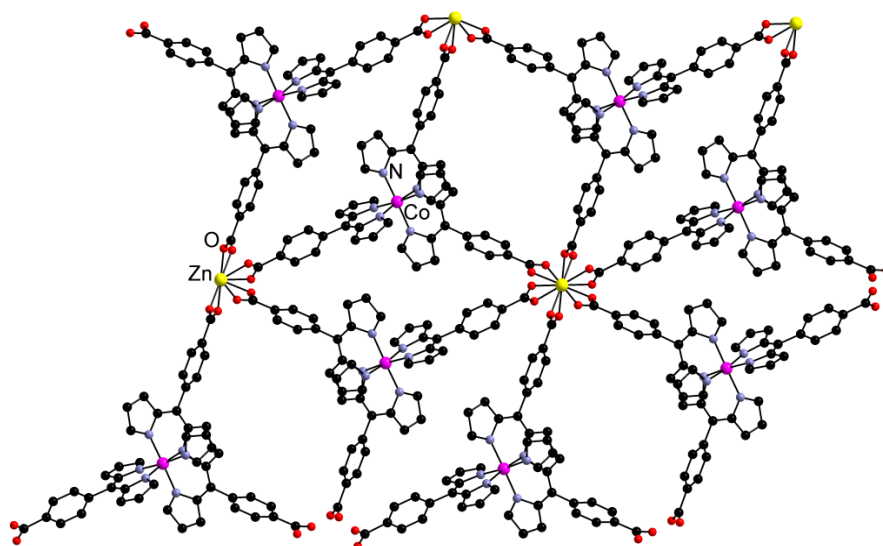


Fig. 92: A 2-D MOF obtained by solvothermal reaction between *rac*- $\text{Co}(\text{DPM-}p\text{-PhCO}_2\text{H})_3$ and $\text{Zn}(\text{NO}_3)_2 \cdot 4\text{H}_2\text{O}$.²⁴ Hydrogen atoms and solvent molecules have been omitted for clarity.

An attempt to obtain MOFs starting from pure enantiomers of homoleptic Co(III) complexes was performed by Cohen, Telfer and coworkers using $\text{Co}(\text{DPM-}p\text{-PhCO}_2\text{H})_3$.²⁴ Starting from the racemic mixture of both Δ and Λ enantiomers, solvothermal reaction with $\text{Zn}(\text{NO}_3)_2 \cdot 4\text{H}_2\text{O}$ led to the isolation of two crystalline MOFs depending on the reaction conditions. Both MOFs are thermally stable up to 400 °C. They differ by the nuclearity of the Zn cluster formed acting as a node and by their dimensionality, one being 2-D (**Fig. 92**) while the other is 3-D. Rather surprisingly, under the same reactions conditions, the use of the enantiopure Δ or Λ species yielded only amorphous and thermally unstable compounds.

III.1.3.2.2. Assistance of Ag- π interactions

In our laboratory, the self assembly of homo- and heteroleptic complexes bearing peripheral nitrile groups with silver salts has been investigated.^{6,12} Interestingly, it has been observed that reaction of $(\text{hfac})\text{Cu}(\text{DPM-}p\text{-PhCN})$ and $\text{Cu}(\text{DPM-}p\text{-PhCN})_2$ with $\text{Ag}(\text{OTf})$ afforded crystals of heterometallic architectures where the Ag^+ ion is coordinated to the triflate anion, the peripheral nitrile of the metallatecton but located above a C=C bond of the pyrrolic ring of the DPM with an average Ag-C distance of 2.56 Å (**Fig. 93**).¹² This suggests a Ag- π interaction as observed with many aromatics.²⁵ Interestingly, while this interaction was been observed and studied in solution with pyrrolic derivatives, it had not been characterized in the solid state.²⁶

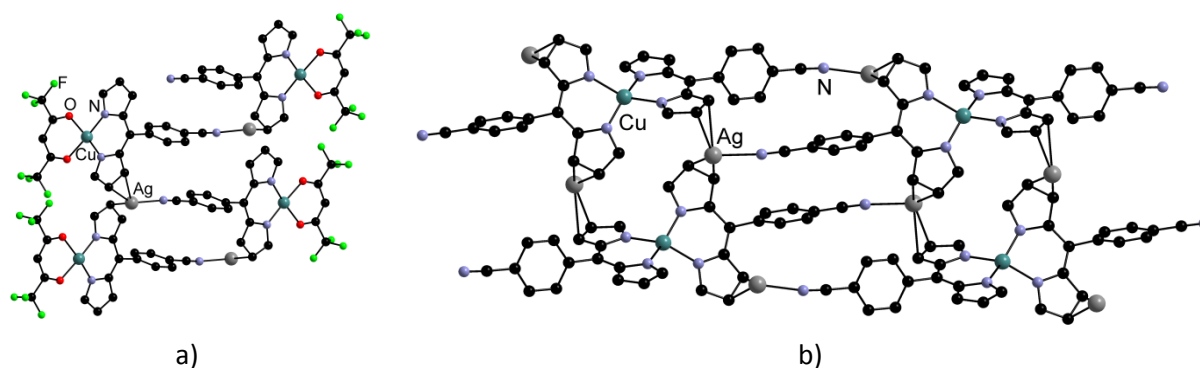


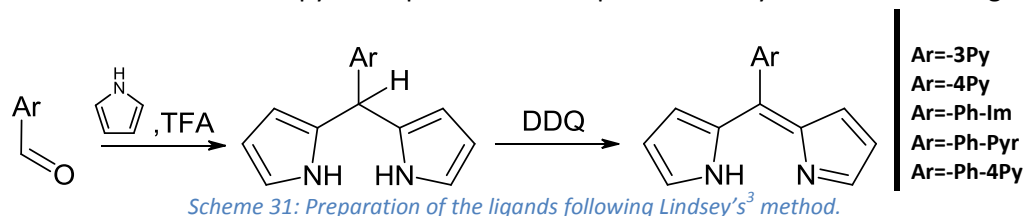
Fig. 93: Ag- π interactions in $\{[(\text{hfac})\text{Cu}(\text{DPM-}p\text{-PhCN})]\text{Ag}\}_\infty(\text{OTf})(\text{C}_6\text{H}_6)_{1.5}$ (a) and in $\{[\text{Cu}(\text{DPM-}p\text{-PhCN})_2]\text{Ag}_2(\text{H}_2\text{O})\}_\infty(\text{OTf})_2$ (b). Hydrogen atoms, anions and solvent molecules have been omitted for clarity.

The same type of complexation is also observed with $\text{Zn}(\text{DPM-}m\text{-Ph}(\text{CN})_2)_2$, $(\text{hfac})\text{Cu}(\text{DPM-}m\text{-Ph}(\text{CN})_2)$ and $(\text{salen})\text{Co}(\text{DPM-}p\text{-PhCN})$ ($\text{salen} = \text{N,N}'\text{-bis}(\text{salicylidene})\text{ethylenediamine}$) upon association with various silver salts.^{6,12} This underlines the absence of directing effect of the metal centre, of the position of the nitrile group(s) as well as of the nature of the silver salt in the presence of the Ag- π interaction in this system. It should be noted that the absence of such mode of complexation in the reported chiral MOF $\{[\text{Co}(\text{DPM-}p\text{-PhCN})_3]\text{Ag}\}_\infty(\text{OTf})$ might be explained by the homoleptic nature of the octahedral metallatecton which sterically hinders the access to the C=C bond of the pyrrolic rings.²³

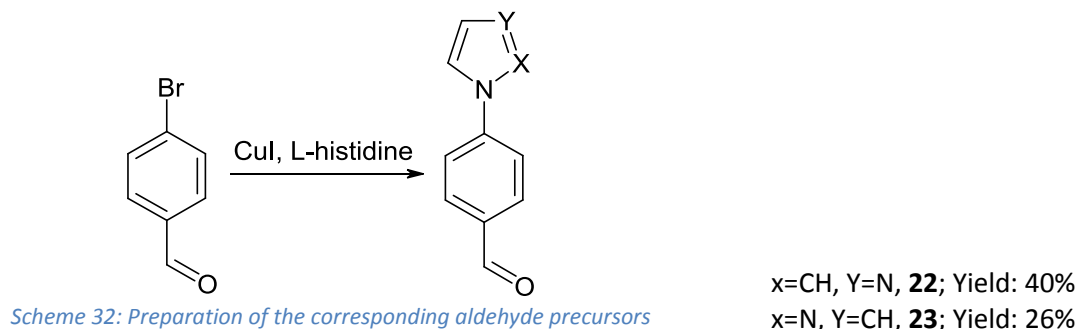
In light of these results, it appears that α,β -unsubstituted dipyrins bearing a peripheral secondary coordinating group are interesting ligands for the preparation of extended homo- and heterometallic architectures. In this work, the emphasis has been put on such derivatives bearing a peripheral heterocyclic nitrogen coordinating group. Indeed, pyridines as well as imidazole and pyrazole are known to form complexes with a variety of metal ions. The result of these investigations is reported in the following section.

III.2. Preparation of the ligand

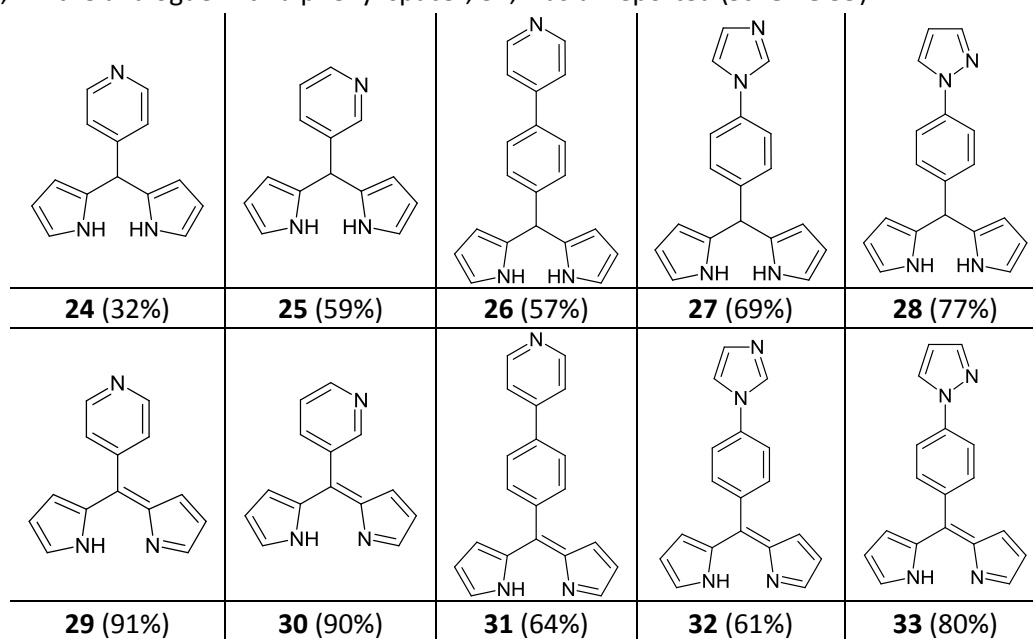
Five ligands consisting of a DPM group as a primary coordination pole and a nitrogen based heterocyclic moieties as a second coordination pole were synthesized. Pyridine, imidazole and pyrazole groups were employed. These compounds were prepared following the synthetic pathway developed by Lindsey and co-workers (**Scheme 31**).³ Reaction of the corresponding aldehyde in neat pyrrole in the presence of a catalytic amount of TFA provides the desired dipyrromethane. The latter is readily oxidized with DDQ to afford the dipyrin in pure form after purification by column chromatography.



While the aldehyde precursors for the synthesis of the pyridine functionalized DPMs are commercially available, the ones for the imidazole and pyrazole appended were prepared by a Cu(I)-catalyzed reaction of *p*-bromobenzaldehyde with the corresponding heterocycle (**Scheme 32**).²⁷



While the synthesis of the two dipyrromethanes containing 4- and 3-pyridine as a secondary coordination pole (**24**, **25**) and the corresponding dipyrins has been already described by Cohen and co-workers,^{11,14} the analogue with a phenyl spacer, **31**, was unreported (**Scheme 33**).



*Scheme 33: Ligands **29-33** and corresponding dipyrromethanes **25-28**. Yields are given in parantheses.*

The structure of two dipyrromethane derivatives, **27** and **28**, and two dipyrrens, **31** and **32**, was determined by single crystal X-ray diffraction. Both dipyrromethanes **27** and **28** were crystallized by slow diffusion of *n*-pentane vapors into a THF solution containing the ligand. The former crystallizes in the triclinic space group *P*-1, while the latter crystallizes in the monoclinic space group *P*2₁/*n* with one molecule in general position. In **27**, one imidazole nitrogen atom is hydrogen bonded with the pyrrolic N-H of two neighboring molecules, leading thus to the formation of one-dimensional chains along the *c* axis (**Fig. 94a**). This type of arrangement is reminiscent of reported crystal structures of other α,β -unsubstituted dipyrromethanes⁴ for example with 4-benzamide moiety^{4b} (**Fig. 81**). In **28**, a single hydrogen bond is identified between a pyrrolic N-H and a pyrazole N atom leading again to a 1-D chain (**Fig. 94b**) analogous to the organization of DPM-Py¹⁴ (**Fig. 80**).

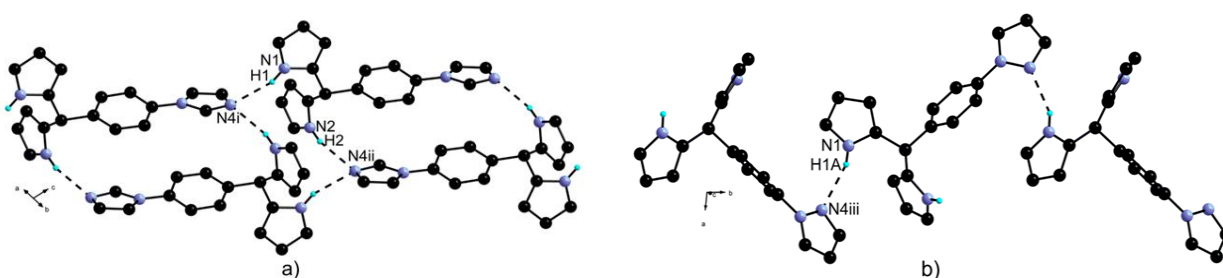


Fig. 94: H-bond interactions in crystal structure of dipyrromethanes **27** (a) and **28** (b).

Dipyririn **32** crystallized by slow diffusion of *n*-pentane in a THF solution of the ligand. It crystallizes in the monoclinic space group *C*2/*c* with one molecule in general position (**Fig. 95a**). Owing to the conjugation, the two pyrrolic rings are almost coplanar (6.7 °).

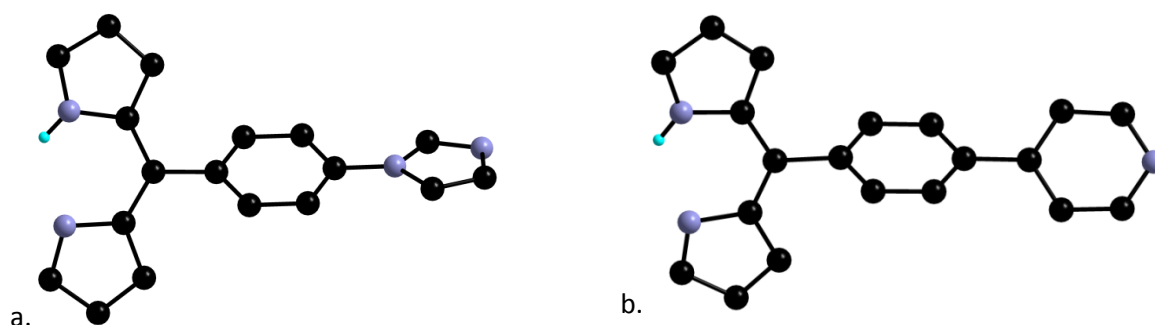


Fig. 95: Structure of ligands **32** (a) and **31** (b).

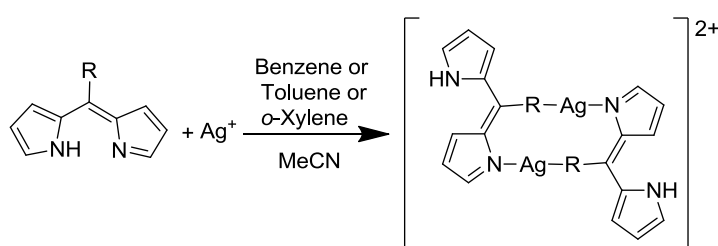
Dipyririn **31** crystallized by slow diffusion of *n*-pentane vapors into a CHCl₃ solution of the ligand. Compound **31** crystallizes in the monoclinic space group *P*2₁/*n* with one molecule in general position (**Fig. 95b**). The two pyrrolic rings are here again almost coplanar (dihedral angle 4.2 °). The phenyl and pyridine rings are not coplanar but form an angle of 31.7 °. In neither of the two structures, any strong hydrogen bonds could be identified, unlike in the reported structure of **24** (**Fig. 80**).¹⁴

III.3. Preparation of complexes and networks

III.3.1. Neutral dipyrrens as ligands for the preparation of [2+2] macrocycles with silver ions

As described in the introduction, only one example of a metal complex, a [2+2] metallamacrocycle, incorporating a neutral dipyrren has been reported. It therefore appeared interesting to use dipyrrens **29-33** for such purpose and, in particular, to investigate the possibility to expand the family of metallamacrocycles with silver ions using ligands **29**, **31** and **32** which show structural similarity with the reported DPM-Ph-CN. Unfortunately, no complexes could be obtained in crystalline form with dipyrrens **30** and **33**.

Reaction of a solution of dipyrren with a solution (benzene or toluene or *o*-xylene) of silver salts under stoichiometric conditions (1:1), subsequent addition of MeCN to dissolve the resulting precipitate and crystallization of the complexes by slow solvent evaporation (**Scheme 34**) at room temperature in the absence of light led to the isolation of a series of macrocycles in yields ranging from 42 % to 74 % (**Table 12**). These compounds were analyzed by single-crystal X-ray diffraction, UV visible spectroscopy and elemental analysis. Depending on the solubility of these species, ^1H -, ^{13}C - and DOSY-NMR studies were also performed.



Scheme 34: Preparation of the macrocycles **34-40**.

Macrocycles/Yields(%)		
34	$[\text{Ag}(\text{DPM-4Py})_2(\text{OTf})_2(\text{Benzene})_3]$	42
35	$[\text{Ag}(\text{DPM-4Py})_2(\text{SbF}_6)_2]$	67
36	$[\text{Ag}(\text{DPM-4Py})_2(\text{BF}_4)_2(\text{H}_2\text{O})_2]$	61
37	$[\text{Ag}(\text{DPM-Ph-4Py})_2(\text{PF}_6)_2]$	67
α - 38	$\alpha\text{-}[\text{Ag}(\text{DPM-Ph-4Py})_2(\text{BF}_4)_2(\text{MeCN})_2]$	74
β - 38	$\beta\text{-}[\text{Ag}(\text{DPM-Ph-4Py})_2(\text{BF}_4)_2(\text{MeCN})_2]$	mix
39	$[\text{Ag}(\text{DPM-Ph-4Py})_2(\text{OTf})_2]$	52
40	$[\text{Ag}(\text{DPM-Ph-Im})_2(\text{OTf})_2(\text{MeCN})_3]$	68

Table 12: Macrocycles and corresponding yields.

In all cases, dicationic [2+2] metallamacrocycles composed of two Ag^+ cations bridged by two dipyrrens were obtained. The silver ions are linearly coordinated to the secondary coordination pole of the ligand and the non-protonated pyrrolic nitrogen of the DPM moiety of the second dipyrren. As expected, this type of organization is very similar to the one observed with DPM-Ph-CN ligand (**Fig. 83**).⁶ In this type of macrocycles, three different isomers can be imagined (**Fig. 96**), depending on the configurations of the ligand moieties. In the case of the reported⁶ macrocycle $[\text{Ag}_2(\text{DPM-Ph-CN})_2](\text{BF}_4)_2$ the structure of the DPM moieties is not the same as the one observed in the structure of the free ligand and adopts an *E*-anti arrangement with formation of “out-out” isomer. Depending on the crystallization conditions and the nature of the anion, these macrocycles organize either into discrete complexes or extended networks. We will now describe the crystal structure and conformational preferences of these compounds.

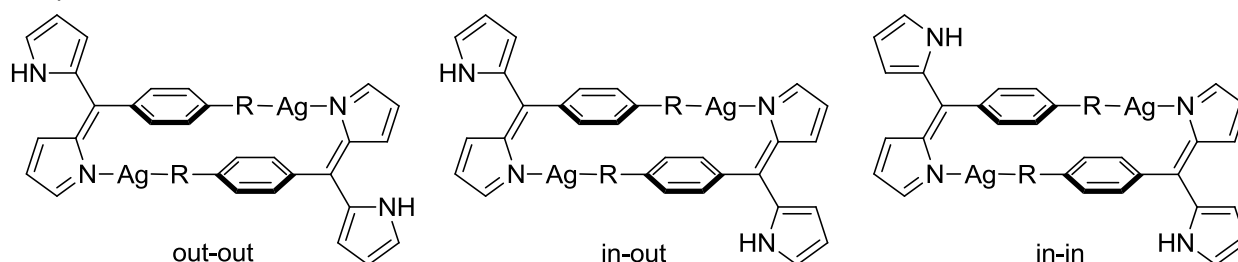


Fig. 96: Different possible conformations of the free pyrrolic rings in the [2+2] metallamacrocycle $[\text{Ag}_2(\text{DPM-Ph-R})_2]^{2+}$.

Macrocycle $[\text{Ag}(\text{DPM-4Py})]_2(\text{OTf})_2(\text{Benzene})_3$, **34**, crystallizes in the triclinic space group $P-1$ with one ligand **29**, a silver cation, a triflate anion and one benzene solvent molecule in general positions and an additional benzene molecule on an inversion centre. The macrocycle features an “out-out” conformation (**Fig. 97**). The Ag^+ is in a linear coordination environment bonded to one nitrogen atom of a pyrrolic ring and the pyridyl nitrogen atom of another molecule of **29** with bond distances close to the ones expected for such compounds (**Table 13**).⁶ A long Ag-O distance of 2.755(7) Å is observed with the triflate anion. Within the macrocycle, the Ag^+ cation is located above the pyridyl ring with the shortest Ag-C distance of 3.037(9) Å, rather long to suggest any Ag- π interactions.^{25d} The pyrrolic NH pointing outward the macrocycle is hydrogen bonded to an oxygen atom of a triflate anion ($d(\text{N-H}\cdots\text{O})=2.907(9)$ Å; $\alpha(\text{N-H}\cdots\text{O})=148.7^\circ$), leading to the formation of a 1-D H-bond network (**Fig. 97**). The two pyrrolic rings are coplanar within the DPM moieties. The latter seem to stack within the network with distances between centroids of corresponding pyrrole rings of 3.333 Å and 3.567 Å, suggesting additional π - π staking between the macrocycles.

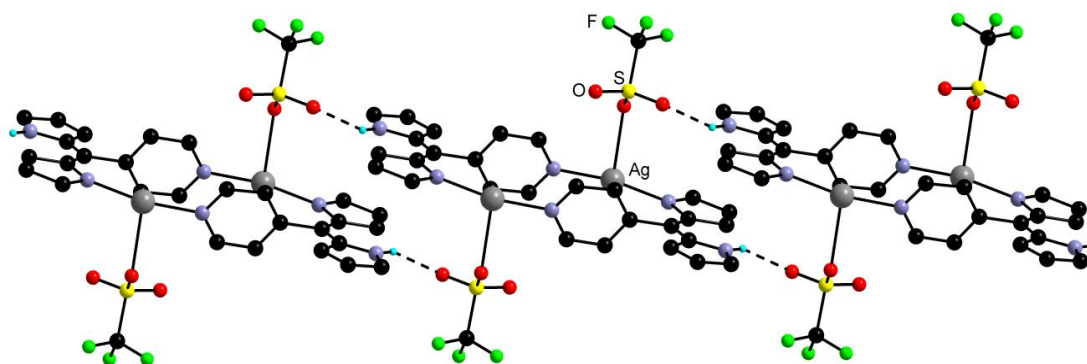


Fig. 97: 1-D H-bond network in the structure of macrocycle 34.

Macrocycle $[(\text{DPM-4Py})\text{Ag}]_2(\text{SbF}_6)_2$, **35**, crystallizes in the monoclinic space group $C2/c$ with one ligand **29**, a silver cation and one SbF_6^- anion in general positions. Here again the Ag^+ cation is in a linear coordination environment with Ag-N distances (**Table 13**) similar to the ones observed in **34**, but in this case the macrocycle features an “in-in” conformation. Long Ag-F distances of 2.896 and 2.936 Å are observed with the SbF_6^- anion. The pyrrolic N-H pointing inward also interacts with the SbF_6^- anion via a N-H \cdots F hydrogen bond. This leads to the formation of a 1-D H-bond network (**Fig. 98**).

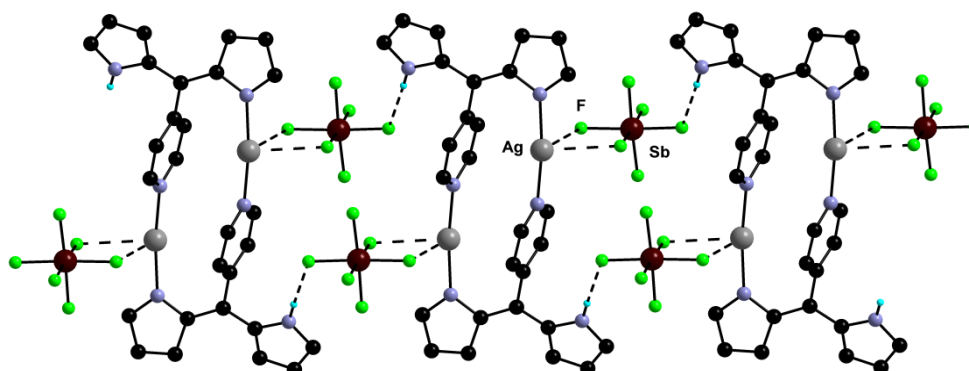


Fig. 98: 1-D H-bond network in the structure of macrocycle 35.

Macrocycle $[(\text{DPM-4Py})\text{Ag}(\text{H}_2\text{O})]_2(\text{BF}_4)_2$, **36**, crystallizes in the monoclinic space group $P2_1/n$ with one ligand, silver cation, water and anion molecules in general position. It adopts an “out-out” conformation. The Ag^+ cation is in a linear coordination environment the pyridyl and pyrrolic groups (**Table 13**). A water molecule is bound to the silver ion (2.612 Å), leading to an overall T-shape environment. Hydrogen bonding interactions between fluorine atoms of the BF_4^- anion and the hydrogen atoms of the water molecule ($d(\text{F}\cdots\text{H-O})=2.795(6); 2.876(6)\text{Å}$) combined with interaction with the pyrrolic N-H ($d(\text{F}\cdots\text{H-N})=2.927(3)\text{Å}$, $\alpha((\text{F}\cdots\text{H-N})=144.5^\circ$) lead to the formation of a 3-D H-bond network (**Fig. 99**).

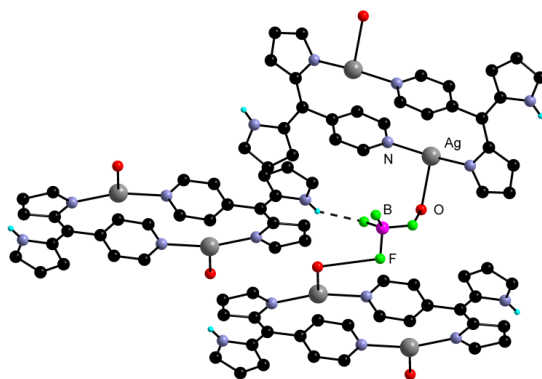


Fig. 99: 3-D H-bond network in the structure of macrocycle **36**.

Three of the four fluorine atoms of BF_4^- anion are included in H-bond interactions. Each water molecule in turn interacts with two fluorine atoms of two neighboring anions molecules. Finally, water molecules and fluorine atoms form a 1-D H-bond network with alternate $\{\text{O-H}\cdots\text{F-B-F}\cdots\text{H}\}$ fragments, the second dimensionality takes place via the $\text{F}\cdots\text{H-N}$ interaction and finally the third dimension stems from the O-Ag fragment.

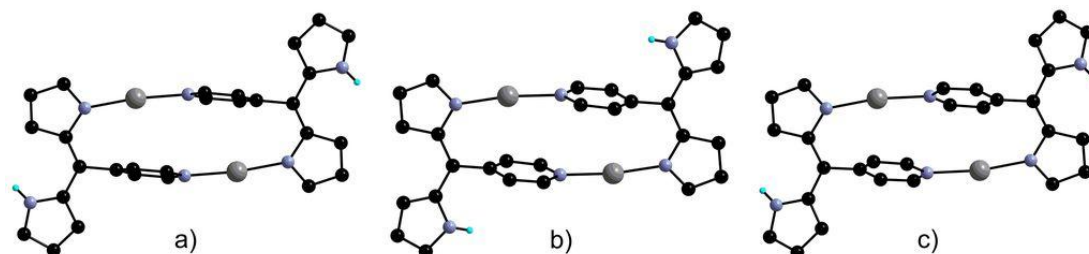


Fig. 100: Macrocycles **34-36**.

Within this series, no striking difference in the geometry of the macrocycles themselves are observed (**Fig. 100**, **Table 13**). This is not surprising given that the most important degree of freedom is in the angle between the coordinated pyrrolic and pyridyl rings. Two of the complexes adopt “out-out” conformation (**34** and **36**) and only one is in “in-in”. The extension to ligand **29** featuring an additional phenyl ring demonstrates the flexibility yet robustness of this architecture (**Fig. 106**).

	Ag-N(pyrrole) Å	Ag-N(py/im) (Å)	N-Ag-N (°)
$[\text{Ag}(\text{DPM-4Py})]_2(\text{OTf})_2(\text{Benzene})_3$	2.132(6)	2.152(6)	169.7(2)
$[\text{Ag}(\text{DPM-4Py})]_2(\text{SbF}_6)_2$	2.127(9)	2.131(8)	170.8(3)
$[\text{Ag}(\text{DPM-4Py})]_2(\text{BF}_4)_2(\text{H}_2\text{O})_2$	2.1475(19)	2.178(2)	165.30(8)
$[\text{Ag}(\text{DPM-Ph-4Py})]_2(\text{OTf})_2$	2.132(2)	2.153(2)	171.89(8)
$\alpha\text{-}[\text{Ag}(\text{DPM-4Py})]_2(\text{BF}_4)_2(\text{MeCN})_2$	2.146(3)	2.168(3)	170.97(11)
$\beta\text{-}[\text{Ag}(\text{DPM-4Py})]_2(\text{BF}_4)_2(\text{MeCN})_2$	2.121(2)	2.141(2)	171.15(19)
$[\text{Ag}(\text{DPM-Ph-4Py})]_2(\text{PF}_6)_2$	2.127(3)	2.157(3)	169.37(11)

Table 13: Bond distances (Å) and angles (°) in silver environment of macrocycles **34-40**.

Macrocycle $[(\text{DPM-Ph-4Py})\text{Ag}]_2(\text{PF}_6)_2$, **37**, crystallizes in the monoclinic space group $P2_1/n$ with one ligand **31**, a silver cation and a PF_6^- anion in general positions. In this case, the phenyl and pyridyl rings are almost coplanar with a 7.57° dihedral angle. As in **34-36**, the silver cation features a linear coordination environment with similar Ag-N distances (**Table 13**). The PF_6^- anion is hydrogen bonded to the pyrrolic N-H pointing inward (**Fig. 101**), the distance between silver ions and neighboring fluorine atoms is $3.107(2) \text{ \AA}$. No extended network is observed in this structure.

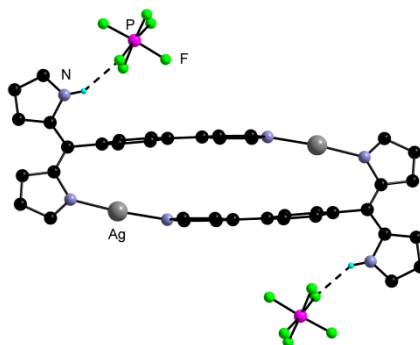


Fig. 101: Structure of macrocycle **37**.

Upon reacting ligand **31** with AgBF_4 , two polymorphs were obtained depending on the mixture of solvents used for crystallization. Upon slow evaporation of a benzene/MeCN mixture, crystals of α - $[(\text{DPM-Ph-4Py})\text{Ag}]_2(\text{BF}_4)_2(\text{MeCN})_2$ (α -**38**), were obtained (**Fig. 102**). This phase crystallizes in the triclinic space group $P-1$ with one ligand **31**, a silver cation, a BF_4^- anion and an acetonitrile molecule in general positions. The phenyl and pyridyl rings are almost coplanar as in **34** (9.12°). In the case of a toluene/MeCN mixture, crystals of both α - and β - $[(\text{DPM-Ph-4Py})\text{Ag}]_2(\text{BF}_4)_2(\text{MeCN})_2$ (β -**38**) were obtained (**Fig. 103**). This second phase, β , crystallizes in the monoclinic $P2_1/n$ space group with one ligand **31**, a silver cation, a BF_4^- anion and an acetonitrile molecule in general positions. Although these two structures are rather similar (**Table 13**), they differ in the orientation of the MeCN solvate molecules and the angles between the phenyl and pyridine rings (27.07° for β -**38**). Both compounds form discrete complexes with BF_4^- anion hydrogen bonded to the pyrrolic N-H (**Table 14**).

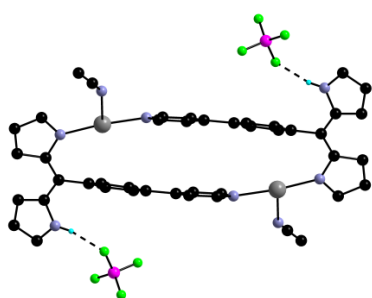


Fig. 102: Structure of macrocycle α -**38**

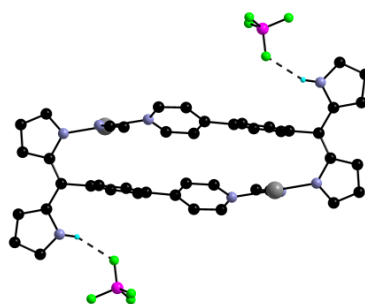


Fig. 103: Structure of macrocycle β -**38**

Bonds and angles	Bond distances (\AA) and angles ($^\circ$)
	α -complex (α - 38)
$d(\text{F}\cdots\text{H-N})$	2.812(6)
$\alpha(\text{F}\cdots\text{H-N})$	167.7
	β -complex (β - 38)
$d(\text{F}\cdots\text{H-N})$	2.970(5)
$\alpha(\text{F}\cdots\text{H-N})$	154.7

Table 14 Bond distances (\AA) and angles ($^\circ$) in compounds α -**38** and β -**38**.

Macrocycle $[(\text{DPM-Ph-4Py})\text{Ag}]_2(\text{OTf})_2$, **39**, crystallizes in the triclinic space group $P-1$ with one ligand **31**, a silver cation and a triflate anion in general positions. The pyridyl and phenyl rings of the ligand are not coplanar as in the structure of **37** with a dihedral angle of 23.11° . As in the former macrocycles, the silver cation is in a linear coordination geometry with similar Ag-N distances (**Table 13**). As in **34**, one oxygen atom of the triflate anion weakly interacts with the Ag^+ cation ($d(\text{Ag-O})=2.774(4) \text{ \AA}$) and another is hydrogen bonded to the pyrrolic NH pointing outward ($d(\text{N-H}\cdots\text{O})=2.873(4) \text{ \AA}$ and $\alpha(\text{N-H}\cdots\text{O})=162.7^\circ$). This leads to the formation of 1-D H-bond networks along the a axis (**Fig. 104**).

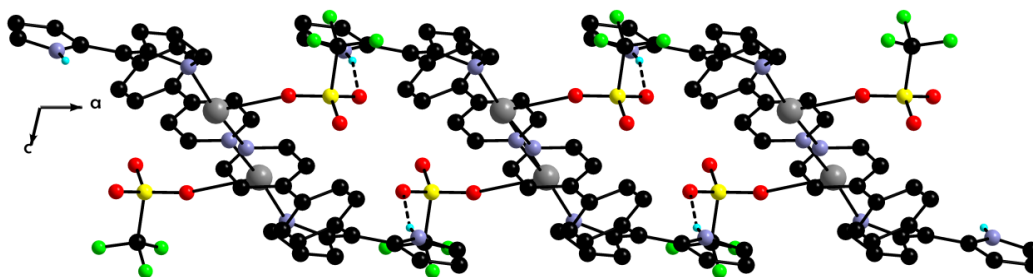


Fig. 104: Crystal structure of macrocycle **39**. View along the *b* axis.

However, one salient difference between **39** and the former triflate analogue **34** is in the presence of a long Ag-Ag interaction (3.627(5) Å) between neighboring macrocycles (**Fig. 105**). This leads to an overall 2-D architecture. This Ag-Ag $d^{10}-d^{10}$ interaction is slightly weaker than in the case of the reported macrocycle compound⁶ ($d_{\text{Ag-Ag}} = 3.396$ Å) with DPM-Ph-CN ligand.

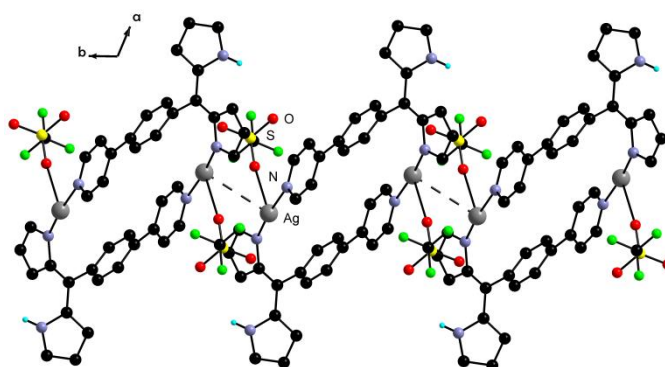


Fig. 105: Crystal structure of macrocycle **39**; view along the *c* axis.

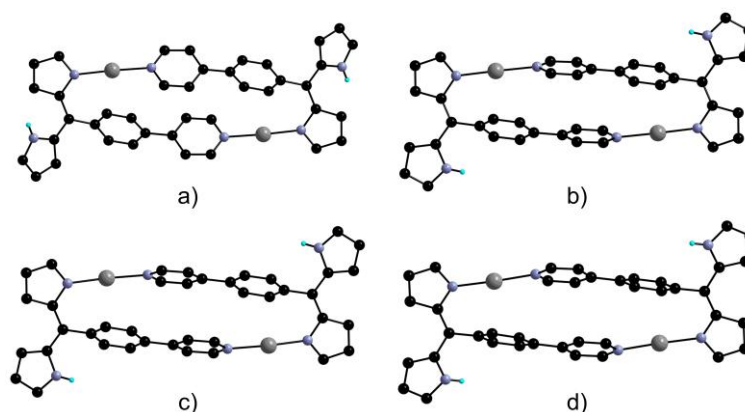


Fig. 106: Macrocycles **37-39**.

As in the former series of macrocycles, in the case of compounds with an additional phenyl spacer, no striking differences in the overall geometry of the macrocycles themselves are observed (**Fig. 106**). Within this series, the preferential conformation was “in-in”. Macrocycles α - and β -**38** with the BF_4^- anion adopt the “in-in” conformation, unlike the parent complex **36** with the same anion which adopts the “out-out” conformation. Both macrocycles **34** and **39** with the OTf anion adopt the “out-out” conformation. However, the phenyl and pyridine rings can go from almost coplanar to very twisted and still retain the macrocyclic motif.

A 2-D architecture is also observed in the crystal structure of macrocycle **[(DPM-Ph-Im)Ag]₂(CH₃CN)₃(OTf)₂, 40**. This compound crystallized in the monoclinic space group *P2₁/c* with one ligand, silver cation, anion molecules in general position. Here again, the Ag⁺ is in a linear coordination environment bonded to one nitrogen atom of a pyrrolic ring and the imidazole nitrogen atom of another molecule of **27** (Table 15). One of the two OTf anions is coordinated perpendicularly to the one of the silver centers with a long Ag-O distance (*d*_{Ag-O} = 2.787(6) Å). The second anion is not involved in any interactions with silver centers, but nevertheless participate in hydrogen bonding with two N-H pyrrolic protons of neighboring macrocycles (*d*(N-H[⋯]O)=2.811(4) Å; 3.014(4)Å and α (N-H[⋯]O)=154.3; 155.2 °). This interaction in turn leads to the formation of a 1-D H-bond network. As in the two previous complexes **34** and **39** with the OTf anion, an “out-out” conformation of the pyrrole rings is observed (Fig. 107).

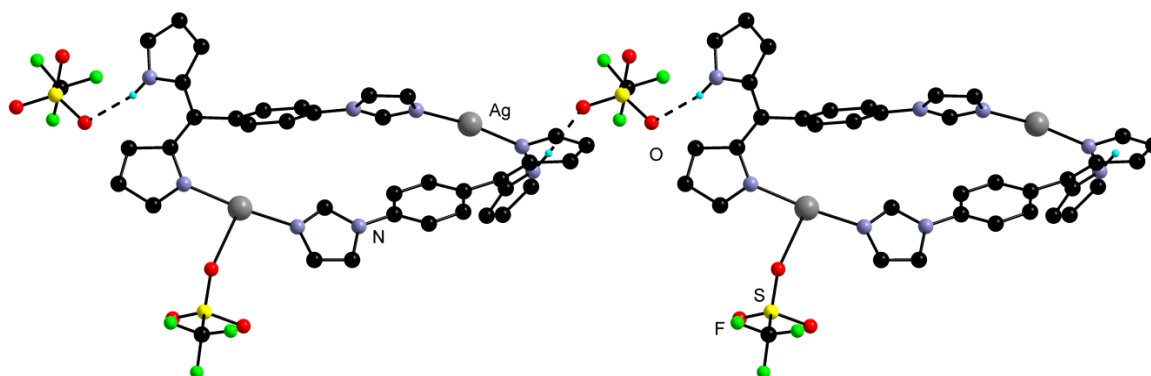


Fig. 107: Structure of **40**, formation of 2-D network via H-bond interaction anion.

The *d*¹⁰-*d*¹⁰ interaction between silver atoms (3.435(1) Å) expands the dimensionality of the network, thus 2-D, along the *c* axis (Fig. 108). This interaction is stronger than observed in the case of **39** and comparable with the distance reported in the literature example (*d*_{Ag-Ag} = 3.396 Å).⁶ The imidazole and phenyl rings of the ligand are not coplanar as in the structure of **32** with a dihedral angle of 32.16 °.

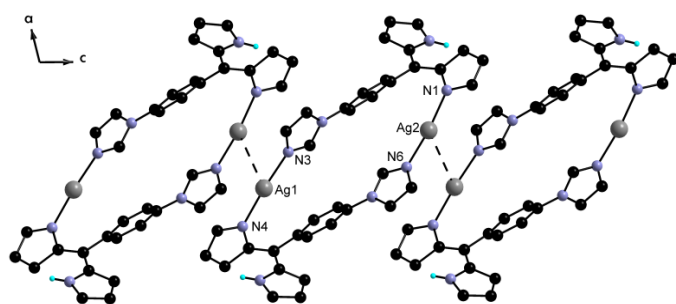


Fig. 108: Structure of **40**, formation of 1-D network via Ag-Ag interaction between metallomacrocycles. View along axis *b*.

Bonds and angles	Bond distances (Å) and angles (°)
N4 [⋯] Ag1	2.128(2)
N3 [⋯] Ag1	2.117(2)
N1 [⋯] Ag2	2.117(2)
N6 [⋯] Ag2	2.115(2)
N4-Ag-N3	174.74(10)
N6-Ag-N1	171.76(10)

Table 15: Bond distances (Å) and angles (°) in compound **40**.

III.3.1.1. Behavior in solution

In order to investigate the stability of metallamacrocycles **34-40** in solution, an NMR study was performed on compounds **36**, **37** and **40**. These compounds were chosen as illustrative examples of the behavior in solution for the complexes based on ligand **29**, **31** and **32**. Owing to the low solubility of complexes **36** and **37**, these complexes were analyzed only by ^1H -NMR spectroscopy. The complex with the DPM-Ph-Im ligand (**40**) was also investigated by ^{13}C -NMR (see experimental section) and DOSY. In all three cases, a shift of all peaks are down field shifted and a splitting of the three DPM signals integrating for two protons in the free ligand into six different peaks integrating for one proton in the case of the complex are observed (**Fig. 109**, **Fig. 110**). This suggests the presence of a complex in solution in which both the dipyrin and the peripheral group are coordinated to the Ag(I) ions.

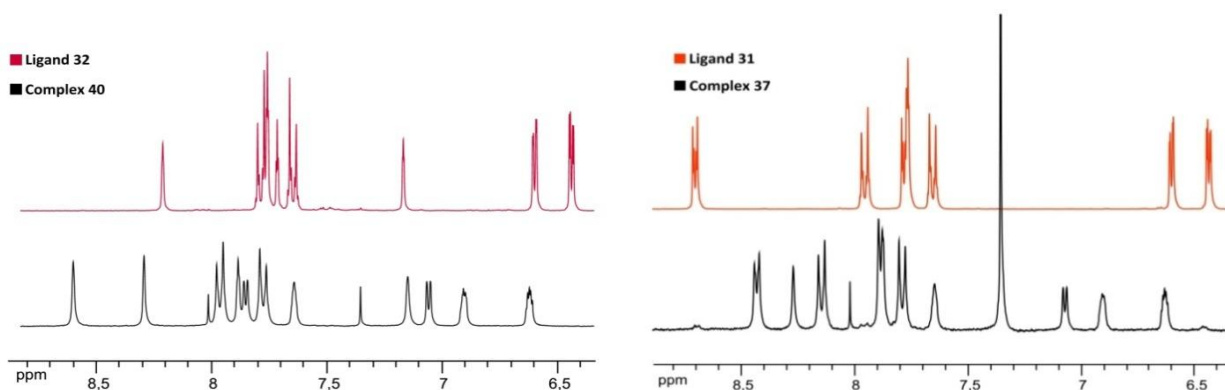


Fig. 109: Comparison of the aromatic region of the ^1H NMR spectra in acetone- d_6 of ligand **32** and macrocycle **40** (left) and ligand **31** and macrocycle **37** (right).

In the case of the **37** and **40**, no signal for the free ligand is detected. In the case of compound **36**, signals of the starting dipyrin are detected, suggesting partial decomposition of the macrocycle (**Fig. 110**) and a relative lower stability of this compound.

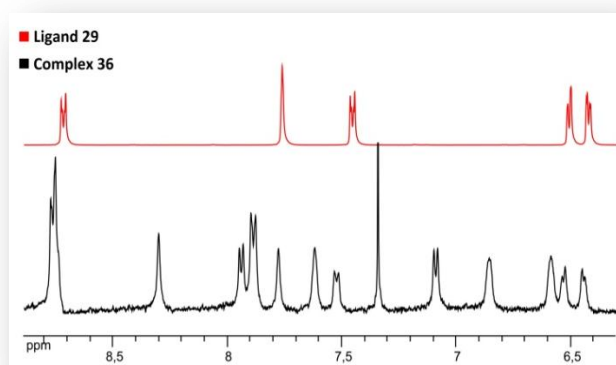


Fig. 110: Comparison of the aromatic region of the ^1H NMR spectra in acetone- d_6 of ligand **29** and macrocycle **36**.

This study clearly demonstrates the coordination of both functional groups of the ligands. In order to assess whether these complexes are [2+2] metallamacrocycles as in the solid state or complexes of higher nuclearity, a DOSY-NMR experiment on **40** in acetone- d_6 solution was performed. The DOSY (Diffusion-Ordered Spectroscopy) is a powerful technique based on differences in apparent diffusion coefficients (D) of compounds in solution and allows the measurement of these coefficients either in the case of single compounds or for mixtures. Using the *Stokes-Einstein* equation (**Scheme 35**)

gives access to the determination of the dimensions for the molecules (r), all the other coefficients in this equations being constant (viscosity of the solvent $\eta=f(T)$) or measured individually during the experiment, $\mu_{25^\circ\text{C}}=0.0003095 \mu\text{Pa/S}$ (for Acetone d_6 at $T=298 \text{ }^\circ\text{K}$). It is worth noting that this equation considers in first approximation a spherical model for the species in solution.

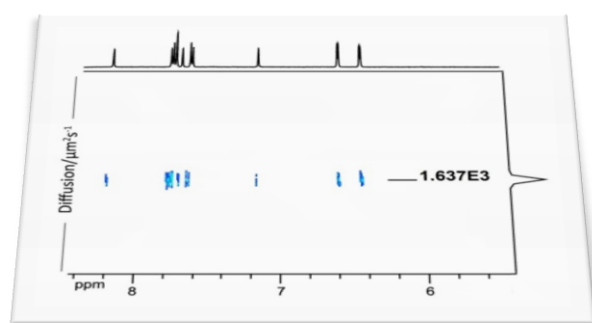
$$r = \frac{KT}{6\pi\mu D}$$

r = Dimension of the molecule
 K = Boltzman constant

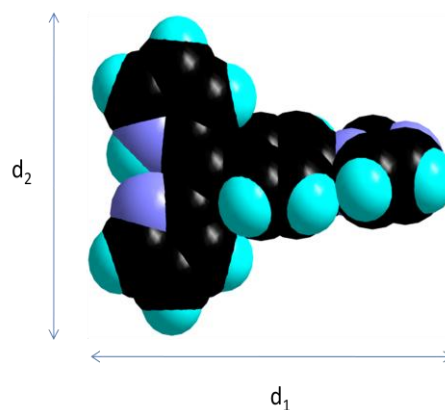
μ = Viscosity ($\mu\text{Pa/S}$)
 D = Diffusion coefficient ($\mu\text{m}^2/\text{s}$)
 T = Temperature (K°)

Scheme 35: Stokes-Einstein equation.

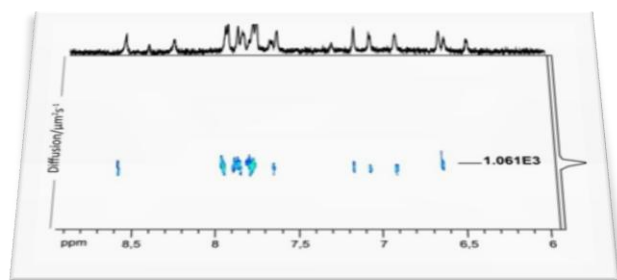
The DOSY investigations were performed for the free ligand **32** and its silver complex **40**. Based on the data obtained from the crystal structure, the theoretical values (r_{Calc}) of dimension were calculated for both compounds (Fig. 111).



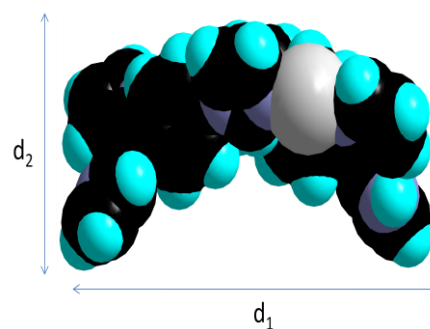
$D(\text{Ligand})= 1.6369001\text{E}3 \text{ } (\mu\text{m}^2/\text{s})$
 $r(\text{Ligand})= 4.3 \text{ \AA}$



$d_1=12.188\text{ \AA}$; $d_2=8.703 \text{ \AA}$
 $r_{\text{Calc}}(\text{Ligand})=5.22 \text{ \AA}$



$D(\text{Complex})= 1.0612806\text{E}3 \text{ } (\mu\text{m}^2/\text{s})$
 $r(\text{Complex})= 6.7 \text{ \AA}$



$d_1=18.216 \text{ \AA}$; $d_2=8.647 \text{ \AA}$
 $r_{\text{Calc}}(\text{Complex})= 6.71 \text{ \AA}$

Fig. 111: DOSY-NMR measurements and theoretical calculations of dimension value (r) of the ligand **32**(top) and complex **40** (bottom).

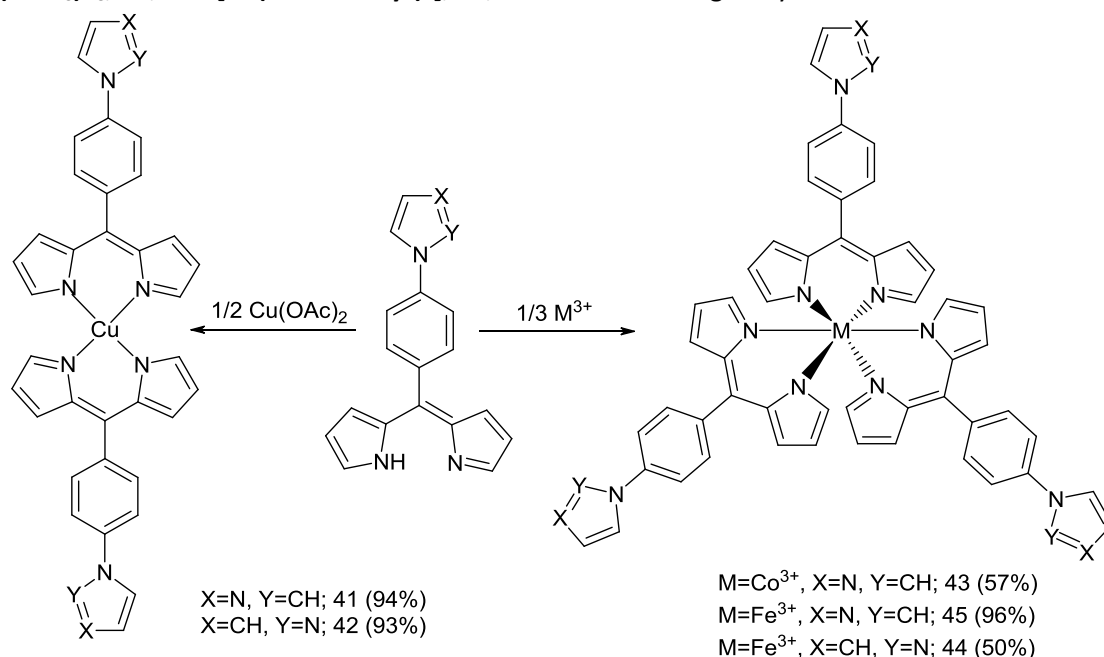
In both cases, only one species is observed in solution. The agreement between the determined dimension (r) of the molecules and theoretical data suggests that a [2+2] macrocycle is present in acetone- d_6 solution.

In conclusion, the [2+2] macrocyclic motif appears as a robust motif in the self-assembly of 5-aryl-dipyrrens bearing an additional coordinating group in *para* position and silver(I) salts. The organization of these compounds in the solid state is dependent on the nature of the anions and the conformations of the uncoordinated pyrrole rings. Furthermore, NMR studies have demonstrated that this macrocyclic arrangement is retained in solution.

III.3.2. Coordination chemistry of dipyrinate

III.3.2.1. Homoleptic discrete complexes

As mentioned in the introduction, many metal complexes have been reported with dipyrinate ligands acting as a monoanionic chelate. Several homoleptic complexes with the pyridine appended ligands have been reported with Cu(II), Co(III), Fe(III), In(III), Ga(III).¹³ We have then explored the coordination chemistry of the new imidazole and pyrazole appended ligands **32** and **33** to prepare a series of homoleptic complexes that could be potential metallatectons for the formation of heterometallic architectures. New Cu(II), Co(III) and Fe(III) complexes were prepared (**Scheme 36**). Upon reaction of the DPM ligands with copper acetate in a 2/1 ratio, two copper complexes **[Cu(DPM-Ph-Im)₂](CHCl₃)_{1.5}**, **41**, and **[Cu(DPM-Ph-Pyr)₂]**, **42**, were obtained in good yields.



Scheme 36: Preparation of homoleptic complexes 41-45.

In the first case (**41**), green-red crystals were grown by slow diffusion of *n*-pentane vapor into a CHCl₃ solution of the complex (**Fig. 112**). The complex crystallized in the monoclinic space group *C2/c* with one molecule in general position and a chloroform molecule on a twofold rotation axis. The copper ion is surrounded by two DPM moieties (**Table 16**) in a pseudo-tetrahedral environment. The two chelates form a dihedral angle of 46.32°, similar to the one observed for other Cu(DPM)₂ complexes.^{11,16,20,28}

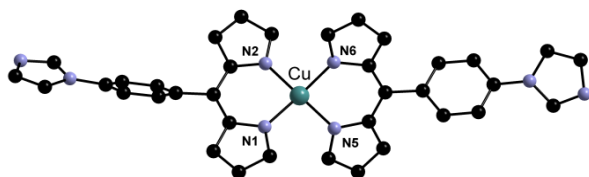


Fig. 112: Structure of the homoleptic complex 41.

Bonds	Distances (Å)
Cu-N1	1.955(3)
Cu-N2	1.949(3)
Cu-N5	1.961(3)
Cu-N6	1.952(3)

Table 16: Bond distances in compound 41.

The analogous complex **42** with the pyrazole appended ligand **33** was obtained in 93 % yield and characterized by elemental analysis. Unfortunately, all attempts to obtain this complex in crystalline form afforded only polycrystalline materials or powders.

Both homoleptic copper complexes **41** and **42** were analyzed in CH_2Cl_2 solution by UV-Visible spectroscopy. The absorption spectra (**Fig. 113**, **Table 17**) of both compounds are similar to the one reported in the literature²⁸ for analogous complexes and show bands in the 228-280 nm and 300-400 nm regions which can be attributed to $\pi-\pi^*$ transitions of the aromatic fragments. Two bands between 430-530 nm with maxima at 468 and 499 nm can be attributed to ligand-to-metal charge transfer and $\pi-\pi^*$ transitions of the dipyrinato moiety.

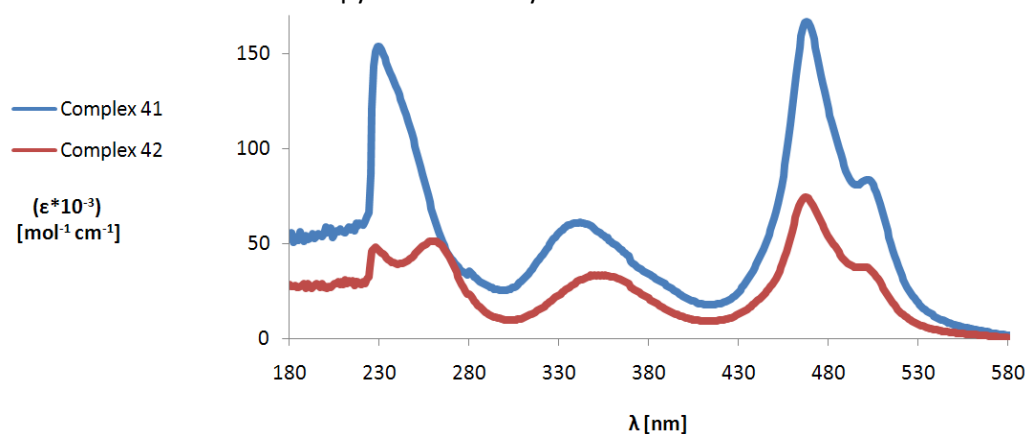


*Fig. 113: UV Visible spectra of homoleptic copper complexes **41** and **42** in CH_2Cl_2 .*

Compound	λ_{max} [nm] (ϵ) [$\text{mol}^{-1}\text{cm}^{-1}$]				
	41	230 (154000)	342 (61000)	468 (167000)	502 (8400)
42	228 (48000)	260 (51000)	350 (34000)	468 (74000)	499 (38000)

*Table 17: Absorption data for homoleptic copper complexes **41** and **42** in CH_2Cl_2 .*

Regarding complexes with trivalent metals, three complexes with cobalt(III) and iron(III) were obtained. Upon reaction of ligand **32** with $\text{Na}_3\text{Co}(\text{NO}_2)_6$ (**Scheme 36**) in a 3/1 ratio, complex **43** was obtained in 57 % yield. Crystallization by slow diffusion of *n*-pentane vapors into a 2-propanol solution of the complex (at 5 °C), afforded red crystals of $[\text{Co}(\text{DPM-Ph-Im})_3](2\text{-propanol})_3$ (**43**) (**Fig. 114a**). It crystallized in the triclinic space group *P*-1 with one complex and three solvent molecules in general position. Complexes $[\text{Fe}(\text{DPM-Ph-Im})_3]$ (**44**) and $[\text{Fe}(\text{DPM-Ph-Pyr})_3]$ (**45**) were obtained by reaction of ligands **32** and **33** with $\text{FeCl}_3 \cdot \text{H}_2\text{O}$ in a 3/1 ratio in 96 % and 50 % yields respectively. Both complexes **44** and **45** crystallized as dark red crystals by slow diffusion of *n*-pentane vapors into an acetone and dioxane solution of the complexes respectively. Complex **44** crystallized in the triclinic space group *P*-1 (**Fig. 114b**), while compound **45** crystallized in the monoclinic space group $P2_1/n$ (**Fig. 114c**) with the complex in general position. In all three cases (**43-45**), the metal centers are in a slightly distorted octahedral environment (**Table 18**), very similar to what has been reported for analogues by Cohen.¹³ Regarding the ligand moieties, in all three complexes, the angles between the planes of the phenyl rings and the imidazole or pyrazole groups are different in each ligand (**Table 18**).

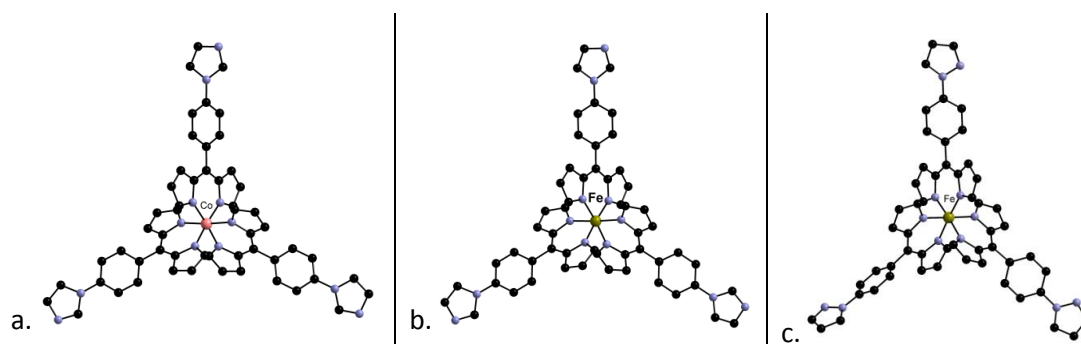


Fig. 114: Structure of the homoleptic complexes **43** (a), **44** (b), **45** (c.).

Bonds	43	Bonds	44	45
N1-Co	1.956(3)	N1-Fe	1.9595(18)	1.962(2)
N2-Co	1.934(3)	N2-Fe	1.9678(19)	1.968(2)
N3-Co	1.939(3)	N3-Fe	1.963(2)	1.965(2)
N4-Co	1.944(4)	N4-Fe	1.9649(19)	1.970(2)
N5-Co	1.938(4)	N5-Fe	1.9651(19)	1.954(2)
N6-Co	1.948(3)	N6-Fe	1.9563(19)	1.984(2)
Range of the angles between corresponding planes of phenyl and imidazole (or pyrazole) rings				
$\alpha(^{\circ})$	15.51-33.31		3.82-30.77	7.64-19.63

Table 18: Bond distanced and range of the angles between plans of phenyl and imidazole (or pyrazole) rings in **43-45**.

Regarding the UV-Visible spectroscopy in the case of the trivalent metals, as in the copper case, it was measured in CH_2Cl_2 solution. Here again (**Fig. 115, Table 19**) the absorption bands in the 228-380 nm region which can be attributed to π - π^* transitions of aromatic fragments and the bands between 380-580 nm correspond to ligand-to-metal charge transfer and π - π^* transitions of the dipyrinato moiety. These data are in agreement with those for Co^{III} or Fe^{III} /DPM complexes.¹⁶

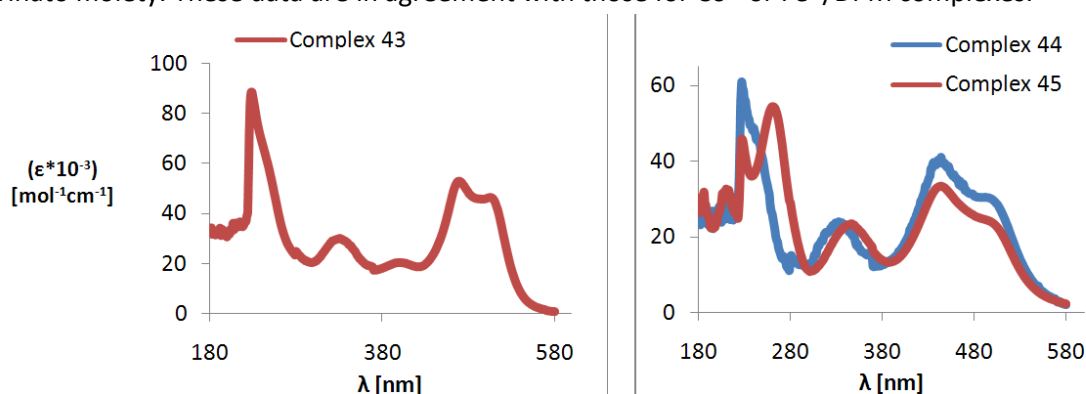


Fig. 115: UV Visible spectra of homoleptic complexes **43**, **44** and **45** in CH_2Cl_2 .

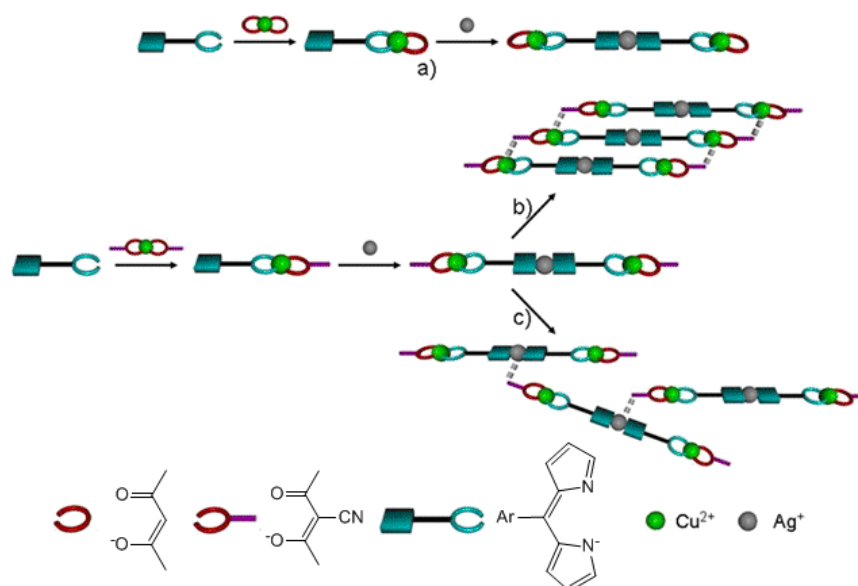
Compound	λ_{max} [nm] (ϵ) [$\text{mol}^{-1}\text{cm}^{-1}$]				
	43	227 (61000)	333 (24000)	444 (41000)	494 (31000)
44	229 (86000)	331 (30000)	399 (20000)	491 (46000)	505 (47000)
45	227 (46000)	261 (54000)	347 (24000)	444 (33000)	490 (25000)

Table 19: Absorption data for homoleptic complexes **43**, **44** and **45** in CH_2Cl_2 .

In our attempt to obtain heterometallic architectures, homoleptic complexes **41-45** were used as metallatectons in the reaction with a variety of metal salts. In particular, owing to several examples in the literature of imidazole²⁹ (and pyrazole³⁰) based silver or cadmium complexes, these latter metals were used. Unfortunately, only amorphous or very unstable crystalline materials were obtained. We then pursued to develop the proposed strategy using heteroleptic metallatectons.

III.3.2.2. Heteroleptic complexes and networks

There are only few examples reporting the elaboration of extended heterometallic systems based on heteroleptic metallatectons incorporating a DPM.^{6,12} These examples involve a Ag- π interaction between silver ions and the pyrrolic system of the DPM. In the absence of such an interaction, heteroleptic metallatectons such as (acac)Cu(DPM)^{6,12,33,11,19,20,21} or (salen)Co(DPM)^{6,12} complexes (acac = acetylacetonate, salen = *N,N'*-bis(salicylidene)ethylenediamine) incorporating a DPM bearing a coordinating site in the *para* position should only lead to discrete heterometallic complexes upon reaction with a second metal center as illustrated in **Scheme 37a**. Two approaches can be considered to obtain extended systems with such species. The first one consists in using a DPM ligand bearing more than one peripheral coordinating site. An example of such unit may be obtained by functionalizing both *meta* positions on the aryl moiety. The second strategy relies on the use of the capping ligand itself for further coordination. For example, when considering the association of a (acac)Cu(DPM) heteroleptic complex with silver salts (**Scheme 37b and c**), introduction of a coordinating group on the capping ligand should allow the self-assembly by coordination processes of the heterometallic discrete complexes.



Scheme 37: The coordination of a (acac)Cu(DPM) complex with silver ions leads to a trinuclear complex (a), while with the nitrile appended (acacCN)Cu(DPM) complexes, coordination networks can be obtained (b and c).

It is worth noting that at least two modes of self-assembly can be foreseen for these species. The silver ion can feature coordination numbers higher than 2 and is therefore capable of interaction with the additional peripheral coordinating group (**Scheme 37c**). It has also been demonstrated that (acac)Cu(DPM) complexes self-assemble upon coordination of the peripheral group on the DPM to a metal center of another complex leading to a penta-coordinated Cu ion.^{11,19,20,21} In the case of discrete heterometallic complexes bearing peripheral coordinating sites, such a self assembly mode should also lead to extended architectures (**Scheme 37b**). Recently, several homoleptic complexes with the acac-Py or acacCN ligands (acacPy = 3-(4-pyridyl)acetylacetonate; acacCN = 3-cyanoacetylacetonate) have been prepared. It is worth noting that, in particular, in the case of homoleptic copper complex with acacCN ligands, a 1-D network was observed via the interaction between the nitrile group and the copper centre ($d(\text{Cu-N})=2.468(2)\text{\AA}$) of a neighboring molecule (**Fig. 116**). These homoleptic complexes were successfully used for the elaboration of heterometallic coordination polymers upon association with silver salts^{31,32} (**Fig. 117**).

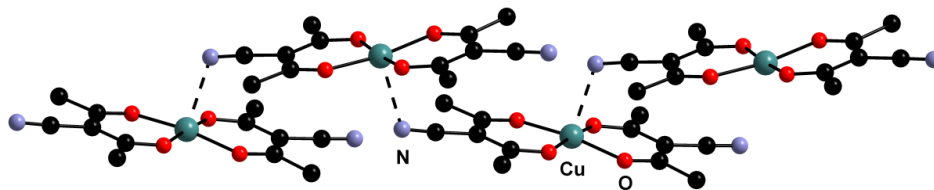


Fig. 116: Structure of self complimentary 1-D network $\{[Cu(acacCN)_2]\}_x$.

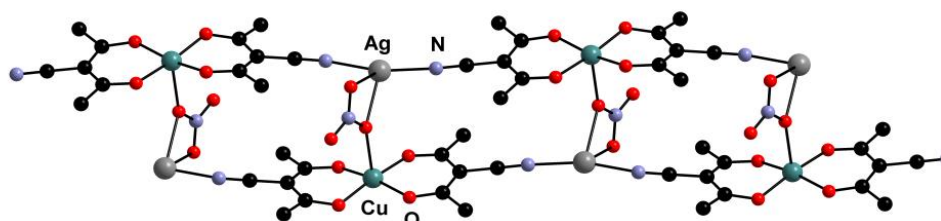
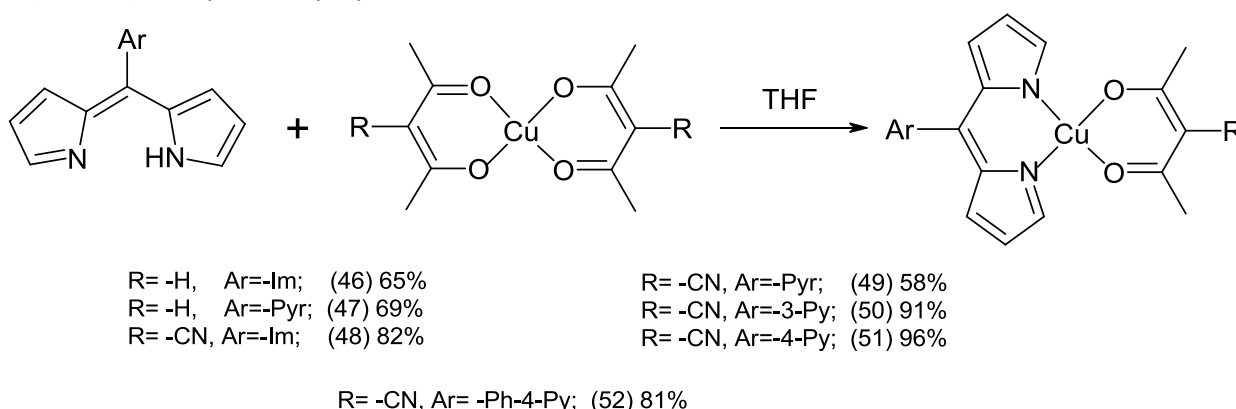


Fig. 117: Structure of 1-D heterometallic network $\{Ag(Cu(acacCN)_2(NO_3))\}_x$.^{32a}

Interestingly, no $(acacCN)Cu(DPM)$ or $(acacPy)Cu(DPM)$ complexes have, to our knowledge, been reported. The novel dipyrins **32**, **33** and **31** bearing peripheral imidazole, pyrazole and pyridine groups respectively as well as ligands **29** and **30** were used for the preparation of $(acacCN)Cu(DPM)$ complexes. Their self-assembly was investigated as well as their reaction with silver salts to afford heterometallic coordination polymers. Furthermore, extension of this strategy to architectures of higher dimensionality was addressed. In that aim, novel $(acacCN)Co(DPM)_2$ complexes were prepared and used as metallatectons.

III.3.2.2.1. *Heteroleptic complexes and networks with copper (II)*

All heteroleptic copper (II) complexes were prepared by reaction of the corresponding ligands with $Cu(acac)_2$ or $Cu(acacCN)_2$ complexes in a 1/1 ratio in THF (**Scheme 38**) in good yields ranging from 58 to 96 % and characterized by UV-Visible and IR spectroscopies and elemental analyses or HRMS. Note that in the presence of an excess of ligand, homoleptic complexes were obtained instead. The starting $Cu(acacCN)_2$ complex was prepared as described.³⁷



Scheme 38: Preparation of the heteroleptic copper (II) complexes **46-52**.

Crystals of **[(acac)Cu(DPM-Ph-Im)]**, **46**, were obtained by slow diffusion of Et₂O vapors into a CHCl₃ solution. Complex **46** crystallizes in the triclinic space group *P*-1 with one molecule in general position. Complex **[(acac)Cu(DPM-Ph-Pyr)]**, **47**, obtained upon slow evaporation of CHCl₃, crystallizes in the monoclinic space group *P*2₁/*c* with one molecule in general position. For both compounds, the copper atom is in a square planar environment with Cu-N and Cu-O distances close to those reported for other analogous complexes (**Fig. 118**).^{33,6,12} Interestingly, unlike other reported (acac)Cu(DPM) or (hfac)Cu(DPM) species^{11,19,20,21}, the peripheral coordinating group, the diazole here, does not coordinate the Cu(II) center. A difference between the two complexes lies in the angle between the diazole and the phenyl ring, 30.9° for **46** and 13.9° for **47**. The angle for the latter might explain the absence of coordination to a neighboring complex.

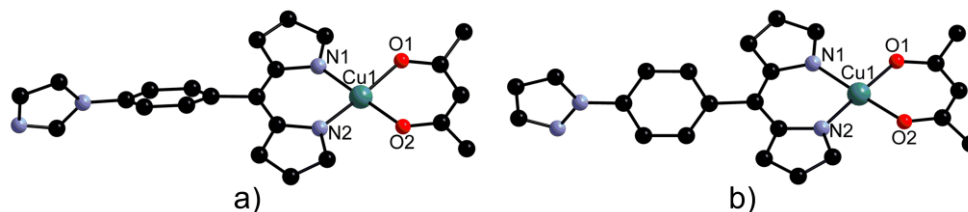


Fig. 118: Crystal structure of complexes **46** (a) and **47** (b). Hydrogen atoms have been omitted for clarity.

Complex 46				Complex 47			
Bonds	Distances (Å)	Bonds	Distances (Å)	Bonds	Distances (Å)	Bonds	Distances (Å)
Cu1-O1	1.9554(17)	Cu1-N1	1.9286(15)	Cu1-O1	1.9411(19)	Cu1-N1	1.942(2)
Cu1-O2	1.9478(16)	Cu1-N2	1.9391(14)	Cu1-O2	1.9225(19)	Cu1-N2	1.961(2)

Table 20: Bond distances in compounds **46** and **47**.

Crystals of **[(acacCN)Cu(DPM-Ph-Im)]**, **48**, were obtained by slow evaporation of a CHCl₃ solution. Complex **48** crystallizes in the monoclinic space group *P*2₁/*c* with two molecules in general position. In both molecules, the Cu ion is coordinated to both chelates, the DPM and the acacCN, and to the imidazole group of a neighboring complex with Cu-N_{imid} distances of 2.245(2) and 2.302(2) Å, leading to the formation of 1-D coordination networks (**Fig. 119**). This parallels the crystal structure of other heteroleptic Cu(acac)(DPM) where the DPM bears a coordinating peripheral nitrogen atom, such as pyridine or quinoline.^{11,19,20,21,33} The main difference between the two independent complexes lies in the coordination geometry around the copper atoms (**Table 21**). While one complex deviates from planarity with an angle of 42.9° between the acacCN and the DPM chelates (**Fig. 119**), the other is less distorted with an angle of 8.8° between the two groups. Such a concave arrangement away from the additional coordinating atom has been observed for other (acac)Cu(DPM) species.^{11,19,20,21,33}

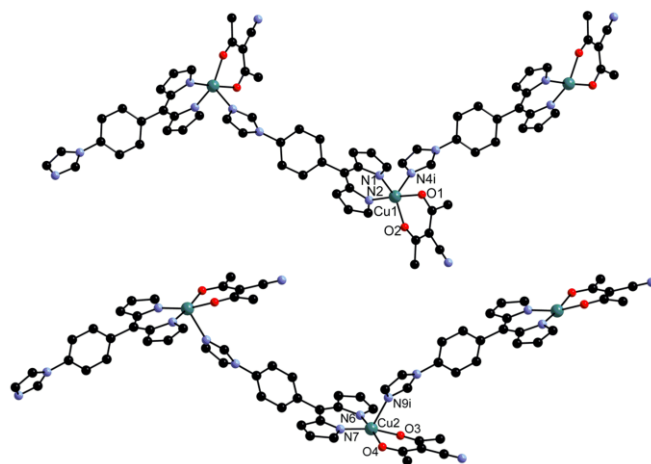


Fig. 119: Two independent 1-D networks in the crystal structure of complex **48**. Hydrogen atoms have been omitted for clarity.

Bonds and angles	Distances (Å) and angles (°)
Cu1-O1	1.9732(18)
Cu1-O2	1.9931(19)
Cu1-N1	1.966(2)
Cu1-N2	1.948(2)
Cu1-N4i	2.245(2)
Cu2-O3	1.9694(19)
Cu2-O4	1.9930(19)
Cu2-N6	1.968(2)
Cu2-N7	1.957(2)
Cu2-N9	2.302(2)

Table 21: Bond distances in compound **48**. (*i* = 1 - *x*, 1/2 + *y*, 3/2 - *z*; *ii* = -*x*, 1/2 + *y*, 1/2 - *z*)

For compound **49**, depending on the solvent of crystallization used, two different crystal structures were obtained. In both cases, the arrangement of the copper complexes is quite different from the one observed for **48**. Upon slow diffusion of *n*-pentane vapors into a dioxane solution of **49**, crystals of a dioxane solvate $[(\text{acacCN})\text{Cu}(\text{DPM-Ph-Pyr})](\text{DiOX})$, **49a**, were obtained (**Fig. 120**). The latter crystallizes in the triclinic space group *P*-1 with one copper complex and one solvent molecule in general position. The copper center features square pyramidal coordination geometry, being coordinated to the acacCN and the DPM chelates, as well as to an oxygen atom of the dioxane molecule (**Table 22**). Unlike in the case of **48**, the azole nitrogen atom is not coordinated to the copper center.

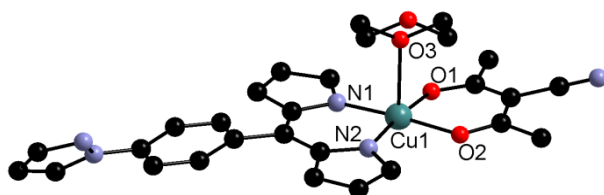


Fig. 120: Crystal structure of the **49a** solvate showing the axially coordinated dioxane molecule. Hydrogen atoms have been omitted for clarity.

Bonds and angles	Distances (Å)
Cu1-O1	1.9573(11)
Cu1-O2	1.9470(12)
Cu1-N1	1.9534(12)
Cu1-N2	1.9628(13)
Cu1-O3	2.443(2)

Table 22: Bond distances in compound **49a**.

The pseudo-polymorph **49b** crystallizes in the monoclinic space group *P*2₁ with one molecule in general position. The copper ion is coordinated to the acacCN and DPM chelates with bond distances as expected for such complexes. Here again, the azole nitrogen atom is not coordinated to the copper center but a one-dimensional chain is nonetheless formed owing to a weak interaction of the metal center with the nitrogen atom of the CN group of a neighboring complex (**Fig. 121**). The Cu-N(acacCN) distance of 2.489(2) Å is rather long and the CN-Cu angle of 114.4° deviates largely from linearity. These geometrical parameters are however similar to the ones observed in the crystal structure of other reported Cu(acacCN)₂ complexes^{37,38} (**Table 23**). This structure illustrates the coordination, although weak, of the peripheral nitrile group to the copper center as depicted in **Scheme 37b**.

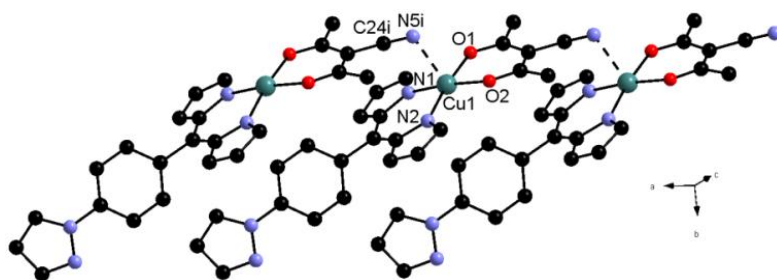


Fig. 121: One-dimensional network in the crystal structure of complex **49b**. Hydrogen atoms have been omitted for clarity.

Bonds and angles	Distances (Å) and angles (°)
Cu1-O1	1.9706(16)
Cu1-O2	1.9465(16)
Cu1-N1	1.9586(18)
Cu1-N2	1.9648(19)
Cu1-N5i	2.489(2)
C24i-N5i-Cu1	114.4

Table 23: Selected bond lengths and angles for compound **49b**. ($i = 1+x, y, z$).

The analogues incorporating the pyridine appended ligands **29** and **30** differing only by the position of the peripheral nitrogen atom have been prepared and characterized in solution and in the solid state. These compounds illustrate the influence of this variation on the solid state organization. In both cases, 1-D networks are formed, analogous to what has been observed in the structure of **48** (**Fig. 119**) with pyridine moiety coordinated to the copper center and a non coordinated nitrile pole. This type of pyridine coordination has been observed in the case of heteroleptic complexes with acac and hfac moieties (**Fig. 89**)^{11, 19}.

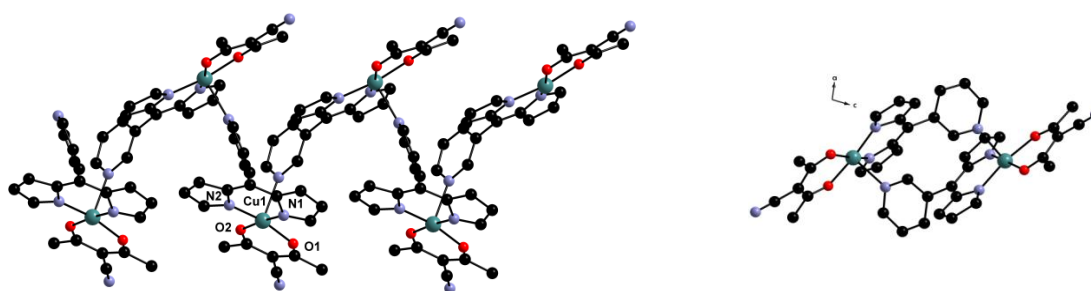


Fig. 122: One-dimensional network in the crystal structure of complex 50. Hydrogen atoms have been omitted for clarity.

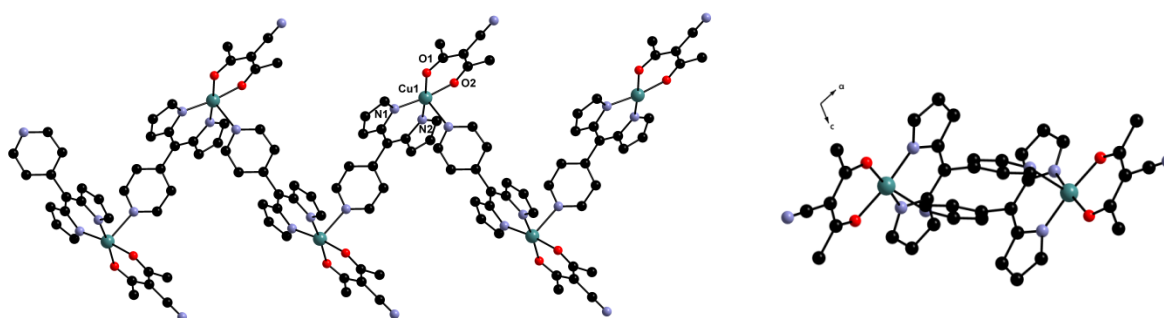


Fig. 123: One-dimensional network in the crystal structure of complex 51. Hydrogen atoms have been omitted for clarity.

Complex $[(\text{acacCN})\text{Cu}(\text{DPM-3Py})]$, **50**, with the 3-pyridine appended ligand crystallized by slow diffusion of *n*-pentane vapours into a chloroform solution of the complex in the monoclinic $P2_1/c$ space group with two molecules of complex in general position. In both units, the copper centers adopt a square pyramidal coordination environment. The angles between DPM and pyridine moieties are almost identical (56.92° and 56.17°). Regarding the complex $[(\text{acacCN})\text{Cu}(\text{DPM-4Py})]$, **51**, it crystallized by slow evaporation of a dioxane solution in the monoclinic $C2/c$ space group with one molecule of complex in general position. The coordination environment is very similar to the one observed in **48**, with a distance between the copper ion and the basal plane of 0.125 \AA . The pyridine group is tilted by an angle of 74.40° with respect to the rest of the complex. The bond distances in the CuN_2O_2 core (**Table 24**) are similar to what has been observed in the above-mentioned complexes.

Complex 50				Complex 51	
Bonds	Distances (\AA)	Bonds	Distances (\AA)	Bonds	Distances (\AA)
N(1)-Cu(1)	1.958(3)	N(4)-Cu(2)	1.964(3)	N(1)-Cu(1)	1.955(2)
N(2)-Cu(1)	1.949(3)	N(5)-Cu(2)	1.956(3)	N(2)-Cu(1)	1.962(2)
O(1)-Cu(1)	1.972(3)	O(3)-Cu(2)	1.964(3)	O(1)-Cu(1)	1.9590(18)
O(2)-Cu(1)	1.966(3)	O(4)-Cu(2)	1.970(3)	O(2)-Cu(1)	1.9705(18)

Table 24: Bond distances in compounds **50** and **51**.

In the case of complex **50** with the 3-pyridyl group, a helix is formed (**Fig. 122**), whereas in the second case **51**, a zigzag organization (**Fig. 123**) is observed, as in the case of the $[(\text{acac})\text{Cu}(\text{DPM-3Py})]$ and $[(\text{acac})\text{Cu}(\text{DPM-3Py})]$ complexes.¹¹ Bond distances between the copper centers and the coordinated pyridine nitrogen atoms of a neighboring unit are almost identical for both structures ($2.322(3) \text{ \AA}$ and $2.376(2) \text{ \AA}$ respectively).

The analogue incorporating the extended ligand **31** containing an additional phenyl ring, complex **[(acacCN)Cu(DPM-Ph-4Py)]**, **52**, was obtained. This compound crystallized in the monoclinic $P2_1/c$ space group with one molecule in general position by slow diffusion of *n*-pentane vapors in a THF solution of the complex. By analogy with **51**, the complexes organize in 1-D zigzag networks by interaction between the pyridyl nitrogen atom and the copper cation of a neighboring unit (**Fig.124**) with a bond distance, 2.493(2) Å, longer than in the previous examples. Here again, a square pyramidal coordination environment of the metallic core is observed (**Table 25**). While the DPM moiety is flat, the phenyl spacer is perpendicular to the DPM plane. The angle between the phenyl and pyridine rings is 23.03°.

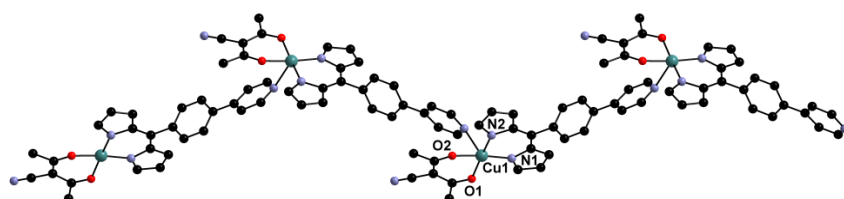


Fig. 124: One-dimensional network in the crystal structure of complex **52**. Hydrogen atoms have been omitted for clarity.

Bonds	Distances (Å)
N(1)-Cu(1)	1.9632(15)
N(2)-Cu(1)	1.9644(14)
O(1)-Cu(1)	1.9659(13)
O(2)-Cu(1)	1.9624(13)

Table 25: Bond distances in compound **52**.

All heteroleptic complexes were investigated by UV-Visible spectroscopy in CH_2Cl_2 solution (**Table 26**). For all compounds, the observed spectrum is similar to the one obtained for the homoleptic analogues. It features bands in the 228-300 nm and 300-400 nm regions which can be attributed to π - π^* transitions of aromatic fragments (**Fig. 125**). Two bands between 430-530 nm corresponding to ligand-to-metal charge transfer and π - π^* transitions of the dipyrinato moiety are observed. However, unlike in the spectrum of the homoleptic species, the relative intensity of these two latter bands is reversed. This intensity inversion of the bands in heteroleptic copper complexes has been mentioned in the literature for other (acac)Cu(DPM) derivatives.¹¹

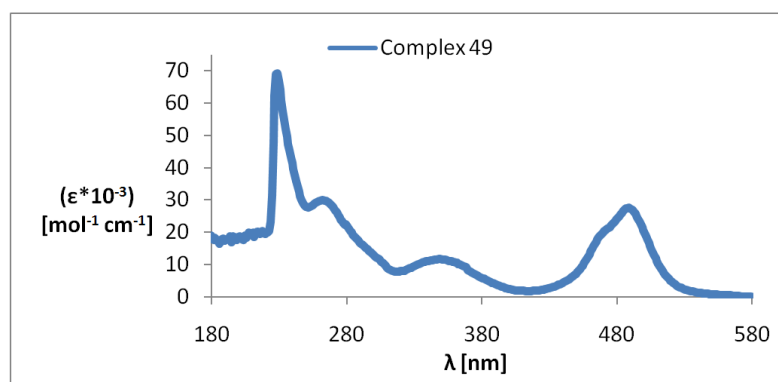


Fig. 125: Example of a UV visible spectrum for heteroleptic copper complexes. The case of complex **49** in CH_2Cl_2 .

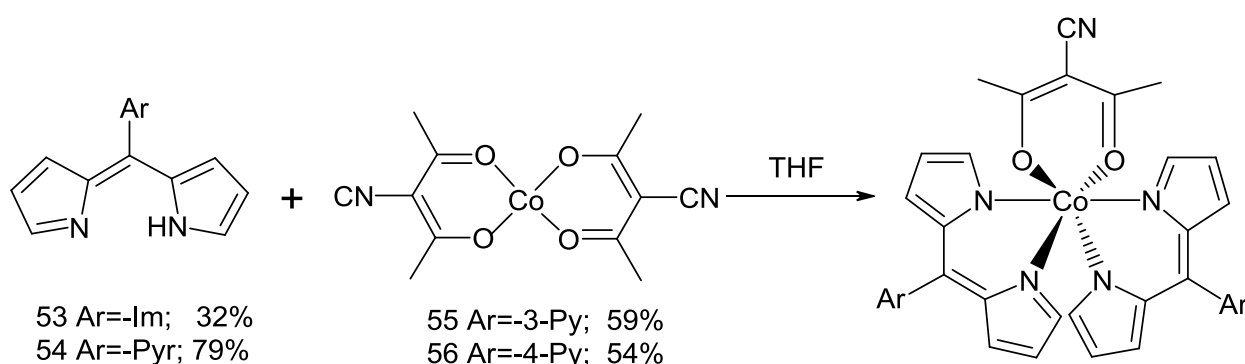
Compound	λ_{max} [nm] (ϵ) [$\text{mol}^{-1}\text{cm}^{-1}$]				
46	229 (34000)	297 (15000)	329 (11000)	479 (25000)	493 (32000)
47	227 (33000)	294 (24000)	342 (15000)	482 (32000)	493 (39000)
48	227 (28000)	288 (12000)	333 (9000)	479 (21000)	491 (27000)
49	229 (69000)	263 (30000)	349 (12000)	478 (23000)	489 (27000)
50	229 (20000)	296 (14000)	342 (5000)	474 (23000)	491 (36000)
51	228 (27000)	293 (16000)	357 (5000)	468 (18000)	492 (36000)
52	227 (27000)	266 (23000)	282 (23000)	318 (14000)	469 (18000)

Table 26: Data of UV Visible spectra for heteroleptic copper complexes **46-52** in CH_2Cl_2 .

III.3.2.2.2. *Heteroleptic complexes with cobalt (III)*

As mentioned in the introduction, only few examples of heteroleptic complexes have been reported in the literature, the largest series of compounds being the (acacR)Cu(DPM) one. During his Ph. D., Domingo Salazar-Mendoza prepared a series of (acac)Co(DPM)₂ complexes.³⁴ In the frame of the strategy illustrated **Scheme 38**, it appeared interesting to prepare analogues of the (acacCN)Co(DPM)₂ type.

These compounds were prepared by reaction of dipyrins with the starting Co(acacCN)₂ complex in a 2/1 ratio in THF (**Scheme 39**) with yields ranging from 32 to 79 % and analyzed by IR, UV-Visible specocopy and HRMS. Interestingly, in the presence of an excess of ligand, conversion to the homoleptic species is not detected. The starting Co(acacCN)₂ complex was prepared as described in the literature.³⁷ We should note here that this reaction involves the oxidation of the cobalt from the divalent to the trivalent state.



Scheme 39: Preparation of the heteroleptic cobalt (III) complexes 53-56.

Red crystals of [Co(DPM-Ph-Im)₂(acacCN)](DiOX), **53**, and [Co(DPM-Ph-Pyr)₂(acacCN)](THF), **54**, (**Fig. 126**) were obtained by slow diffusion of *n*-pentane vapors into a DiOX solution and *n*-pentane into a THF solution of the complexes respectively. Both complexes crystallize in the orthorhombic space group *Pbcn*. In the case of **53**, the complex lies on a two-fold axis and one dioxane molecule lies on an inversion center. In the case of **54**, both the complex and the THF molecules are on a two-fold axis. In both compounds, the cobalt atoms are in an octahedral environment with similar Co-N and Co-O distances (**Table 27**). A difference between the two complexes lies in the angle between the diazole and the phenyl ring, 40.2 ° for **53** and 30.3 ° for **54**.

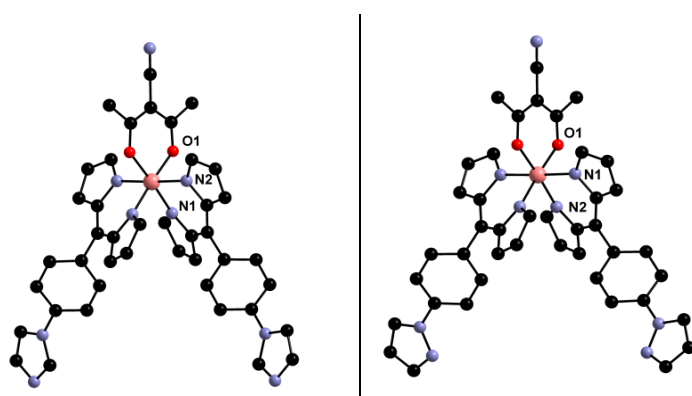


Fig. 126: Crystal structure of heteroleptic cobalt (III) complexes 53 and 54. Hydrogen atoms have been omitted for clarity.

Bonds	Bond distances (Å)
Complex (53)	
N1-Co	1.922(3)
N2-Co	1.941(3)
O-Co	1.910(3)
Complex (54)	
N1-Co	1.936(2)
N2-Co	1.918(2)
O-Co	1.9124(18)

Table 27: Bond distances in compounds 53 and 54.

In the same manner, complexes with the 3- and 4-pyridine appended ligands **[Co(DPM-3Py)₂(acacCN)](CHCl₃)_{0.5}, **55**, and **[Co(DPM-4Py)₂(acacCN)](DiOX)_{1.5}, **56**, were synthesized. Complex **55** crystallized (**Fig. 127a**) by slow diffusion of *n*-pentane vapours into a chloroform solution of the compound in the triclinic *P*-1 space group with a complex in general position and a chloroform molecule on an inversion centre.****

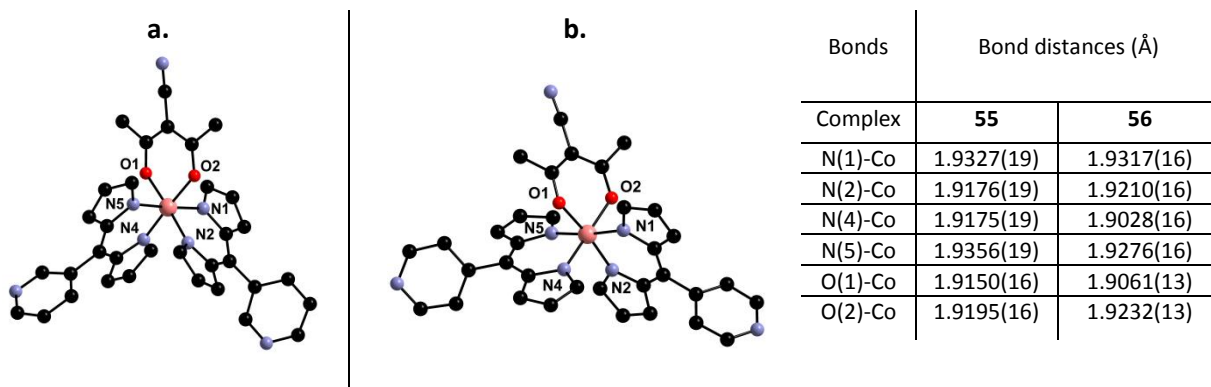


Fig. 127: Crystal structure of heteroleptic cobalt (III) complexes **55** (a) and **56** (b). Hydrogen atoms have been omitted for clarity.

Table 28 Bond distances in compounds **55** and **56**.

Complex **56** crystallized (**Fig. 127b**) by slow diffusion of *n*-pentane vapors into a dioxane solution of the compound in the triclinic *P*-1 space group with one complex and one dioxane molecule in general position and a second dioxane molecule on an inversion centre. The cobalt center is in an octahedral coordination environment with bond distances (**Table 28**) similar to the ones observed for complexes **53** and **54**.

It is worth noting that these heteroleptic cobalt(III) species, like the homoleptic cobalt(III) and iron(III) complexes, are isolated as a racemate mixture of Δ and Λ enantiomers.

All heteroleptic cobalt(III) complexes were investigated in CH₂Cl₂ solution by UV-Visible spectroscopy (**Table 29**). As for the corresponding homoleptic complexes described previously (**Fig. 115**) and in the literature,¹⁶ the absorption bands at 227-300 nm and 300-415 nm correspond to π - π^* transitions of the aromatic fragments in the *meso* position of the DPM. The bands in the 430-550nm region with a maximum at 480(2) nm are attributed to LMCT and π - π^* transitions of dipyrinato moiety (**Fig. 128**).

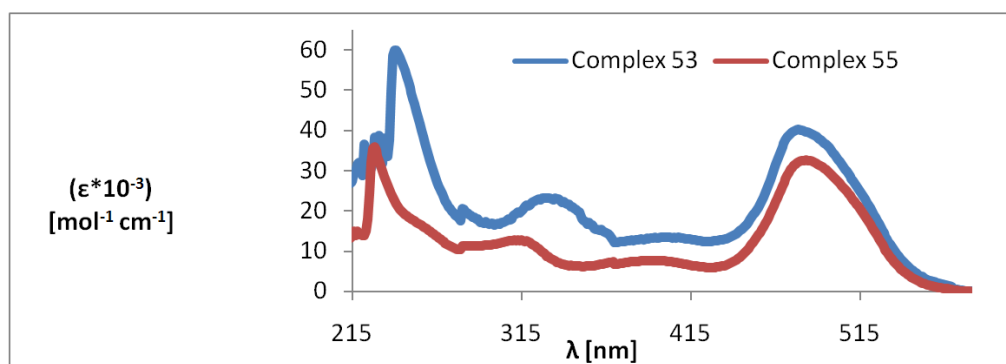


Fig. 128: Examples of spectra of heteroleptic complex **53** and **55** in CH₂Cl₂.

Compounds	λ_{max} [nm] (ϵ) [mol ⁻¹ cm ⁻¹]			
53	228 (66000)	334 (20000)	401 (13000)	481 (40000)
54	228 (71000)	258 (63000)	349 (28000)	480 (48000)
55	227 (36000)	311 (13000)	395 (8000)	483 (33000)
56	233 (78000)	302 (17000)	393 (10000)	485 (41000)

Table 29: Absorption data for heteroleptic copper complexes **53-56** in CH₂Cl₂.

Both pyridine appended heteroleptic cobalt(III) complexes **55** and **56** were investigated by cyclic voltammetry in a 0.1M (*n*-Bu₄N)PF₆ CH₂Cl₂ solution as supporting electrolyte solution at room temperature with a scanning speed of 100 mV.s⁻¹. In both cases (**Fig. 129**), quasi reversible Co^{III}/Co^{II} and Co^{II}/Co^I reduction processes are observed (**Table 30**). These results are in agreement with the electrochemistry of the parent heteroleptic Co(hfac)(DPM) complexes studied in our laboratory³⁴.

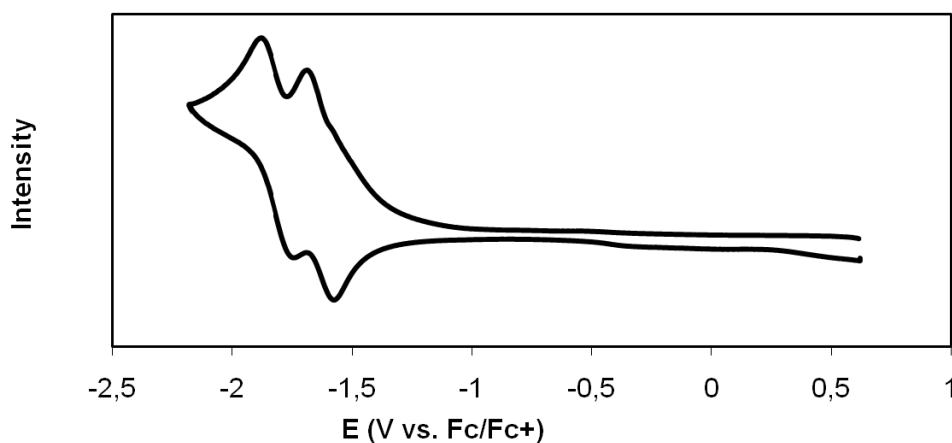


Fig. 129: Cyclic voltammetry investigation (CH₂Cl₂) for heteroleptic cobalt complex 56.

	Complex 55		Complex 56	
	E _{1/2} (V)	ΔE (V)	E _{1/2} (V)	ΔE (V)
Co ^{III} /Co ^{II}	-1.67	0.080	-1.63	0.082
Co ^{II} /Co ^I	-1.87	0.087	-1.81	0.104

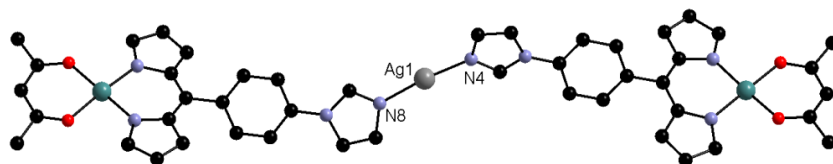
Table 30: Data of cyclic voltammetry investigation for heteroleptic cobalt complexes 55 and 56.

This series of heteroleptic copper and cobalt complexes bearing two different types of peripheral coordinating groups were used as metallatectons in attempts to obtain heterometallic architecture by reactions with different metal salts such as silver salts and rhodium acetate, among other.

III.3.2.3. Heterometallic architecturesⁱ

The preparation of heteronuclear species was attempted by reaction of heteroleptic complexes with silver salts. Unfortunately, the two pyrazole functionalized complexes **47** and **49** did not form crystalline heterometallic systems. This is rather surprising given that other phenyl-pyrazole derivatives have been reported to coordinate silver ions.³⁵ We will illustrate hereafter the strategy presented in **Scheme 37** and describe the results based on the copper complexes **46**, **48**, **50-52** and then on the cobalt species **55** and **56**.

To prepare a discrete heteronuclear complex such as the one presented schematically in **Scheme 37a**, complex **46** was reacted with silver salts. Upon slow diffusion of a benzene solution of AgSbF₆ into a CHCl₃ solution of **46**, crystals of the heterometallic complex [Ag(acac)Cu(DPM-Ph-Im)₂](SbF₆)₂(Benzene)₂, **57**, were obtained. This compound crystallizes in the triclinic space group *P*-1 with two complexes **46**, one silver ion, a SbF₆⁻ anion and two benzene molecules in general positions. The coordination geometry around the copper atoms is similar to the one observed in the structure of **46**. The Ag⁺ cation is coordinated in a linear fashion to two imidazole groups belonging to two copper complexes (**Fig. 130**) with Ag-N_{imid} distance (**Table 31**) close to the one previously observed for similar compounds.^{29c,36} As expected (**Scheme 37a**), the absence of further coordinating group in **46** prevents the self-assembly process through coordination bond to take place and thus a discrete species is formed. To investigate the role played by a peripheral nitrile group on the copper complexes, **48** was reacted with silver salts in a 2:1 stoichiometry.



Bonds and angles	Bond distances (Å) and angles (°)
[Ag(7) ₂](SbF ₆)(C ₆ H ₆) ₂ (57)	
Ag1-N4	2.079(3)
Ag1-N8	2.074(3)
N4-Ag1-N8	171.89(14)

Fig. 130: Complex [Ag(46)₂]⁺ in **57**. Hydrogen atoms, solvent molecules as well as the SbF₆⁻ anion have been omitted for clarity.

Table 31: Bond distances and angles in compound **57**.

Interestingly, upon reacting complex **48** with either AgPF₆ or AgBF₄ salts, isomorphous heterometallic systems were obtained (**Fig. 131**). Orange crystals of {[acacCN)Cu(DPM-Ph-Im)]₂Ag}_∞(PF₆)(THF), **58**, were obtained upon slow diffusion of a EtOH solution of AgPF₆ into a THF solution of **48**, while crystals of {[acacCN)Cu(DPM-Ph-Im)]₂Ag}_∞(BF₄)(Benzene), **59**, were obtained from a CHCl₃/benzene mixture. Both compounds crystallize in the triclinic space group *P*-1 with silver ions, anions and solvent molecules on an inversion center and one copper complex **48** in general position. The silver ion is coordinated linearly to the imidazole group of two molecules of **48**, as in **57**, hence forming a trinuclear species. Owing to the interaction of the peripheral nitrile groups with copper atoms of neighboring complexes, the trinuclear complexes are interconnected (**Table 32**) affording 1-D networks along the *c* axis. Consequently, the copper centers are in a square pyramidal environment. As stated above, this type of coordination mode has been also observed for the complex **49**. Although the Cu-N_{acacCN} distances observed for **58** and **59** are longer than the one observed for **49**, it is nevertheless in the same range as those observed for other self-assembled heteroleptic complexes incorporating the [(acacCN)Cu]⁺ fragment.^{37,38}

ⁱ Work on pyridyl appended complexes and networks has been partly performed by Brandon Kilduff as part of his two-month stay in the laboratory in the frame of the REU program.

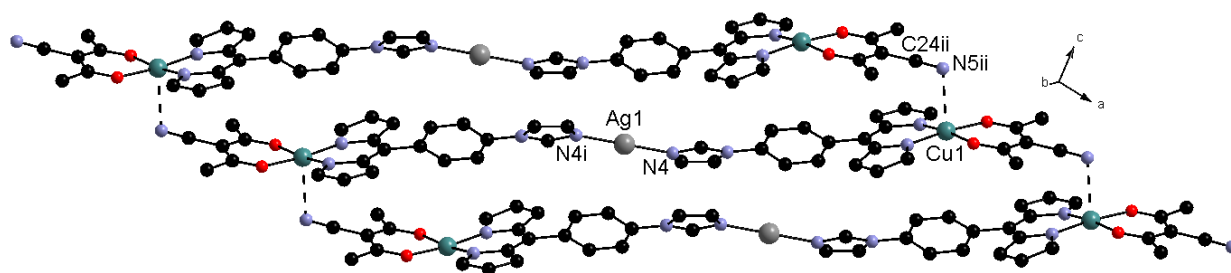


Fig. 131: Coordination ribbon $[Ag(48)_2]^+_{\infty}$ observed for **58** and **59**. Hydrogen atoms, solvent molecules as well as the anions have been omitted for clarity.

$\{[(acacCN)Cu(DPM-Ph-Im)]_2Ag\}_{\infty} (PF_6) (THF) (\mathbf{58})$				$\{[(acacCN)Cu(DPM-Ph-Im)]_2Ag\}_{\infty} (Benzene) (\mathbf{59})$			
Bonds	Distances (Å)	Angles	Angles (°)	Bonds	Distances (Å)	Angles	Angles (°)
Ag1-N4	2.090(3)	N4-Ag1-N4i	180.0(3)	Ag1-N4	2.084(3)	N4-Ag1-N4i	180.0(3)
Cu1-N5ii	2.631(4)	C24ii-N5ii-Cu1	103.6	Cu1-N5ii	2.620(4)	C24ii-N5ii-Cu1	105.4

Table 32: Selected bond lengths and angles for compounds **58** and **59**.

Slow evaporation of a MeCN/*o*-Xylene solution of **48** and AgOTf afforded orange crystals of $\{[(acacCN)Cu(DPM-Ph-Im)]_2Ag(OTf)\}_{\infty} (o\text{-Xylene}) (\mathbf{60})$ (63 %). It crystallizes in the triclinic space group *P*-1 with two complexes **48**, one Ag⁺ cation, one triflate anion and an *o*-xylene molecule in general position. The two complexes **48** differ in the geometry around the copper centers (Fig. 132). While one shows a square planar arrangement, the other is in a square pyramidal coordination environment owing to an interaction with an oxygen atom of the triflate anion ($d_{Cu-O} = 2.405(3)$ Å). The bond distances in the CuN₂O₂ cores (Table 33) are similar to the ones observed in the starting heteroleptic complex (**48**) (Table 21).

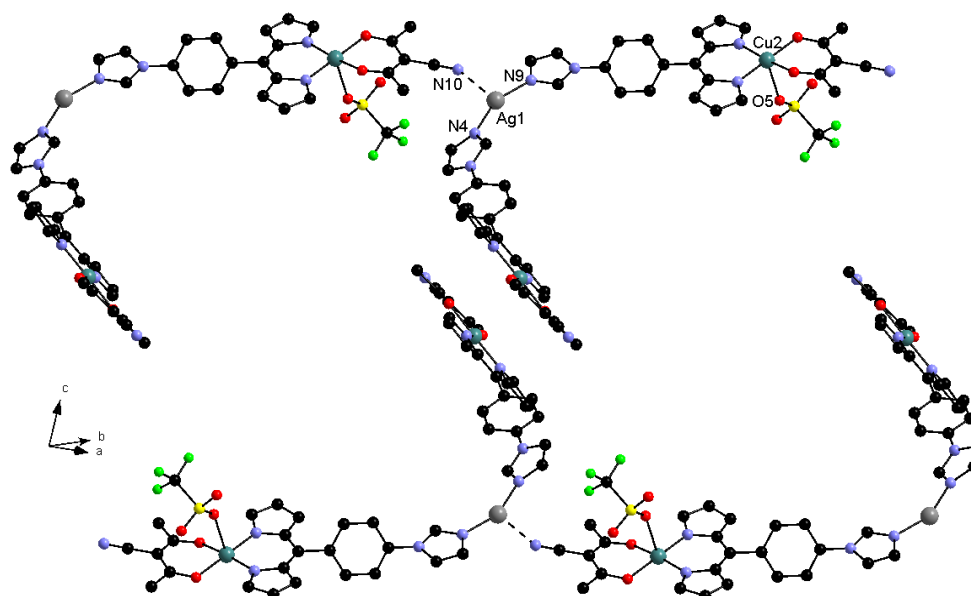


Fig. 132: Portions of 1-D networks $[Ag(9)_2(OTf)]_{\infty}$ in **60** showing the interdigitation of consecutive networks. Hydrogen atoms and solvent molecules have been omitted for clarity.

Bonds	Distances (Å)	Bonds	Distances (Å)	Bonds	Distances (Å)	Bonds	Distances (Å)
Cu1-N1	1.952(3)	Cu1-O1	1.934(2)	Cu2-N6	1.957(3)	Cu2-O3	1.956(2)
Cu1-N2	1.941(3)	Cu1-O2	1.945(2)	Cu2-N7	1.947(2)	Cu2-O4	1.964(2)

Table 33: Selected bond lengths and angles for compound **60**.

As in the case of **57-59**, the Ag^+ center is coordinated to the two copper complexes *via* the imidazole groups (**Fig. 132**). The coordination geometry around the silver ion however deviates from linearity with a N(im)-Ag-N(im) angle of $154.93(10)^\circ$. This is due to an additional weak $\text{CN}\cdots\text{Ag}$ interaction (**Table 34**) with the nitrile group of the *acacCN* capping ligand of a neighbouring complex (**Fig. 132**). This leads to the formation of one-dimensional chains of trinuclear species. Since only one of the two complexes **48** interact with the silver ion, the resulting chain possesses a comb shape. The consecutive comb shape arrangements are interdigitated with a face-to-face organization of the copper complexes. The space between combs is occupied by *o*-xylene molecules.

Bonds	Distances (Å)	Angles	Angles (°)
Ag1-N4	2.135(3)	N4-Ag1-N9	154.93(10)
Ag1-N9	2.141(3)	N4-Ag1-N10	109.79(10)
Ag1-N10	2.627(3)	N9-Ag1-N10	93.94(10)

Table 34: Bond distances and angles in the silver environment of compound **60**.

Heterometallic networks based on the pyridine appended metallatectons **50** and **51** were obtained in crystalline form by reaction with the corresponding silver salts and slow evaporation of CH_3CN /Benzene (or *o*-Xylene) solution mixtures. These systems illustrate the dependence on the organization of the bimetallic networks of the position of the nitrogen atom in the pyridine moiety of the starting metallatectons.

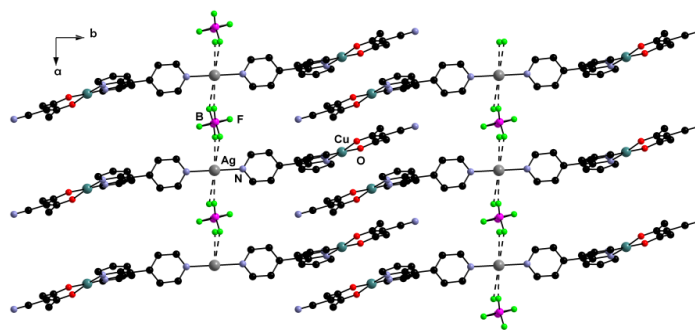


Fig. 133: Structure of 1-D network **61**. Hydrogen atoms and solvent molecules have been omitted for clarity.

Network $\{[\text{Ag}(\text{acacCN})\text{Cu}(\text{DPM-4Py})_2](\text{BF}_4)\}_n$, **61**, crystallized by slow evaporation of a $\text{CH}_3\text{CN}/o\text{-Xylene}$ mixture (59 %) in the monoclinic $P2_1/n$ space group with one copper complex in general position, a silver ion on an inversion center and the anion disordered around the inversion center. The silver ion is linearly coordinated to two pyridine groups ($d(\text{N-Ag})=2.137(3)$ Å). Along the *a* axis, the trinuclear units organize into 1-D networks *via* Ag-F interactions between silver cations and fluorine atoms of the BF_4^- anions ($d(\text{Ag-F})=2.827(5)$ Å; $2.844(6)$ Å) (**Fig. 134**). This bridging mode of the BF_4^- anion is unusual, although some examples have been described in the literature.^{39,40} Along the *b* axis, these comb-like 1-D networks interdigit with metallatectons **51** facing each other. The coordination geometry around the copper center is similar to the one observed for the starting complex albeit without interaction with the pyridyl group leading to a slightly distorted square planar environment with Cu-N and Cu-O distances (**Table 35**) close to those of **51** (**Table 24**). Although compound bears a peripheral secondary coordination poles, these nitriles are not involved in the coordination.

Bonds	Distances (Å)	Bonds	Distances (Å)
Cu-N1	1.942(2)	Cu-O1	1.941(2)
Cu-N2	1.947(2)	Cu-O2	1.940(2)

Table 35: Bond distances around the copper center in compound **61**.

Two isomorphous compounds were obtained by reaction of **50** with $\text{Ag}(\text{BF}_4)$ and crystallized as $\{[\text{Ag}((\text{acacCN})\text{Cu}(\text{DPM-3Py}))_2]\text{BF}_4(\text{Benzene})\}_\infty$, **62a**, and $\{[\text{Ag}((\text{acacCN})\text{Cu}(\text{DPM-3Py}))_2]\text{BF}_4(\text{o-Xylene})\}_\infty$, **62b**, by slow evaporation of $\text{CH}_3\text{CN}/\text{Benzene}$ and $\text{CH}_3\text{CN}/\text{o-Xylene}$ mixtures. Both of them crystallized in the monoclinic $C2/c$ space group with a copper complex in general position and a silver ion, a BF_4^- anion and solvent molecules on a twofold screw axis. These two structures are almost identical (**Fig. 134**). The sole difference lies in the solvate molecules. They are facing the silver ion but at a distance higher than 4 Å suggesting the absence of interactions. In these structure, the silver cations is here again linearly coordinated to two pyridyl nitrogen atoms to form trinuclear $[\text{Ag}((\text{acacCN})\text{Cu}(\text{DPM-3Py}))_2]^+$ units. The latter self-assemble into 1-D network owing to the interaction of the peripheral nitrile groups with the silver ions.

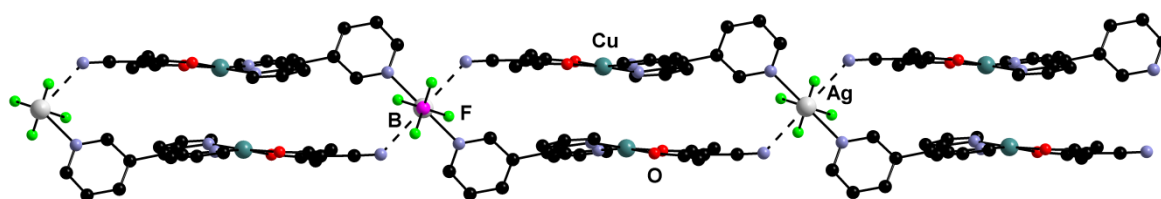


Fig. 134: View on the networks 62(a and b) along B-Ag axis. Hydrogen atoms and solvent molecules have been omitted for clarity.

The silver atom adopts therefore a distorted tetrahedral coordination environment with bond distances and angles presented in **Table 36**. As expected, these geometrical data are practically identical for both networks. The copper metallatecton **50** has a structure similar to the one observed in the free complex.

Network 62a				Network 62b			
Bonds	Distances (Å)	Angles	Angles (°)	Bonds	Distances (Å)	Angles	Angles (°)
Ag-N _{Py}	2.216(3)	N _{Py} -Ag-N _{Py}	147.24(12)	Ag-N _{Py}	2.219(2)	N _{Py} -Ag-N _{Py}	148.39(11)
Ag-N _{CN}	2.668(4)	N _{CN} -Ag-N _{Py}	95.56(10)	Ag-N _{CN}	2.700(3)	N _{CN} -Ag-N _{Py}	94.91(9)
Ag-F	2.838(3)	N _{CN} -Ag-N _{CN}	162.18(10)	Ag-F	2.868(3)	N _{CN} -Ag-N _{CN}	162.00(7)

Table 36: Bond distances and angles around the silver ions in 62a and 62b.

While BF_4^- is usually considered a rather non-coordinating anion, it acts here as a chelate to the silver ions via two weak Ag-F interactions (**Table 36, Fig. 135**). This chelate type of coordination with silver cations has already been described in the literature^{35e,40,41} with a $\text{F}\cdots\text{Ag}$ distance of 2.886(2) Å in $[\text{Ag}(1,4\text{-dithiane})]\text{BF}_4$ ^{35e,41}, for example, in agreement with what is seen here. Overall, the silver centers are hexacoordinated considering these weak $\text{F}\cdots\text{Ag}$ interaction.

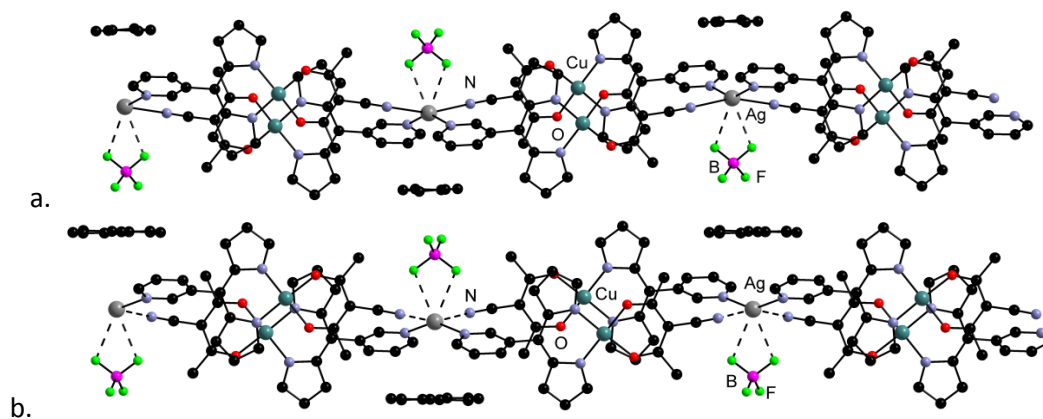


Fig. 135: Solvent and anion molecules in the networks 62a (a) and 62b (b). Hydrogen atoms have been omitted for clarity.

A similar architecture is observed in the network $\{[(\text{Cu}(\text{acacCN})(\text{DPM-3Py}))_2\text{Ag}]\text{OTf}\}_\infty$, **63**, obtained upon reaction of **50** with AgOTf. This heterometallic 2-D network crystallized (41 %) by slow evaporation of a $\text{CH}_3\text{CN}/o\text{-xylene}$ mixture in the triclinic $P-1$ space group with a copper metallatecton in general position and one silver ion and a disordered triflate anion on inversion centers. Along the c axis, the network formed (**Fig. 136**) is almost identical to the one observed for AgBF_4 (**62a** and **62b**). The silver atom is coordinated to two pyridine groups and interacts with two nitrile groups. The distance between copper centres is $3.658(1)$ Å, less than in **62a** and **62b** (>4 Å). Here again the structure of the copper complex itself is unchanged (**Table 37**).

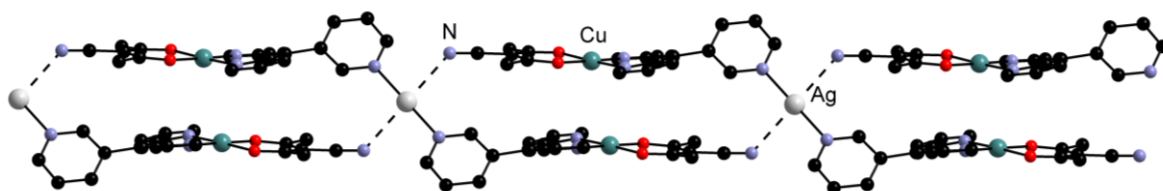


Fig. 136: Structure of network **63**. View along the b axis. Hydrogen atoms as well as the anions have been omitted for clarity.

Along the b axis, these 1-D coordination networks are connected *via* interactions between the silver centers and the disordered triflate anions ($d_{\text{Ag-O}}=2.825(19)$ Å) (**Fig. 137**, **Table 37**). Unlike the two previous structures (**62a** and **62b**), two OTf anions are coordinated to the silver centre symmetrically, resulting in an overall octahedral coordination environment.

It is interesting to note that in the case of the pyridyl appended copper metallatecton, there is no striking effect on the organization of the trinuclear Cu_2Ag units and that the nitrile groups interact rather with the Ag ion than with the copper ions.

A common feature in these architectures is that the organization of the coordination networks is mostly one-dimensional. Only one 2-D network has been obtained with the assistance of the triflate anions in **63**. The situation should be different in the case of the cobalt metallatectons. Indeed, the coordination sphere of these complexes is filled and no interaction with the nitrile groups is to be expected. However, the presence of three peripheral coordinating groups, namely two dipyrins and one nitrile, should increase the dimensionality of the heterometallic architectures.

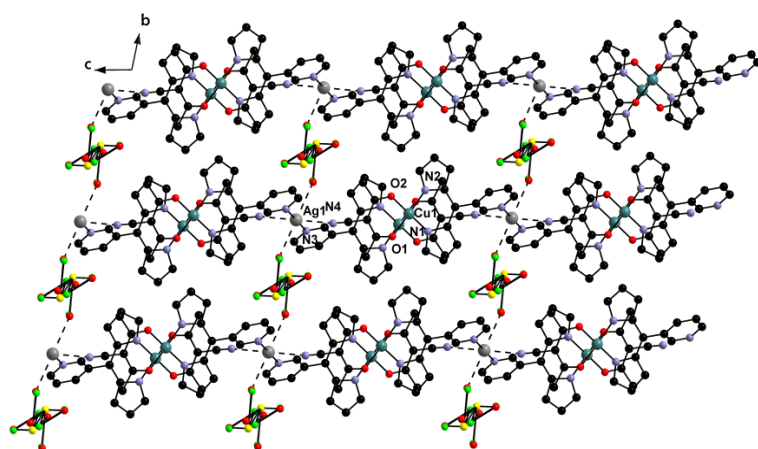


Fig. 137: Formation of 2-D network via interactions between silver centers and triflate anions in network **63**.

Bonds	Bond distances (Å)
$\{[(\text{acacCN})\text{Cu}(\text{DPM-3py}))_2\text{Ag}](\text{Otf})\}_\infty$ (63)	
Ag-N _{Py}	2.177(5)
Ag-N _{CN}	2.711(6)
Ag-O _{OTf}	2.825(19)
Cu-N1	1.959(5)
Cu-N2	1.942(6)
Cu-O1	1.938(5)
Cu-O2	1.937(6)

Table 37: Selected bond lengths for network **63**.

Reaction of the pyrazole and imidazole appended cobalt complexes did not afford any networks in crystalline form, but two heterometallic networks were obtained by reaction of the heteroleptic complexes **55** and **56** containing 3- and 4-pyridine moieties as a secondary coordination poles with silver salts.

The association of the heteroleptic metalloligand **55**, containing 3-pyridyl groups, with AgOTf led to the formation of the bimetallic 2-D architecture $\{[(\text{acacCN})\text{Co}(\text{DPM-3py})_2]\text{AgOTf}\}_\infty(\text{CH}_3\text{CN})$, **64**. Network **64** was obtained by slow evaporation of a $\text{CH}_3\text{CN}/o\text{-xylene}$ mixture in 46 % yield and crystallized in the monoclinic $P2_1/n$ space group with one cobalt complex, one silver center, one triflate anion and one acetonitrile molecule in general position. Each silver(I) center is linearly coordinated to two different metallatectons (**55**) *via* the pyridine groups hence resulting in 1-D zigzag chains (**Fig. 138**). One oxygen atom of the triflate anion is coordinated to the Ag^+ cations providing a T-shape coordination environment (**Table 38**). The structure of the metallatecton in the network is practically identical to the one of the starting complex (**55**). The nitrile coordination pole is not included in the coordination sphere in this case and remains free.

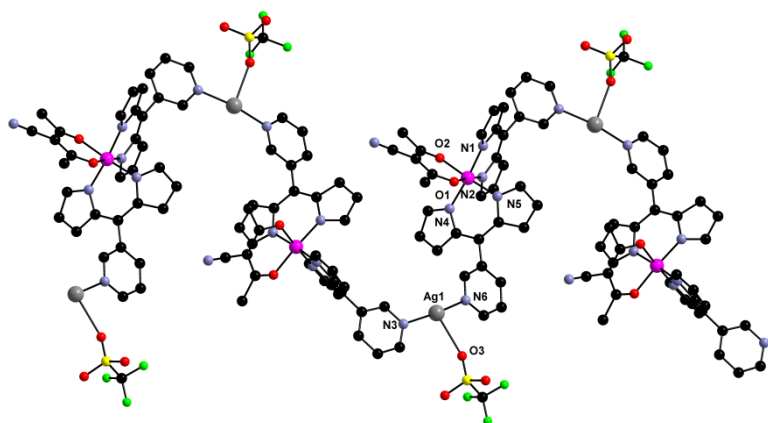


Fig. 138: Formation of 1-D zigzag chain of network **64**. Hydrogen atoms have been omitted for clarity.

Bonds	Bond distances (Å)
$\{[(\text{acacCN})\text{Co}(\text{DPM-3py})_2]\text{AgOTf}\}_\infty(\text{CH}_3\text{CN})$, (64)	
N(3)-Ag	2.154(4)
N(6)-Ag	2.147(4)
O(3)-Ag	2.665(5)
N1—Co1	1.927(4)
N2—Co1	1.911(4)
N4—Co1	1.917(4)
N5—Co1	1.913(4)
O1—Co1	1.906(4)
O2—Co1	1.910(3)
Angles	Angles (°)
N(6)-Ag-N(3)	171.10(14)

Table 38: Selected bond lengths and angles for network **64**.

These zigzag chains organize into a 2-D network via $d^{10}\text{-}d^{10}$ interaction between silver atoms (3.224(2) Å) of neighboring chains (**Fig. 139**). This Ag-Ag distance is similar to what has been observed in the structure of macrocycles **39** and **40**.

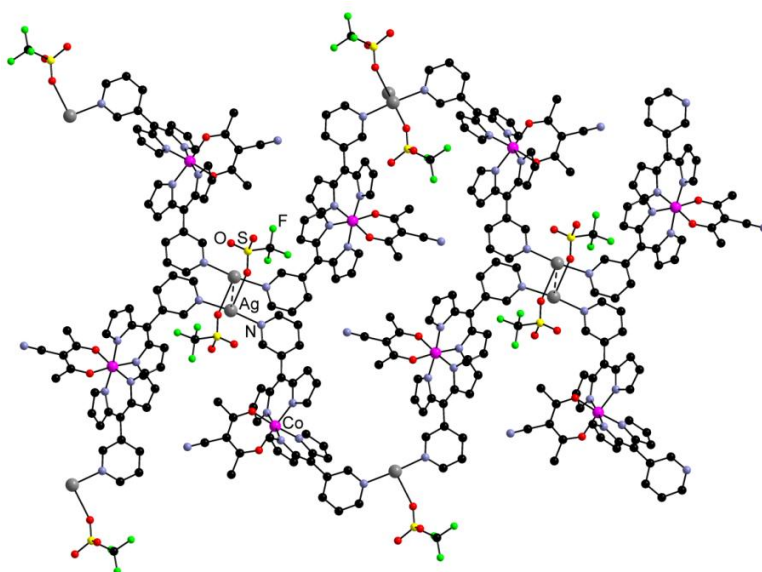


Fig. 139: Formation of a 2-D network via Ag-Ag $d^{10}\text{-}d^{10}$ interaction in compound **64**.

Each individual 1-D chain is homochiral but they are connected via $d^{10}-d^{10}$ interaction around an inversion center, thus leading to an overall racemic mixture.

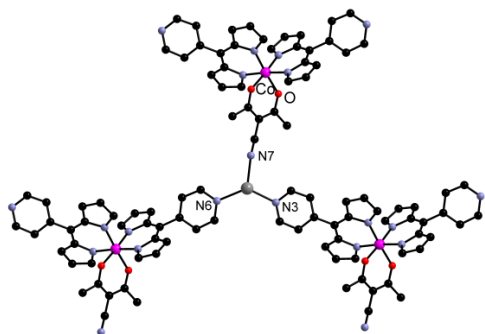


Fig. 140: Silver environment in network **65**.

Bonds	Bond distances (Å)
$\{[(\text{acacCN})\text{Co}(\text{DPM-4py})_2]\text{Ag}\}_\infty(\text{BF}_4)(\text{Benzene})_{0.5}(\text{CH}_3\text{CN})_3$, (65)	
N(3)-Ag	2.253(3)
N(6)-Ag	2.236(3)
N(7)-Ag	2.277(4)
Angles	Angles (°)
N(6)-Ag-N(3)	129(8)
N(7)-Ag-N(3)	118.93(11)
N(7)-Ag-N(6)	107.64(13)

Table 39: Selected bond lengths and angles for network **65**.

The bimetallic 2-D network $\{[(\text{Co}(\text{DPM-4Py})_2(\text{acacCN}))_2\text{Ag}](\text{BF}_4)\}_\infty(\text{Benzene})_{0.5}(\text{CH}_3\text{CN})_3$ (**65**) based on the 4-pyridyl appended metallatecton (**56**) was obtained by slow evaporation of a $\text{CH}_3\text{CN}/\text{Benzene}$ mixture in 56 % yield. It crystallized in the triclinic space group $P-1$ with one copper metallatecton, one silver ion and one triflate anion and MeCN molecules in general position and a benzene molecule on an inversion centre. The silver center is coordinated to two pyridine and one nitrile groups (Fig. 141, Table 39), interacting therefore with three different heteroleptic $\{\text{Co}(\text{acac-CN})(\text{DPM-4Py})\}$ metalloligands, leading thus to the formation of a (6,3) 2-D honeycomb network (Fig. 141a). This organization is analogous to the one reported by Cohen²² in the case of the assembly of homoleptic $\{\text{Co}(\text{DPM-4Py})_3\}$ complexes with AgSbF_6 and AgPF_6 (Fig. 90c). Interestingly, using AgBF_4 as a silver source, Cohen obtained a 3-D network unlike what is obtained here. Another difference with this latter structure is the fact that no interaction of the fluorine atoms of the BF_4^- anions with the $\text{Ag}(\text{I})$ cations is observed here.

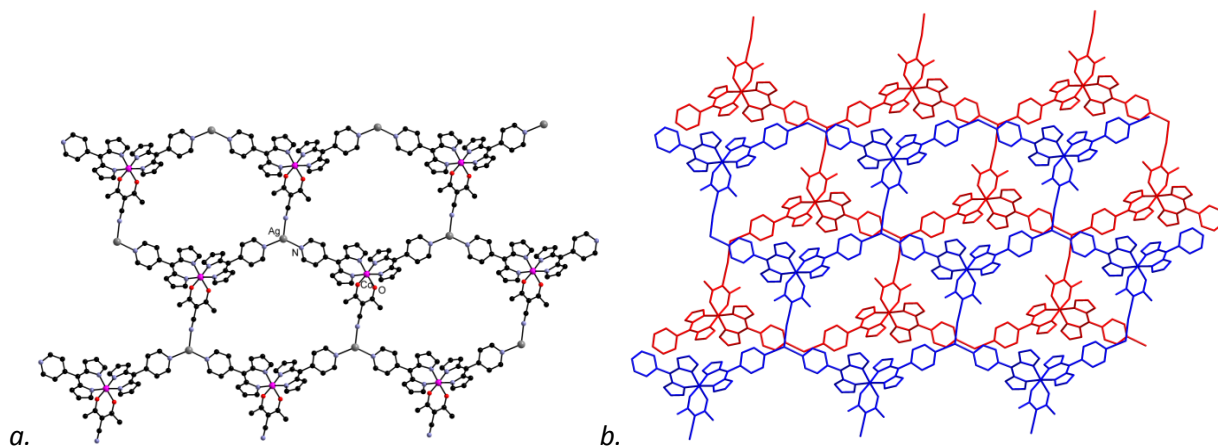


Fig. 141: Honeycomb 2-D network **65** (a) and alternation of neighboring homochiral layers (b). Hydrogen atoms as well as the anions and solvents have been omitted for clarity.

While the cobalt complexes are chiral, both Λ and Δ enantiomers are present in **65**, and the structure contains a racemic mixture. However, it is worth noting that the 2-D layers of the network are homochiral, containing either enantiomers (Fig. 141b). These enantiomerically pure layers alternate in a $\Lambda\Delta\Delta\Delta$ pattern. Along the b axis, the space between these slabs differ (Fig. 142). Two $\Lambda\Delta$ layers associate without any solvent present within this double layer. Between these double-slabs, benzene and acetonitrile molecules are present. The position of the benzene molecule parallel to the 2-D layers

and facing two silver ions slightly shifted from the N-N-N coordination plane (0.246 Å) is worth emphasizing. Such an orientation suggests a Ag- π interaction which would result in a bridging of the 2-D networks. However, the shortest distance between silver atom and carbon atoms of the benzene ring (2.922(6) Å) is rather long for this type of interactions (2.41 ± 0.05 Å).^{25d}

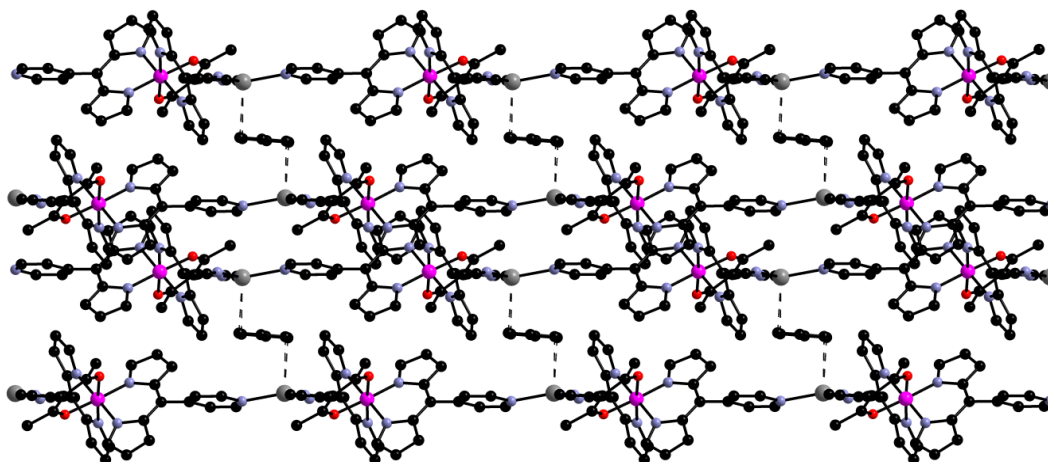
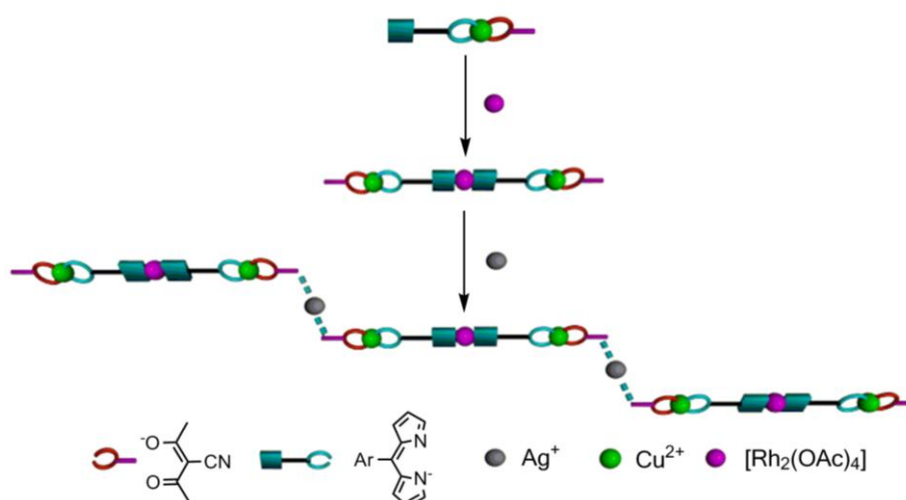


Fig. 142: Alternation of the 2-D layers along the *b* axis in compound 65. Hydrogen atoms have been omitted for clarity.

Owing to the presence of two potential coordination poles with different coordination behavior on these metallatectons, a new synthetic approach towards trimetallic architectures was developed (**Scheme 40**). Instead of the direct assembly of the heteroleptic metallatectons with silver salts, which leads to the formation of bimetallic networks, an additional step can be introduced. During this step, the metallatecton reacts with a first metal center selectively by one of the coordination poles with the formation of an intermediate discrete bimetallic complex. Subsequently, this bimetallic building block can be reacted with silver salts, thus leading to trimetallic networks. Rhodium acetate was chosen as a linear spacer between two molecules of metallatecton. Two heteroleptic copper complexes (**51**) and (**48**), appended with 4-Py and -Ph-Im groups respectively, were reacted with rhodium acetate in a 2:1 stoichiometric ratio.



Scheme 40: Synthetic approach to the preparation of trimetallic architectures.

Two bimetallic tetranuclear discrete complexes $[\text{Rh}_2(\text{OAc})_4((\text{acacCN})\text{Cu}(\text{DPM-4Py}))_2](\text{DiOX})_4$, **66**, and $[\text{Rh}_2(\text{OAc})_4((\text{acacCN})\text{Cu}(\text{DPM-Ph-Im}))_2](\text{CHCl}_3)_3$, **67**, were obtained in 41 % and 70 % yields respectively (**Fig. 143**).

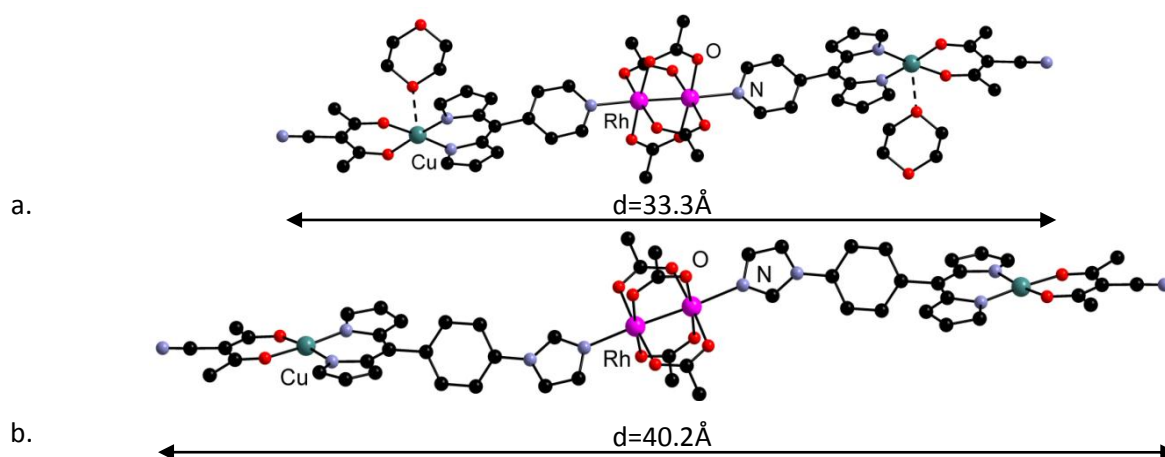
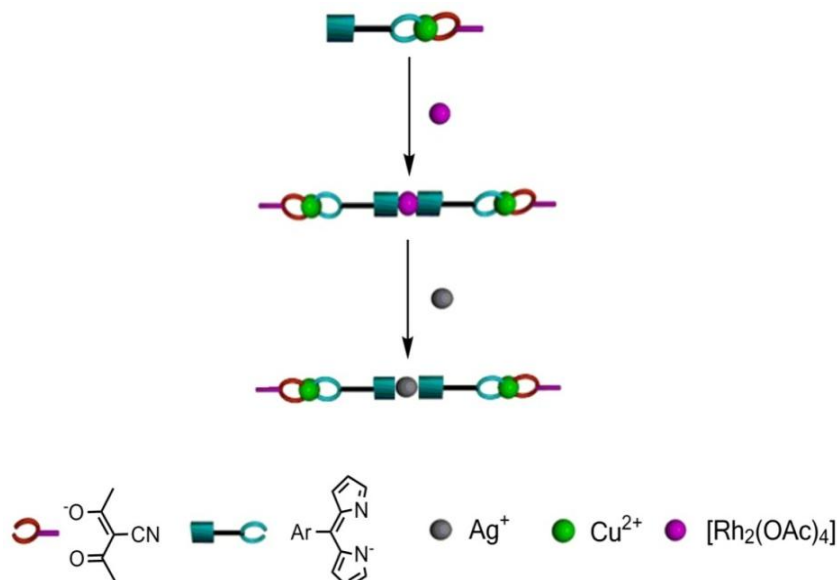


Fig. 143: Structure and length of the bimetallic complexes 66 (a) and 67 (b).

Complex **66** crystallized by slow diffusion of *n*-pentane into a dioxane solution, in the triclinic *P*-1 space group with one starting metallatecton moiety in general position and the rhodium acetate fragment on an inversion center.

Complex **67** crystallized by slow diffusion of *n*-pentane into a CHCl_3 solution of the complex, in the monoclinic *P*₂₁/*c* space group with a copper complex in general position and both the chloroform solvate molecule and the rhodium acetate on inversion centers. Both molecules organized in the same manner, with two molecules of starting metallatectons (**51** and **48**) coordinated to the two axial positions of the dimer *via* N-Rh interactions ($d(\text{N-Rh})= 2.232(2)\text{\AA}$ and $2.220(3)\text{\AA}$ respectively) with the imidazole and pyridine coordination pole respectively. These discrete bimetallic species possess two peripheral nitrile groups available for further coordination. In both complexes, no intermolecular interactions between the peripheral nitrile groups and copper atoms of neighboring molecules are observed. It is worth noting the length of these linear metalloligands with the two available nitrile coordinating groups separated by a distance 33.3\AA and 40.2\AA respectively.



Scheme 41: Substitution of rhodium acetate fragment with formation of bimetallic copper and silver appended networks.

Unfortunately at the final step, all attempts to obtain trimetallic architecture upon reactions with silver salts led to the decomposition of these metalloligands and substitution of the rhodium acetate fragments by silver centers leading to the formation of Cu/Ag networks such as the ones described above, for example for **58** (Scheme 41).

III.4. Conclusion

The DPM appended ligands were synthesized and used for the preparation of discrete complexes and extended homo- and hetero-metallic architectures. As for 7-azaindole, two modes of coordination were defined and exploited. The DPM fragments can be used as such, without deprotonation, to afford a family of macrocyclic compounds upon reaction with silver (I) salts. These species were characterised by X-ray single crystal diffraction. Depending on the nature of the anion and the peripheral coordination poles, different architectures, ranging from discrete macrocycles to extended 3-D networks were observed in the solid state. The stability and behaviour of these compounds in solution were investigated by $^1\text{H-NMR}$, $^{13}\text{C-NMR}$ and DOSY-NMR measurements.

A series of homo- and hetero-leptic complexes illustrating the coordination of the dipyrinate moiety has been obtained. The homoleptic species were prepared upon reaction with $\text{Cu}(\text{OAc})_2$, $\text{Na}_3\text{Co}(\text{NO}_2)_6$ and FeCl_3 . The compounds were characterised by X-ray single crystal diffraction, UV-Visible spectroscopy, $^1\text{H-NMR}$ and $^{13}\text{C-NMR}$. Unfortunately all attempts to use these homoleptic complexes as metalloligands for the preparation of extended heterometallic architectures led to the formation of non-crystalline or unstable materials. A broader series of heteroleptic complexes was obtained by reaction of -Ph-Im, -Ph-Pyr, -3Py, -4Py and -Ph-4Py appended ligands with $\text{Cu}(\text{acac})_2$, $\text{Cu}(\text{acacCN})_2$ and $\text{Co}(\text{acacCN})_2$ and characterised in the solid state and in solution. Depending on the nature of the secondary coordination pole and the solvent of crystallisation, different extended architectures and discrete complexes were observed for the copper species, while only discrete complexes were obtained with cobalt. The $(\text{acacCN})\text{Cu}(\text{DPM})$ complexes self-assemble into one-dimensional chains but with different connectivity patterns. In the case of the imidazole or pyridines appended complexes, the peripheral nitrogen is coordinated to the copper atom in a square pyramidal coordination environment. Rather interestingly, in the case of the pyrazole analogue, **49b**, the peripheral nitrile group of the acacCN capping ligand is weakly coordinated to a copper atom.

Both groups of cobalt (III) and copper (II) heteroleptic complexes were used for the preparation of heterometallic architectures by reaction with silver (I) salts and rhodium acetate.

Upon self-assembly of the heteroleptic copper complexes **46**, **48-52** with silver salts, trinuclear species are formed. While, in the case of $(\text{acac})\text{Cu}(\text{DPM-Ph-Im})$ **46**, the absence of peripheral coordinating nitrile groups prevents any self-assembly. In other cases coordination processes lead to formation of extended architectures. For the networks based on $(\text{acacCN})\text{Cu}(\text{DPM-Ph-Im})$ **48** complex, in the presence of a weakly coordinating anion such as BF_4^- or PF_6^- , weak interactions between the CN groups and the copper atoms of another trinuclear unit are observed. In the case of the slightly more coordinating OTf anion, the axial position of the copper center is occupied and thus not available. Consequently, the interaction of the nitrile group takes place with the silver ion of another trinuclear unit. In the case of complex **50** with the 3-Py moiety as a secondary coordination pole, a double layer architecture with the silver centre surrounded by two pyridine and two CN groups is formed. A 1-D network was obtained by assembly of the heteroleptic complex **51**, with the -4Py coordination pole, with AgBF_4 . The silver centre is coordinated to the two copper complexes *via* the pyridyl groups forming a trinuclear species, and the two -CN are not involved in any coordination. Unfortunately, the two pyrazole functionalized complexes **47** and **49** did not form crystalline heterometallic systems.

Upon self-assembly of the heteroleptic cobalt complexes **55** and **56** with silver salts, two bimetallic networks were obtained. In the case of the -3Py appended complex 1-D zigzag chains, connected via $\text{Ag-Ag } d^{10}\text{-}d^{10}$ interactions, are observed with the silver centre surrounded by two pyridine groups and one anion molecule. In contrast, the self-assembly of the heteroleptic cobalt complexes **56**

with -4Py moiety as a coordination pole, afforded a bimetallic 2-D honeycomb network with the silver atom surrounded by two pyridines and one -CN moiety.

Two heterometallic tetranuclear complexes based on heteroleptic copper complexes **48** and **51** with rhodium acetate were obtained. These compounds crystallized as discrete complexes with the absence of any coordination of the -CN groups. All attempts to use these complexes as metallatectons for the preparation of trimetallic architectures by reactions with silver salts led to decomplexation of the metalloligands and substitution of the rhodium acetate fragments by silver centers.

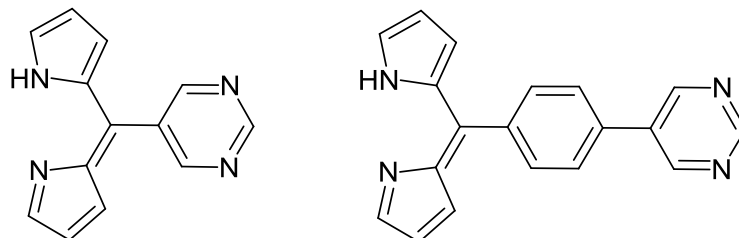


Fig. 144: Potential ligands for preparation of heterometallic architectures.

As a perspective, it could be interesting to use ligands bearing pyrimidine units as a secondary coordination poles and their complexes to form heterometallic architectures (**Fig. 144**). The additional nitrogen coordination centre should induce the formation of different types of architectures.

III.5. References

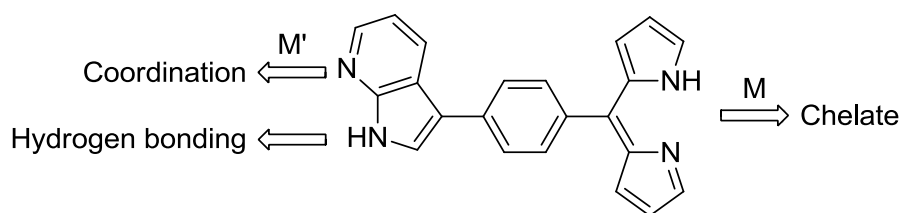
- ¹ Sazanovich, I. V., Kirmaier, C., Hindin, E., Yu, L., Bocian, D. F., Lindsey, J. S., Holten, D., *J. Am. Chem. Soc.* **2004**, *126*, 2664.
- ² Arsenault, G. P., Bullock, E., MacDonald, S. F., *J. Am. Chem. Soc.* **1960**, *82*, 4384.
- ³ (a) Wagner, R. W., Lindsey, J. S., *Pure Appl. Chem.* **1996**, *68*, 1373; (b) Littler, J., Miller, M. A., Hung, C. H., Wagner, R. W., O'Shea, D. F., Boyle, P. D., Lindsey, J. S., *J. Org. Chem.* **1999**, *64*, 1391.
- ⁴ (a) Heinze, K., Reinhart, A., *Z. Naturforsch.* **2005**, *60b*, 758; (b) Baudron, S. A., Salazar-Mendoza, D., Hosseini, M. W., *CrystEngComm* **2009**, *11*, 1245; (c) Lin, K. J., Wu, J. Y., Chen, C. T., *Acta Cryst.* **1996**, *C52*, 3114; (d) Bennis, V., Gallagher, J. F., *Acta Cryst.* **1998**, *C54*, 130; (e) Foxon, S. P., Smith, J. R. L., O'Brien, P., Reginato, G., *J. Chem. Soc., Perkin Trans. 2* **2001**, 1145; (f) Patra, G. K., Diskin Posner, Y., Goldberg, I., *Acta Cryst.* **2002**, *E58*, o530; (g) Gokulnath, S., Prabhuraja, V., Sankar, J., Chandrashekar, T. K., *Eur. J. Org. Chem.* **2007**, 191; (h) Senge, M. O., *Acta Cryst.* **2007**, *E63*, o3679; (i) Maeda, H., Hasewaga, M., Ueda, A., *Chem. Commun.* **2007**, 2726; (j) Easson, M. W., Fronczek, F. R., Jensen, T. J., Vicente, M. G. H., *Bioorg. Med. Chem.* **2008**, *16*, 3191; (k) Kumar, R., Misra, R., Prabhuraja, V., Chandrashekar, T., *Chem. Eur. -J.* **2005**, *11*, 5695.
- ⁵ Shin, J. Y., Dolphin, D., Patrick, B. O., *Cryst. Growth Des.* **2004**, *4*, 659.
- ⁶ Salazar-Mendoza, D., Baudron, S. A., Hosseini, M. W., *Inorg. Chem.* **2008**, *47*, 766.
- ⁷ Pyykkö, P., *Chem. Rev.* **1997**, *97*, 597.
- ⁸ Hall, J. D., McLean, T. M., Smalley, S. J., Waterland, M. R., Telfer, S. G., *Dalton Trans.* **2010**, *39*, 437.
- ⁹ Brückner, C., Karunaratne, V., Rettig, S. J., Dolphin, D., *Can. J. Chem.* **1996**, *74*, 2182.
- ¹⁰ Gill, H. S., Finger, I., Božidarević, I., Szydlo, F., Scott, M., *New J. Chem.* **2005**, *29*, 68.
- ¹¹ Halper, S. R., Malachowski, M. R., Delaney, H. M., Cohen, S. M., *Inorg. Chem.* **2004**, *43*, 1242.
- ¹² Salazar-Mendoza, D., Baudron, S. A., Hosseini, M. W., *Chem. Commun.* **2007**, 2252.
- ¹³ Halper, S. R., Cohen, S. M., *Inorg. Chem.* **2005**, *44*, 486.
- ¹⁴ Stork, J. R., Thoi, V. S., Cohen, S. M., *Inorg. Chem.* **2007**, *46*, 11213.
- ¹⁵ Brückner, C., Zhang, Y., Rettig, S. J., Dolphin, D., *Inorg. Chim. Acta* **1997**, *263*, 279.
- ¹⁶ Miao, Q., Shin, J. Y., Patrick, B. O., Dolphin, D., *Chem. Commun.* **2009**, 2541.
- ¹⁷ (a) Murakami, Y., Sahara, K., *Inorg. Chim. Acta* **1968**, *2*, 273; (b) March, F. C., Conch, D. A., Emerson, K., Fergusson, J. E., Robinson, W. T., *J. Chem. Soc. A* **1971**, 440; (c) Johnson, A. W., Kay, I. T., Markham, E., Price, R., Shaw, K. B., *J. Chem. Soc.* **1959**, 3416; (d) Fergusson, J. E., Ramsay, C. A., *J. Chem. Soc.* **1965**, 5222; (e) Murakami, Y., Matsuda, Y., Sakata, K., *Inorg. Chem.* **1971**, *10*, 1728.
- ¹⁸ (a) Sano, Y., Tanaka, M., Koga, N., Matsuda, K., Iwamura, H., Rabu, P., Drillon, M., *J. Am. Chem. Soc.* **1997**, *119*, 8246; (b) Dong, Y. B., Smith, M. D., Layland, R., Loye, H. C., *Inorg. Chem.* **1999**, *38*, 5027; (c) Tabellio, F. M., Seidel, S. R., Arif, A. M., Stang, P. J., *J. Am. Chem. Soc.* **2001**, *123*, 7740; (d) Horikoshi, R., Mochida, T., Moriyama, H., *Inorg. Chem.* **2001**, *40*, 2430; (e) Zaman, M. B., Smith, M. D., Ciurtin, D. M., Loye, H. C., *Inorg. Chem.* **2002**, *41*, 4895; (f) Zaman, M. B., Udachin, K. A., Ripmeester, J. A., *CrystEngComm* **2002**, *4*, 613.
- ¹⁹ Halper, S. R., Cohen, S. M., *Angew. Chem. Int. Ed.* **2004**, *43*, 2385.
- ²⁰ Do, L., Halper, S. R., Cohen, S. M., *Chem. Commun.* **2004**, 2662.
- ²¹ Halper, S. R., Cohen, S. M., *Inorg. Chem.* **2005**, *44*, 4139.
- ²² Halper, S. R., Do, L., Stork, J. R., Cohen, S. M., *J. Am. Chem. Soc.* **2006**, *128*, 15255.
- ²³ Murphy, D. L., Malachowski, M. R., Campana, C. F., Cohen, S. M., *Chem. Commun.* **2005**, 5506.
- ²⁴ Garibay, S., Stork, J. R., Wang, Z., Cohen, S. M., Telfer, S. G., *Chem. Commun.* **2007**, 4881.
- ²⁵ (a) Hall Griffith, E. A., Amma, E. L., *J. Am. Chem. Soc.* **1974**, *96*, 743; (b) Shelly, K., Finster, D. C., Lee, Y. J., Scheidt, R., Reed, C. A., *J. Am. Chem. Soc.* **1985**, *107*, 5955; (c) Munakata, M., Wu, L. P., Ning, G. L., *Coord. Chem. Rev.* **2000**, *198*, 171; (d) Lindeman, S. V., Rathore, R., Kochi, J. K., *Inorg. Chem.* **2000**, *39*, 5707.
- ²⁶ (a) Thompson, A., Dolphin, D., *Org. Lett.* **2000**, *2*, 1315; (b) Ikeda, M., Tanida, T., Takeuchi, M., Shinkai, S., *Org. Lett.* **2000**, *2*, 1803; (c) Ikeda, M., Takeuchi, M., Shinkai, S., Tani, F., Naruta, Y., Sakamoto, S., Yamaguchi, K., *Chem. Eur. -J.* **2002**, *8*, 5541; (d) Ali, A. A. S., Benson, R. E., Blumentritt, S., Cameron, T. S., Linden, A., Wolstenholme, D., Thomspson, A., *J. Org. Chem.* **2007**, *72*, 4947.

- ²⁷ Sreedhar, B., Shiva K. B., Srinivas, P., Balasubrahmanyam, V., Venkanna, G. T., *J. Mol. Catal. A: Chem.* **2007**, *265*, 183.
- ²⁸ Halper, S. R., Cohen, S. M., *Chem. Eur. -J.* **2003**, *9*, 4661.
- ²⁹ (a) Zuo-Xim, L., Tong-Liang, H., Hong, M., Yong-Fei, F., Cui-Jin, L., Ming-Liang, T., Xian-He, B., *Cryst. Growth Des.* **2010**, *10*, 1138; (b) Zhao, W., Z., Fan, J., Okamura, T., Sun, W., Ueyama, N., *New J. Chem.* **2004**, *28*, 1142; (c) Fan, J., Okamura, T., Sun, W., Ueyama, N., Tang, W., Ueyama, N., *Inorg. Chem.* **2003**, *42*, 3168.
- ³⁰ (a) Zhou, H. P., Wang, P., Hu, Z. J., Lim L., Chen, J. J., Cuim C., Tianm Y. P., Wu, G. Y., Yang, J. X., Tao, X. T., Jiang, M. H., *Eur. J. Inorg. Chem.* **2007**, 1854; (b) Liddle, B. J., Hall, D., Lindeman, S. V., Smith, M. D., Gardinier, J. R., *Inorg. Chem.* **2009**, *48*, 8404.
- ³¹ (a) Chen, B., Fronczek, F. R., Maverick, A. W., *Inorg. Chem.* **2004**, *43*, 8209; (b) Vreshch, V. D., Lysenko, A. B., Chernega, A. N., Howard, J. A. K., Krautscheid, H., Sieler, J., Domasevitch, K. V., *Dalton Trans.* **2004**, 2899; (c) Zhang, Y., Chen, B., Fronczek, F. R., Maverick, A. W., *Inorg. Chem.* **2008**, *47*, 4433.
- ³² (a) Burrows, A. D., Cassar, K., Mahon, M. F., Warren, J. E., *Dalton Trans.* **2007**, 2499; (b) Kondracka, M., Englert, U., *Inorg. Chem.* **2008**, *47*, 10246.
- ³³ Heinze, K., Reinhart, A., *Inorg. Chem.* **2006**, *45*, 2695.
- ³⁴ Salazar-Mendoza, D., Ph.D. Dissertation, Université Louis Pasteur, Strasbourg, **2007**.
- ³⁵ (a) Francisco, R. H. P., Mascarhenas, Y. P., Lechat, J. R., *Acta Cryst. Sect. B* **1979**, *35*, 177. (b) Loi, M., Hosseini, M. W., Jouaiti, A., De Cian, A., Fischer, J. *Eur. J. Inorg. Chem.* **1999**, 1981; (c) Jouaiti, A., Hosseini, M. W., Kyritsakas, N. *Eur. J. Inorg. Chem.* **2003**, 57; (d) Shu, M., Tu, C., Xu, W., Jin, H., Sun, J. *Cryst. Growth Des.* **2006**, *6*, 1890; (e) Liddle, B. J., Hall, D., Lindeman, S. V., Smith, M. D., Gardinier, J. R. *Inorg. Chem.* **2009**, *48*, 8404; (f) Ehrhart, J., Planeix, J. M., Kyritsakas-Gruber, N., Hosseini, M. W., *Dalton Trans.* **2009**, 2552; (g) Ehrhart, J., Planeix, J.M., Kyritsakas-Gruber, N., Hosseini, M. W., *Dalton Trans.* **2009**, 6309.
- ³⁶ See, for example: (a) Hoskins, B. F., Robson, R., Slizys, D. A., *J. Am. Chem. Soc.* **1997**, *119*, 2952. (b) Jin, C. M., Lu, H., Wu, L. Y., Huang, J., *Chem. Commun.* **2006**, 5039; (c) Fan, J., Zhu, H. F., Okamura, T., Sun, W. Y., Tang, W. X., Ueyama, N., *Chem. Eur. -J.* **2003**, *9*, 4724; (d) Dobrzanska, L., Llyod, G. O., Raubenheimer, H. G., Barbour, L. J., *J. Am. Chem. Soc.* **2005**, *127*, 13134; (d) Zhu, H. F., Fan, J., Okamura, T., Sun, W. Y., Ueyama, N., *Cryst. Growth Des.* **2005**, *5*, 289; (e) Liu, C. S., Chen, P. Q., Yang, E. C., Tian, J. L., Bu, X. H., Li, Z. M., Sun, H. W., Lin, Z., *Inorg. Chem.* **2006**, *45*, 5812.
- ³⁷ (a) Angelova, O., Petrov, G., Macicek, J., *Acta Cryst. Sect. C* **1989**, *45*, 710; (b) Angelova, O., Macicek, J., Atanasov, M., Petrov, G., *Inorg. Chem.* **1991**, *30*, 1943; (c) Tsiamis, C., Tzavellas, L. C., Stergiou, A., Anesti, V., *Inorg. Chem.* **1996**, *35*, 4984; (d) Tsiamis, C., Hatzidimitriou, A. G., Tzavellas, L. C., *Inorg. Chem.* **1998**, *37*, 2903; (e) Silvernail, C. M., Yap, G., Sommer, R. D., Rheingold, A. L., Day, V. W., Belot, J. A., *Polyhedron* **2001**, *20*, 3113; (f) Burdukov, A. B., Roschuplina, G. I., Gatilov, Y. V., Gromilov, S. A., Reznikov, V. A., *J. Supramol. Chem.* **2002**, *2*, 359; (g) Yoshida, J., Nishikiori, S., Kuroda, R., *Chem. Eur.-J.* **2008**, *14*, 10570.
- ³⁸ (a) Soldatov, D. V., Ripmeester, J. A., Shergina, S. I., Sokolov, I. E., Zanina, A. S., Gromilov, S. A., Dyadin, Y. A., *J. Am. Chem. Soc.* **1999**, *121*, 4179; (b) Ma, B. Q., Gao, S., Yi, T., Xu, G. X., *Polyhedron* **2001**, *20*, 1255; (c) Soldatov, D. V., Tinnemans, P., Enright, G. D., Ratcliffe, C. I., Diamente, P. R., Ripmeester, J. A., *Chem. Mater.* **2003**, *15*, 3826; (d) Yoshida, J., Nishikiori, S., Kuroda, R., *Chem. Lett.* **2007**, *36*, 678.
- ³⁹ (a) Li, H., Lee, G. H., Peng, S. M., *J. Mol. Str.* **2004**, *707*, 179; (b) Kuzu, I., Neumüller, B., *Z. Anorg. Allg. Chem.* **2007**, *633*, 941.
- ⁴⁰ (a) Horn, E., Snow, M. R., Tiekink, E. R. T., *Aust. J. Chem.* **1987**, *40*, 761; (b) Blake, A. J., Poorters, L., Armspach, D., Matt, D., Toupet, L., Jones, P. G., *Angew. Chem. Int. Ed.* **2007**, *46*, 2663.
- ⁴¹ Blake, A. J., Brooks, N. R., Champness, N. R., Cunningham, J. W., Hubberstey, P., Schroder, M., *CrystEngComm.* **2000**, *2*, 41.

IV. Chapter 3

IV.1. Introduction

As seen in Chapter 1, the 7-azaindole group self-organizes into a hydrogen bonded dimers and is capable of forming metal complexes in particular with the $[\text{Rh}_2(\text{OAc})_4]$ paddlewheel *via* coordination of the pyridyl nitrogen atom assisted by N-H...O interactions. On the other hand, as described in Chapter 2, dipyrriins can form metal complexes with a wide range of metal centres affording homo- and heteroleptic complexes. It, therefore, appeared that derivative **70** (**Scheme 42**) could be seen as an appealing candidate for the construction of extended architectures built upon both coordination and hydrogen bonding events. Indeed, it incorporates a dipyrriin unit, acting as a chelate in its conjugate base form, and a 7-azaindole group, which can be employed either for hydrogen bonding or coordination processes. One may take advantage of versatility of the latter group to build both homo- and hetero-metallic systems based on compound **70**. Before reporting our results using ligand **70**, both construction strategies will be described.



Scheme 42: 5-(4-(7-azaindol-3-yl)phenyl)-dipyrriin (**70**).

IV.1.1. Strategy towards homometallic networks

As we have seen with functionalized mono-azaindole derivatives in Chapter 1 (3-(4-benzonitrilyl)-7-azaindole and 3-Tricyanovinylene-7-azaindole), the $R_2^2(8)$ motif¹ leading to the formation of a dimer is often observed. When considering molecules comprising several 7-azaindole groups, this motif leads to the formation of extended networks such as in the crystal structures of the bis(1*H*-7-azaindol-3-yl)-methane² or bis(1*H*-7-azaindol-3-yl)(2,4,5-trimethylphenyl)methane³ ligands (**Fig. 145**). The former arranges into zigzag chains whereas the latter organizes into crenellated 1-D networks.

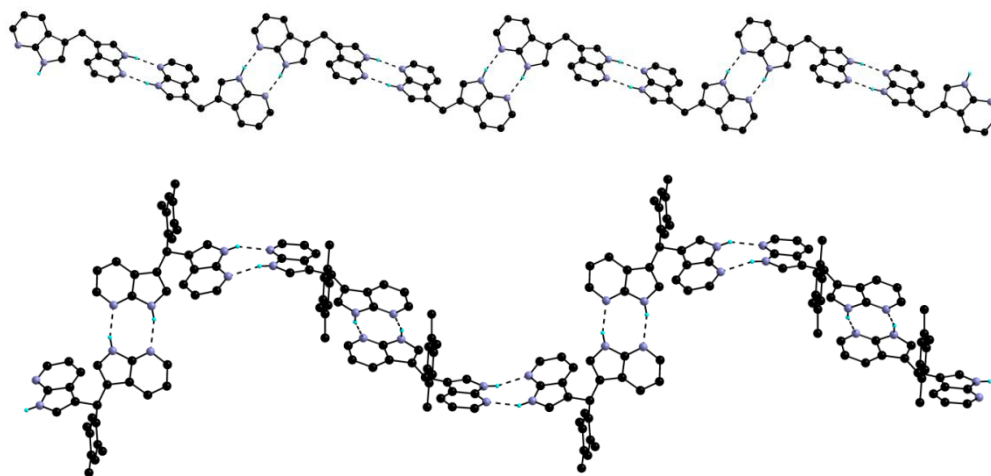
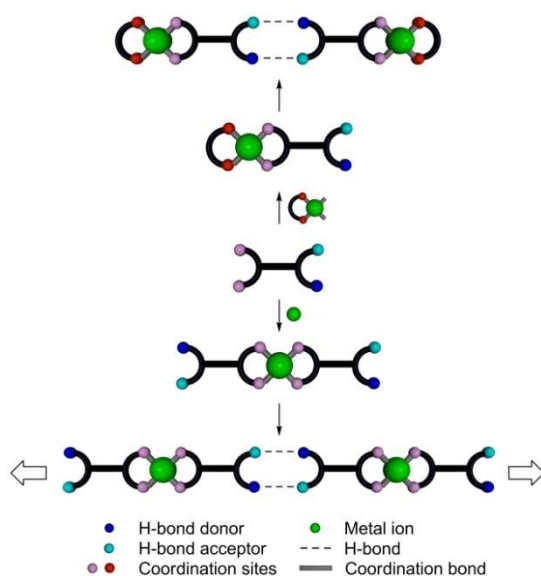


Fig. 145: Structure of bis(azaindol-3-yl)-methane and bis(1*H*-7-azaindol-3-yl)(2,4,5-trimethylphenyl)methane.

It can therefore be envisioned that the self-assembly by hydrogen bonding of metal complexes formed upon coordination of the dipyrins to metal centers as described in **Scheme 43** should lead to the formation of discrete systems in the case of heteroleptic complexes and networks in the case of homoleptic species. We should note here that this strategy is based on a hierarchy between the two coordination poles resulting from the expected prevalence of the chelate effect of the monoanionic dipyrinato over the pyridyl group of the 7-azaindole upon reaction with metal centers bearing at least two available coordination sites in *cis* positions.



Scheme 43: Self-assembly by hydrogen bonding of hetero- (top) and homo-leptic (bottom) complexes bearing peripheral 7-azaindole groups.

In the literature, the self-assembly of such functionalized metal dipyrin complexes has been reported. Indeed, several dipyrins functionalized with a hydrogen bond donor/acceptor group have been described^{4,5,6,7,8,9}. Heinze and Reinhart have showed that the heteroleptic copper complex (acac)Cu(dpm-*p*-PhCONH*i*Pr) (acac = acetylacetonate) incorporating a secondary amide group organizes into one-dimensional chains in the solid state owing to the formation of N-H...O hydrogen bonds between amide groups⁴. The primary amide analogue, dpm-*p*-PhCONH₂, has been prepared in the laboratory and the crystal structures of a series of homo- and hetero-leptic metal complexes have been determined⁶. Depending on the presence of competing donor/acceptor groups such as crystallization solvent molecules or capping ligands, either 1-D or 2-D networks could be observed. The crystal structure of the homoleptic copper complex Cu(dpm-*p*-PhCONH₂)₂ which arranges into a 2-D network as a result of the formation of $R_4^2(8)$ motifs¹⁰ as usually observed with the self-complementary primary amides is presented **Fig. 146**.⁶

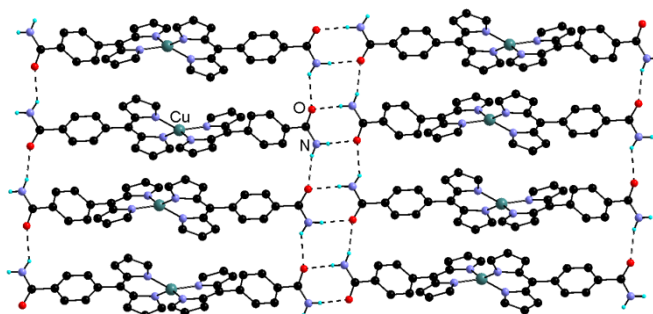


*Fig. 146: 2-D organization of Cu(dpm-*p*-PhCONH₂)₂. CH hydrogen atoms have been omitted for clarity.*

The combined effect of hydrogen bonding and chirality on the self-assembly of this class of complexes has been elegantly investigated by Telfer and Wuest in a series of octahedral cobalt complexes of the $\text{Co}(\text{dpm})_3$ type^{11,7b,8}. The two enantiomers of the tris chelate $\text{Co}(\text{dpm-}p\text{-PhCO}_2\text{H})_3$ complex could be resolved by formation of the diastereomeric salts upon reaction with (–)-cinchonidine^{7b}. The Δ and Λ enantiomers have been shown to have mirror CD spectra in THF. In the solid state, the self-complementary $R_2^2(8)$ motif¹⁰ is formed between carboxylic acid groups. Surprisingly, out of the three available self-complementary groups, only two form this motif leading to 1-D chains (**Fig. 147**). The same type of arrangement is observed in the crystal structure of Δ - and *rac*- $\text{Co}(\text{dpm-}p\text{-PhCO}_2\text{H})_3$ revealing the absence of influence of chirality on the overall organization in this case^{7b}. More recently, similar arrangements have been reported for $\text{Rh}(\text{dpm-}p\text{-PhCO}_2\text{H})_3$ and $(\text{bpy})\text{Ru}(\text{dpm-}p\text{-PhCO}_2\text{H})_2$ ⁹. Given the analogy (see Chapter 1) between the 7-azaindole and carboxylic acid groups, the structure presented **Fig. 147** supports the strategy illustrated **Scheme 43**.

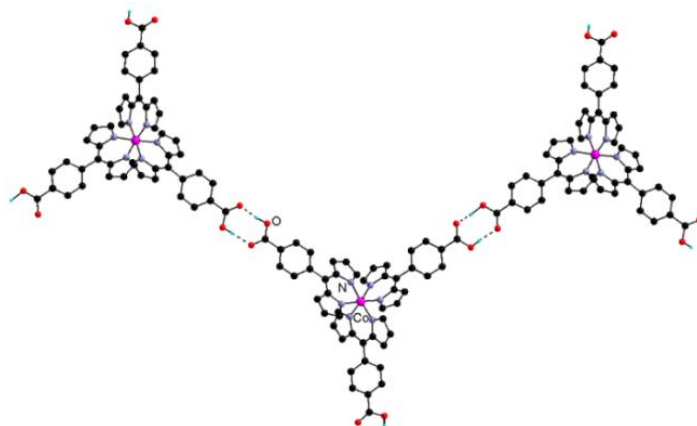


Fig. 147: 1-D chain in the crystal structure of $\Delta\text{-Co}(\text{dpm-}p\text{-PhCO}_2\text{H})_3$ ¹¹. C-H hydrogen atoms and solvent molecules have been omitted for clarity.

Interestingly, the pure Λ enantiomer and the racemic mixture of the Co(III) complex incorporating the diaminotriazinyl (DAT) appended dipyrin, *dpm-p-PhDAT*, feature different structural arrangements.^{7, 11} In the case of $\Lambda\text{-Co}(\text{dpm-}p\text{-PhDAT})_3$, six peripheral groups organize into a rosette motif leading to a 2-D hydrogen bonded network (**Fig. 148a**).¹¹ The structure of crystals of *rac*- $\text{Co}(\text{dpm-}p\text{-PhDAT})_3$ obtained under the same conditions reveals also a 2-D organization albeit without the rosette motif but with a S-shape motif involving here again six DAT groups (**Fig. 148b**).¹² Both structures feature a fraction of accessible volume and surprisingly, it's higher in the case of the *rac* complex (40 % vs 32 %).

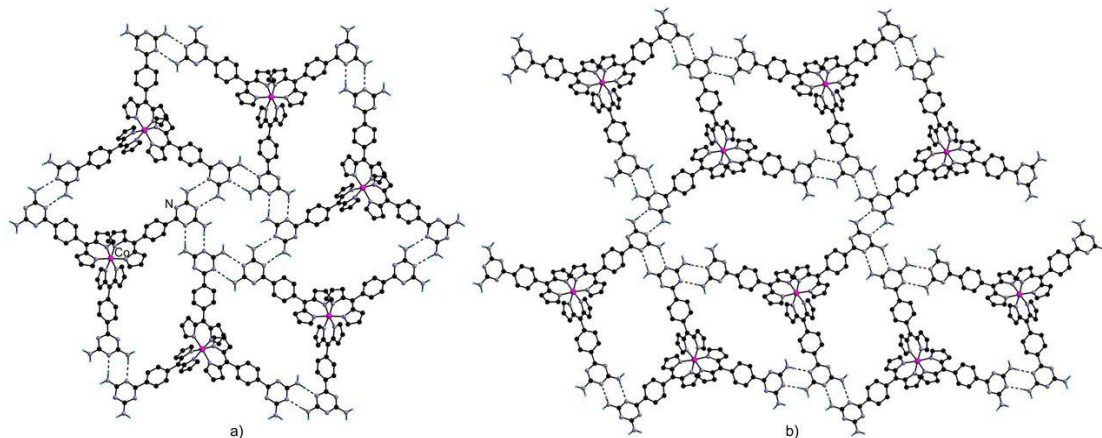
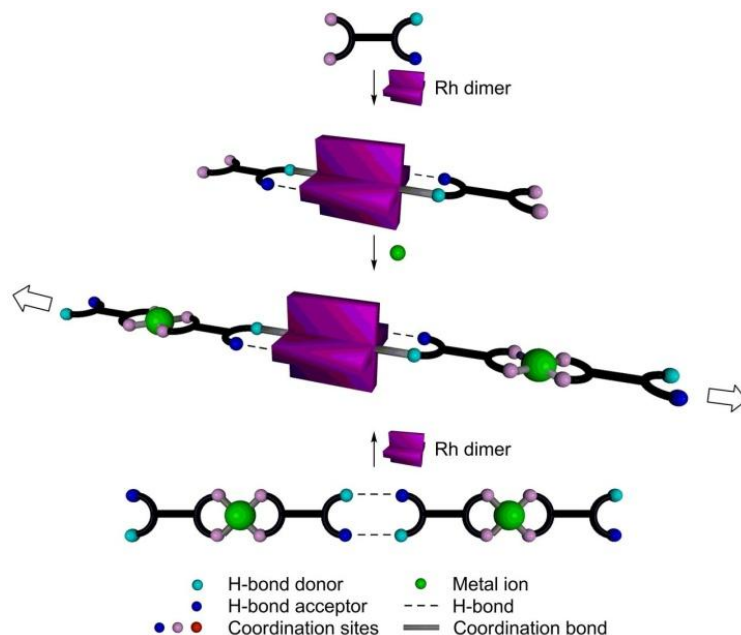


Fig. 148: 2-D hydrogen bonded networks in the crystal structures of $\Lambda\text{-Co}(\text{dpm-}p\text{-PhDAT})_3$ (a) and *rac*- $\text{Co}(\text{dpm-}p\text{-PhDAT})_3$ (b). C-H hydrogen atoms and solvent molecules have been omitted for clarity.

IV.1.2. Strategy towards heterometallic architectures

Owing to the presence of two potential coordination poles, either the dipyrin or the 7-azaindole can act as a primary coordination poles. This determines an order in the sequence of coordination leading to two approaches (**Scheme 44**) to form heterometallic architectures.

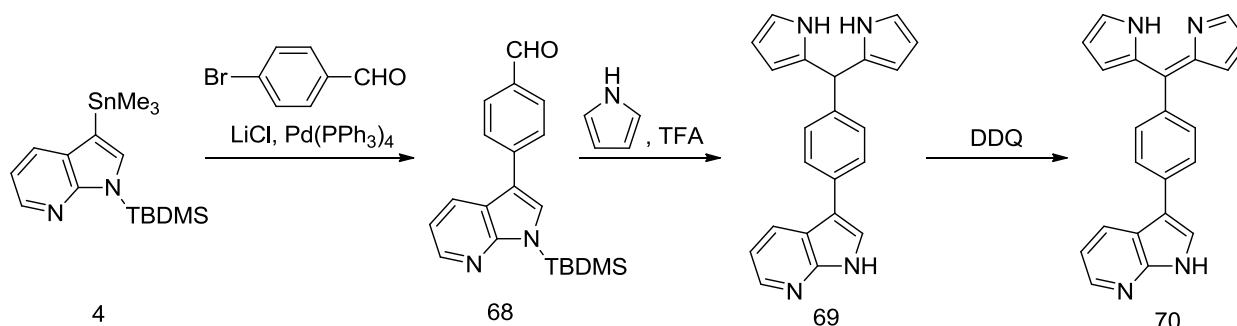


Scheme 44: Strategy for the construction of heterometallic systems with two different sequences.

As described in **Scheme 43**, the dipyrin group can act as the primary coordination pole leading to self-assembled metal complexes. These species offer peripheral 7-azaindole group which could act as secondary coordination poles in the presence of $[\text{Rh}_2(\text{OAc})_4]$ units (**Scheme 44 bottom**). On the other hand, the same heterometallic system can be prepared by a reverse sequence with 7-azaindole as a primary coordination pole. In a first step, ligand **70** can interact with rhodium acetate forming discrete complexes resulting from the coordination of the pyridyl group of the by the 7-azaindole moiety and featuring two available dpm poles. Supposing that this compound is stable, its combination with a second metal centre should lead to the formation of the final heterometallic system.

IV.2. Ligand

The synthesis of compound **70** is based on reactions developed in the first two chapters. The Pd-catalyzed coupling of 1-*tert*-Butyldimethylsilyl-3-trimethylstannyl-7-azaindole (see Chapter 1 for its synthesis), **4**,¹³ with *p*-bromobenzaldehyde afforded aldehyde **68** in 17 % yield. Subsequent reaction of the latter in neat pyrrole in the presence of a catalytic amount of trifluoroacetic acid (TFA), as described by Lindsey¹⁴, gave dipyrromethane **69** in 89 %. Oxidation of **69** by DDQ afforded the desired compound **70** in 92 % yield (**Scheme 45**).



Scheme 45: Synthesis of dipyrin **70**.

Crystals of dipyrromethane **69** were obtained by slow vapour diffusion of *n*-pentane into a dioxane solution of this compound. Ligand **69** crystallizes in the triclinic space group *P*-1 with one dipyrromethane in general position and two dioxane molecules on inversion centres. As observed in the crystal structure of other dipyrromethanes^{14,15}, the two pyrrolic rings are not coplanar and form an angle of 68.2 °. As expected, two consecutive 7-azaindole groups form the $R_2^2(8)$ hydrogen bonding motif (**Fig. 149**). The two pyrrolic NH interact with the two oxygen atoms of the dioxane solvate molecules thus leading to the formation of a 2-D network (**Table 40**).

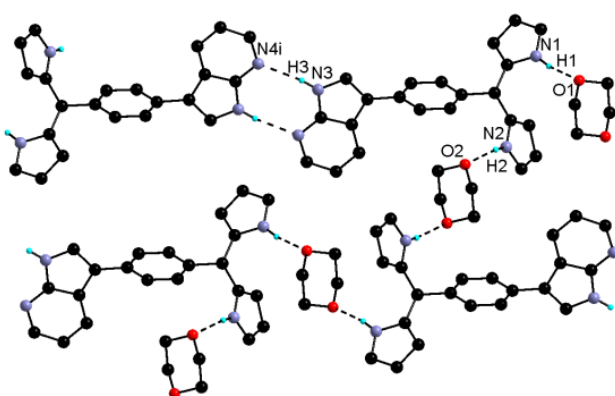


Fig. 149: 2-D hydrogen bonding network in the crystal structure of **69** (Dioxane).

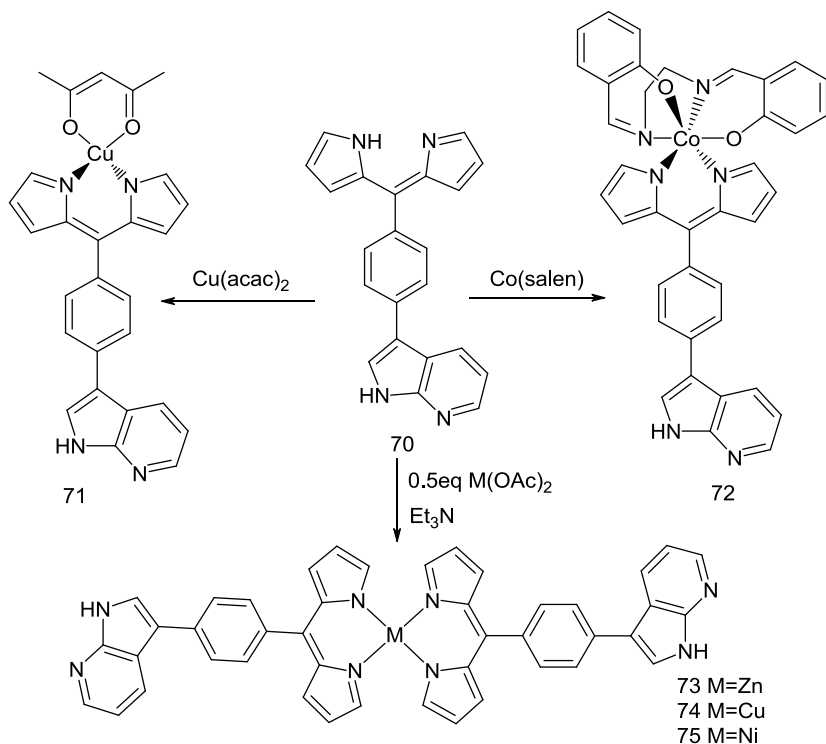
Only the NH hydrogen atoms are shown for clarity.

Bonds	Bond distances (Å) and angles (°)
N3 ^{''} N4i	2.947(4)
N1 ^{''} O1	2.878(3)
N2 ^{''} O2	2.914(4)
N3-H3 ^{''} N4i	167.7
N1-H1 ^{''} O1	164.1
N2-H2 ^{''} O2	165.6

Table 40: Bond distances (Å) and angles (°) of compound **69**. (*i* = 1-*x*, -*y*, 2-*z*)

IV.3. Preparation of complexes and H-bond networks upon coordination of the dipyrin pole

Reaction of the ditopic ligand **70** with one equivalent of $(\text{acac})_2\text{Cu}$ (acac = acetylacetonate) afforded the heteroleptic complex **71** in 74 % yield (**Scheme 46**). Analogous reaction with $(\text{salen})\text{Co}$ (salen = N,N' -bis(salicylidene)ethylenediamine) afforded **72** in 40 % yield. Reaction of two equivalents of **70** with one equivalent of $\text{M}(\text{OAc})_2$ (M = Zn, Cu, Ni) afforded the homoleptic complexes $(\text{70})_2\text{M}$ (M = Zn, **73**; Cu, **74**; Ni, **75**) in 80 to 85 % yield. The latter three complexes are only poorly soluble in organic solvents, probably owing to the formation of insoluble oligomers *via* hydrogen bonding.



Scheme 46: Synthesis of complexes 71-75.

Crystals of two polymorphs of **71** (**71a** and **71b**) were obtained by slow vapour diffusion of *n*-pentane into a CHCl_3 solution of the complex. Complex **71a** crystallizes in the monoclinic space group $P2_1/n$ with two complexes in general positions, whereas complex **71b** crystallizes in the monoclinic space group $P2_1/c$ with one complex in general position. Within each complex, the copper atom is coordinated both to the acac unit and the dpm ligand with Cu-O and Cu-N distances close to those observed for other complexes of this type¹⁶ (**Table 41**). The two complexes organize into dimers through the formation of two hydrogen bonds with $R_2^2(8)$ motif as in the case of dipyrromethane **69**, with similar $\text{N-H}\cdots\text{N}$ distances (**Fig. 150**).

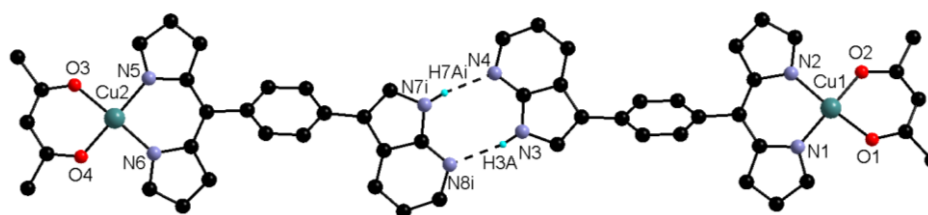


Fig. 150: Hydrogen bonded dimer in the crystal structure of 71. Only the NH hydrogen atoms are shown for clarity.

Regarding polymorph **71a**, two complexes in general positions contain the two non equivalent copper centres, the two chelates surrounding the Cu(II) ions are not coplanar and form an angle between the N-Cu-N and O-Cu-O planes 13.42 and 11.60 ° respectively. In the second polymorph **71b**, the N₂CuO₄ core is more planar with an angle between chelate planes of 4.65 ° (**Fig. 151**).

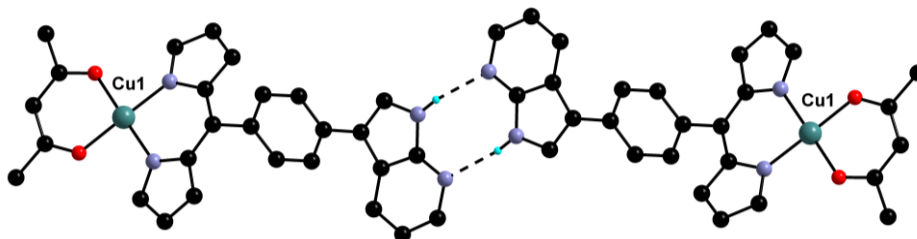


Fig. 151: Hydrogen bonded dimer in the crystal structure of 71b. Only the NH hydrogen atoms are shown for clarity.

Another difference between the two structures lies in the hydrogen bonding interactions. In the case of **71b**, both 7-azaindole moieties are practically coplanar, whereas in the case of the **71a** polymorph, the two 7-azaindole groups form an angle of 7.04 °. These minor differences between the two polymorphs may be explained by packing effects.

	Complex 71a				Complex 71b	
Bond distances (Å)	Cu1-O1	1.9331(17)	Cu2-O3	1.9282(17)	Cu-O1	1.9319(16)
Bond distances (Å)	Cu1-O2	1.9305(17)	Cu2-O4	1.9405(17)	Cu-O2	1.9414(16)
Bond distances (Å)	Cu1-N1	1.9549(19)	Cu2-N5	1.9531(19)	Cu-N1	1.9585(19)
Bond distances (Å)	Cu1-N2	1.9503(19)	Cu2-N6	1.9435(19)	Cu-N2	1.9556(19)
Bond distances (Å)	N3 ⁱⁱⁱ -N8 ⁱ	2.982(3)	N7 ⁱ -N4	2.924(3)	N3 ⁱⁱⁱ -N4 ⁱⁱ	2.930(3)
Angles (°)	N3-H3A ⁱⁱⁱ -N8 ⁱ	167.1	N7 ⁱ -H7A ⁱ -N4	160.4	N3-H3A ⁱⁱⁱ -N4 ⁱⁱ	167.7

Table 41: Bond distances and angles observed in 71a and 71b polymorphs. (i = -2+x, y, -1+z; ii = 1-x, -y, 3-z)

Crystals of compound **72** were obtained by slow vapour diffusion of pentane into a dioxane solution of this compound. It crystallizes in the triclinic space group *P*-1 with one complex and two dioxane solvate molecules in general positions and an additional dioxane molecule on an inversion centre. As observed for other (salen)Co(dpm) complexes^{17,18}, the Co(III) ion is in an octahedral N₄O₂ environment. The salen ligand is twisted and the dipyrroin chelate non-planar with a dihedral angle of 27.4 ° between the two pyrrolic rings. Here again, the complexes adopt a dimeric arrangement but not as a result of H bonds with R₂²(8) motif between two 7-azaindole groups (**Table 42**). Indeed, as it has been observed in the case of a primary amide appended analogue¹⁷, the oxygen atom of the salen capping ligand acts as a strong hydrogen bond acceptor and interacts with the pyrrolic NH moiety of the 7-azaindole (**Fig. 152**).

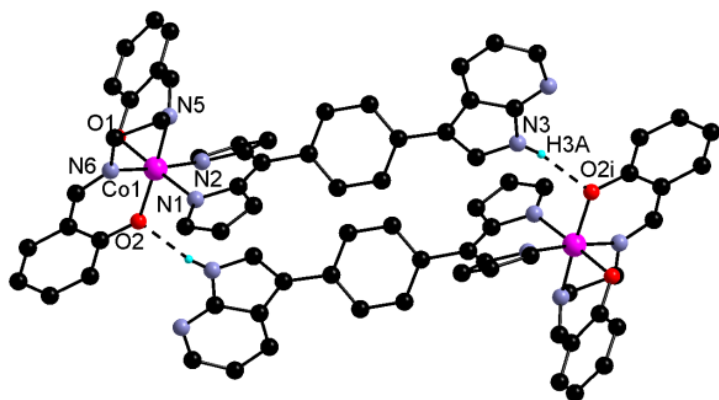


Fig. 152: Hydrogen bonded dimer in the crystal structure of **72**. Only the NH hydrogen atoms are shown for clarity. Dioxane solvent molecules are not shown for clarity.

Bonds	Bond distances (Å) and angles (°)
Co1-O1	1.9091(19)
Co1-O2	1.9155(19)
Co1-N1	1.922(2)
Co1-N2	1.911(2)
Co1-N5	1.897(2)
Co1-N6	1.914(2)
N3...O2i	2.973(3)
N3-H3A...O2i	168.7

Table 42: Bond distances (Å) and angles (°) of compound **72**. (*i* = 1-x, -y, 2-z)

Owing to the insolubility of homoleptic complexes **73-75**, single crystals were obtained by the liquid-liquid diffusion method. Thus, crystals of **73** were grown by diffusion of a benzene solution of **70** into a MeOH solution of Zn(OAc)₂. It crystallizes in the triclinic space group *P*-1 with one Zn complex and three benzene molecules in general positions. The Zn ion adopts a tetrahedral coordination environment with a dihedral angle of 74.2 ° between the two dpm chelates and Zn-N distances ranging from 1.9731(14) to 1.9837(14) Å as observed for other Zn(dpm)₂ complexes^{19,20}. The complexes organize into 1-D chains as a result of the formation of the $R_2^2(8)$ motif (**Table 43**) between consecutive 7-azaindole groups (**Fig. 153a**). The organization is similar to the one observed for **71**, but owing to the homoleptic nature of **73**, both extremities are engaged in H-bonding pattern and thus a network is formed.

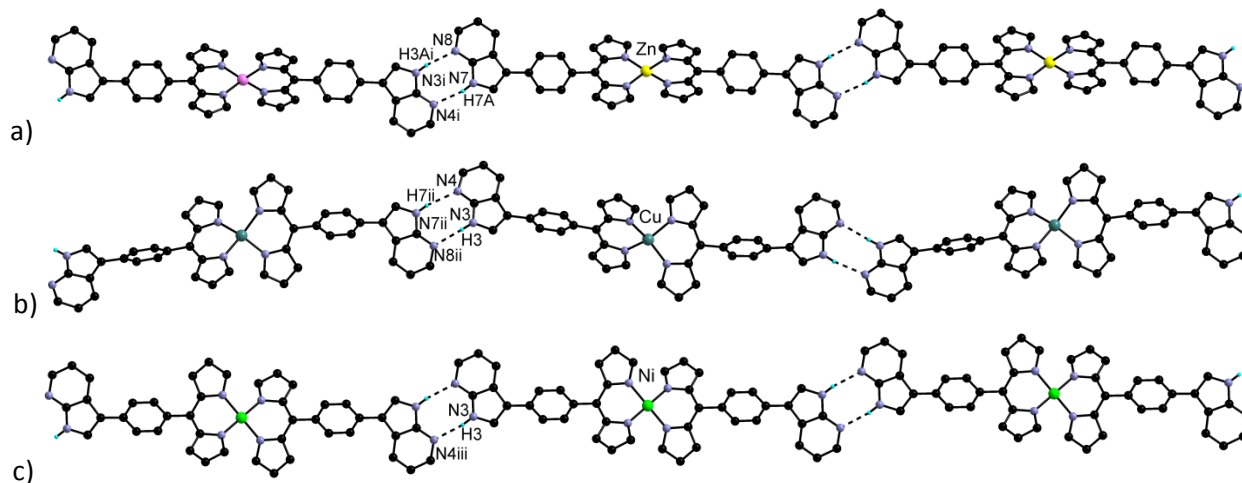


Fig. 153: Networks formed by a combination of coordination and hydrogen bonding in the structure of Zn complex **73** (a), Cu complex **74** (b) and Ni complex **75** (c). Only the NH hydrogen atoms are shown for clarity.

Crystals of **74** were obtained by slow diffusion of a MeOH solution of Cu(OAc)₂ into a dioxane solution of **70**. It crystallizes in the monoclinic space group $P2_1/n$ with one complex in general position. The copper ion is coordinated to two dpm groups with Cu-N distances ranging from 1.939(2) to 1.969(2) Å in a pseudo-tetrahedral environment as the two chelates form a dihedral angle of 43.2 ° similar to the one observed for other Cu(dpm)₂ complexes^{21,22,23}. As in the structure of **73**, a 1-D hydrogen bonded network is formed again by formation of $R_2^2(8)$ motifs (**Table 43**) between neighbouring complexes along the *b* axis (**Fig. 153b**).

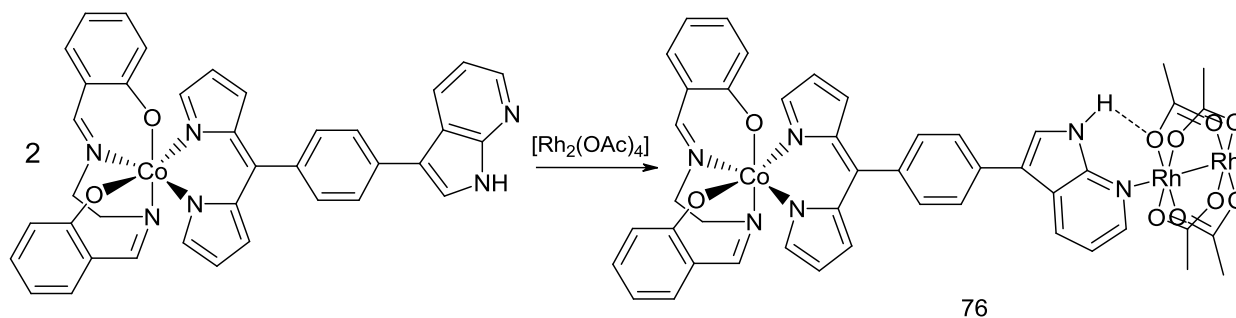
Crystals of **75** were obtained by slow diffusion of a MeOH solution of Ni(OAc)₂ into a dioxane solution of **70**. It crystallizes in the monoclinic space group $P2_1/c$ with one complex on a 2-fold axis. The nickel ion is coordinated to two dpm chelates in a square planar environment with an average Ni-N distance of 1.897(3) Å (**Fig. 153c**). This is surprising given that in the crystal structure of the other reported Ni(dpm)₂ complexes incorporating an α,β -unsubstituted dipyrin^{24,25,26}, the metal centre is in a pseudo-tetrahedral coordination geometry, a likely result of the repulsion between the α -CH of the two dpms. This repulsion, also present here, induces a substantial deviation from planarity of the dpm chelate. As a consequence, the two pyrrolic rings form a dihedral angle of 35.4° as observed recently for Pd(dpm)₂ and (Ppy)M(dpm) (Ppy = 2-phenylpyridine; M = Pt, Pd) complexes^{27,28}. In spite of the different coordination geometry around the metal centre, compared to **73** and **74**, again a 1-D network is formed owing to the presence of $R_2^2(8)$ motifs (**Table 43**) along the c axis (**Fig. 153c**).

73	d (N-H...N)	2.953(3)(Å)	74	d (N7-H...N4)	3.036(3)(Å)	75	d (N-H...N)	2.935(4)(Å)
	α (N-H...N)	157.7(°)		d (N8-H...N3)	2.936(3)(Å)		α (N-H...N)	163.1(°)
				α (N7-H...N4)	164.7(°)			
				α (N8-H...N3)	157.5(°)			

Table 43: H-Bond distances and angles for complexes **73-75**.

IV.4. Towards heterometallic architectures

In a first attempt to prepare heterometallic systems, the strategy described in **Scheme 44 bottom** was considered. The homoleptic complexes **73-75** were seen as metallatectons which could form 1-D networks upon assembly with the [Rh₂(OAc)₄] paddlewheel. Unfortunately, these complexes offer extremely low solubility in common organic solvents, owing to the probable formation of oligomeric assemblies by strong hydrogen bonding interactions between the 7-azaindole poles. Use of DMSO and DMF as solvents did not allow to generate crystalline compounds. This prevented the further exploration of this approach. Unlike their homoleptic counterparts, the heteroleptic complexes **71** and **72** were more soluble in organic solvents. They were therefore reacted with [Rh₂(OAc)₄] (**Scheme 47**) in an attempt to form discrete analogues of the architectures presented **Scheme 44**. The resulting heterometallic products were also soluble but could not be isolated in the crystalline form. Although these species could not be crystallized, their formation was studied by ¹H NMR (300MHz) in chloroform as illustrated in the case of compound **76**.



Scheme 47: Preparation of heterobimetallic complex **76**.

In spite of the 2:1 stoichiometry used in this reaction, the product $[\text{Rh}_2(\text{OAc})_4(\mathbf{72})]$ incorporated only one coordinated Co complex instead of the expected $[\text{Rh}_2(\text{OAc})_4(\mathbf{72})_2]$ species. Compared to the starting complex **72**, proton signals of the 7-azaindole moiety are down field shifted for the complex (**Fig. 154**), contrary to the signals of the salen fragment, which are not modified in comparison with the starting Co species. In addition, a singlet in aliphatic region integrating for 12 protons is observed. This indicates the formation of the heterometallic discrete complex **76** and its stability in chloroform solution.

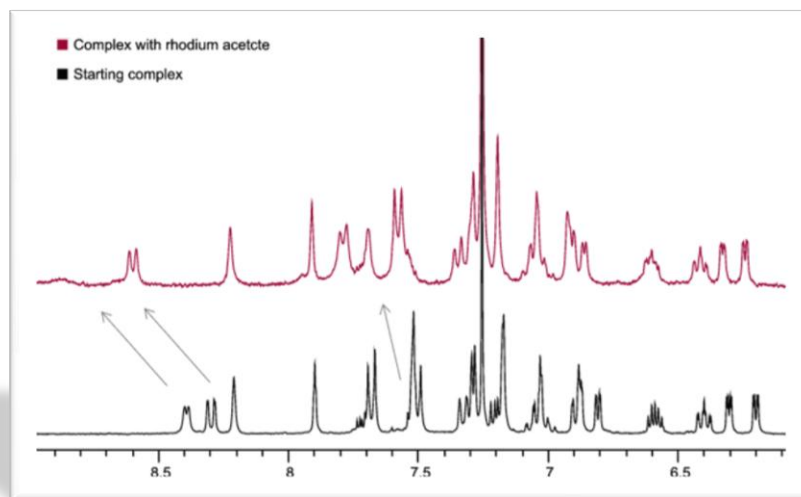
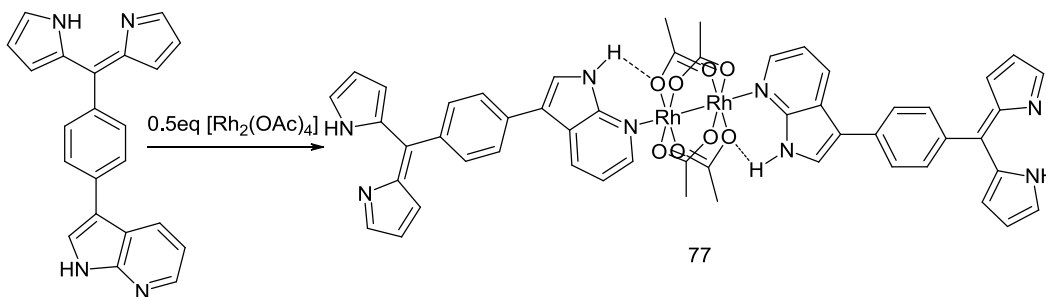


Fig. 154: Comparison of complex **76** and starting complex **72** spectra.

As illustrated in **Scheme 44** top, a reversed coordination sequence was considered using the 7-azaindole group as a primary coordination pole. Two equivalents of **70** were reacted with one equivalent of $[\text{Rh}_2(\text{OAc})_4]$ to afford complex **77** in 65 % yield.



Scheme 48: Preparation of complex **77**.

Crystals of **77** were obtained by slow diffusion of *n*-pentane into a dioxane solution of the complex (**Scheme 48**). It crystallizes in the monoclinic space group $P2_1/n$ with one complex **77** on an inversion centre and two dioxane solvate molecules in general positions. The structure of this compound (**Fig. 155**) is similar to the one observed in Chapter 1 (see complexes **13-16**). Two ligands **70** are coordinated in the axial positions of the $[\text{Rh}_2(\text{OAc})_4]$ paddlewheel *via* the pyridyl nitrogen atom of the 7-azaindole groups (Rh-N distances are 2.268(3) Å) and both pyrrolic N-H protons are hydrogen bonded to oxygen atoms of the acetate moieties. Interestingly, the N-H...O distance and angle (2.896 Å and 143.4 ° respectively) suggest a weaker interaction than in the previous examples (the O-H-N distances observed in Chapter 1 are in the range 2.7-2.8 Å). This is correlated to the fact that the 7-azaindole and acetate groups do not lie in the same plane but form an angle of 11.97 ° (**Fig. 156**) unlike in the examples presented Chapter 1. This might be due to packing effect.

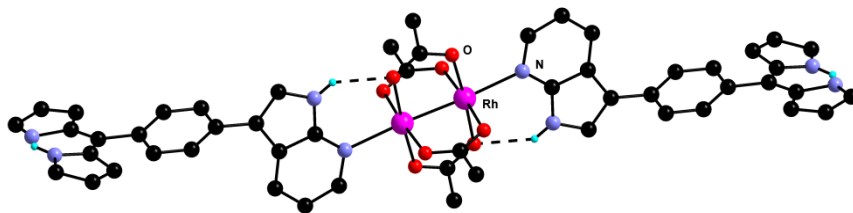


Fig. 155: Structure of rhodium complex **77**.

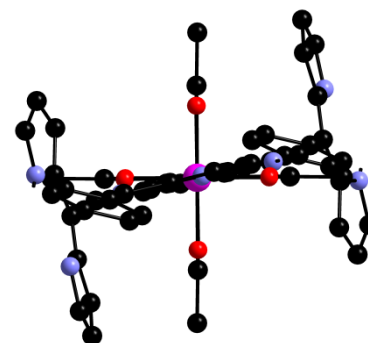
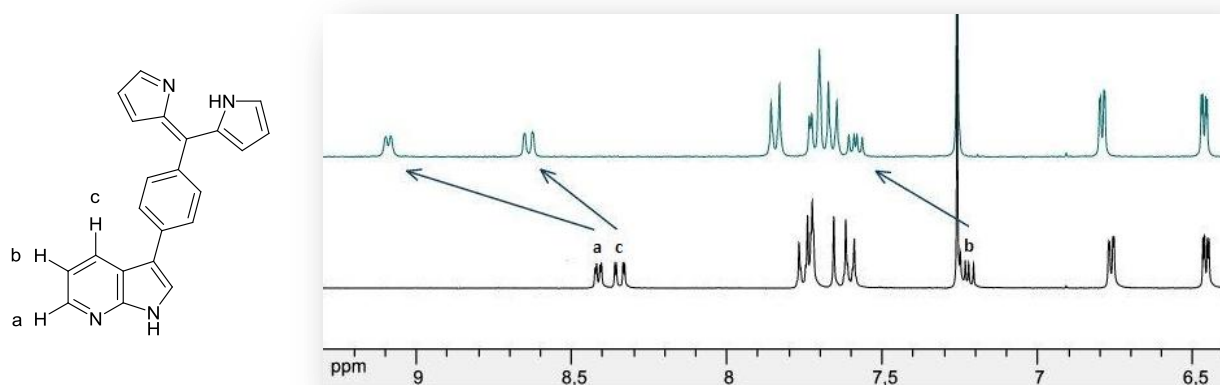


Fig. 156: Structure of rhodium complex **77**, view along Rh-Rh axes.

Before using this complex for coordination to a second metal centre, its stability in chloroform solution was studied by $^1\text{H-NMR}$ (300 MHz) (**Scheme 49**). Comparison of the spectra obtained for the ligand and corresponding complex showed strong downfield shift of the proton of the pyridine ring of the ligand and slight shift of the phenyl protons. This deshielding indicates that the pyridine, hence ligand **70**, remains coordinated to the $[\text{Rh}_2(\text{OAc})_4]$ paddlewheel and demonstrate the stability of **77** in chloroform solution. As expected from the crystal structure, the protons of the DPM are observed at almost identical chemical shifts in the spectra of **70** and **77**.



Scheme 49: Comparison of the $^1\text{H NMR}$ (300MHz, CDCl_3) spectra of ligand **70** (black) with corresponding rhodium acetate complex **77** (green). Only the aromatic region is shown for clarity; full spectra with chemical shifts are presented in the experimental section.

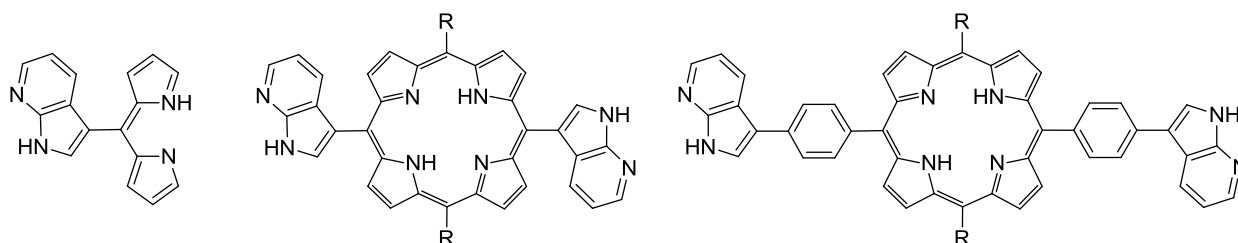
Complex **77** appeared as a suitable and stable metallatecton in organic solvents. Unfortunately, upon diffusion of a solution of a second metal salt into a solution of **77**, no single-crystals could be obtained, in spite of numerous trials in various solvent mixtures. Only pink insoluble polycrystalline materials were isolated.

IV.5. Conclusion

A 7-azaindole appended dipyrin ligand was synthesized and was employed to form both homo- and hetero-metallic architectures. Homometallic systems were prepared upon self-assembly of hetero- and homoleptic complexes bearing peripheral 7-azaindole group(s) as hydrogen bond donor/acceptor site(s). As observed for dipyrromethane **69**, the heteroleptic copper complex **71** forms a hydrogen bonded dimer *via* the $R_2^2(8)$ motif. In the case of the heteroleptic Co(III) complex, the presence of a competing hydrogen bond acceptor, namely the oxygen atom of the capping salen ligand, disrupts the $R_2^2(8)$ motif. The dimeric organization is restored in the crystal structure of the homoleptic complexes containing Zn^{2+} (**73**), Cu^{2+} (**74**) and Ni^{2+} (**75**). Because of the homoleptic nature of these complexes, the $R_2^2(8)$ motif is translated and consequently one-dimensional chains are generated regardless of the coordination sphere around the metal ions. In spite of several attempts to investigate the structure of analogous homoleptic octahedral complexes with trivalent metal centers such as Co(III) or Fe(III), no crystalline materials could be obtained so far. Nonetheless, the results obtained here demonstrate that 7-azaindole, a rather robust self-complementary hydrogen bonding unit, is a structure directing group and thus of interest for crystal engineering.

The preparation of heterometallic coordination networks was then attempted. Owing to the poor solubility of the complexes bearing peripheral 7-azaindole groups, these species could not be assembled with the $[Rh_2(OAc)_4]$ paddlewheel. A reverse approach was explored consisting in the use of the 7-azaindole group as a primary coordination pole. The resulting complex **77** was characterized by X-Ray single crystal diffraction in the solid state and 1H -NMR in $CDCl_3$. The latter experiment demonstrated its stability in this solvent. However, further attempts to react this compound with a secondary metal salt did not afford crystalline material hampering the demonstration of the strategy illustrated **Scheme 44**.

One way to circumvent these problems and obtain the desired heterometallic architectures could be to prepare an analogue of ligand **70** (**Scheme 50**) without a spacer between the two coordination poles. Such a compound may improve the solubility of the resulting complexes. Extension to other polypyrrolic systems such as porphyrins can also be considered (**Scheme 50**). These compounds are rather appealing owing to the variety of solubilizing groups which may be introduced in the 10,20 *meso* positions. These derivatives are currently being synthesized in the laboratory.



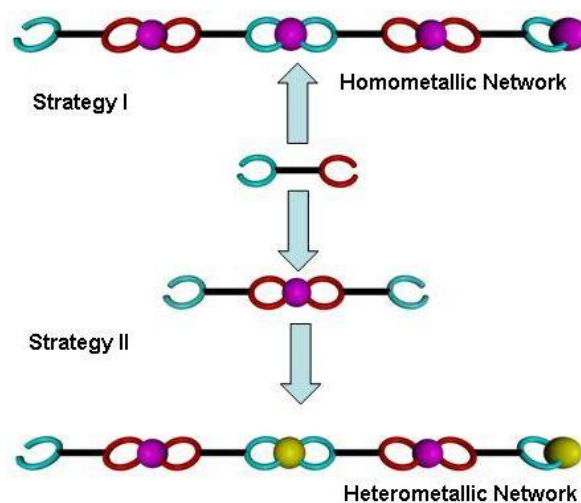
Scheme 50: Potential ligands for the preparation of heterometallic systems.

IV.6. Reference

- ¹ Etter, M. C., *Acc. Chem. Res.* **1990**, *23*, 120.
- ² Deacon, G. B., Junk, P. C., Leary, S. G., *Adv. Synth. Catal.* **2003**, *345*, 1115.
- ³ Song, D., Schmider, H., Wang, S., *Org. Lett.* **2002**, *4*, 4049.
- ⁴ Heinze, K., Reinhart, A., *Inorg. Chem.* **2006**, *45*, 2695.
- ⁵ Heinze, K., Reinhart, A., *Z. Naturforsch.* **2005**, *60b*, 758.
- ⁶ Baudron, S. A., Salazar-Mendoza, D., Hosseini, M. W., *CrystEngComm.* **2009**, *11*, 1245.
- ⁷ (a) Brückner, C., Zhang, Y., Rettig, S. J., Dolphin, D., *Inorg. Chim. Acta* **1997**, *263*, 279; (b) Telfer, S., Wuest, J. D., *Chem. Commun.* **2007**, 3166.
- ⁸ Telfer, S. G. Wuest, J. D., *Cryst. Growth Des.* **2009**, *9*, 1923.
- ⁹ Hall, J. D., McLean, T. M., Smalley, S. J., Waterland M. R., Telfer, S. G., *Dalton Trans.* **2010**, *39*, 439.
- ¹⁰ Etter, M. C., *Acc. Chem. Res.* **1990**, *23*, 120.
- ¹¹ Brückner, C., Zhang, Y. S., Rettig, J., Dolphin, D., *Inorg. Chim. Acta* **1997**, *263*, 279.
- ¹² (a) Hosseini, M. W., *Acc. Chem. Res.* **2005**, *38*, 313; (b) Hosseini, M. W., *Chem. Commun.*, **2005**, 5825.
- ¹³ Alvarez, M., Fernandez, D., Joule, J. A., *Synthesis* **1999**, *4*, 615.
- ¹⁴ Littler, J., Miller, M. A., Hung, C. H., Wagner, R. W., O'Shea, D. F., Boyle, P. D., Lindsey, J. S., *J. Org. Chem.* **1999**, *64*, 1391.
- ¹⁵ (a) Lin, K. J., Wu, J. Y., Chen, C. T., *Acta Cryst.* **1996**, *C52*, 3114; (b) Bennis, V., Gallagher, J. F., *Acta Cryst.* **1998**, *C54*, 130; (c) Foxon, S. P., Smith, J. R. L., O'Brien, P., Reginato, G. J., *Chem. Soc. Perkin Trans.* **2001**, *2*, 1145; (d) Patra, G. K., Diskin, Y., Goldberg, I., *Acta Cryst.* **2002**, *E58*, o530; (e) Kumar, R., Misra, R., Prabhuraja, V., Chandrashekar, T., *Chem. Eur. J.* **2005**, *11*, 5695; (f) Heinze, K., Reinhart, A., *Z. Naturforsch. B* **2005**, *60*, 758; (g) Gokulnath, S., Prabhuraja, V., Sankar, J., Chandrashekar, T. K., *Eur. J. Org. Chem.* **2007**, 191; (h) Senge, M. O., *Acta Cryst.* **2007**, *E63*, o3679; (i) Maeda, H., Hasewaga, M., Ueda, A., *Chem. Commun.* **2007**, 2726; (j) Easson, M. W., Fronczek, F. R., Jensen T. J., Vicente, M. G. H., *Bioorg. Med. Chem.* **2008**, *16*, 3191.
- ¹⁶ (a) Halper, S. R., Malachowski, M. R., Delaney, H. M., Cohen, S. M., *Inorg. Chem.*, **2004**, *43*, 1242; (b) Halper, S. R., Cohen, S. M., *Angew. Chem. Int. Ed.*, **2004**, *43*, 2385; (c) Do, L., Halper, S. R., Cohen, S. M., *Chem. Commun.*, **2004**, 2662; (d) Halper, S. R., Cohen, S. M., *Inorg. Chem.* **2005**, *44*, 4139.
- ¹⁷ Salazar-Mendoza, D., Baudron, S. A., Hosseini, M. W., *CrystEngComm.* **2009**, *11*, 1245.
- ¹⁸ Salazar-Mendoza, D., Baudron, S. A., Hosseini, M. W., *Inorg. Chem.* **2008**, *47*, 766.
- ¹⁹ Salazar-Mendoza, D., Baudron, S. A., Hosseini, M. W., *Chem. Commun.* **2007**, 2252.
- ²⁰ (a) Muthukumar, K., L. Yu, Sazanovich, I. V., Kirmaier, C., Hindin, E., Diers, J. R., Boyle, P. D., Bocian, D. F., Holten, D., Lindsey, J. S., *Inorg. Chem.* **2003**, *42*, 6629; (b) Maeda, H., Hasegawa, M., Hashimoto, T., Kakimoto, T., Nishio, S., Nakanishi, T., *J. Am. Chem. Soc.* **2006**, *128*, 10024; (c) Maeda, H., Hashimoto, T., *Chem. Eur. J.* **2007**, *13*, 7900.
- ²¹ Halper, S. R., Malachowski, M. R., Delaney, H. M., Cohen, S. M., *Inorg. Chem.* **2004**, *43*, 1242.
- ²² Do, L., Halper, S. R., Cohen, S. M., *Chem. Commun.* **2004**, 2662.
- ²³ (a) Halper, S. R., Cohen, S. M., *Chem. Eur. J.*, **2003**, *9*, 4661; (b) Miao, Q., Shin, J. Y., Patrick, B. O., Dolphin, D., *Chem. Commun.* **2009**, 2541.
- ²⁴ Brückner, C., Karunaratne, V., Rettig, S. J., Dolphin, D., *Can. J. Chem.* **1996**, *74*, 2182.
- ²⁵ Miao, Q., Shin, J. Y., Patrick, B. O., Dolphin, D., *Chem. Commun.* **2009**, 2541.
- ²⁶ Gill, H. S., Finger, I., Bozidarevic, I., Szydlo, F., Scott, M. J., *New. J. Chem.* **2005**, *29*, 68.
- ²⁷ Hall, J. D., McLean, T. M., Smalley, S. J., Waterland, M. R., Telfer, S. G., *Dalton Trans.* **2010**, *39*, 439.
- ²⁸ Bronner, C., Baudron, S. A., Hosseini, M. W., Strassert, C. A., Guenet, A., De Cola, L., *Dalton Trans.* **2010**, *39*, 180.

V. General conclusion and perspective

In this work, two different approaches for the elaboration of homo- and heterometallic architectures were followed (**Scheme 51**). The first one consists in the preparation of homometallic architectures upon association of the same metal centre with a ditopic ligand bearing two similar coordinating poles (**Scheme 51 top**). The second strategy is based on a ditopic ligand offering different coordinating poles and relies on stepwise processes. Intermediate metallatectons are obtained upon coordination of a first metal centre to the primary coordination poles of the ligands (**Scheme 51 bottom**). Heterobimetallic architectures are prepared upon subsequent coordination of a second metal centre to the secondary coordination poles. For the preparation of homo- and hetero-metallic complexes and networks, 7-azaindole and dipyrin (DPM) moieties as coordinating poles were chosen as demonstrators for the proposed strategy. Three types of ligands, appended by either 7-azaindole or dipyrin and or a combination of both were designed and synthesized.



Scheme 51: Elaboration of homo- and heterometallic architectures.

Following the first strategy, several ligands based on 7-azaindole and DPM coordinating poles were engaged in reactions with metal salts, leading to the formation of the corresponding homometallic discrete complexes and extended networks.

Upon reaction of ligands bearing both a 7-azaindole and a carboxylic acid moiety with copper (II) and cobalt (II) salts, three extended networks **17**, **18** and **19** were obtained. Depending on the position of the carboxylic acid groups within the ligand framework, the porosity and dimensionality of the architectures are modified although the coordination environment around the copper center remained almost the same in **17** and **18**. The nitrogen sorption property of the porous metal organic framework **18** was analyzed by BET measurement. These examples illustrate the coordination of 7-azaindole without deprotonation.

Upon reaction of the 7-azaindole/TCV ligand (**12**) with copper (II) salts, a discrete complex and a 1-D network were obtained. These examples illustrate the coordination chemistry of 7-azaindolate, similar to the one of the carboxylate group.

Regarding the second group of ligands appended with the DPM coordinating pole, their use for the preparation of homometallic networks by coordination to metal centres (**Scheme 51 top**) was illustrated with the family of macrocyclic compounds (**34-40**), obtained by reaction with silver (I) salts. Depending on the nature of the anion and the peripheral coordination poles attached at the *meso* position of the DPM, different arrangements, ranging from discrete macrocycles to extended 3-D networks, were observed in the solid state. However, all these compounds are practically based on a

rather identical macrocyclic core and illustrate the coordination of metals by DPM without deprotonation.

In our attempts to use 7-azaindole derivatives for the preparation of heterometallic architectures, two different approaches were followed depending on whether this group was considered as a primary or secondary coordinating pole. Considering the 7-azaindole moiety as a primary coordination pole, compounds **13-16** were obtained by reaction of 7-azaindole appended ligands with the $[\text{Rh}_2(\text{OAc})_4]$ dimer. Depending on the nature of the secondary coordination pole, discrete complexes (**13, 14**) or hydrogen bonded networks (**15, 16**), in the case of the ligands appended by peripheral carboxylic acid groups, were observed. However, owing to the low solubility of these metallatectons, further coordination was found to be difficult and the products obtained were amorphous or polycrystalline materials. Owing to the tendency of 7-azaindole species to form strong self-complementary hydrogen bonding patterns, compounds bearing such peripheral groups as secondary poles were poorly soluble preventing thus the application of *Strategy II* for the stepwise elaboration of heterometallic systems. Nevertheless, the family of hydrogen bonded homometallic networks **73, 74, 75** based on the homoleptic complexes incorporating the Aza-Ph-DPM ligand (**70**) with zinc, copper and nickel was obtained.

Regarding the stepwise elaboration of heterometallic architectures in the case of DPM ligands, the DPM moiety was mostly used as primary coordination pole. Homo- and hetero-leptic complexes were prepared and used as metallatectons. Unfortunately, reactions of homoleptic complexes **41-45** with a second metal centre led to the formation of only amorphous, polycrystalline or unstable crystalline materials. A broader series of heteroleptic complexes was obtained by reaction of -Ph-Im, -Ph-Pyr, -3Py, -4Py and -Ph-4Py appended ligands with $\text{Cu}(\text{acac})_2$, $\text{Cu}(\text{acacCN})_2$ and $\text{Co}(\text{acacCN})_2$ and characterised in the solid state and in solution. Depending on the nature of the secondary coordinating pole and the crystallisation conditions, discrete copper complexes (**46, 47, 49a**) or self-complementary extended networks (**48-52**) were observed. Two different recognition patterns were observed in these networks. Whereas a 1-D network *via* weak interaction of the copper center with the nitrogen atom of the CN group of a neighbouring complex in the case of the pyrazole appended complex $(\text{acacCN})\text{Cu}(\text{DPM-Ph-Pyr})$ (**49b**) was observed, in all the other copper heteroleptic complexes, this arrangement results from the coordination of the metal center to the nitrogen atom of the pyridine or imidazole groups of a neighbouring complex. Upon reactions of heteroleptic copper (II) and cobalt (III) complexes with different silver (I) salts, the formation of heterometallic architectures was observed. Unfortunately, the two pyrazole functionalized complexes **47** and **49** did not form crystalline heterometallic systems. In the case of the complex $(\text{acac})\text{Cu}(\text{DPM-Ph-Py})$ **46**, the absence of peripheral coordinating nitrile groups prevents any self-assembly and leads to a discrete heterobimetallic complex **57**. In the other cases, the formation of different heterobimetallic networks was observed. Depending on the nature of the coordinating poles and anions, the networks were organized in different modes. In the case of the imidazole based networks **58** and **59** with PF_6^- and BF_4^- anions, weak interactions between the CN groups and the copper atoms of another trinuclear unit were observed. In the case of the slightly more coordinating OTf anion (**60**), two imidazole and one CN groups of the neighboring unit are coordinated to the silver (I) center. Networks based on the 3-Py appended metallatecton adopt a double layer architecture with the silver centre surrounded by two pyridine and two CN groups, whereas in the 4-Py case (**61**) the -CN groups are not involved in any coordination and the network is formed *via* silver-anion bridging. Two 2-D networks with the cobalt -3Py and -4Py appended metallatectons were obtained upon reaction of $\text{Ag}(\text{OTf})$ and AgBF_4 respectively. In the first case (**65**), the -CN groups are not involved in any coordination and the network is formed *via* weak Ag-Ag $d^{10}-d^{10}$

interactions, whereas, in the second case, two pyridine and one –CN group of three neighbouring molecules are coordinated to the silver cation, forming a 2-D honeycomb heterobimetallic network.

In perspective, it will be interesting to apply these strategies to ligands without a spacer or with an aliphatic one in the 7-azainole and 7-azainole/DPM cases (**Fig. 157**). This substitution may improve the solubility of the ligands and of the resulting metallatectons. Considering π - π staking as one of the forces stabilising the interpenetration in the case of network **18**, the use of an aliphatic spacer can represent one approach to solve this problem, although other arrangements might be also observed. On the other hand, the macrocyclic spacer, such as a porphyrin, can be another possibility for the elaboration of 7-azainole based heterometallic architectures. These derivatives are currently being synthesized in the laboratory (**Fig. 157**, compounds a, b, d).

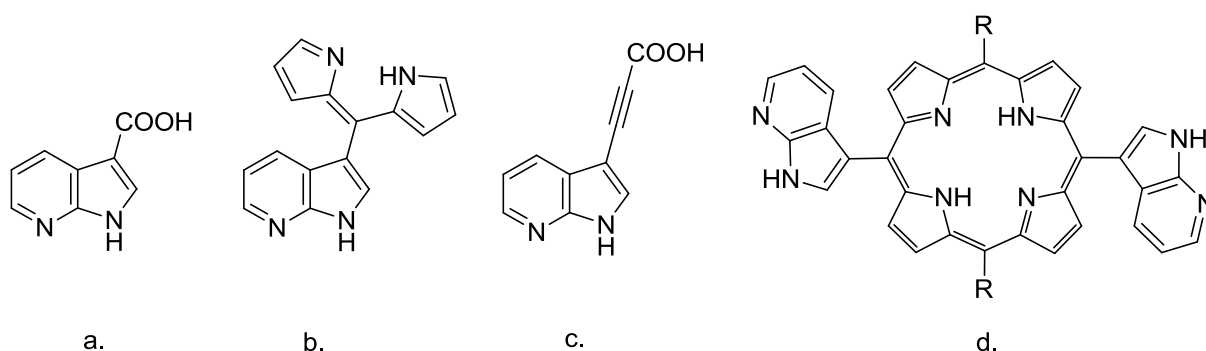


Fig. 157: Potential ligands for the preparation of 7-azainole based homo- and heterometallic architectures.

In the case of the DPM based ligands, the introduction of divergent secondary coordinating poles, such as pyrimidine, triazole or tetrazole, may be a way to induce the formation of different architectures with higher dimensionality (**Fig. 158**). Regarding the heteroleptic DPM complexes, only the formation of (acac)Cu(DPM), (acacCN)Cu(DPM), (acacCN)Co(DPM)₂, and (SALEN)Co(DPM) type heteroleptic complexes were investigated. The substitution of the –CN group by a pyridine¹ or another coordinating pole within the starting M(acacCN)_n complexes may be a further possibility for the formation of new architectures with different topologies.

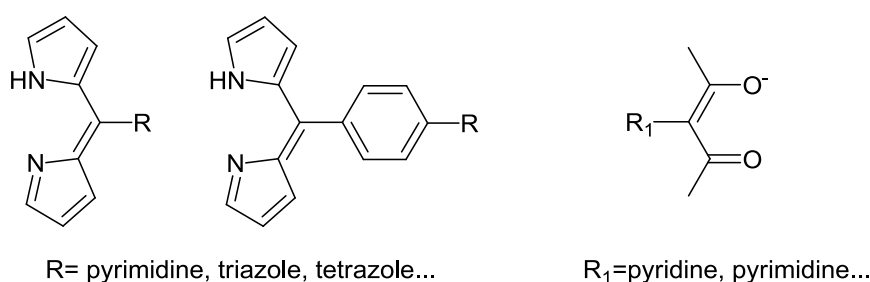


Fig. 158: Potential ligands for the preparation of DPM based homo- and heterometallic architectures.

¹ (a) Turner, S. S., Collison, D., Mabbs, F. E., Halliwell, M., *J. Chem. Soc., Dalton Trans.* **1997**, 1117; (b) Chen, B., Fronczek, F. R., Maverick, A.W., *Inorg. Chem.* **2004**, 43, 8209; (c) Vreshch, V. D., Lysenko, A. B., Chernega, A. N., Howard, J. A. K., Krautscheid, H., Sieler, J., Domasevitch, K. V., *Dalton Trans.* **2004**, 2899.

VI. Experimental section

VI.1. General remarks

I. Solvents and reagents:

Unless otherwise noted, all reagents were obtained from commercial suppliers and used without further purification. In case of hygroscopic solvents or solvents sensitive to oxygen, they were distilled with appropriate reagents under inert (Argon) atmosphere:

- Dichloromethane was dried over P₂O₅.
- Tetrahydrofuran was dried over sodium with benzophenone.
- Benzene was dried over sodium with benzophenone.

Chloroform	Riedel-de Haën	(≥99.8 %)	Acetone	Carlo Erba	(≥99.0 %)
Tetrahydrofuran	Riedel-de Haën	(≥99.9 %)	Ethyle Acetate	Carlo Erba	(≥99.0 %)
Ethanol	Riedel-de Haën	(≥99.8 %)	Chloroform	Carlo Erba	(≥99.8 %)
Benzene	Riedel-de Haën	(≥99.0 %)	Dichloromethane	Carlo Erba	(≥99.5 %)
1-Propanol	Riedel-de Haën	(≥99.0 %)	Methanol	Carlo Erba	(≥99.9 %)
Dimethylsulfoxyd	Alfa Aesar	(≥99.9 %)	Ethanol	Carlo Erba	(≥99.8 %)
N,N-Diethylformamide	Alfa Aesar	(≥99.0 %)	Ether	Carlo Erba	(≥99.8 %)
N,N-Dimethylformamide	Aldrich	(≥99.0 %)	<i>n</i> -Pentane	Carlo Erba	(≥99.0 %)
<i>o</i> -Xylene	Fluka	(≥98.0 %)	Isopropanol	Carlo Erba	(≥99.7 %)
Acetonitrile	Sds	(≥99.0 %)			

Preparative column chromatography:

- Silica gel: Silicagel Si 60 (0.040-0.063 mm), Merck TA1337567 943
- Aluminum oxide: Aluminium oxide 90 (0.063-0.200 mm) standardized, Merck TA1599097 011

Thin-layer chromatography (≥TLC):

- Silica gel: TLC Silica gel 60 F₂₅₄ on aluminum sheets, Merck HX934320
- Aluminum oxide: Polygram Alox N/UV254, Macherey-Nagel 802021

II. Analysis and characterizations:

Unless otherwise noted, compounds and complexes were characterized by ¹H-NMR, ¹³C-NMR, IR, UV and elemental analysis or/and HRMS.

- **NMR:** The ¹H and ¹³C NMR spectra were recorded at 298 K on a Bruker DRX-500 (500 MHz), Bruker AV 300 (300 MHz), Bruker AV 400 (400 MHz), Bruker MSL-400 (400 MHz) spectrometers, instruments of «Service central de RMN de la Federation de Recherche de Chimie de Université de Strasbourg». The ¹H-NMR and ¹³C-NMR spectra were recorded with the deuterated solvent as the lock and residual solvent as the internal reference. NMR chemical shifts and *J* values are given in ppm and in Hz respectively.

¹ H-NMR		¹³ C-NMR		Supplier;purity
CDCl ₃	7.26 ppm	CDCl ₃	77.2 ppm	Euriso-top®; H ₂ O+D ₂ O≤0.01 %
CD ₂ Cl ₂	5.30 ppm	CD ₂ Cl ₂	53.7 ppm	Euriso-top®; H ₂ O+D ₂ O≤0.01 %
CD ₃ OD	3.31 ppm	CD ₃ OD	49.0 ppm	Euriso-top®; H ₂ O+D ₂ O≤0.03 %
DMSO-d ₆	2.50 ppm	DMSO-d ₆	39.5 ppm	Euriso-top®; H ₂ O+D ₂ O≤0.02 %
Acetone-d ₆	2.05 ppm.	Acetone-d	29.8 ppm.	Euriso-top®; H ₂ O+D ₂ O≤0.02 %

•**IR:** IR Spectra were obtained on a Perkin Elmer FTIR 1600 spectrometer using ATR mode.

•**UV-visible:** The UV-visible spectrometer was a UVIKON XL.

•**Elemental analyses:** Elemental analyses were performed by the Service de Microanalyses de la Federation de Recherche de Chimie de Universite de Strasbourg.

•**X-Ray Crystallography:** The X-Ray Crystallography structures were determined by Dr. Stéphane Baudron. Data were collected on a Bruker SMART CCD diffractometer with Mo-K α radiation. The structures were solved using SHELXS-97 and refined by full matrix least-squares on F2 using SHELXL-97 with anisotropic thermal parameters for all non hydrogen atoms. The hydrogen atoms were introduced at calculated positions and not refined (riding model).

III. Crystallizations technique.

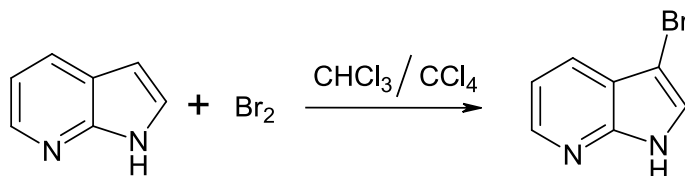
•**Slow diffusion technique:** a solution of the first reagent is slowly diffused into a solution of the second reagent in a diffusion tube 15x20cm with diameter 4mm.

•**Slow evaporation technique:** a vial (\varnothing 22.00x65x1 mm) containing a solution of the compound ($\frac{1}{3}$ of total volume) is placed in a jar containing another solvent. Depending on the solvents, there are two possible modes of crystallization. In the first case there is a slow evaporation of solvent from the vial and condensation in the crystallization jar (for example, in the system CHCl₃/DMSO). In the second case, the situation is reversed with diffusion of the vapors of the solvent from the crystallization chamber into the solution of the compound (for example system CHCl₃/*n*-pentane).

VI.2. Compounds reported in Chapter 1

Compound 1

3-Bromo-7-azaindole



A solution of 7-azaindole (25 g, 0.212 mol) in chloroform (350 mL) was cooled in an ice-bath and a CCl₄ solution (425 mL) of bromine (33.82 g, 0.212 mol) was added dropwise. The reaction mixture was extracted with aq. HCl (10 %) solution, the aqueous extract was basified with K₂CO₃ and the obtained tan precipitate was filtered off. The crude product was purified by flash chromatography (SiO₂, EtOAc) and recrystallized from toluene (32.63 g, 78.2 %)¹.

¹H NMR (300 MHz, CDCl₃): δ(ppm) 10.88 (s, 1H), 8.37 (dd, J¹=4.7 Hz, J²=1.6 Hz, 1H), 7.93 (dd, J¹=7.9 Hz, J²=1.6 Hz, 1H), 7.41(s, 1H), 7.19 (dd, J¹=7.9 Hz, J²=4.7 Hz, 1H).

¹³C NMR (75 MHz, CDCl₃): δ(ppm) 147.5, 143.7, 128.0, 124.4, 120.0, 116.6, 89.4.

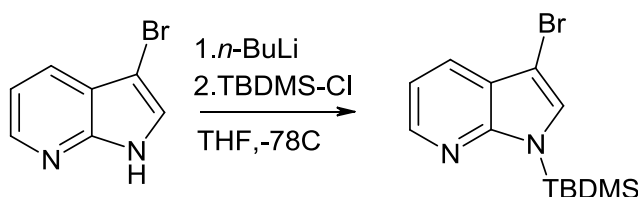
Elemental Analysis: C₇H₅N₂Br (Mw: **197.04** g/mole)

Calculated: C 42.67 %, N 14.22 %, H 2.56 %.

Found: C 42.21 %, N 14.39 %, H 2.70 %.

Compound 2

N-TBDMS-3-Bromo-7-azaindole



To a solution of 3-Bromo-7-azaindole (30 g, 0.152 mol) in dry THF (300 mL), cooled at -78°C, under an argon atmosphere, *n*-BuLi (1.6 M in hexane, 95.6 mL, 0.153 mol) was added slowly. After addition and stirring for 15 min, the solution had a deep color and a solution of TBDMS-Cl (23.06 g, 0.153 mol) in dry THF (100 mL) was added. Upon completion of addition, the cooling bath was removed and the mixture was allowed to come slowly to RT. The reaction mixture was diluted with Et₂O, washed with brine, dried and evaporated. The crude product was purified by flash chromatography (CH₂Cl₂/hexane: 1/5, *R*_f= 0.8). The resulting colorless oil was washed with *n*-pentane (200mL) to afford the product as white crystals (41.8 g, 88.2 %)².

$^1\text{H NMR}$ (300 MHz, CDCl_3): δ (ppm) 8.30 (dd, $J^1=4.7$ Hz, $J^2=1.6$ Hz, 1H), 7.81 (dd, $J^1=7.9$ Hz, $J^2=1.6$ Hz, 1H), 7.23(s, 1H), 7.10 (dd, $J^1=7.9$ Hz, $J^2=4.7$ Hz, 1H), 0.93 (s, 9H), 0.62 (s, 6H).

$^{13}\text{C NMR}$ (75 MHz, CDCl_3): δ (ppm) 152.6, 143.6, 129.5, 126.7, 121.7, 116.6, 91.2, 26.5, 18.9, -4.2.

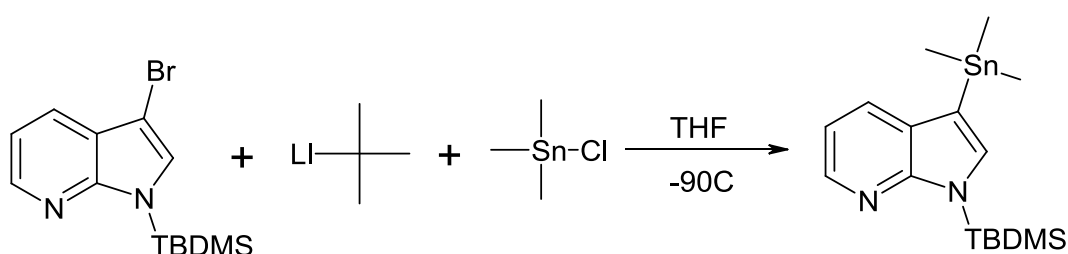
Elemental Analysis: $\text{C}_{13}\text{H}_{19}\text{BrN}_2\text{Si}$ (Mw: **311.29** g/mole)

Calculated: C50.16 %, N 9.00 %, H 6.15 %.

Found: C49.99 %, N 8.80 %, H 6.20 %.

Compound 3

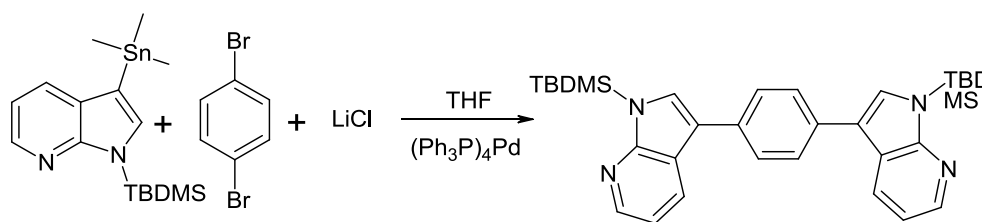
3-Trimethylstannyl-7-azaindole



To a solution of N-TBDMS-3-Bromo-7-azaindole (8 g, 25.72 mmol) in dry THF (100 mL), cooled at -90°C , under an argon atmosphere, *t*-BuLi (1.7M in hexane, 30.3 mL, 51.44 mmol) was quickly added. After addition and stirring for 5 min, solution had turned green and Me_3SnCl (7.69 g, 38.58 mmol) was added slowly. When the addition was complete, mixture was stirred for 1h at -90°C and then for 1h at RT; The mixture was diluted with Et_2O , washed with brine, dried and evaporated to afford the product as a white solid (9.56g, 97.2 %)².

$^1\text{H NMR}$ (300 MHz, CDCl_3): δ (ppm) 8.26 (dd, $J^1=4.7$ Hz, $J^2=1.6$ Hz, 1H), 7.81 (dd, $J^1=7.8$ Hz, $J^2=1.6$ Hz, 1H), 7.13(s, 1H), 7.01 (dd, $J^1=7.8$ Hz, $J^2=4.7$ Hz, 1H), 0.95 (s, 9H), 0.63 (s, 6H), 0.35 (s, 9H).

$^{13}\text{C NMR}$ (75 MHz, CDCl_3): δ (ppm) 155.6, 142.1, 136.9, 130.7, 128.7, 115.6, 109.7, 26.5, 19.0, -4.3, -9.2.

Compound 4**1,4-Di(7-azaindol-3-yl)-benzene (Two step synthesis)****Step I:**

A solution of N-TBDMS-3-trimethylstannyl-7-azaindole (3 g, 7.59 mmol), 1,4 dibromobenzene (0.90 g, 3.80 mmol), LiCl (0.96 g, 22.77 mmol) and $(\text{Ph}_3\text{P})_4\text{Pd}$ (0.1 g) in dry THF (100 mL) was refluxed for 72h under argon. The mixture was then diluted with Et_2O and the precipitate was filtered off. The solution was evaporated and the solid residue was purified by flash chromatography in chloroform, concentrated and diluted with hexane. The obtained white precipitate was separated and washed with *n*-pentane to afford the product as a white powder (0.9 g, 44.1 %).

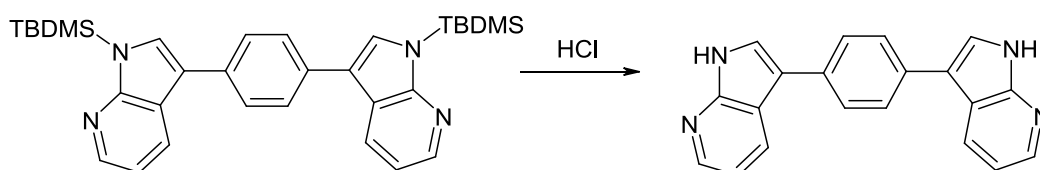
$^1\text{H NMR}$ (300 MHz, CDCl_3): δ (ppm) 8.33 (dd, $J^1=4.7$ Hz, $J^2=1.7$ Hz, 2H), 8.21 (dd, $J^1=7.9$ Hz, $J^2=1.6$ Hz, 2H), 7.73(s, 4H), 7.45 (s, 2H), 7.12 (dd, $J^1=7.9$ Hz, $J^2=4.8$ Hz, 2H), 0.99 (s, 18H), 0.69 (s, 12H).

$^{13}\text{C NMR}$ (75 MHz, CDCl_3): δ (ppm) 150.5, 142.8, 133.1, 127.8, 127.5, 127.3, 120.7, 118.0, 116.3, 26.6, 19.0, -4.1.

Elemental Analysis: $\text{C}_{32}\text{H}_{42}\text{N}_4\text{Si}_2$ (Mw: **538.89** g/mole)

Calculated: C 71.32 %, N 10.40 %, H 7.86 %,

Found: C 70.74 %, N 10.42 %, H 8.02 %.

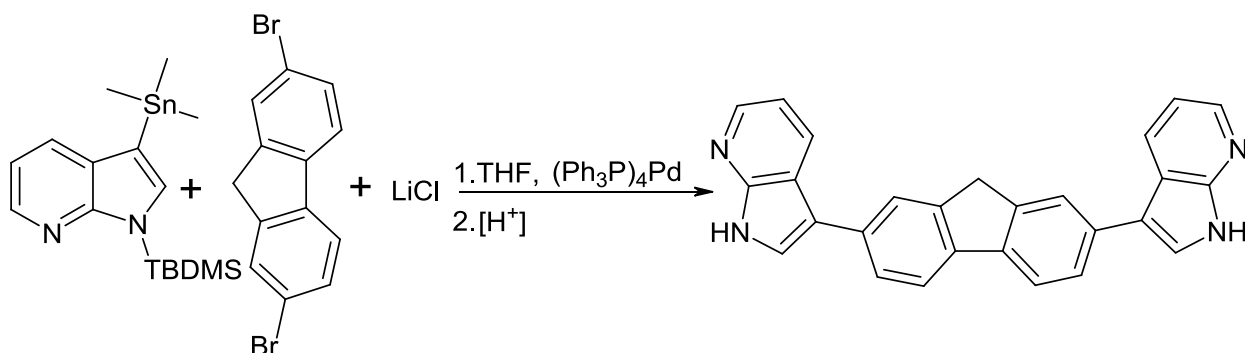
Step II:

A solution of 1,4-di(N-TBDMS-7-azaindol-3-yl)-benzene (0.9 g, 1.67 mmol) in THF (200 mL) was extracted (3x300 mL) with aq HCl (10 %) and the aqueous extract was basified with NaOH (50 %). The obtained white precipitate was separated and washed with ether (350 mL) to afford the product as a white powder (0.33 g, 63.6 %).

$^1\text{H NMR}$ (300 MHz, DMSO-d_6): δ (ppm) 11.91 (s, 2H), 8.33 (dd, $J^1=8.0$ Hz, $J^2=1.3$ Hz, 2H), 8.29 (dd, $J^1=4.5$ Hz, $J^2=1.3$ Hz, 2H), 7.90(s, 2H), 7.80 (s, 4H), 7.17 (dd, $J^1=7.8$ Hz, $J^2=4.7$ Hz, 2H).

$^{13}\text{C NMR}$ (75 MHz, DMSO-d_6): δ (ppm) 149.6, 143.3, 132.9, 128.0, 127.1, 124.0, 117.8, 116.5, 114.6.

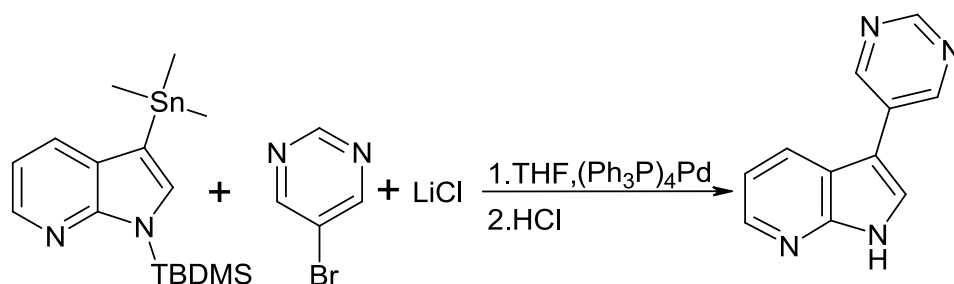
HRMS (ESI), m/z : $[\text{M} + \text{H}]^+$ calc. for $\text{C}_{20}\text{H}_{15}\text{N}_4$: 311.129, found 311.128.

Compound 5**2,7-di(7-azaindol-3-yl)-fluorene**

A solution of N-TBDMS-3-trimethylstannyl-7-azaindole (1 g, 2.53 mmol), 2,7-dibromofluorene (0.41 g, 1.275 mmol), LiCl (0.64 g, 15.180 mmol) and $(\text{Ph}_3\text{P})_4\text{Pd}$ (0.1 g) was refluxed for 72h under argon in dry THF (50 mL). The mixture was diluted with Et_2O , the precipitate was filtered off and the solution was evaporated to dryness. The residue was purified by flash chromatography (SiO_2 , CHCl_3), concentrated and diluted with hexane. The resulting white powder was dissolved in THF (200 mL) and extracted (3X150 mL) with aq HCl (10 %); the aqueous extract was basified with NaOH (50 %). After 1h of stirring, the precipitate obtained was filtered and washed with ether (300 mL) to afford the product (0.125 g, 12.4 %) as a white precipitate.

$^1\text{H NMR}$ (300 MHz, DMSO-d_6): δ (ppm) 11.93 (s, 2H), 8.39 (d, $J=7.8$ Hz, 2H), 8.29 (d, $J=3.9$ Hz, 2H), 7.95 (d, $J=7.9$ Hz, 6H), 7.76 (d, $J=8.1$ Hz, 2H), 7.19 (dd, $J_1=8.0$ Hz, $J_2=4.7$ Hz, 2H), 4.07 (s, 2H).

$^{13}\text{C NMR}$ (75 MHz, DMSO-d_6): δ (ppm) 149.6, 144.3, 143.3, 139.3, 133.9, 128.1, 125.5, 124.1, 123.3, 120.6, 117.8, 116.4, 115.1, 37.1.

Compound 6**3-(Pyrimidin-5-yl)-7-azaindole**

A solution of N-TBDMS-3-trimethylstannyl-7-azaindole (1 g, 2.53 mmol), 5-bromo-pyrimidine (1.6 g, 10.12 mmol), LiCl (0.32 g, 7.59 mmol) and $(\text{Ph}_3\text{P})_4\text{Pd}$ (0.1 g) in dry THF (50 mL) was refluxed for 48h under argon. After this time, the mixture was diluted with Et_2O and extracted with aq. HCl (10 %), the aqueous extract was basified with NaHCO_3 . The resulting precipitate was filtered off and washed by preheated chloroform and ether to afford the product as a white powder (0.254 g, 51.24 %)².

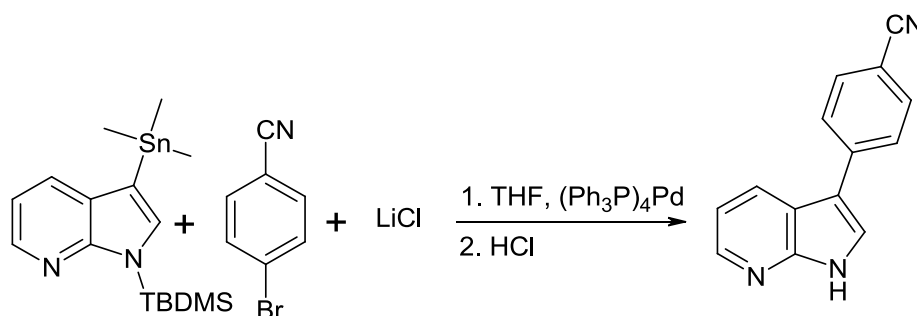
$^1\text{H NMR}$ (300 MHz, DMSO-d_6): δ (ppm) 12.22 (s, 1H), 9.21 (s, 2H), 9.06 (s, 1H), 8.40 (dd, $J^1=8.1$ Hz, $J^2=1.1$ Hz, 1H), 8.32 (dd, $J^1=4.7$ Hz, $J^2=1.5$ Hz, 1H), 8.18 (d, $J=2.8$ Hz, 1H), 7.20 (dd, $J^1=8.0$ Hz, $J^2=4.7$ Hz, 1H).

^{13}C NMR (75 MHz, DMSO- d_6): δ (ppm) 155.9, 154.0, 149.5, 143.9, 129.7, 128.2, 125.9, 117.3, 117.0, 107.8.

HRMS (ESI), m/z : $[M + H]^+$ calcd for $\text{C}_{11}\text{H}_9\text{N}_4$: 197.082, found 197.081.

Compound 7

3-(4-benzonitrilyl)-7-azaindole



A solution of N-TBDMS-3-trimethylstannyl-7-azaindole (1 g, 2.53 mmol), 4-bromo-benzonitrile (0.69 g, 3.80 mmol), LiCl (0.21 g, 7.59 mmol) and $(\text{Ph}_3\text{P})_4\text{Pd}$ (0.2 g) in dry THF (50 mL) was refluxed for 72h under argon. The mixture was diluted with Et_2O , the precipitate was filtered off and the solution evaporated. The crude product was purified by chromatography (SiO_2 , CHCl_3 /pentane: 1/3). The resulting product was dissolved in THF and mixed with HCl solution in dioxane (4M, 10 ml). After 1h of stirring, the precipitate which formed was filtrated and washed with ether (0.092 g, 16.6 %).

^1H NMR (300 MHz, DMSO- d_6): δ (ppm) 12.20 (s, 1H), 8.38 (dd, $J^1=8.38$ Hz, $J^2=1.4$ Hz, 1H), 8.31 (dd, $J^1=4.6$ Hz, $J^2=1.4$ Hz, 1H), 8.15(d, $J=2.5$ Hz, 1H), 7.96 (d, $J=8.2$ Hz, 2H), 7.86 (d, $J=8.2$ Hz, 2H), 7.21 (dd, $J^1=8.1$ Hz, $J^2=4.8$ Hz, 1H).

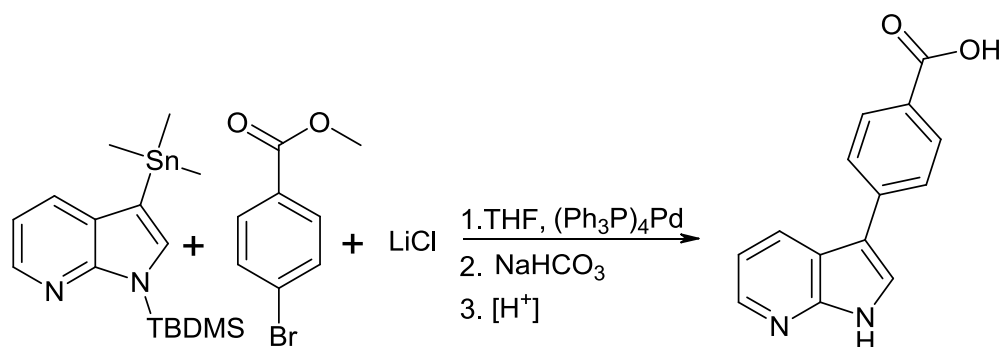
^{13}C NMR (75 MHz, DMSO- d_6): δ (ppm) 149.7, 143.8, 140.6, 133.2, 128.2, 126.8, 126.6, 119.7, 117.4, 117.1, 113.0, 107.9.

IR: ν 2218 (CN) cm^{-1} .

Elemental Analysis: $\text{C}_{14}\text{H}_9\text{N}_3$ (Mw: 219.25 g/mole)

Calculated: C 76.70 %, N 19.17 %, H 4.14 %,

Found: C 75.97 %, N 19.17 %, H 4.25 %

*Compound 8***4-(7-azaindol-3-yl) benzoic acid**

A solution of N-TBDMS-3-trimethylstannyl-7-azaindole (1 g, 2.53 mmol), 4-bromo-benzoic acid methyl ester (0.82 g, 3.81 mmol), LiCl (0.321 g, 7.57 mmol) and (Ph₃P)₄Pd (0.1 g) in dry THF (50 mL) was refluxed for 72h under argon. The mixture was then diluted with Et₂O. The precipitate was filtered off and the solution evaporated. The residue was purified by chromatography (SiO₂, CHCl₃/pentane: 1/3). The isolated white powder was dissolved in a minimum amount of MeOH and mixed with aq. NaHCO₃ solution (100 mL). Obtained suspension was refluxed before full dissolution. Then, an aq. HCl solution was added until the pH reached 3-5. Obtained solution was basified with aq. NaHCO₃ until the pH reached 7-8 and formed white precipitate was filtered off. The resulting solid was washed with ether (100mL) to afford the product as a white powder (0.175 g, 29.0 %).

¹H NMR (300 MHz, DMSO-d₆): δ(ppm) 12.81 (s, 1H), 12.10 (s, 1H), 8.38 (d, J=7.8 Hz, 1H), 8.30 (d, J=4.7 Hz, 1H), 8.06 (d, J=2.5, 1H), 7.99 (d, J=8.2 Hz, 2H), 7.88 (d, J=8.2 Hz, 2H), 7.19 (dd, J¹=8.0 Hz, J²=4.6 Hz, 1H).

¹³C NMR (75 MHz, DMSO-d₆): δ(ppm) 167.7, 149.6, 143.6, 140.1, 130.4, 128.2, 127.9, 126.2, 125.7, 117.5, 116.8, 113.7.

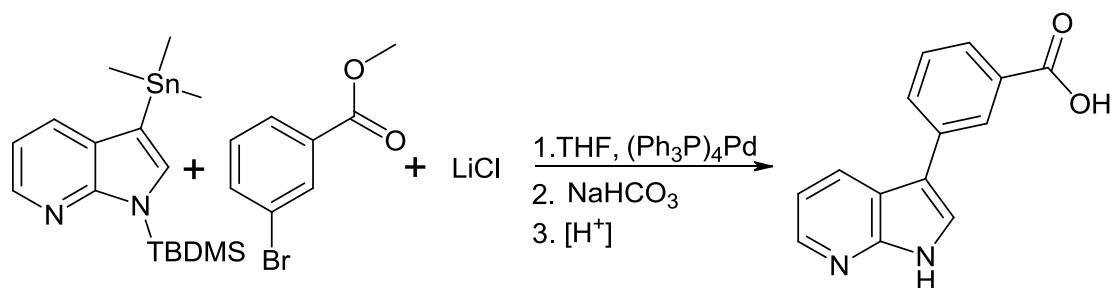
IR: ν 3226 (OH), 1691 (C=O), 1314 (C-O). cm⁻¹.

Elemental Analysis: C₁₄H₁₀N₂O₂ (Mw: **238.25 g/mole**)

Calculated: C 70.58 %, N 11.76 %, H 4.23 %.

Found: C 69.24 %, N 11.11 %, H 4.26 %.

HRMS (ESI), m/z: [M + H]⁺ calcd for C₁₄H₁₁N₂O₂: 239.082, found 239.081.

*Compound 9***3-(7-azaindol-3-yl) benzoic acid**

A solution of N-TBDMS-3-trimethylstannyl-7-azaindole (3.40 g, 8.60 mmol), 3-bromo-benzoic acid methyl ester (3.64 g 16.93 mmol), LiCl (1.28 g, 30.29 mmol) and (Ph₃P)₄Pd (0.2g) in dry THF (150 mL) was refluxed for 72h under argon. After evaporation of the mixture, the residue was dissolved in a minimum amount of MeOH and mixed with an aq. NaHCO₃ solution (150 mL). Obtained suspension was refluxed before full dissolution. Then, an aq. HCl solution was added until the pH reached 3-5. Obtained solution was basified with aq. NaHCO₃ until the pH reached 7-8 and formed white precipitate was filtered off. The resulting solid was washed with MeOH and ether to afford the product as a white powder (0.99 g, 48.1 %).

¹H NMR (300 MHz, DMSO-d₆): δ(ppm) 13.06 (s, 1H), 12.01 (s, 1H), 8.31-8.25 (m, 3H), 7.98-7.95 (m, 2H), 7.83(dt, J₁=7.6 Hz, J₂=1.5 Hz, 1H), 7.56 (t, J=7.6 Hz, 1H), 7.19 (dd, J¹=7.9 Hz, J²=4.7 Hz, 1H).

¹³C NMR (75 MHz, DMSO-d₆): δ(ppm) 167.9, 149.5, 143.5, 135.8, 132.1, 130.9, 129.6, 127.6, 127.2, 126.9, 124.8, 117.6, 117.0, 113.8.

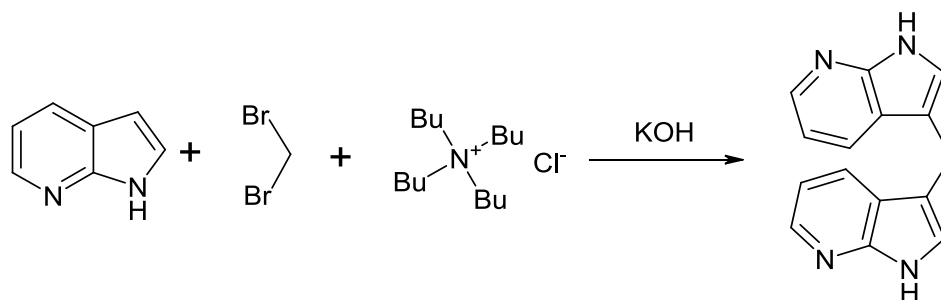
IR: ν 3144-2551 (OH), 1698 (C=O), 1303 (C-O). cm⁻¹.

Elemental Analysis: C₁₄H₁₀N₂O₂ (Mw: **238.25** g/mole)

Calculated: C 70.58 %, N 11.76 %, H 4.23 %.

Found: C 69.50 %, N 11.37 %, H 4.06 %.

HRMS (ESI), m/z: [M + H]⁺ calcd for C₁₄H₁₁N₂O₂: 239.082, found 239.080.

Compound 10**Bis(7-azaindol-3-yl)-methane**

7-Azaindole (1.5 g, 12.70 mmol), dibromomethane (1.10 g, 6.33 mmol) and tetrabutylammonium bromide (0.32g, 1.15mmol) were dissolved in toluene (40 mL) and mixed with an aqueous solution (100 mL) of KOH (1.06 g, 18.89 mmol). The mixture was strongly stirred and heated at 120°C for 72 h. The reaction mixture was then cooled down thoroughly and the precipitate was collected by vacuum filtration followed by washing with water and ether (0.272 g, 17.3 %)³.

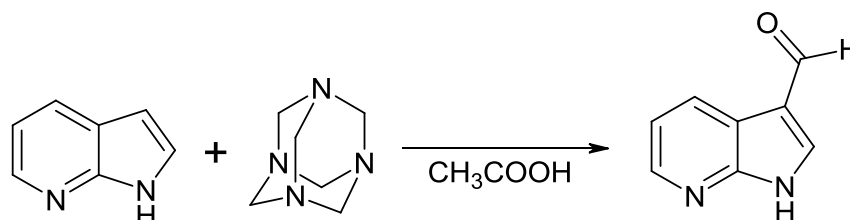
¹H NMR (300 MHz, DMSO-d₆): δ(ppm) 11.31 (s, 2H), 8.14 (dd, J¹=4.8 Hz, J²=1.8 Hz, 2H), 7.88 (dd, J¹=7.7 Hz, J²=1.5 Hz, 2H), 7.31(s, 2H), 6.96 (dd, J¹=7.9 Hz, J²=4.7 Hz, 2H), 4.13 (s, 2H).

¹³C NMR (75 MHz, DMSO-d₆): δ(ppm) 149.2, 142.7, 127.1, 123.6, 119.7, 115.1, 113.2, 21.5.

Elemental Analysis: C₁₅H₁₂N₄•(H₂O) (Mw: 266.30 g/mole)

Calculated: C 67.65 %, N 21.01 %, H 5.30 %.

Found: C 67.71 %, N 21.81 %, H 4.46 %.

Compound 11A**7-azaindole-3-carboxaldehyde**

A solution of 7-azaindole (1 g, 8.46 mmol) and hexamethylenetetramine (1.78 g, 12.7 mmol) in acetic acid (10 mL, aq. 30 %) was refluxed at 110°C. After 6 hours, the yellow solution became pale and the mixture was allowed to rise to RT. Water (20 mL) was added and the mixture was left at 4°C for 12h. The precipitate was filtered and recrystallized from water (0.807 g, 65.0 %)⁴.

¹H NMR (300 MHz, Acetone-d₆): δ(ppm): 10.02 (s, 1H), 8.49 (dd, J¹=7.9 MHz, J²=1.6 MHz, 1H), 8.38 (m, 2H), 7.28 (dd, J¹=7.8 MHz, J²=4.7 MHz, 1H).

¹³C NMR (75 MHz, DMSO-d₆): δ(ppm) 185.8, 149.8, 145.3, 139.2, 129.6, 118.8, 116.9, 117.0.

IR (KBr): ν: 1665 cm⁻¹(CO)

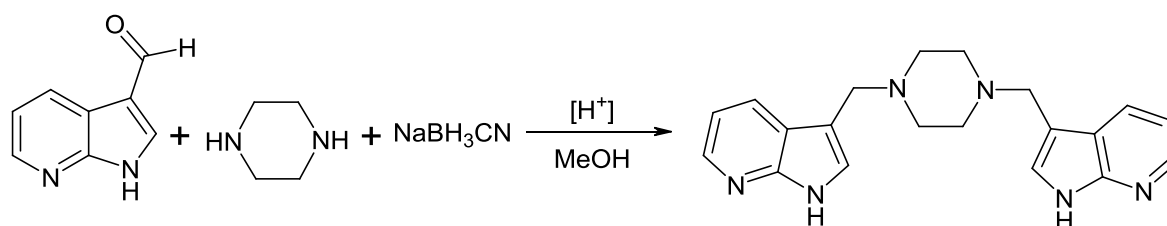
Elemental Analysis: C₈H₆N₂O (Mw: **146.15** g/mole)

Calculated: C 65.75 % H 4.14 % N 19.17 %

Found: C 65.46 % H 4.15 % N 19.42 %

Compound 11

N,N-Bis((7-azaindol-3-yl)methyl)-piperazine



7-azaindol-3-carboxaldehyde (0.50 g, 3.42 mmol) and piperazine (0.21 g, 1.71 mmol) were dissolved in methanol (8 mL). The pH of the reaction mixture was adjusted to 5 with acetic acid and stirred for 12h at RT. NaBH₃CN was added and after 12h of stirring, the precipitate was filtrated and washed with water (100 mL) and ether (300 mL) to afford the product (0.46 g, 78.4 %) as a white precipitate.

¹H NMR (300 MHz, DMSO-d₆): δ(ppm) 11.43 (s, 1H), 8.17 (dd, J¹=4.6 Hz, J²=1.6 Hz, 1H), 7.99 (dd, J¹=7.8 Hz, J²=1.5 Hz, 1H), 7.30(s, 1H), 7.01 (dd, J¹=7.8 Hz, J²=4.7 Hz, 1H), 3.59 (s, 2H), 2.37 (s, 4H).

¹³C NMR (75 MHz, DMSO-d₆): δ(ppm) 149.1, 142.8, 127.7, 125.2, 120.2, 115.4, 110.4, 53.7, 53.1.

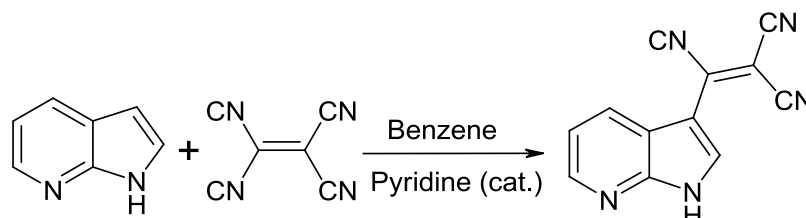
Elemental Analysis: C₂₀H₂₂N₆•(H₂O) (Mw: **364.44** g/mole)

Calculated: C 65.91 %, N 23.06 %, H 6.63 %.

Found: C 66.15 %, N 23.41 %, H 5.94 %

Compound 12

3-Tricyanovinylene-7-azaindole



A benzene (10 mL) solution of 7-azaindole (0.5 g, 4.23 mmol) was added to a refluxing benzene (8 mL) solution of TCNE (0.3g, 2.34mmol). The solution immediately turned black. Addition of few drops of pyridine resulted in the precipitation of a green solid. The mixture was further refluxed for 2 hours. The solution was then filtered and the solid washed with benzene and cold CHCl₃ to afford 3-tricyanovinylene-7-azaindole (0.48 g, 97.0 % based on TCNE)⁵.

$^1\text{H NMR}$ (300 MHz, DMSO- d_6): δ (ppm) 13.78 (br s, 1H), 8.78 (s, 1H), 8.49 (dd, $J^1=1.4$ Hz, $J^2=4.5$ Hz, 1H), 8.44 (dd, $J^1=1.5$ Hz, $J^2=8.2$ Hz, 1H), 7.45 (dd, $J^1=4.5$ Hz, $J^2=8.2$ Hz, 1H).

$^{13}\text{C NMR}$ (75 MHz, DMSO- d_6): δ (ppm) 149.5, 146.5, 137.4, 133.5, 129.4, 119.6, 117.1, 115.0, 114.3, 113.9, 107.7, 81.4.

UV-VIS, (CH_2Cl_2) λ_{max} (nm), ϵ ($\text{mol}^{-1} \text{L cm}^{-1}$): 228 (14000), 281 (6000), 423 (8000), 478 (3000).

IR: ν 2223 (CN) cm^{-1} .

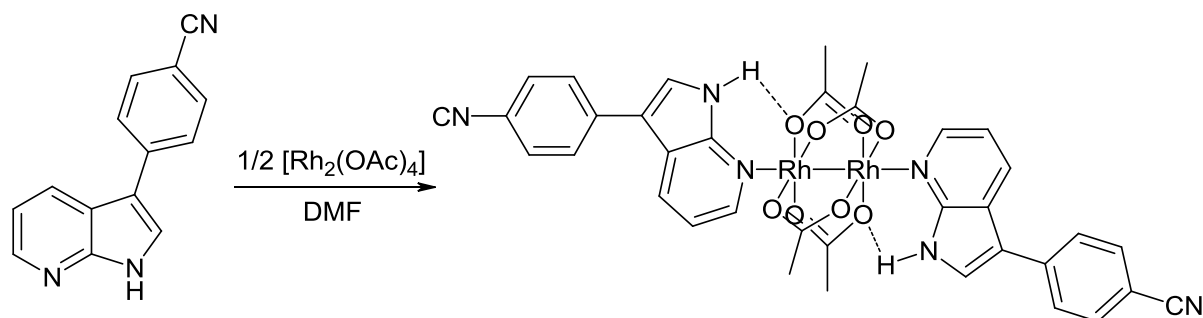
Elemental Analysis: $\text{C}_{12}\text{H}_5\text{N}_5$ (Mw: **219.20** g/mole)

Calculated: C 65.75 %, N 31.95 %, H 2.30 %,

Found: C 65.16 %, N 31.62 %, H 2.67 %

Compound 13:

Complex [Bis(3-(4-benzonitrilyl)-7-azaindole)($\text{Rh}_2(\text{OAc})_4$)]



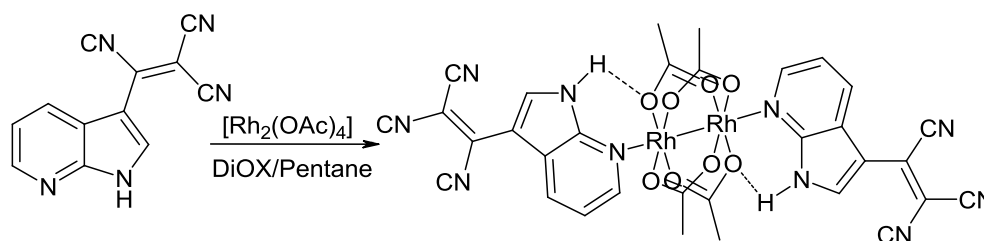
A solution of 3-(4-benzonitrilyl)-7-azaindole (25 mg, 0.114 mmol) in DMF (5mL) was mixed with a DMF solution (5 mL) of $[\text{Rh}_2(\text{OAc})_4]$ (25.2 mg, 0.057 mmol) in a tube (16x1 cm). Red crystals were obtained by slow diffusion of water into a DMF solution of the complex. (35.5 mg, 60.6 %).

IR: ν 2220(CN) 1437(COO^-), 1591 (COO^-) cm^{-1} .

Elemental Analysis: $\text{C}_{36}\text{H}_{30}\text{N}_6\text{O}_8\text{Rh}_2 \cdot 2(\text{DMF})$ (Mw: **1026.67** g/mole)

Calculated: C 49.14 %, N 10.91 %, H 4.32 %.

Found: C 48.38 %, N 11.04 %, H 4.64 %

Compound 14**Complex [Bis(3-Tricyanovinylene-7-azaindole)](Rh₂(OAc)₄)**

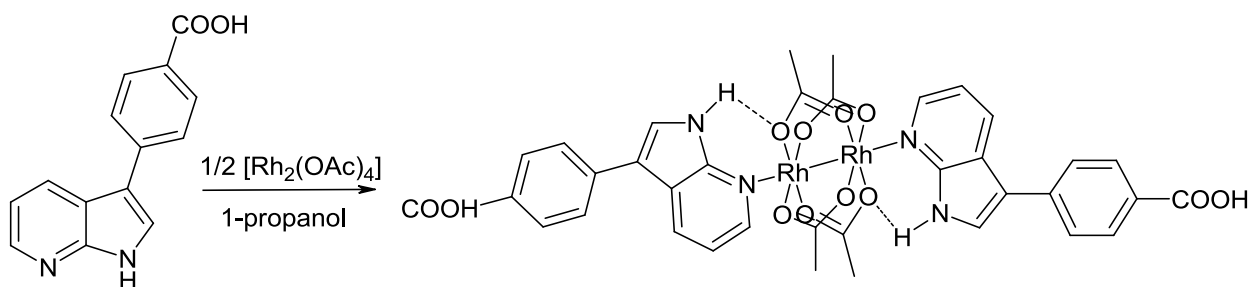
A solution of 3-Tricyanovinylene-7-azaindole (25.7 mg, 0.117 mmol) in THF (10 mL) was mixed with a THF solution (10mL) of [Rh₂(OAc)₄] (25.8 mg, 0.058 mmol). The solution was evaporated and the residue remains was dissolved in dioxane. Red crystals were grown by slow diffusion of *n*-pentane vapors into the DiOX solution of the complex (25.5 mg, 35.3 %).

¹H NMR (300 MHz, CDCl₃): δ(ppm) 11.84 (br s, 1H), 9.23 (dd, J¹=5.1 Hz, J²=1.0 Hz, 1H), 9.03 (dd, J¹= 8.2 Hz, J²=1.1 Hz, 1H), 8.88 (d, J=3.3 Hz, 1H), 7.81 (dd, J¹=8.4 Hz, J²=5.2 Hz, 1H), 1.98 (s, 6H).

¹³C NMR (75 MHz, CDCl₃): δ(ppm) 192.6, 151.0, 147.8, 133.8, 133.2, 130.9, 120.8, 119.3, 114.0, 113.5, 112.0, 108.0, 78.5, 24.2.

¹H NMR (300 MHz, Acetone-d₆): δ(ppm) 8.93 (s, H), 8.59 (dd, J¹=8.1 Hz, J²=1.5 Hz, 1H), 8.52 (dd, J¹= 4.7 Hz, J²=1.5 Hz, 1H), 7.48 (dd, J¹=8.1 Hz, J²=4.7 Hz 1H), 2.05 (s, 6H).

IR: ν 2224 (CN), 1415 (COO⁻), 1588(COO⁻). cm⁻¹.

Compound 15:**Complex [Bis(3-(7-azaindol-3-yl)benzoic acid)](Rh₂(OAc)₄)**

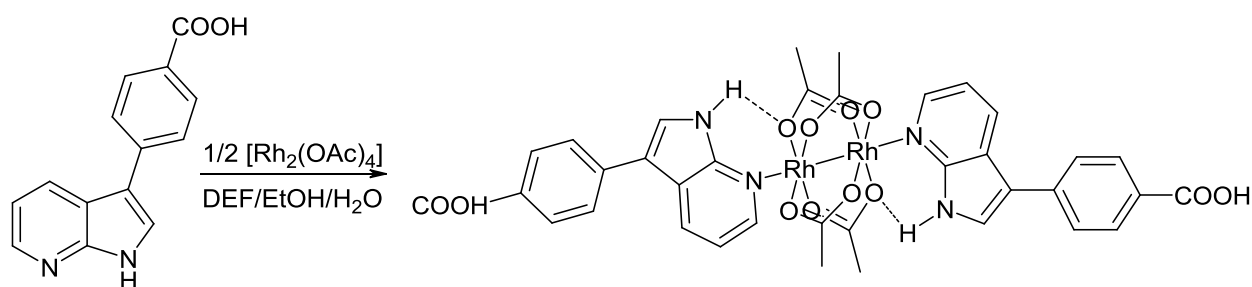
The solutions of 7-azaindol-3-yl-benzoic acid (25 mg, 0.105 mmol) and [Rh₂(OAc)₄] (22.2 mg, 0.052mmol) in 1-propanol were mixed. Red crystals (insoluble in any common solvents) were grown in two weeks (39.5 mg, 81.9 %).

IR: ν 3259 (OH), 1710 (C=O), 1232 (C-O), 1440 (COO⁻), 1589(COO⁻). cm⁻¹.

Elemental Analysis: C₃₆H₃₂N₄O₁₂Rh₂ (Mw: **918.47** g/mole)

Calculated: C 47.08 %, N 6.10 %, H 3.51 %.

Found: C 47.77 %, N 6.80 %, H 4.08 %.

Compound 16**Complex [Bis(4-(7-azaindol-3-yl) benzoic acid))(Rh₂(OAc)₄)](DEF)₂**

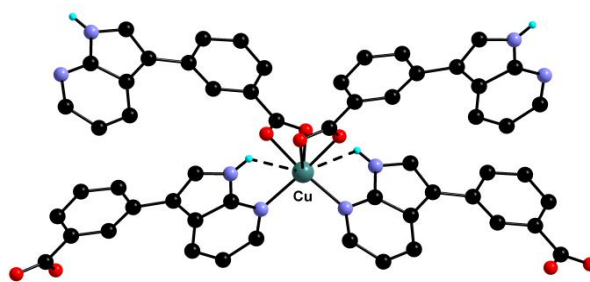
The solutions of 7-azaindol-3-yl-benzoic acid (25 mg, 0.105mmol) and [Rh₂(OAc)₄] (22.2 mg, 0.052mmol) in mixture DEF/EtOH/H₂O: 3/2/2 was mixed. Red crystals (insoluble in any common solvents) were grown in two weeks (37.8 mg, 62.3 %).

IR: ν 3295 (OH), 1720 (C=O), 1221 (C-O), 1435(COO⁻), 1582(COO⁻). cm⁻¹.

Elemental Analysis: C₃₆H₃₂N₄O₁₂Rh₂ •2(DEF) (Mw: **1120.78** g/mole)

Calculated: C 49.29 %, N 7.50 %, H 4.86 %.

Found: C 49.06 %, N 7.07 %, H 4.94 %.

Compound 17**Network {[Bis(4-(7-azaindol-3-yl) benzoic acid))Cu(II)]}_∞**

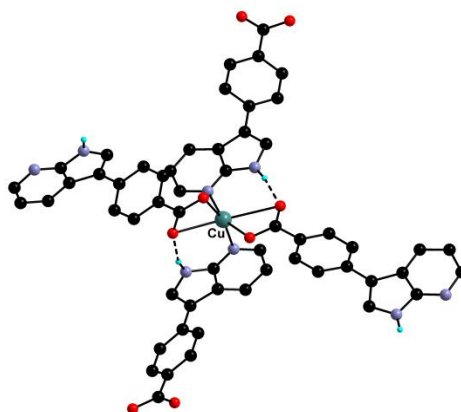
Solutions of 3-(7-azaindol-3-yl)-benzoic acid (25 mg, 0.105 mmol) and Cu(NO₃)₂•3H₂O (25.3 mg, 0.105 mmol) in mixture DEF/EtOH/H₂O (3/1/3) were mixed and left to stand for two weeks, upon which time, green crystals (insoluble in any common solvents) were grown (18 mg, 63.8 %).

IR: ν 1566 (C=O), 1387 (C-O). cm⁻¹.

Elemental Analysis: C₂₈H₁₈CuN₄O₄ (Mw: **538.00** g/mole)

Calculated: C 62.51 %, N 10.41 %, H 3.37 %.

Found: C 61.87 %, N 10.27 %, H 3.77 %

Compound 18**Network {[Bis(4-(7-azaindol-3-yl) benzoic acid))Cu(II)]_∞ (Solvent)}**

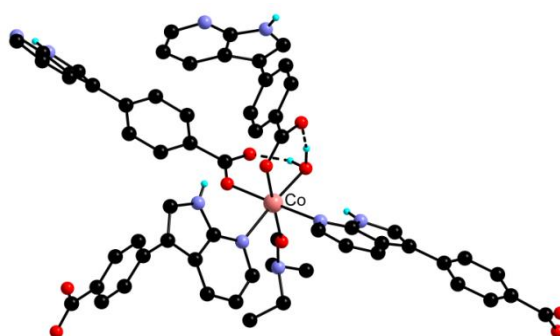
The solutions of 4-(7-azaindol-3-yl)-benzoic acid (100 mg, 0.420mmol) and $\text{Cu}(\text{NO}_3)_2 \cdot 6\text{H}_2\text{O}$ (61.2 mg, 0.210mmol) in a DEF/EtOH/ H_2O (3/1/1) mixture were mixed. Green crystals (insoluble in any common solvents) were grown after two weeks. (70 mg, 62.0 %). The network contains solvents in the canals.

IR: ν 1673 (C=O), 1390 (C-O). cm^{-1} .

Elemental Analysis: $\text{C}_{28}\text{H}_{18}\text{CuN}_4\text{O}_4 \cdot (\text{solvents H}_2\text{O or/and DEF or/and EtOH})$ (Mw: **538.00** g/mole)

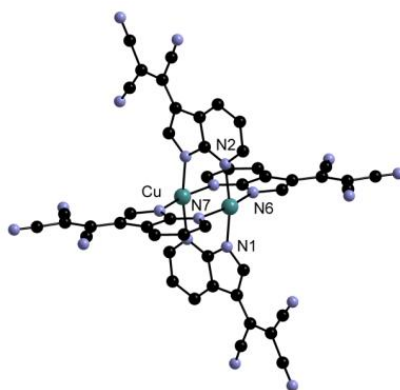
Calculated: C 62.51 %, N 10.41 %, H 3.37 %.

Found: C 59.52 %, N 10.08 %, H 5.11 %.

Compound 19**Network {[Bis(4-(7-azaindol-3-yl) benzoic acid))(DEF)(H_2O))Co(II)]_∞}**

The solutions of 4-(7-azaindol-3-yl)-benzoic acid (5 mg, 0.020 mmol) and CoCl_2 (4.8 mg, 0.020 mmol) in DEF/EtOH/ H_2O (3/2/2) mixture was mixed. Pink crystals (insoluble in any common solvents) were grown in obtained after six months.

IR: ν 1641 (C=O), 1386 (C-O). cm^{-1} .

Compound 20**Complex $[\text{Cu}_2(\text{3-Tricyanovinylene-7-azaindoly})_4(\text{DMF})_2]$** 

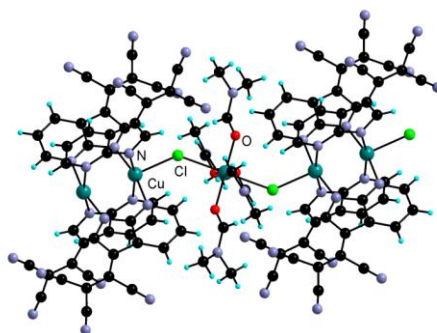
The solutions of 3-Tricyanovinylene-7-azaindoly (50 mg, 0.228 mmol) and $\text{Cu}(\text{OTf})_2$ (41.3 mg, 0.114 mmol) in DMF were mixed and left to stand. Green-blue crystals (insoluble in any common solvents) were obtained after two weeks (38.4 mg, 58.8 %).

IR: ν 2213 (CN) cm^{-1} .

Elemental Analysis: $\text{C}_{48}\text{H}_{16}\text{Cu}_2\text{N}_{20} \cdot 2(\text{DMF})$ (Mw: **1146.06** g/mole)

Calculated: C 56.59 %, N 26.89 %, H 2.64 %.

Found: C 56.08 %, N 26.58 %, H 3.16 %.

Compound 21**Network $\{[(\text{Cu}_2(\text{3-Tricyanovinylene-7-azaindoly})_4)(\text{CuCl}_2)(\text{DMF})_4](\text{DMF})\}_\infty$** 

The solutions of 3-Tricyanovinylene-7-azaindoly (45.5 mg, 0.208 mmol) and CuCl_2 (35.4 mg, 0.208 mmol) in DMF were mixed and left to stand at RT. Green-blue crystals (insoluble in any common solvents) were obtained after two months (22.0 mg, 28.3 %).

IR: ν 2210 (CN) cm^{-1} .

Elemental Analysis: $\text{C}_{48}\text{H}_{16}\text{Cu}_3\text{N}_{20}\text{Cl}_2 \cdot 4(\text{DMF})$ (Mw: **1499.81** g/mole)

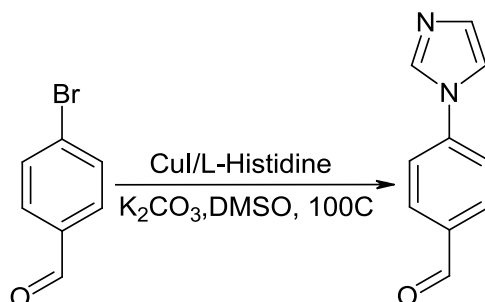
Calculated: C 50.45 %, N 23.35 %, H 3.43 %.

Found: C 49.71 %, N 23.25 %, H 3.66 %

VI.3. Compounds reported in Chapter 2

Compound 22

4-(1H-imidazol-1-yl)-benzaldehyde



A DMSO solution (60 mL) of CuI (0.21 g, 1.1 mmol) and *L*-histidine (0.34 g, 2.2 mmol) was stirred in a preheated oil bath (100°C) under nitrogen for 30 minutes. Then, 4-bromobenzaldehyde (2g, 11.1 mmol), imidazole (0.9 g, 13.2 mmol) and potassium carbonate (3.06 g, 22.2 mmol) were added. After 36 h, the reaction mixture was washed with aqueous NaHCO₃ (750mL) and the product was extracted in chloroform (3x500 mL). The organic extracts were dried over mgSO₄ and concentrated. The crude product was purified by chromatography (SiO₂, EtOAc *R_f*=0.37) to afford the compound as a white solid (0.76 g, 40 %)⁶.

¹H NMR (300 MHz, CDCl₃): δ(ppm) 10.04 (s, 1H), 8.01 (d, *J*=8.7 Hz, 2H), 7.96 (s, 1H), 7.57(d, *J*=8.7 Hz, 2H), 7.37 (t, *J*=1.4 Hz, 1H), 7.24 (t, *J*=1.1 Hz, 1H).

¹³C NMR (75 MHz, CDCl₃): δ(ppm) 190.6, 141.7, 135.4, 135.0, 131.6, 131.4, 121.1, 117.7

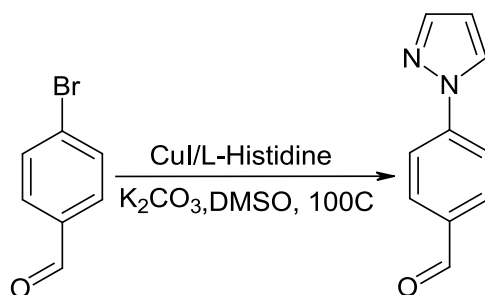
Elemental Analysis: C₁₀H₈N₂O (Mw: 172.19 g/mole)

Calculated: C 69.76 %, N 16.27 %, H 4.68 %,

Found: C 69.72 %, N 16.55 %, H 4.87 %

Compound 23

4-(1H-pyrazol-1-yl)-benzaldehyde



A DMSO solution (60 mL) of CuI (0.5 g, 2.6 mmol) and *L*-histidine (0.34 g, 2.2 mmol) was stirred in a preheated oil bath (100°C) under nitrogen for 30 minutes. Then, 4-bromobenzaldehyde (5 g, 27.70 mmol), pyrazole (2.26 g, 33.2 mmol) and K₂CO₃ (7.65 g, 55.43 mmol) were added. After 36h, the reaction mixture was washed with aqueous K₂CO₃ (1.5 L) and the product was extracted in chloroform (4x500 mL). The organic extracts were dried over mgSO₄ and concentrated. The crude product was purified by flash chromatography (SiO₂, CHCl₃, *R_f* = 0.34) in CHCl₃/pentane (1/1) and then in CHCl₃ to afford the product as a white solid (1.25 g, 26.4 %).

¹H NMR (300 MHz, CDCl₃): δ(ppm) 10.01 (s, 1H), 8.03 (d, *J*=2.6 Hz, 1H), 8.00-7.96 (m, 2H), 7.91-7.87(m, 2H), 7.78 (d, *J*=1.8 Hz, 1H), 6.53 (dd, *J*¹=2.6, *J*²=1.8 Hz, 1H).

¹³C NMR (75 MHz, CDCl₃): δ(ppm) 191.0, 144.3, 142.3, 134.1, 131.3, 127.0, 118.8, 108.9

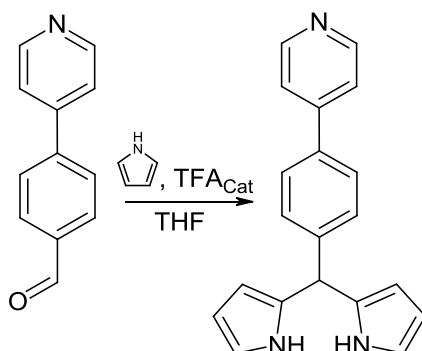
Elemental Analysis: C₁₀H₈N₂O (Mw: 172.19 g/mole)

Calculated: C 69.76 %, N 16.27 %, H 4.68 %.

Found: C 68.95 %, N 16.07 %, H 4.41 %

Compound 26

5-(4-(4-pyridin-1-yl)phenyl)-dipyrromethane

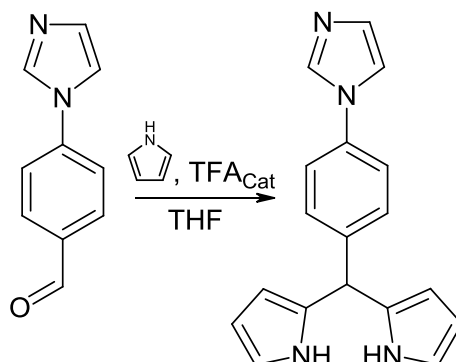


Solid 4-formylphenylpyridine (1 g, 5.458 mmol) was added to degassed pyrrole (20 mL). Few drops of TFA were added and the mixture was heated at 70°C under argon in the absence of light for 24 hours. Pyrrole was then removed under vacuum and the residue was dissolved in EtOAc (100 mL). This solution was washed with 0.1M NaOH (3x50 mL) and water (3x50 mL) and dried over MgSO₄. Purification by column chromatography (Al₂O₃, CH₂Cl₂) afforded the product as a yellow solid (0.896g, 57 %).

¹H NMR (300 MHz, CDCl₃): δ(ppm) 8.61 (dd, *J*¹=1.5 Hz, *J*²=4.4 Hz, 2H), 8.14 (s, 2H), 7.58 (d, *J*= 8.2, 2H), 7.47 (dd, *J*¹=1.5 Hz, *J*²=4.4 Hz, 2H), 7.34 (d, *J*=8.2 Hz, 2H), 6.72 (dd, *J*¹=3.3 Hz, *J*²=3.7 Hz, 2H), 6.17 (dd, *J*¹=3.7 Hz, *J*²=5.7 Hz, 2H), 5.93 (m, 2H), 5.34 (s, 1H).

¹³C NMR (75 MHz, CDCl₃): δ(ppm) 150.1, 147.9, 143.4, 136.7, 132.1, 129.2, 127.2, 121.5, 117.5, 108.5, 107.4, 43.7.

HRMS (ESI), *m/z*: [M + H]⁺ calcd for C₂₀H₁₈N₃: 300.150, found 300.149.

Compound 27**5-(4'-(1H-imidazol-1-yl)phenyl)-dipyrromethane**

Several drops of TFA were added to a solution of 4-(1H-imidazol-1-yl) benzaldehyde (2.5 g, 15.52 mmole) in an excess of degassed pyrrole (40 mL). The mixture was heated at 75°C for 24h under argon and protected from light. Pyrrole was then removed under vacuum and the resulting residue was dissolved in CHCl₃ (300 mL) and washed with 0.1M NaOH (3x150 mL) solution. The organic extracts were dried over mgSO₄ and concentrated. The crude product was purified by flash chromatography (SiO₂, CHCl₃, *R_f*(EtOAc)=0.53). The resulting solid was washed with EtOAc to afford the product as a beige solid (2.63 g, 69.1 %).

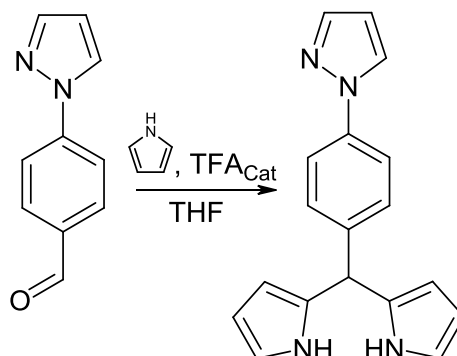
¹H NMR (300 MHz, Acetone-d₆): δ(ppm) 9.81 (s, 1H), 7.97 (s, 1H), 7.53 (dt, *J*¹=2.3 Hz, *J*²=8.7 Hz, 2H), 7.34 (dt, *J*¹=2.3 Hz, *J*²=8.7 Hz, 2H), 7.08(t, *J*=1.1 Hz, 1H), 6.70 (m, 2H), 6.00 (dd, *J*¹=2.8 Hz, *J*²=5.8 Hz, 2H), 5.76(m, 2H), 5.52 (s, 1H).

¹³C NMR (75 MHz, DMSO-d₆): δ(ppm) 143.1, 135.9, 135.5, 133.2, 130.2, 129.8, 120.3, 118.5, 106.6, 43.3.

Elemental Analysis: C₁₈H₁₆N₄ (Mw: **288.35** g/mole)

Calculated: C 74.98 %, N 19.43 %, H 5.59 %.

Found: C 74.32 %, N 19.46 %, H 5.56 %

*Compound 28***5-(4'-(1H-pyrazol-1-yl)phenyl)-dipyrromethane**

Several drops of TFA were added to a solution of 4-(1H-pyrazol-1-yl)benzaldehyde (1.25 g, 6.98 mmol) in an excess of degassed pyrrole (40 mL). The mixture was heated at 75°C for 24h under nitrogen and protected from light. Few drops of Et₃N were added to the mixture and pyrrole was removed under vacuum. The resulting residue was dissolved in CHCl₃ (300 mL) and washed with 0.1M NaOH (3x150mL). The organic extracts were dried over mgSO₄ and concentrated. The crude product was purified by flash chromatography on SiO₂ (CHCl₃) and then on Al₂O₃ (CHCl₃/pentane: 1/1, *R_f*(CHCl₃) = 0.17) to afford a yellow solid (1.61 g, 76.9 %).

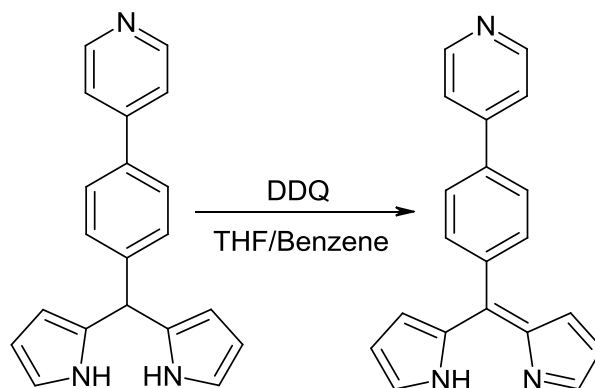
¹H NMR (300 MHz, CDCl₃): δ(ppm) 8.00 (s, 2H), 7.89 (d, *J*=2.4 Hz, 1H), 7.71 (d, *J*=1.6 Hz, 1H), 7.65-7.60 (m, 2H), 7.31-7.27 (m, 2H), 6.72 (dd, *J*¹=4.2, *J*²=2.8 Hz, 2H), 6.46 (t, *J*=2.1 Hz, 1H), 6.17 (dd, *J*¹=6.0 Hz, *J*²=2.6 Hz, 2H), 5.93 (m, 2H), 5.51 (s, 1H)

¹³C NMR (75 MHz, CDCl₃): δ(ppm) 141.1, 140.5, 139.1, 132.2, 129.4, 126.8, 119.5, 117.4, 108.6, 107.6, 107.4, 43.5.

Elemental Analysis: C₁₈H₁₆N₄ (Mw: **288.35** g/mole)

Calculated: C 74.98 %, N 19.43 %, H 5.59 %.

Found: C 74.64 %, N 19.59 %, H 5.45 %

Compound 31**5-(4'-(4-pyridin-1-yl)phenyl)-dipyrrin**

To a THF (75 mL) solution of 5-(4'-(4-pyridin-1-yl)phenyl)dipyrromethane (0.5 g, 1.670 mmol) in an ice bath, DDQ (380 mg, 1.674 mmol) in THF (75 mL) was added dropwise. The solution quickly turned dark. After stirring overnight, the mixture was evaporated to dryness. Purification by column chromatography (Al_2O_3 , CH_2Cl_2) afforded the product as a golden-orange solid (320 mg, 64 %).

$^1\text{H NMR}$ (300 MHz, DMSO-d_6): δ (ppm) 12.65 (s, 1H), 8.69 (dd, $J=4.5$ Hz, $J^2=1.6$ Hz, 2H), 7.97-7.94 (m, 2H), 7.82 (dd, $J^1=4.6$ Hz, $J^2=1.6$ Hz, 2H), 7.78 (t, $J=1.3$, 2H), 7.63-7.61 (m, 2H), 6.54 (dd, $J^1=4.2$, $J^2=1.0$, 2H), 6.45 (dd, $J^1=4.2$, $J^2=1.4$, 2H).

$^1\text{H NMR}$ (300 MHz, Acetone-d_6): δ (ppm) 8.70 (dd, $J^1=4.5$ Hz, $J^2=1.7$ Hz, 2H), 7.95 (dt, $J^1=8.4$ Hz, $J^2=2$ Hz, 2H), 7.78 (dd, $J^1=4.5$ Hz, $J^2=1.6$ Hz, 2H), 7.76 (t, $J=1.3$ Hz, 2H), 7.65 (dt, $J^1=8.4$ Hz, $J^2=2.0$ Hz, 2H), 6.59 (dd, $J^1=4.2$ Hz, $J^2=1.1$ Hz, 2H), 6.43 (dd, $J^1=4.2$ Hz, $J^2=1.4$ Hz, 2H).

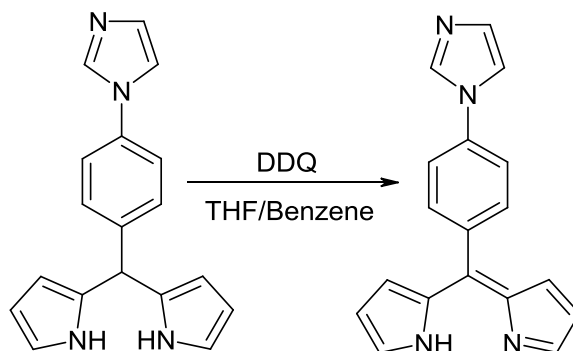
$^{13}\text{C DEPT NMR}$ (75 MHz, DMSO-d_6): δ (ppm) 150.8, 145.2, 131.8, 128.8, 126.8, 121.7, 118.5.

UV-VIS, (CH_2Cl_2) λ_{max} (nm), ϵ ($\text{mol}^{-1} \text{L cm}^{-1}$): 227 (29000), 256 (22000), 319 (15000), 438 (22000), 478 (15000).

Elemental Analysis: $\text{C}_{20}\text{H}_{15}\text{N}_3$ (Mw: **297.35** g/mole)

Calculated: C 80.78 %, N 14.13 %, H 5.08 %.

Found: C 80.44 %, N 13.66 %, H 5.28 %.

Compound 32**5-(4'-(1H-imidazol-1-yl)phenyl)-dipyrrin**

A benzene solution (100mL) of DDQ (2.75 g, 12.09 mmol) was added dropwise over a period of 30 min to a THF solution (300mL) of 5-(4'-(1H-imidazol-1-yl)phenyl)dipyrromethane (2.63 g, 11.52 mmol). TLC analysis indicated complete consumption of the starting material after stirring for 1h. The solvent was removed under vacuum and the resulting residue was dissolved in CHCl₃ (300 mL) and purified by mixing with activated carbon. The CHCl₃ solution was separated by filtration and the crude product was purified by flash chromatography (SiO₂, EtOAc with addition of Et₃N, *R_f*=0.45) to afford the product as a yellow solid (1.6g, 61.4 %).

¹H NMR (300 MHz, Acetone-d₆): δ(ppm) 8.21 (s, 1H), 7.78 (dt, *J*¹=8.52 Hz, *J*²=2.1 Hz, 2H), 7.76(t, *J*=1.4, 2H), 7.71 (t, *J*=1.4, 1H), 7.65 (dt, *J*¹=8.5 Hz, *J*²=2.1 Hz, 2H), 7.17 (t, *J*=1.1 Hz, 1H), 6.60 (dd, *J*¹=4.2, *J*²=1.3 2H), 6.44 (dd, *J*¹=4.2, *J*²=1.3 2H).

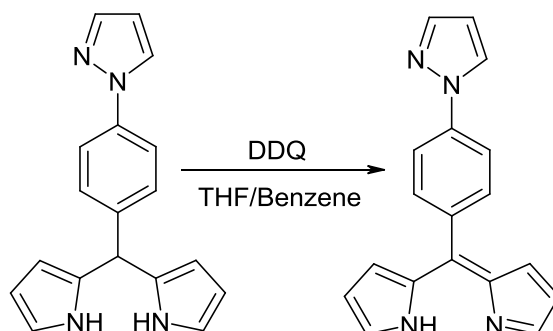
¹³C NMR (75 MHz, CDCl₃): δ(ppm) 144.1, 140.8, 140.1, 137.8, 136.5, 135.5, 132.3, 130.8, 128.5, 121.5, 120.4, 118.1, 118.0, 117.6, 108.5, 107.4.

UV-VIS, (CH₂Cl₂) λ_{max}(nm), ε(mol⁻¹ L cm⁻¹): 228 (30000), 323 (11000), 434 (26000)

Elemental Analysis: C₁₈H₁₄N₄ (Mw: **286.34** g/mole)

Calculated: C 75.51 %, N 19.57 %, H 4.93 %.

Found: C 75.52 %, N 19.86 %, H 5.21 %

Compound 33**5-(4'-(1H-pyrazol-1-yl)phenyl)-dipyrrin**

A benzene solution (100 mL) of DDQ (1.3 g, 5.73 mmol) was added dropwise over a period of 30 min to a THF solution (200 mL) of 5-(4'-(1H-pyrazol-1-yl)phenyl)-dipyrromethane (1.5g, 6.57mmol). TLC analysis indicated complete consumption of the starting material after stirring for 12h. Then, the solvent was removed under vacuum, and the resulting residue was dissolved in CHCl₃ (300mL) and purified by mixing with activated carbon. The organic solution was separated by filtration and the crude product was purified by flash chromatography (SiO₂, CHCl₃/pentane: 1/1 with addition of Et₃N, *R_f*(CHCl₃) = 0.66) to afford a yellow solid (1.2 g, 80.1 %).

¹H NMR (300 MHz, CDCl₃): δ(ppm) 8.01 (d, *J*=2.5 Hz, 2H), 7.82-7.77 (m, 3H), 7.66 (t, *J*=1.2 Hz, 2H), 7.62-7.57 (m, 2H), 6.64 (dd, *J*¹=4.2 Hz, *J*²=1.0 Hz, 2H), 6.52 (t, *J*=2.2 Hz, 1H), 6.42 (dd, *J*¹=4.2 Hz, *J*²=1.5 Hz, 2H)

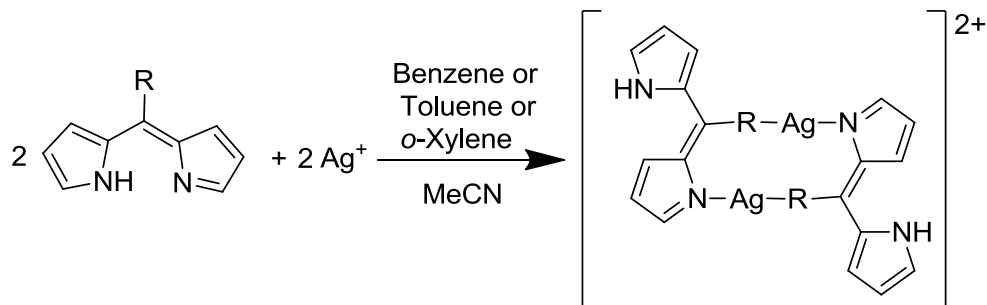
¹³C NMR (75 MHz, CDCl₃): δ(ppm) 143.8, 141.5, 140.8, 140.8, 140.6, 135.4, 132.0, 128.6, 126.8, 118.2, 117.8, 108.1.

UV-VIS, (CH₂Cl₂) λ_{max}(nm), ε(mol⁻¹ L cm⁻¹): 227 (18000), 258 (22000), 338 (12000), 437 (22000), 461 (18000)

HRMS (ESI), *m/z*: (M + H)⁺ calcd for C₁₈H₁₅N₄: 287.129, found 287.126.

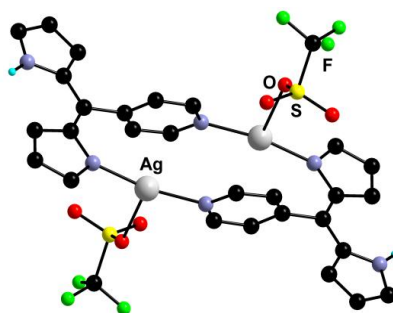
General procedure for the synthesis of compounds 34-40:

A solution of ligand in 3mL of benzene (*o*-xylene) was mixed with a benzene (or Toluene or *o*-Xylene) solution of AgX in 4mL. After 1 min of stirring formation, a red precipitate appeared. CH₃CN (0.5-1.5ml) was added until complete dissolution of the solid. Slow evaporation in the absence of light affords the product as orange-red crystals.



Compound 34

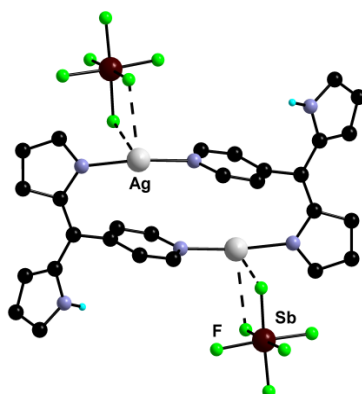
Complex [(5-(4-pyridin-1-yl)-dipyririn)₂Ag₂](OTf)₂(Benzene)₃



From 5-(4-pyridin-1-yl)-dipyririn (20 mg, 0.090 mmol) and AgOTf (23 mg, 0.090 mmol) in benzene. The red crystalline product (22.4 mg, 41.6 %) is insoluble in common organic solvents.

Compound 35

Complex [(5-(4-pyridin-1-yl)-dipyririn)₂Ag₂](SbF₆)₂



From 5-(4-pyridin-1-yl)-dipyririn (20 mg, 0.090 mmol) and AgSbF₆ (31 mg, 0.090 mmol) in *o*-xylene. The product (34.3 mg, 67.2 %) is insoluble in common organic solvents.

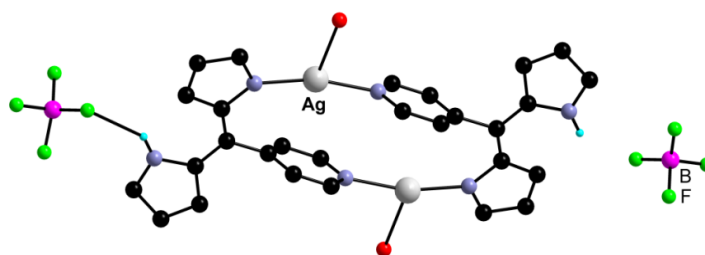
Elemental Analysis: C₂₈H₂₂Ag₂F₁₂N₆Sb₂ (Mw: **1129.76** g/mole)

Calculated: C 29.77 %, N 7.44 %, H 1.96 %.

Calculated: C 29.63 %, N 7.42 %, H 2.29 %.

Compound 36

Complex [(5-(4-pyridin-1-yl)-dipyririn)₂Ag₂](BF₄)₂(H₂O)₂



From 5-(4-pyridin-1-yl)-dipyririn (20 mg, 0.090 mmol) and AgBF₄ (18 mg, 0.090 mmol) in o-xylene. Red crystals (24.0 mg, 61.2 %).

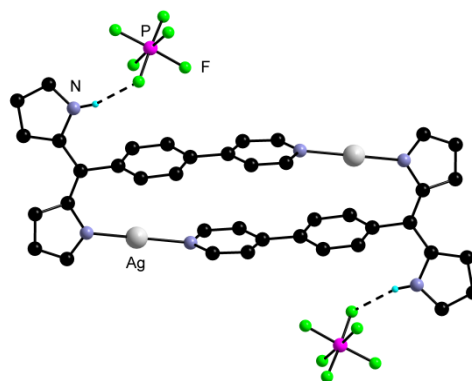
¹H NMR (300 MHz, Acetone-d₆): δ(ppm) 11.19 (s, 1H), 8.78 (dd, J¹=4.6 Hz, J²=1.7 Hz, 2H), 8.32 (s, 1H), 7.95 (dd, J¹=4.9 Hz, J²=1.0 Hz, 1H), 7.91 (dd, J¹=4.6 Hz, J²=1.7 Hz, 2H), 7.65-7.61 (m, 1H), 7.10 (dd, J¹=4.9 Hz, J²=0.7 Hz, 1H), 6.87 (m, J=1.9 Hz, 1H), 6.60 (m, J=1.9 Hz, 1H).

UV-VIS, (Acetone) λ_{max}(nm), ε(mol⁻¹ L cm⁻¹): 431 (39000)

Elemental Analysis: C₂₈H₂₆Ag₂B₂F₈N₆O₂ (Mw: **867.91**g/mole)

Calculated: C 38.75 %, N 9.68 %, H 3.02 %.

Found: C 38.42 %, N 9.79 %, H 3.22 %.

Compound 37**Complex [(5-(4'-(4-pyridin-1-yl)phenyl)-dipyrrin)₂Ag₂](PF₆)₂**

From 5-(4'-(4-pyridin-1-yl)phenyl)-dipyrrin (20 mg, 0.067 mmol) and AgPF₆ (17 mg, 0.067 mmol) in benzene. Red crystals (24.7 mg, 66.7 %).

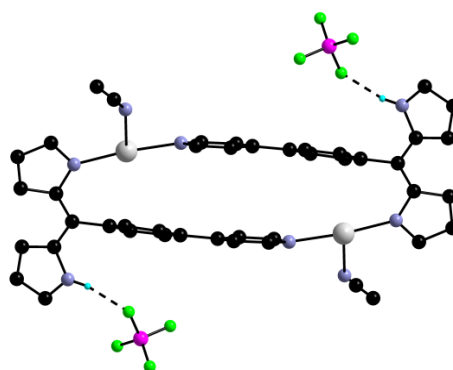
¹H NMR (300 MHz, Acetone-d₆): δ(ppm) 11.22 (s, 1H), 8.42 (dd, J¹=5.0 Hz, J²=1.4 Hz, 2H), 8.26 (s, 1H), 8.14 (d, J=8.3 Hz, 2H), 7.89-7.87 (m, 3H), 7.78 (d, J=8.3 Hz, 2H), 7.64 (m, 1H), 7.07 (d, J=4.7 Hz, 1H), 6.90 (m, 1H), 6.64-6.61 (m, 1H).

UV-VIS, (Acetone) λ_{max}(nm), ε(mol⁻¹ L cm⁻¹): 440 (31000), 511 (15000).

Elemental Analysis: C₄₀H₃₀Ag₂F₁₂N₆P₂ (Mw: **1100.38** g/mole)

Calculated: C 43.66 %, N 7.64 %, H 2.75 %.

Found: C 43.47 %, N 7.45 %, H 3.01 %.

Compound 38**Complex [(5-(4'-(4-pyridin-1-yl)phenyl)-dipyrrin)₂Ag₂](BF₄)₂(CH₃CN)₂**

From 5-(4'-(4-pyridin-1-yl)phenyl)-dipyrrin (20 mg, 0.067 mmol) and AgBF₄ (13 mg, 0.067 mmol) in benzene. Orange crystals (26.5 mg, 73.9 %).

UV-VIS, (Acetone) λ_{max}(nm), ε(mol⁻¹ L cm⁻¹): 442 (36000), 509 (8000).

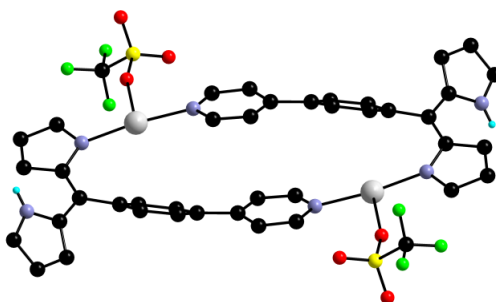
Elemental Analysis: C₄₄H₃₆Ag₂B₂F₈N₈ (Mw: 1066.17 g/mole)

Calculated: C 49.57 %, N 10.51 %, H 3.40 %.

Found: C 49.44 %, N 10.39 %, H 3.54 %.

Compound 39

Complex [(5-(4'-(4-pyridin-1-yl)phenyl)-dipyrrin)₂Ag₂](OTf)₂



From 5-(4'-(4-pyridin-1-yl)phenyl)-dipyrrin (20 mg, 0.067 mmol) and AgOTf (17 mg, 0.067 mmol) in benzene. Red crystals (19.5 mg, 52.3 %)

UV-VIS, (Acetone) λ_{max} (nm), ϵ (mol⁻¹ L cm⁻¹): 445 (37000).

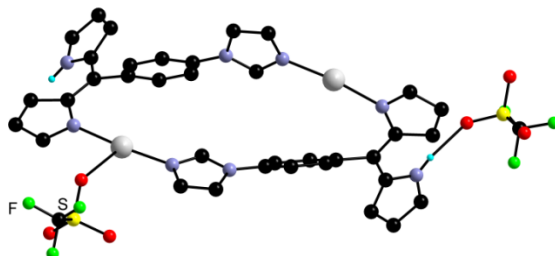
Elemental Analysis: C₄₂H₃₀Ag₂F₆N₆O₆S₂ (Mw: **1108.59** g/mole)

Calculated: C 45.50 %, N 7.58 %, H 2.73 %.

Found: C 45.14 %, N 7.58 %, H 3.05 %

Compound 40

Complex [(5-(4'-(1H-imidazol-1-yl)phenyl)-dipyrrin)₂Ag₂](OTf)₂



From 5-(4'-(1H-imidazol-1-yl)phenyl)-dipyrrin (30 mg, 0.105 mmol) and AgOTf (27 mg, 0.105 mmol) in benzene. Red crystals (43.3 mg, 68.0 %).

¹H NMR (400 MHz, Acetone-d₆): δ (ppm) 11.22 (s, 1H), 8.58 (s, 1H), 8.28 (s, 1H), 7.95 (d, J=8.3 Hz, 2H), 7.87 (t, J=1.5 Hz, 1H), 7.84 (d, J=4.6 Hz, 1H), 7.76 (d, J=8.3 Hz, 2H), 7.63 (s, 1H), 7.14 (s, 1H), 7.04 (d, J=4.7 Hz, 1H), 6.90 (d, J=3.4 Hz, 1H), 6.61 (t, J=3.0 Hz, 1H).

^{13}C NMR (100 MHz, Acetone- d_6): δ (ppm) 160.9, 147.1, 146.2, 137.8, 137.2, 135.7, 134.6, 134.2, 132.0, 131.5, 131.0, 125.0, 125.1, 119.0, 118.0, 114.0.

UV-VIS, (Acetone) λ_{max} (nm), ϵ ($\text{mol}^{-1} \text{L cm}^{-1}$): 453 (51000).

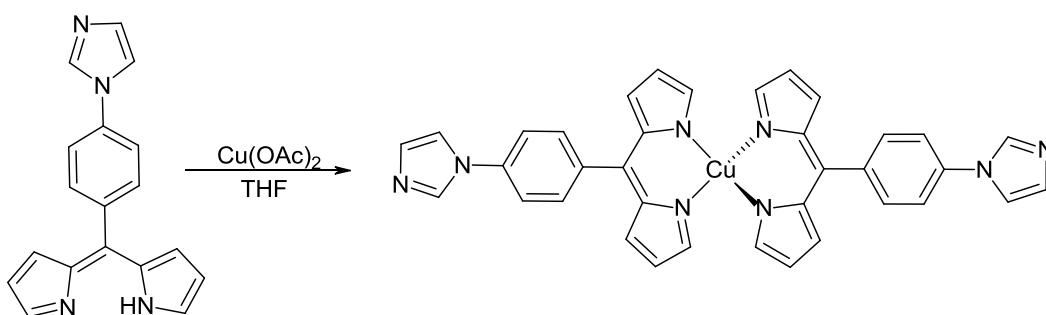
Elemental Analysis: $\text{C}_{38}\text{H}_{26}\text{Ag}_2\text{F}_6\text{N}_8\text{O}_6\text{S}_2$ (Mw: **1084.52** g/mole)

Calculated: C 42.08 %, N 10.33 %, H 2.42 %.

Found: C 41.89 %, N 10.48 %, H 3.03 %.

Compound 41

Complex [Bis(5-(4'-(1H-imidazol-1-yl)phenyl)-dipyrrinato)Cu(II)](CHCl_3) $_{1.5}$



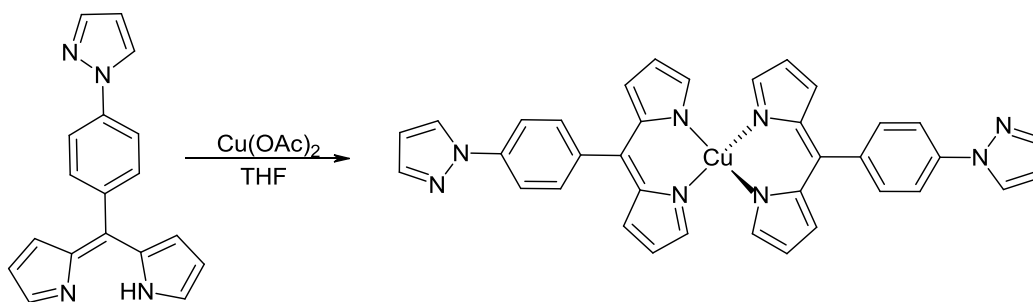
A solution of 5-(4'-(1H-imidazol-1-yl)phenyl)dipyrrin (100 mg, 0.349 mmol) in THF (20 mL) was mixed with a THF solution (30 mL) of $\text{Cu}(\text{OAc})_2$ (31.7 mg, 0.174 mmol). The reaction mixture was stirred for 2h and then solvent was removed under vacuum. The crude product was purified by flash chromatography (SiO_2 , EtOAc, $R_f=0.50$). The resulting solid was washed with *n*-pentane (150 mL) to afford the product as a red solid (104.4 mg, 94.2 %). Green-red crystals were grown by slow diffusion of *n*-pentane into a CHCl_3 solution of the complex.

UV-VIS, (CH_2Cl_2) λ_{max} (nm), ϵ ($\text{mol}^{-1} \text{L cm}^{-1}$): 230 (154000), 342 (61000), 468 (167000), 502 (8400)

Elemental Analysis: $\text{C}_{72}\text{H}_{52}\text{Cu}_2\text{N}_{16} \cdot 3(\text{CHCl}_3)$ (Mw: **1626.55** g/mole)

Calculated: C 55.38 %, N 13.78 %, H 3.41 %.

Found: C 55.59 %, N 14.09 %, H 3.83 %

Compound 42**Complex [Bis(5-(4'-(1H-pyrazol-1-yl)phenyl)dipyrrinato)Cu(II)]**

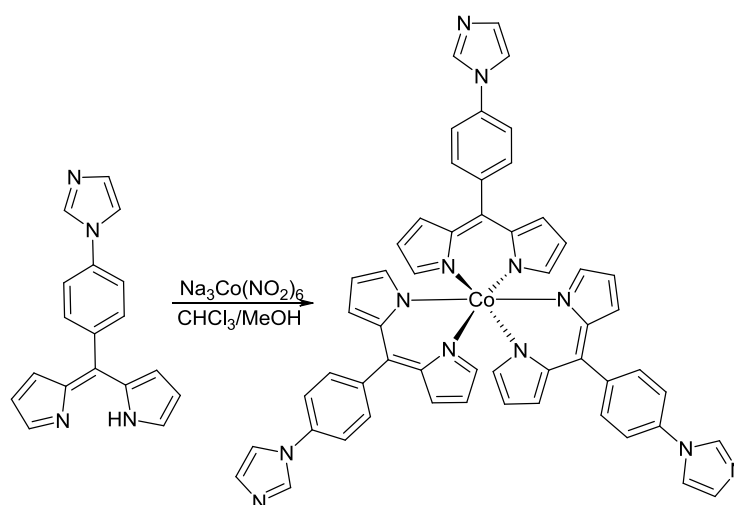
A solution of 5-(4'-(1H-pyrazol-1-yl)phenyl)dipyrrin (100 mg, 0.349 mmol) in THF (20 mL) was mixed with a THF (30mL) solution of $\text{Cu}(\text{OAc})_2$ (31.7 mg, 0.174 mmol). The reaction mixture was stirred for 2h and then, the solvent was removed under vacuum. The crude product was purified by flash chromatography (SiO_2 , CHCl_3 , $R_f=0.59$). The resulting solid was washed with *n*-pentane (150 mL) to afford the product as a green-red solid (103 mg, 93 %). Green-red crystals were grown by slow diffusion of *n*-pentane into a THF solution of the complex.

UV-VIS, (CH_2Cl_2) $\lambda_{\text{max}}(\text{nm})$, $\epsilon(\text{mol}^{-1} \text{ L cm}^{-1})$: 228 (48000), 260 (51000), 350 (34000), 468 (74000), 499 (38000)

Elemental Analysis: $\text{C}_{36}\text{H}_{26}\text{CuN}_8$ (Mw: **634.20** g/mole)

Calculated: C 68.12 %, N 17.67 %, H 4.13 %.

Found: C 68.23 %, N 17.67 %, H 4.27 %.

Compound 43**Complex [Tris(5-(4'-(1H-imidazol-1-yl)phenyl)dipyrrinato)Co(III)]**

A solution of 5-(4'-(1H-imidazol-1-yl)phenyl)dipyrrin (100 mg, 0.349 mmol) and 2 mL of Et_3N in MeOH (20 mL) was stirred for a 5 min and then an aqueous solution (30mL) of $\text{Na}_3\text{Co}(\text{NO}_2)_6$ (47 mg, 0.116 mmol) was added. The reaction mixture was stirred for 24h at 65°C and then the solvent was

removed under vacuum. The crude product was purified by chromatography (SiO_2 , $\text{CHCl}_3/\text{MeOH}:10/1$ $R_f=0.53$). The resulting solid was washed with ether to afford the product as a red solid (61 mg, 57.3 %). Red crystals were grown by slow diffusion of *n*-pentane into a 2-propanol solution of the complex at 5°C.

$^1\text{H NMR}$ (300 MHz, CDCl_3): δ (ppm) 7.95 (s, 1H), 7.58-7.55 (m, 2H), 7.48-7.44 (m, 2H), 7.36 (m, 1H), 7.25 (m, 1H), 6.73 (dd, $J^1=4.4$ Hz, $J^2=1.3$ Hz, 2H), 6.43(t, $J=1.5$ Hz, 2H), 6.36 (dd, $J^1=1.7$, $J^2=4.3$, 2H).

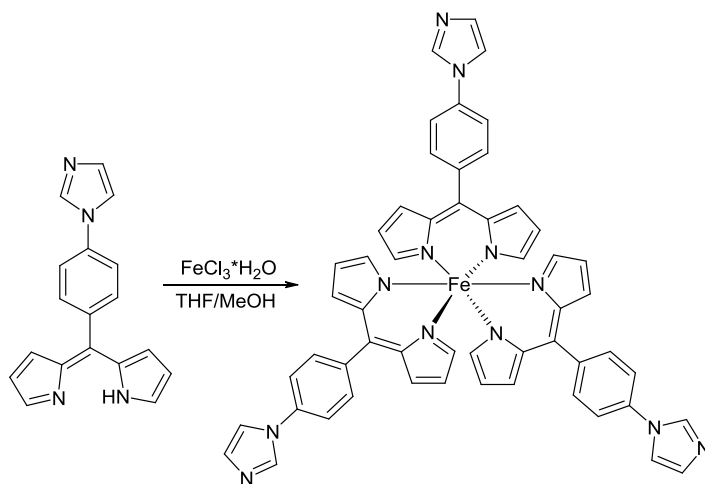
$^{13}\text{C NMR}$ (75 MHz, CDCl_3): δ (ppm) .152.2, 144.6, 137.5, 137.2, 135.6, 135.5, 132.9, 131.9, 130.8, 120.2, 119.1, 118.1.

UV-VIS, (CH_2Cl_2) λ_{max} (nm), ϵ ($\text{mol}^{-1} \text{ L cm}^{-1}$): 229 (86000), 331 (30000), 399 (20000), 491 (46000), 505 (47000)

HRMS (ESI), m/z : $[\text{M} + \text{H}]^+$ calcd for $\text{C}_{54}\text{H}_{40}\text{N}_{12}\text{Co}$: 915.283, found 915.277.

Compound 44

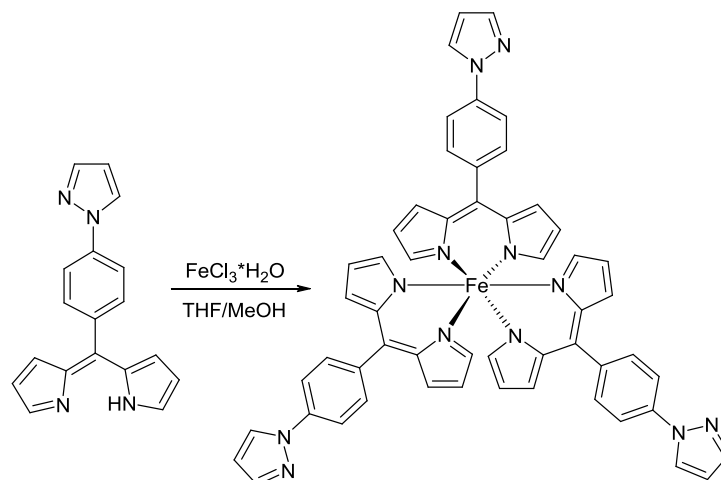
Complex [Tris(5-(4'-(1H-imidazol-1-yl)phenyl)-dipyrrinato)Fe(III)]



A solution of 5-(4'-(1H-imidazol-1-yl)phenyl)-dipyrrin (25 mg, 0.087 mmol) in THF (2 mL) was mixed with a MeOH solution (3 mL) of $\text{FeCl}_3 \cdot \text{H}_2\text{O}$ (7.9 mg, 0.029 mmol) and few drops of Et_3N . The reaction mixture was stirred for 24h at 65°C and then the solvent was removed under vacuum. The crude product was purified by chromatography (SiO_2 , $\text{CHCl}_3/\text{MeOH}:10/1$ $R_f=0.60$). Dark red crystals were grown by slow diffusion of *n*-pentane into an acetone solution of the complex (25.5 mg, 95.7 %).

UV-VIS, (CH_2Cl_2) λ_{max} (nm), ϵ ($\text{mol}^{-1} \text{ L cm}^{-1}$): 227 (61000), 333 (24000), 444 (41000), 494 (31000).

HRMS (ESI), m/z : $[\text{M} + \text{H}]^+$ calcd for $\text{C}_{54}\text{H}_{40}\text{N}_{12}\text{Fe}$: 912.284, found 912.273.

Compound 45**Complex [Tris(5-(4'-(1H-pyrazol-1-yl)phenyl)-dipyrrinato)Fe(III)]**

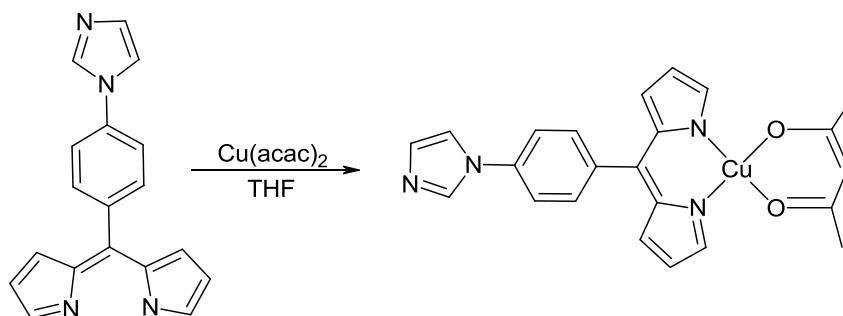
A solution of 5-(4'-(1H-pyrazol-1-yl)phenyl)dipyrrin (25 mg, 0.087mmol) in THF (5 mL) was mixed with a MeOH solution (10mL) of $\text{FeCl}_3 \cdot \text{H}_2\text{O}$ (7.9 mg, 0.029mmol) and few drops of Et_3N . The reaction mixture was stirred for 2h at 75°C and then solvent was removed under vacuum. The crude product was purified by flash chromatography (SiO_2 , CHCl_3 $R_f=0.28$) and reprecipitation from an ether solution by addition of *n*-pentane afforded the product (13.3 mg, 50.0 %). Dark red crystals were grown by slow diffusion of *n*-pentane into a dioxane solution of the complex.

UV-VIS, (CH_2Cl_2) λ_{max} (nm), ϵ ($\text{mol}^{-1} \text{L cm}^{-1}$): 227 (46000), 261 (54000), 347 (24000), 444 (33000), 490 (25000)

Elemental Analysis: $\text{C}_{54}\text{H}_{42}\text{N}_{12}\text{Fe}$ (Mw: **914.84** g/mole)

Calculated: C 70.90 %, N 18.37 %, H 4.63 %,

Found: C 70.66 %, N 18.17 %, H 4.68 %

Compound 46**Complex [((5-(4'-(1H-imidazol-1-yl)phenyl)-dipyrrinato)acac)Cu(II)]**

A solution of 5-(4'-(1H-imidazol-1-yl)phenyl)dipyrrin (25 mg, 0.087 mmol) in THF (8mL) was mixed with THF (8 mL) solution of $\text{Cu}(\text{acac})_2$ (22.9 mg, 0.087 mmol). The reaction mixture was stirred for

20 min. The solvent was then removed under vacuum. The crude product was purified by flash chromatography (SiO_2 , EtOAc, $R_f=0.47$). The resulting solid was washed with *n*-pentane (50 mL) to afford the product as a red solid (25.5 mg, 65 %). Dichroic red-green crystals were grown by slow diffusion of ether into a CHCl_3 solution of the complex.

UV-VIS, (CH_2Cl_2) λ_{max} (nm), ϵ ($\text{mol}^{-1} \text{ L cm}^{-1}$): 229 (34000), 297 (15000), 329 (11000), 479 (25000), 493 (32000)

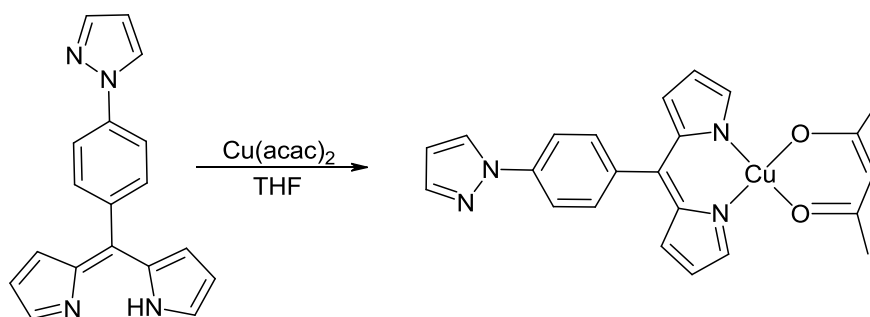
Elemental Analysis: $\text{C}_{23}\text{H}_{20}\text{N}_4\text{O}_2\text{Cu}$ (Mw: **447.99** g/mole)

Calculated: C 61.67 %, N 12.51 %, H 4.50 %.

Found: C 61.19 %, N 12.16 %, H 4.51 %

Compound 47

Complex [((5-(4'-(1H-imidazol-1-yl)phenyl)-dipyrinato)acac)Cu(II)]



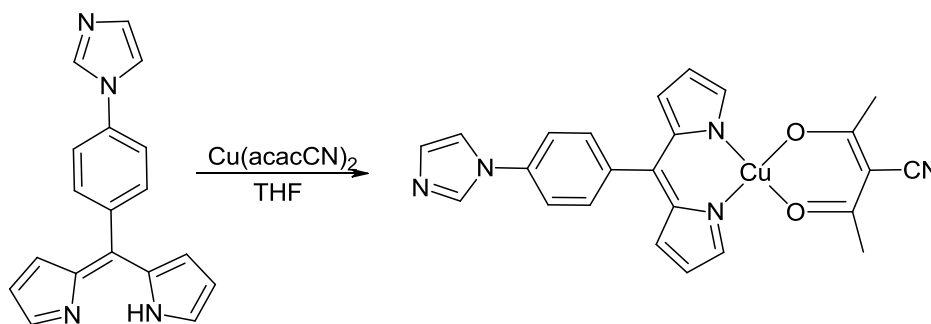
A THF (8 mL) solution of 5-(4'-(1H-imidazol-1-yl)phenyl)dipyrin (25 mg, 0.087 mmol) was mixed with a THF (8 mL) solution of $\text{Cu}(\text{acac})_2$ (22.9 mg, 0.087 mmol). The reaction mixture was stirred for 20 min and then was evaporated to dryness under vacuum. The crude product was purified by chromatography (SiO_2 , CHCl_3 , $R_f = 0.44$). The resulting solid was washed with *n*-pentane (50 mL) to afford the product as a red solid (27.3 mg, 69.5 %). Dichroic red-green crystals were grown by slow evaporation of a CHCl_3 solution of the complex.

UV-VIS, (CH_2Cl_2) λ_{max} (nm), ϵ ($\text{mol}^{-1} \text{ L cm}^{-1}$): 227 (33000), 294 (24000), 342 (15000), 482 (32000), 493 (39000)

Elemental Analysis: $\text{C}_{23}\text{H}_{20}\text{N}_4\text{O}_2\text{Cu}$ (Mw: **447.99** g/mole)

Calculated: C 61.67 %, N 12.51 %, H 4.50 %.

Found: C 61.62 %, N 12.67 %, H 4.82 %.

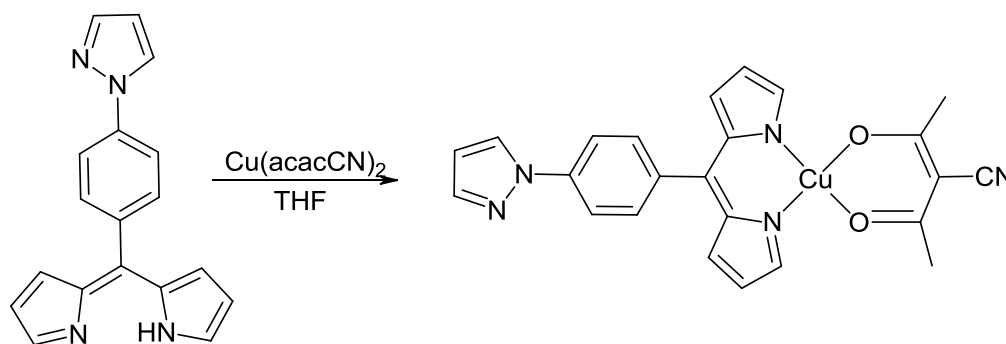
Compound 48**Complex [(5-(4'-(1H-imidazol-1-yl)-phenyl)-dipyrinato)acacnitrillo]Cu(II)]**

A THF (30 mL) solution of 5-(4'-(1H-imidazol-1-yl)phenyl)-dipyrin (100 mg, 0.349 mmol) was added to a THF (20 mL) solution of $\text{Cu}(\text{acacCN})_2$ (109 mg, 0.349 mmol). After stirring for 20 min, the resulting precipitate was filtered off and washed with ether (3x75mL) to afford the product as a green-red solid (136 mg, 82.4 %). Dichroic red-green crystals were grown by slow evaporation of a CHCl_3 solution.

UV-VIS, (CH_2Cl_2) $\lambda_{\text{max}}(\text{nm})$, $\epsilon(\text{mol}^{-1} \text{ L cm}^{-1})$: 227 (28000), 288 (12000), 333 (9000), 479 (21000), 491 (27000)

IR: ν 2206 (CN) cm^{-1} .

HRMS (ESI), m/z : $[\text{M} + \text{H}]^+$ calcd for $\text{C}_{24}\text{H}_{20}\text{N}_5\text{O}_2\text{Cu}$: 473.091, found 473.091.

Compound 49**Complex [(5-(4'-(1H-pyrazol-1-yl)-phenyl)-dipyrinato)acacnitrillo]Cu(II)]**

A THF solution (20 mL) of 5-(4'-(1H-pyrazol-1-yl)phenyl)dipyrin (55 mg, 0.19 mmol) was mixed with a THF solution (30 mL) of $\text{Cu}(\text{acacCN})_2$ (60 mg, 0.19 mmol). The reaction mixture was stirred for 20 min, before removal of the solvent under vacuum. The crude product was purified by flash chromatography (SiO_2 , CHCl_3 , $R_f = 0.42$). The resulting solid was washed with *n*-pentane (150 mL) to afford the product as dichroic red-green crystals (53 mg, 58.1 %). Green-red single crystals were grown either by slow diffusion of *n*-pentane into a dioxane solution of the complex or by slow diffusion of *n*-pentane into a CHCl_3 solution of the complex.

UV-VIS, (CH_2Cl_2) $\lambda_{\text{max}}(\text{nm})$, $\epsilon(\text{mol}^{-1} \text{ L cm}^{-1})$: 229 (69000), 263 (30000), 349 (12000), 478 (23000), 489 (27000).

IR: ν 2197 (CN) cm^{-1} .

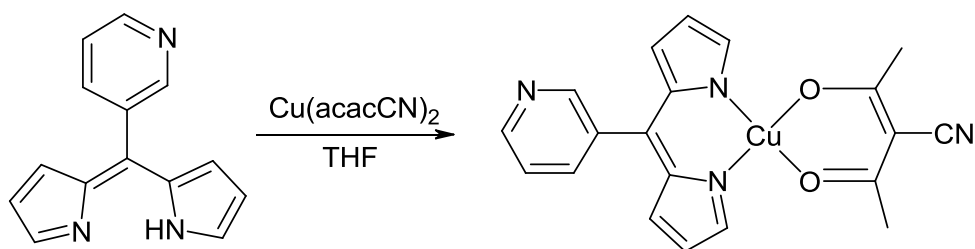
Elemental Analysis: $\text{C}_{24}\text{H}_{19}\text{N}_5\text{CuO}_2 \cdot (\text{DiOX})$ (Mw: **561.10** g/mole)

Calculated: C 59.94 %, N 12.48 %, H 4.85 %.

Found: C 60.12 %, N 12.73 %, H 5.01 %

Compound 50

Complex [(5-(pyridin-3-yl)dipyrrinato)acacnitrillo]Cu(II)



A THF solution (30 mL) of 5-(pyridin-3-yl)dipyrrin (100 mg, 0.45 mmol) was added to a THF solution (20 mL) of $\text{Cu}(\text{acacCN})_2(\text{H}_2\text{O})$ (150 mg, 0.45 mmol). The solution turned immediately red and was stirred for one hour. It was evaporated to dryness and the residue was purified by column chromatography (SiO_2 , $\text{CHCl}_3/\text{EtOAc}$: 90/10) to afford the product as a dichroic red-green solid (178 mg, 96 %).

UV-VIS, (CH_2Cl_2) λ_{max} (nm), ϵ ($\text{mol}^{-1} \text{ L cm}^{-1}$): 229 (14000), 296 (14000), 342 (5000), 474 (23000), 491 (36000)

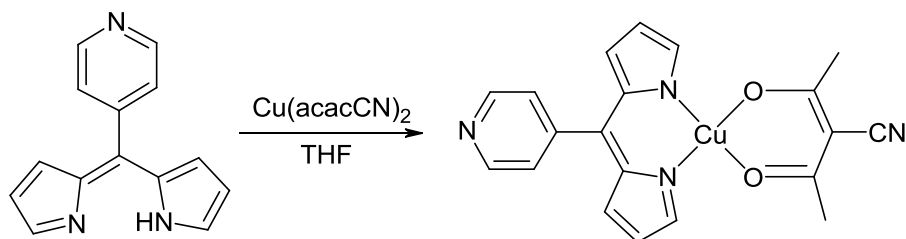
HRMS (ESI), m/z : $[\text{M}+\text{H}]^+$ calc. for $\text{C}_{20}\text{H}_{17}\text{CuN}_4\text{O}_2$: 408.064, found 408.064.

IR: ν 2206 (CN) cm^{-1} .

Elemental Analysis: $\text{C}_{20}\text{H}_{16}\text{CuN}_4\text{O}_2$ (Mw: **407.91** g/mole)

Calculated: C 58.89 %, N 13.73 %, H 3.95 %.

Found: C 58.39 %, N 13.71 %, H 4.26 %

Compound 51**Complex [((5-(pyridin-4-yl)dipyrrinato)acacnitrillo)Cu(II)]**

A THF solution (10 mL) of 5-(pyridin-4-yl)dipyrrin (30 mg, 0.13 mmol) was added to a THF solution (10 mL) of $\text{Cu}(\text{acacCN})_2(\text{H}_2\text{O})$ (44 mg, 0.13 mmol). The solution turned immediately red and was stirred for 30 minutes. It was evaporated to dryness and the residue was purified by column chromatography (SiO_2 , $\text{CH}_2\text{Cl}_2/\text{MeOH}$: 99/1) to afford the product as a dichroic red-green solid (53 mg, 96 %).

UV-VIS, (CH_2Cl_2) $\lambda_{\text{max}}(\text{nm})$, $\epsilon(\text{mol}^{-1} \text{L cm}^{-1})$: 228 (27000), 293 (16000), 357 (5000), 468 (18000), 492 (36000).

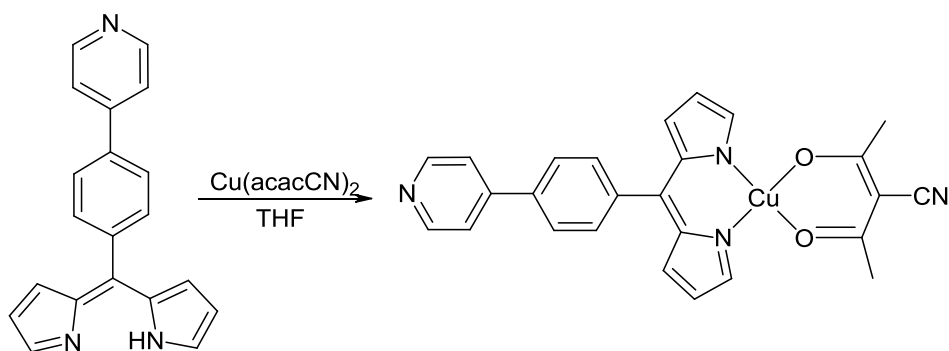
HRMS (ESI), m/z : $[\text{M}+\text{H}]^+$ calcd. for $\text{C}_{20}\text{H}_{17}\text{CuN}_4\text{O}_2$: 408.064, found 408.059.

Elemental Analysis: $\text{C}_{20}\text{H}_{16}\text{CuN}_4\text{O}_2$ (Mw: **407.91** g/mole)

Calculated: C 58.89 %, H 3.95 %, N 13.73 %.

Found: C 58.53 %, H 4.12 %, N 13.86 %.

IR: ν 2203 (CN) cm^{-1} .

Compound 52**Complex [((5-(4'-(pyridin-4-yl)-phenyl)dipyrrinato)acacnitrillo)Cu(II)]**

A THF solution (10 mL) of 5-(4'-(pyridin-4-yl)-phenyl)dipyrrin (50 mg, 0.17 mmol) was added to a THF solution (10 mL) of $\text{Cu}(\text{acacCN})_2(\text{H}_2\text{O})$ (55 mg, 0.17 mmol). The solution turned immediately red and was stirred for 45 minutes. It was evaporated to dryness and the residue was purified by column chromatography (SiO_2 , $\text{CH}_2\text{Cl}_2/\text{MeOH}$: 99/1) to afford the product as a dichroic red-green solid (66 mg, 81 %).

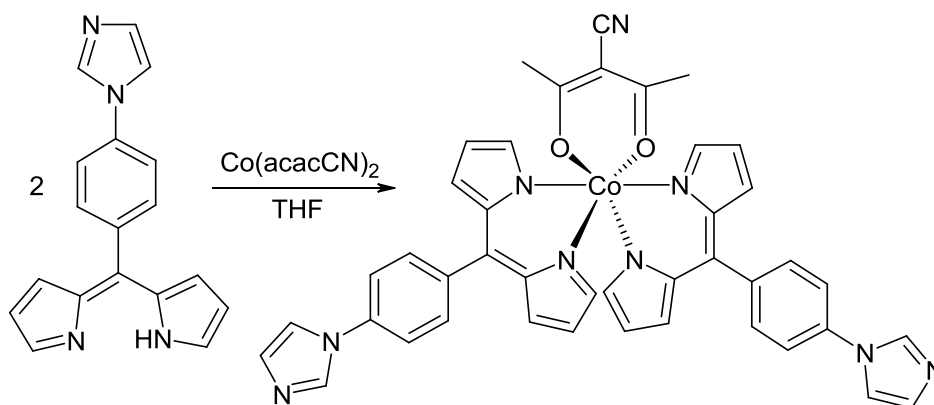
UV-VIS, (CH₂Cl₂) λ_{max}(nm), ε(mol⁻¹ L cm⁻¹): 227 (27000), 266 (23000), 282 (23000), 318 (14000), 469 (18000), 490 (34000).

HRMS (ESI), *m/z*: [M+H]⁺ calcd. for C₂₆H₂₁CuN₄O₂: 484.094, found 484.100.

IR: ν 2200 (CN) cm⁻¹.

Compound 53

Complex [(bis(5-(4'-(1H-imidazol-1-yl)phenyl)dipyrinato)acacnitrillo)Co(III)](DiOX)



A solution of 5-(4'-(1H-imidazol-1-yl)phenyl)dipyrin (100 mg, 0.349 mmol) in THF (30 mL) was mixed with a MeOH (30 mL) solution of Co(acacCN)₃ (53.6 mg, 0.174 mmol) and 0.5 mL of Et₃N. The reaction mixture was stirred for 5h and then, the solvent was removed under vacuum. The crude product was purified by flash chromatography on deactivated SiO₂ by addition of Et₃N to the eluent CHCl₃/MeOH: 10/1. The resulting solid was washed with ether to afford the product as a red solid (42 mg, 32.0 %). Red crystals were grown by slow diffusion of *n*-pentane into a dioxane solution of the complex.

¹H NMR (300 MHz, CD₂Cl₂): δ(ppm) 7.97 (t, *J*=1.1 Hz, 2H), 7.69-7.65 (m, 4H), 7.57-7.54 (m, 4H), 7.45-7.43 (m, 4H), 7.22 (t, *J*=1.1 Hz, 2H), 7.01 (dd, *J*¹=4.3 Hz, *J*²=1.4 Hz, 2H), 6.75 (dd, *J*¹=4.5 Hz, *J*²=1.4 Hz, 2H), 6.68 (t, *J*=1.6, 2H), 6.66 (dd, *J*¹=4.4 Hz, *J*²=1.6 Hz, 2H), 6.28 (dd, *J*¹=4.5 Hz, *J*²=1.6 Hz, 2H), 2.30 (s, 6H).

¹³C NMR (75 MHz, CD₂Cl₂): δ(ppm) 193.6, 170.8, 154.4, 150.5, 145.1, 137.9, 136.3, 135.7, 135.5, 135.4, 133.6, 133.3, 131.9, 130.5, 120.3, 119.4, 118.9, 118.1, 88.7, 27.6.

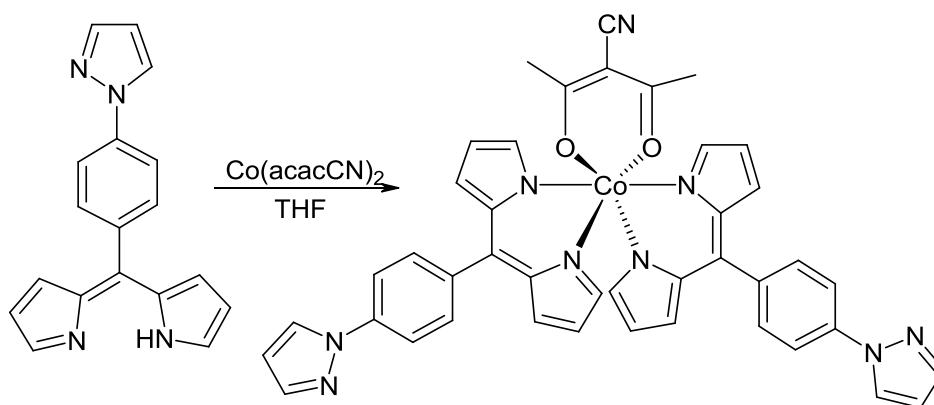
UV-VIS, (CH₂Cl₂) λ_{max}(nm), ε(mol⁻¹ L cm⁻¹): 228 (66000), 334 (20000), 481 (40000)

IR: ν (CN) cm⁻¹. 2208 (CN).

Elemental Analysis: C₄₂H₃₂CoN₉O₂•(DiOX) (Mw: **841.80** g/mole)

Calculated: C 65.63 %, N 14.97 %, H 4.79 %.

Found: C 65.55 %, N 14.68 %, H 5.14 %.

Compound 54**Complex [(bis(5-(4'-(1H-pyrazol-1-yl)phenyl)dipyrrinato)acacnitrilo)Co(III)](THF)**

A solution of 5-(4'-(1H-pyrazol-1-yl)phenyl)-dipyrrin (100 mg, 0.349 mmol) in THF (20 mL) was mixed with a MeOH solution (30 mL) of $\text{Co}(\text{acacCN})_3$ (53.6 mg, 0.174 mmol). The reaction mixture was stirred for 20 min and then, the solvent was removed under vacuum. The crude product was purified by flash chromatography (SiO_2 , CHCl_3 /pentane:1/1, $R_f(\text{CHCl}_3)=0.48$). The resulting solid was washed with Et_2O to afford the product as a red solid (104 mg, 78.7 %). Red crystals were grown by slow diffusion of *n*-pentane into a THF solution of the complex.

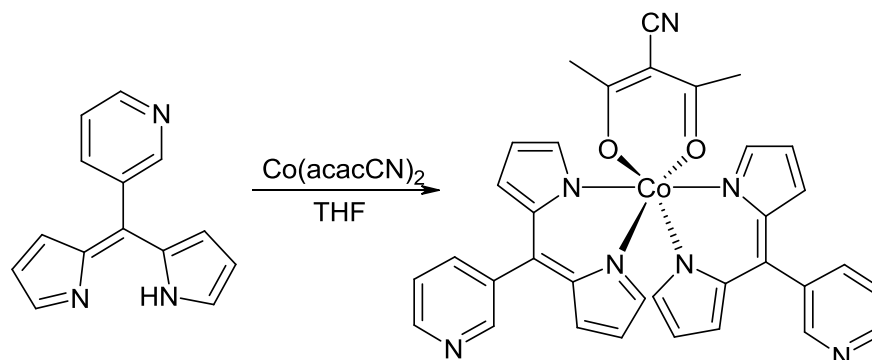
$^1\text{H NMR}$ (300 MHz, CDCl_3): δ (ppm) 8.05 (d, $J=2.4$ Hz, 2H), 7.85-7.82 (m, 4H), 7.80(d, $J=1.9$ Hz, 2H), 7.67-7.64 (m, 4H), 7.40 (t, $J=1.5$ Hz, 2H), 7.01 (dd, $J^1=4.3$ Hz, $J^2=1.4$ Hz, 2H), 6.77(dd, $J^1=4.5$ Hz, $J^2=1.4$ Hz, 2H), 6.71 (t, $J=1.4$, 2H), 6.62 (dd, $J^1=4.4$ Hz, $J^2=1.7$ Hz, 2H), 6.55 (t, $J=2.2$ Hz, 2H), 6.27 (dd, $J^1=4.4$ Hz, $J^2=1.7$ Hz, 2H), 2.28 (s, 6H).

$^{13}\text{C NMR}$ (75 MHz, CDCl_3): δ (ppm) 193.5, 155.0, 149.9, 145.4, 142.5, 141.6, 140.6, 135.7, 135.5, 134.0, 133.9, 132.9, 131.7, 126.8, 119.1, 119.0, 118.1, 108.1, 88.4, 27.7

UV-VIS, (CH_2Cl_2) λ_{max} (nm), ϵ ($\text{mol}^{-1} \text{L cm}^{-1}$): 228 (71000), 258 (63000), 349 (28000), 480 (48000)

IR: ν 2206 (CN) cm^{-1} .

HRMS (ESI), m/z : ($\text{M} + \text{H}$) $^+$ calcd for $\text{C}_{42}\text{H}_{33}\text{N}_9\text{CoO}_2$: 754.208, found 754.198.

Compound 55**Complex [(bis(5-pyridin-3-yl-dipyrrinato)acacnitrilo)Co(III)]**

A CHCl_3 solution (30 mL) of 5-pyridin-3-yl-dipyrrin (100 mg, 0.45 mmol) was added to a MeOH solution (20 mL) of $\text{Co}(\text{acacCN})_2$ (66 mg, 0.21 mmol) was added. The solution turned immediately red and was stirred overnight. After evaporation to dryness, the red solid residue was purified by column chromatography (SiO_2 , $\text{CHCl}_3/\text{MeOH}$: 99/1) to afford the product as a dichroic red-green solid (80 mg, 59 %).

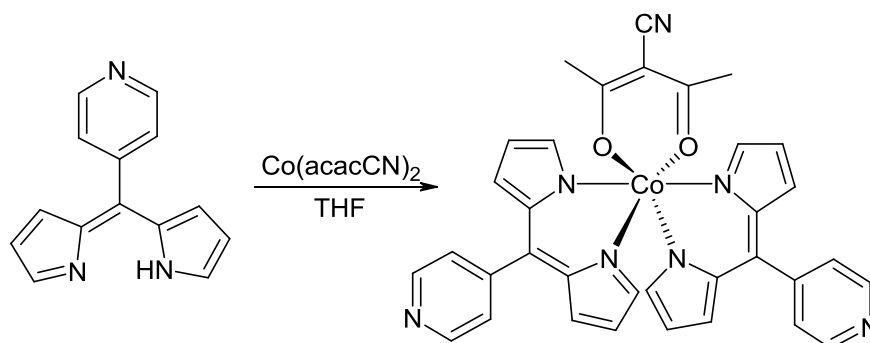
$^1\text{H NMR}$ (300 MHz, CDCl_3): δ (ppm) 8.82 (m, 4H), 7.87 (d, $J=7.6$ Hz, 2H), 7.48 (dd, $J^1=7.5$ Hz, $J^2=4.5$ Hz, 2H), 7.41 (t, $J=1.4$ Hz, 2H), 6.90 (dd, $J^1=4.3$ Hz, $J^2=1.2$ Hz, 2H), 6.71 (t, $J=1.5$, 2H), 6.67 (dd, $J^1=4.3$ Hz, $J^2=1.4$ Hz, 2H), 6.62 (dd, $J^1=4.3$ Hz, $J^2=1.5$ Hz, 2H), 6.28 (dd, $J^1=4.5$ Hz, $J^2=1.5$ Hz, 2H), 2.28 (s, 6H).

$^{13}\text{C NMR}$ (75 MHz, CDCl_3): δ (ppm) 193.6, 155.5, 150.4, 150.3, 150.1, 142.4, 142.3, 137.6, 135.8, 135.7, 133.8, 133.5, 132.8, 122.7, 120.0, 119.5, 88.5, 27.7

UV-VIS, (CH_2Cl_2) λ_{max} (nm), ϵ ($\text{mol}^{-1} \text{L cm}^{-1}$): 227 (36000), 311 (13000), 395 (8000), 483 (33000).

HRMS (ESI), m/z : $[\text{M}+\text{H}]^+$ calcd. for $\text{C}_{34}\text{H}_{27}\text{CoN}_7\text{O}_2$: 624.155, found 624.157.

IR: ν 2207 (CN) cm^{-1} .

Compound 56**Complex [(bis(5-(pyridin-4-yl)phenyl) dipyrrinato)acacnitrilo]Co(III)]**

A CHCl_3 solution (20 mL) of 5-pyridin-4-yl-dipyrin (80 mg, 0.36 mmol) was added to a MeOH solution (20 mL) of $\text{Co}(\text{acacCN})_2$ (55 mg, 0.18 mmol) was added. The solution turned immediately red and was stirred overnight. After evaporation to dryness, the red solid residue was purified by column chromatography (SiO_2 , $\text{CHCl}_3/\text{MeOH}$: 99/1) to afford the product as a dichroic red-green solid (60 mg, 54 %).

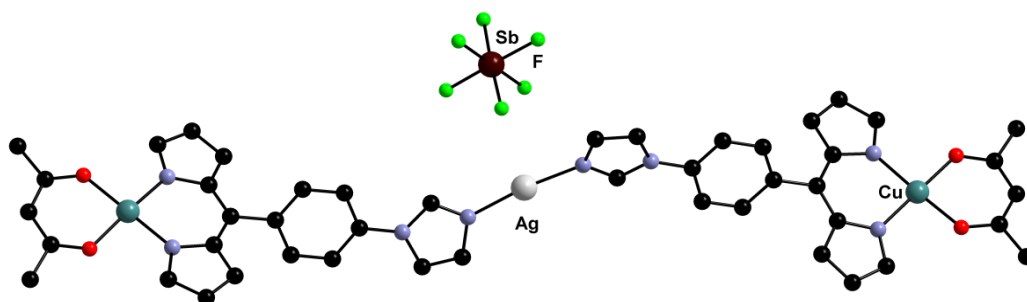
$^1\text{H NMR}$ (300 MHz, CDCl_3): δ (ppm) 8.77 (d, $J=5.5$ Hz, 4H), 7.46 (d, $J=5.8$ Hz, 4H), 7.39 (t, $J=1.3$ Hz, 2H), 6.88 (dd, $J^1=4.6$ Hz, $J^2=1.4$ Hz, 2H), 6.68 (t, $J=1.4$ Hz, 2H), 6.65 (dd, $J^1=4.3$ Hz, $J^2=1.6$ Hz, 2H), 6.61 (dd, $J^1=4.2$ Hz, $J^2=1.7$ Hz, 2H), 6.27 (dd, $J^1=4.2$ Hz, $J^2=1.5$ Hz, 2H), 2.28 (s, 6H).

$^{13}\text{C NMR}$ (75 MHz, CDCl_3): δ (ppm) 193.6, 155.6, 150.5, 149.3, 145.3, 142.3, 134.8, 134.7, 133.7, 132.7, 125.0, 119.9, 119.6, 119.5, 88.5, 27.7

UV-VIS, (CH_2Cl_2) λ_{max} (nm), ϵ ($\text{mol}^{-1} \text{L cm}^{-1}$): 233 (78000), 302 (17000), 393 (10000), 485 (41000).

HRMS (ESI), m/z : $[\text{M}+\text{H}]^+$ calcd. for $\text{C}_{34}\text{H}_{27}\text{CoN}_7\text{O}_2$: 624.155, found 624.157.

IR: ν 2209 (CN) cm^{-1} .

Compound 57**Heterometallic complex:** $[(Ag((acac)Cu(Im-Ph-DPM))_2)(SbF_6)](C_6H_6)_2$ 

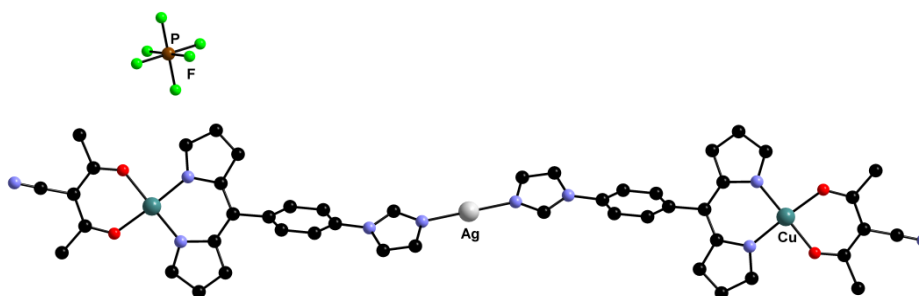
A solution of $[(acac)Cu(Im-Ph-Dpm)]$ complex (34.5 mg, 0.076 mmol) in THF (20 mL) was slowly diffused into a benzene solution (15 mL) of $AgSbF_6$ (13.3 mg, 0.038 mmol) in a tube (16x1cm) protected from light. After two weeks, dichroic green-orange crystals were grown (39 mg, 73.0 %).

UV-VIS, (THF) $\lambda_{max}(nm)$, $\epsilon(mol^{-1} L cm^{-1})$: 237 (65000), 301 (40000), 475 (57000), 494 (98000).

Elemental Analysis: $C_{58}H_{52}AgCu_2F_6N_8O_4Sb$ (Mw: **1395.80** g/mole)

Calculated: C 49.91 %, N 8.03 %, H 3.75 %.

Found: C 48.94 %, N 7.70 %, H 3.78 %

Compound 58**Heterobimetallic network:** $\{[(Ag((acacCN)Cu(Im-Ph-DPM))_2)](PF_6)\}_\infty$ (THF)

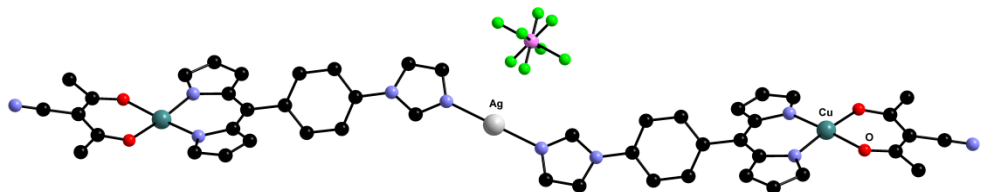
In a vial ($\varnothing 22.00 \times 65 \times 1$ mm) protected from light, a solution of the $[(acacCN)Cu(Im-Ph-Dpm)]$ complex (10 mg, 0.021 mmol) in THF (10 mL) was slowly diffused into an EtOH solution (5 mL) of $AgPF_6$ (2.7 mg, 0.0106 mmol). After two weeks, dichroic green-orange crystals were obtained (7.7 mg, 51.2 %) and analyzed by X-ray diffraction on single crystal.

IR: ν 2196 (CN) cm^{-1} .

Elemental Analysis: $C_{52}H_{46}AgCu_2F_6N_{10}O_5P$ (Mw: **1270.92** g/mole)

Calculated: C 49.14 %, N 11.02 %, H 3.65 %.

Found: C 48.87 %, N 11.35 %, H 3.91 %.

Compound 59**Heterobimetallic network: $\{[(Ag((acacCN)Cu(Im-Ph-DPM))_2)](BF_4)\}_\infty(\text{Benzene})$** 

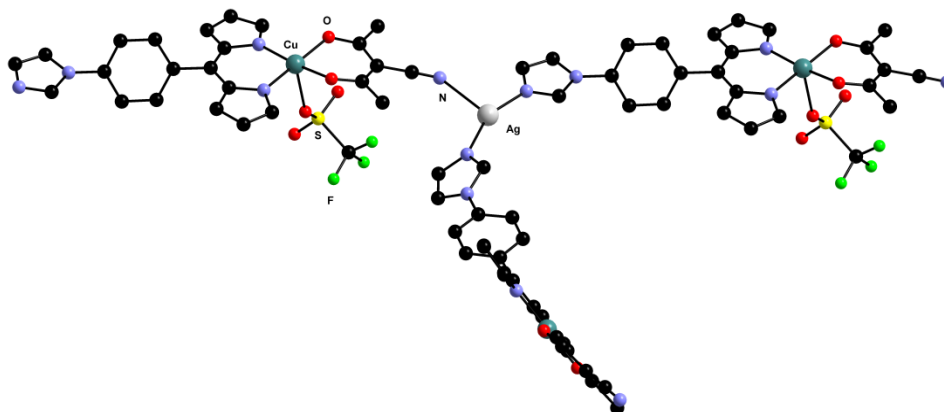
In a crystallization tube ($\varnothing 22.00 \times 65 \times 1 \text{ mm}$) protected from light, a solution of the $[(acacCN)Cu(Im-Ph-Dpm)]$ complex (10 mg, 0.021 mmol) in $CHCl_3$ (7 mL) was slowly diffused into a benzene solution (7 mL) of $AgBF_4$ (2.1 mg, 0.0106 mmol). After two weeks, dichroic green-orange crystals were obtained (7.2 mg, 55.9 %) and analyzed by X-ray diffraction on single crystal.

IR: ν 2194 (CN) cm^{-1} .

Elemental Analysis: $C_{54}H_{44}AgBCu_2F_4N_{10}O_4$ (Mw: **1218.78 g/mole**)

Calculated: C 53.22 %, N 11.49 %, H 3.64 %.

Found: C 52.28 %, N 11.62 %, H 3.88 %.

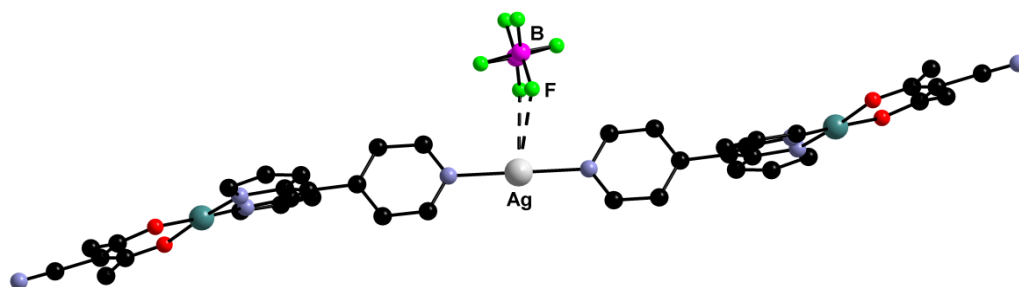
Compound 60:**Heterobimetallic network: $\{[(Ag((acacCN)Cu(Im-Ph-DPM))_2)](OTf)\}_\infty(o\text{-xylene})$** 

A solution of $[(acacCN)Cu(Im-Ph-Dpm)]$ (9 mg, 0.019 mmol) in *o*-xylene (4 mL) was mixed with an *o*-xylene (2 mL) solution of $AgOTf$ (4.8 mg, 0.0095 mmol) and stirred for 1 min. A red precipitate appeared which was dissolved upon addition of CH_3CN (2.5 mL). Slow evaporation of CH_3CN in the absence of light afforded the product as dark-green crystals (7.8 mg, 62.7 %).

IR: ν 2251 (CN) cm^{-1} .

Compound 61:

Heterobimetallic network: $\{[(Ag((acacCN)Cu(4-Py-DPM))_2)](BF_4)\}_\infty$



To a solution of $[(acacCN)Cu(4-Py-Dpm)]$ (15 mg, 0.037mmol) in *o*-xylene (5 mL), a solution of $AgBF_4$ (7.14 mg, 0.037mmol) in *o*-xylene (2mL) was added, causing the immediate precipitation of a red solid. MeCN was added until complete redissolution. The mixture was left for slow evaporation in the absence of light. Crystals appeared after few days (11.0 mg, 59 %).

IR: ν 2212 (CN) cm^{-1} .

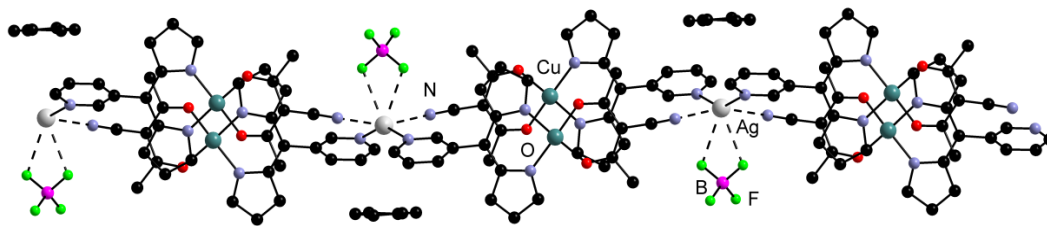
Elemental Analysis: $C_{40}H_{32}AgBCu_2F_4N_8O_4$ (Mw: 1010.50g/mole)

Calculated: C 47.54 %, N 11.09 %, H 3.19 %.

Found: C 47.66 %, N 11.18 %, H 3.50 %.

Compound 62:

Heterobimetallic network: $\{[(Ag((acacCN)Cu(3-Py-DPM))_2)](BF_4)\}_\infty(Benzene)$



To a solution of $[(acacCN)Cu(3-Py-Dpm)]$ complex (15 mg, 0.037 mmol) in benzene (5 mL), a solution of $AgBF_4$ (7.14 mg, 0.037 mmol) in benzene (or *o*-xylene for 62b) (2 mL) was added, causing the immediate precipitation of a red solid. MeCN was added until complete redissolution. The mixture was left for slow evaporation in the absence of light. Crystals appeared after few days (4.5 mg, 24 %).

IR: ν 2213 (CN) cm^{-1} .

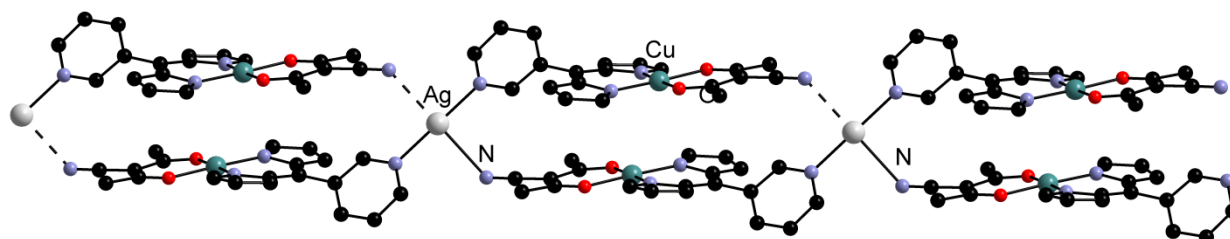
Elemental Analysis: $C_{40}H_{32}AgBCu_2F_4N_8O_4$ (Mw: 1650.48g/mole)

Calculated: C 47.54 %, N 11.09 %, H 3.19 %.

Found: C 47.48 %, N 11.42 %, H 3.53 %.

Compound 63:

Heterobimetallic network: $\{[(Ag((acacCN)Cu(3-Py-DPM))_2)](OTf)\}_\infty$



To a solution of $[(acacCN)Cu(3-Py-Dpm)]$ (15 mg, 0.037 mmol) in *o*-xylene (5 mL), a solution of AgOTf (9.42 mg, 0.037 mmol) in *o*-xylene (2 mL) was added, causing the immediate precipitation of a red solid. MeCN was added until complete redissolution. The mixture was left for slow evaporation in the absence of light. Crystals appeared after few days (8.1 mg, 41 %).

IR: ν 2204 (CN) cm^{-1} .

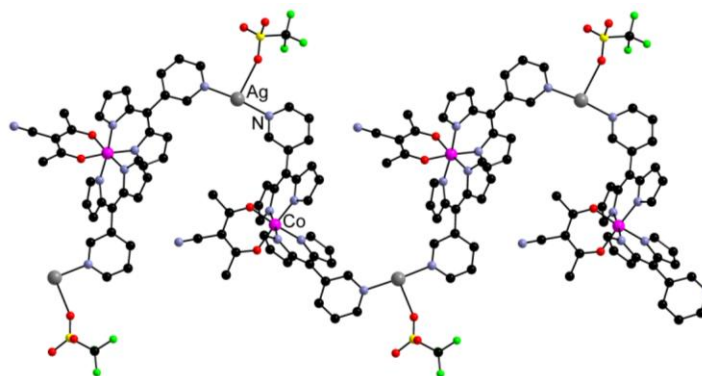
Elemental Analysis: $C_{41}H_{32}AgCu_2F_3N_8O_7S$ (Mw: **1072.77** g/mole)

Calculated: C 45.90 %, N 10.44 %, H 3.00 %.

Found: C 45.07 %, N 8.66 %, H 3.46 %.

Compound 64:

Heterobimetallic network: $\{[(Ag((acacCN)Co(3-Py-DPM))_2)_2](OTf)\}_\infty(CH_3CN)$



To a solution of $[(acacCN)Co(3-Py-Dpm)_2]$ (15 mg, 0.024 mmol) in *o*-xylene (5 mL), a solution of AgOTf (5.9 mg, 0.024 mmol) in *o*-xylene (2 mL) was added, causing the immediate precipitation of a red solid. MeCN was added until complete redissolution. The mixture was left for slow evaporation in the absence of light. Crystals appeared after few days (10.3 mg, 46 %).

IR: ν 2212 (CN) cm^{-1} .

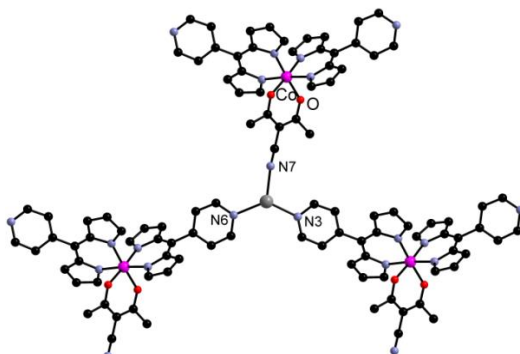
Elemental Analysis: $C_{35}H_{26}AgCoF_3N_7O_5S \cdot (CH_3CN)$ (Mw: **921.54** g/mole)

Calculated: C 48.22 %, H 3.17 %, N 12.16 %.

Found: C 47.98 %, H 3.48 %, N 11.82 %.

Compound 65:

Heterobimetallic network: $\{[(\text{Ag}((\text{acacCN})\text{Co}(4\text{-Py-DPM}))_2)]_2(\text{BF}_4)\}_\infty(\text{Benzene})_{0.5}(\text{CH}_3\text{CN})_3$



To a solution of $[(\text{acacCN})\text{Co}(4\text{-Py-Dpm})_2]$ (15 mg, 0.024 mmol) in benzene (5 mL), a solution of AgBF_4 (4.5 mg, 0.024 mmol) in benzene (2 mL) was added, causing the immediate precipitation of a red solid. MeCN was added until complete redissolution. The mixture was left for slow evaporation in the absence of light. Crystals appeared after few days (13.3 mg, 56 %).

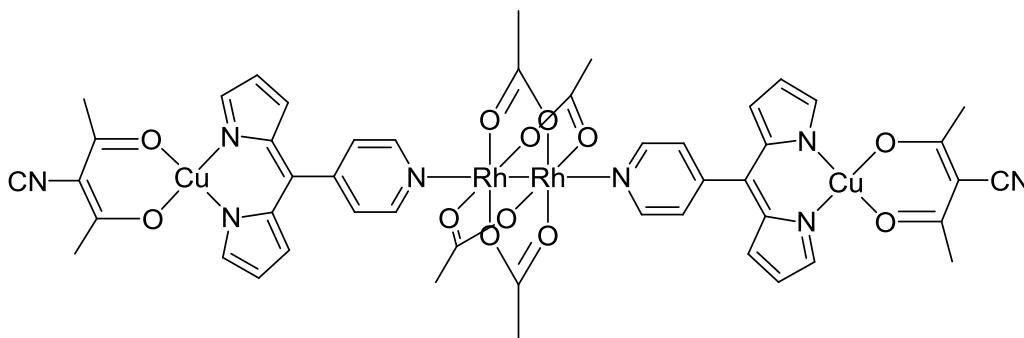
Elemental Analysis: $\text{C}_{43}\text{H}_{38}\text{AgBCoF}_4\text{N}_{10}\text{O}_2$ (Mw: 980.44 g/mole)

Calculated: C 52.67 %, N 14.28 %, H 3.91 %.

Found: C 50.65 %, N 13.07 %, H 3.78 %.

Compound 66

Heterobimetallic complex: $[\text{Rh}_2(\text{OAc})_4((4\text{-Py-Dpm})\text{Cu}(\text{acacCN}))_2] \cdot 8(\text{DiOX})$



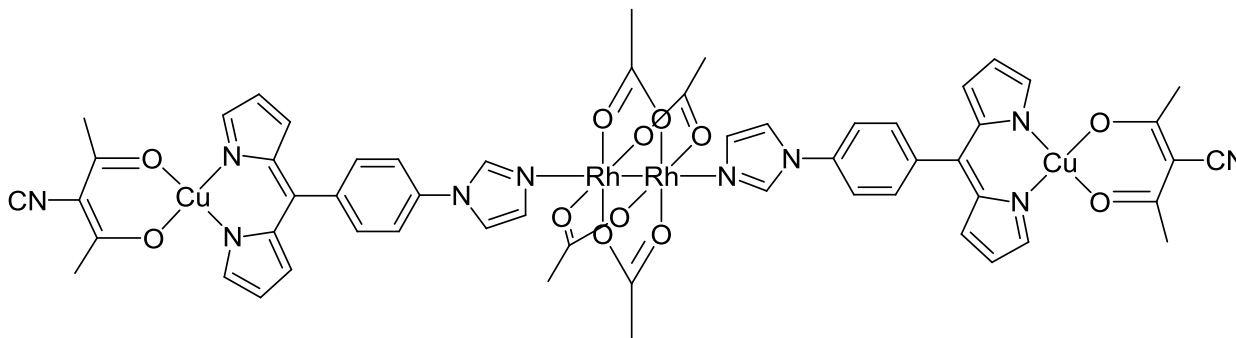
A solution of $[(\text{acacCN})\text{Cu}(4\text{-Py-Dpm})]$ (6.5 mg, 0.016 mmol) in DiOX (5 mL) was mixed with a DiOX solution (5 mL) of $\text{Rh}_2(\text{OAc})_4$ (3.5 mg, 0.008 mmol). The mixture was stirred for 15 minutes and then concentrated to 2 mL. Red crystals were grown by slow diffusion of *n*-pentane into a DiOX solution of the complex (6.5 mg, 41 %).

UV-VIS, (CH_2Cl_2) λ_{max} (nm), ϵ ($\text{mol}^{-1} \text{L cm}^{-1}$): 229 (48000), 296 (29000), 494 (57000)

IR: ν 2207 (CN), 1406(COO^-), 1605 (COO^-). cm^{-1} .

Compound 67

Heterobimetallic complex: $[\text{Rh}_2(\text{OAc})_4((\text{Im-Ph-Dpm})\text{Cu}(\text{acacCN}))_2](\text{CHCl}_3)_3$



A solution of $[(\text{acacCN})\text{Cu}(\text{Im-Ph-Dpm})]$ (15 mg, 0.032 mmol) in THF (5 mL) was mixed with a THF solution (5 mL) of $\text{Rh}_2(\text{OAc})_4$ (7 mg, 0.016 mmol). The mixture was stirred for 15 minutes and then the solvent was removed under vacuum. The resulting solid was dissolved in CHCl_3 . Green-red crystals were grown by slow diffusion of *n*-pentane into a CHCl_3 solution of the complex (15.3 mg, 70 %).

UV-VIS, (CH_2Cl_2) λ_{max} (nm), ϵ ($\text{mol}^{-1} \text{ L cm}^{-1}$): 241 (65000), 278 (38000), 319 (22000), 480 (55000), 491 (71000)

IR: ν 2208 (CN), 1406(COO^-), 1590 (COO^-). cm^{-1} .

Elemental Analysis: $\text{Rh}_2\text{Cu}_2\text{N}_{10}\text{C}_{56}\text{H}_{46}\text{O}_{12} \cdot 3(\text{CHCl}_3)$ (Mw: **1861.45** g/mole)

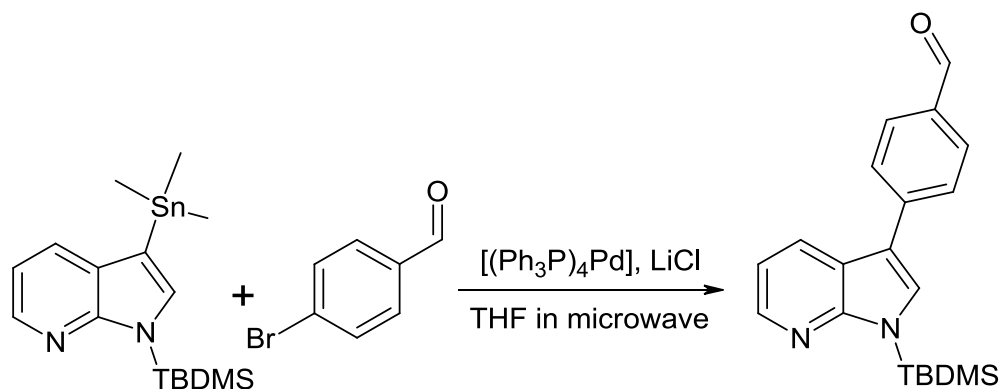
Calculated: C 40.68 %, N 8.04 %, 2.83 %

Found: C 40.41 %, N 7.56 %, 3.31 %

VI.4. Compounds reported in Chapter 3

Compound 68

1-*tert*-Butyldimethylsilyl-3-(4-benzaldehyd-1-yl)-7-azaindole



A solution of 1-*tert*-butyldimethylsilyl-3-trimethylstannyl-7-azaindole (2 g, 5.061 mmol), *p*bromobenzaldehyde (1.87 g, 10.107 mmol), LiCl (0.64g, 15.098mmol) and $(\text{Ph}_3\text{P})_4\text{Pd}$ (0.2g) in dry THF (30 mL) was refluxed for 12h under microwave conditions (60W, 70°C) under argon. The mixture was diluted with Et_2O and the precipitate was filtered off. The filtrate was concentrated under vacuum. The crude product was purified by chromatography (SiO_2 , CHCl_3 /pentane: 1/20) to afford the product as a white solid (0.290 mg, 17.0 %).

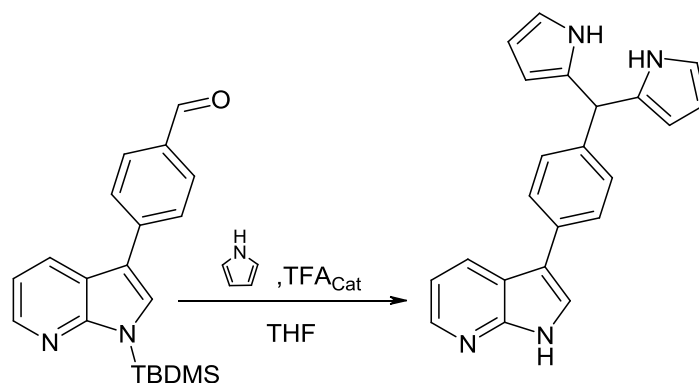
$^1\text{H NMR}$ (300 MHz, CDCl_3): δ (ppm) 10.02 (s, 1H), 8.35 (dd, $J^1=4.6$ Hz, $J^2=1.7$ Hz, 1H), 8.20 (dd, $J^1=8.0$ Hz, $J^2=1.7$ Hz, 1H), 7.97-7.80(m, 4H), 7.56 (s, 1H), 7.15 (dd, $J^1=8.0$ Hz, $J^2=4.6$ Hz, 1H), 0.98 (s, 9H), 0.69 (s, 6H).

$^{13}\text{C NMR}$ (75 MHz, CDCl_3): δ (ppm) 191.7, 154.8, 143.3, 141.8, 134.1, 130.5, 129.6, 127.3, 126.9, 120.1, 117.0, 116.8, 26.6, 19.0, (-4.2).

Elemental Analysis: $\text{C}_{20}\text{H}_{24}\text{N}_2\text{OSi}$ (Mw: **336.51** g/mole)

Calculated: C 71.39 %, H 7.19 %, N 8.32 %

Found: C 71.40 %, H 7.20 %, N 8.47 %

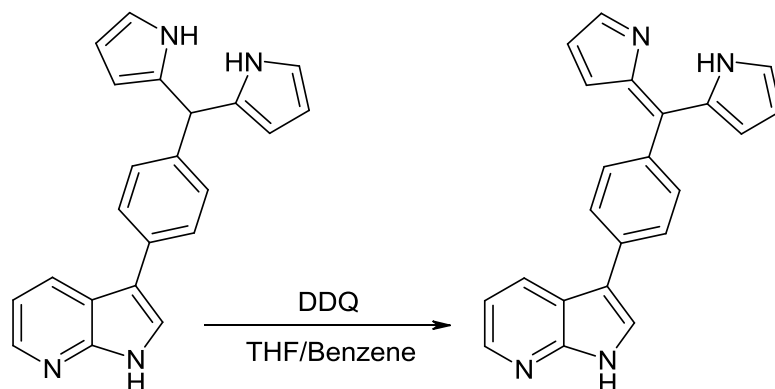
Compound 69**5-(4-(7-azaindol-3-yl)phenyl)-dipyrromethane**

Several drops of TFA were added to a solution of 1-*tert*-Butyldimethylsilyl-3-(4-benzaldehyd-1-yl)-7-azaindole (280 mg, 0.832mmole) in an excess of degassed pyrrole (40 mL). The mixture was stirred at RT for 24h under nitrogen and protected from light. Few drops of Et₃N were added to the mixture and pyrrole was removed under vacuum. The resulting residue was dissolved in chloroform and washed with 0.1M NaOH solution. The organic extracts were dried over magnesium sulfate and concentrated. The crude product was purified by chromatography on SiO₂ (CHCl₃/EtOAc: 1/1, *R_f*=0.74) to afford the product as a white solid (250 mg, 88.8 %). Colorless crystals were grown by slow diffusion of *n*-pentane into a dioxane solution of the complex.

¹H NMR (300 MHz, DMSO): δ(ppm) 11.86 (s, 1H), 10.58 (s, 2H), 8.27 (s, 1H), 8.26-8.24 (m, 1H), 7.80 (d, *J*=2.6 Hz, 1H), 7.65-7.60 (m, 2H), 7.25-7.20 (m, 2H), 7.15-7.11 (m, 1H), 6.63 (dd, *J*¹=4.2 Hz, *J*²=2.6 Hz, 2H), 5.59 (dd, *J*¹=5.3 Hz, *J*²=2.5 Hz, 2H), 5.72 (dd, *J*¹=4.2 Hz, *J*²=3.1 Hz, 2H), 5.38 (s, 1H).

¹³C NMR (75 MHz, DMSO): δ(ppm) 149.0, 142.8, 141.3, 133.2, 132.9, 128.6, 127.5, 126.0, 123.4, 117.3, 116.8, 116.0, 114.2, 106.8, 106.0, 43.2.

HRMS (ESI), *m/z*: [M + H]⁺ calcd for C₂₂H₁₉N₄: 339.160, found 339.157.

*Compound 70***5-(4-(7-azaindol-3-yl)phenyl)-dipyrrin**

A benzene solution (50 mL) of DDQ (0.25 g, 1.10 mmol) was added to a THF solution (100 mL) of 5-(4-(7-azaindol-3-yl)phenyl)-dipyrromethane (0.25 g, 0.73 mmol) dropwise over a period of 30 min. TLC analysis indicated complete consumption of the starting material after stirring for 12h. Then solvent was removed under vacuum and the resulting residue was purified by chromatography (SiO₂, CHCl₃/EtOAc: 1/1 with addition of Et₃N, *R_f*(EtOAc)=0.74) and washed with ether to afford the product as a yellow solid (0.23 g, 92.5 %).

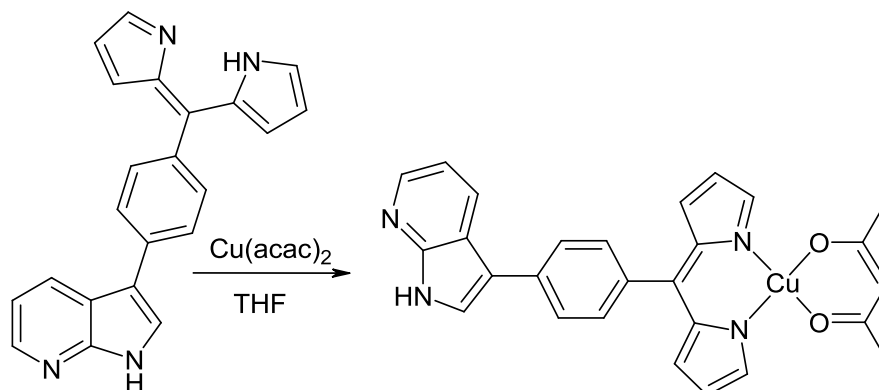
¹H NMR (300 MHz, CDCl₃): δ(ppm) 8.41 (dd, *J*¹=4.8 Hz, *J*²=1.5 Hz, 1H), 8.34 (dd, *J*¹=8.0 Hz, *J*²=1.5 Hz, 1H), 7.77-7.74 (m, 2H), 7.74 (t, *J*=1.3 Hz, 2H), 7.66 (s, 1H), 7.62-7.58 (m, 2H), 7.23 (dd, *J*¹=8.0 Hz, *J*²=4.8 Hz, 1H), 6.76 (dd, *J*¹=4.2 Hz, *J*²=1.1 Hz, 2H), 6.46 (dd, *J*¹=4.2 Hz, *J*²=1.5 Hz, 2H)

¹H NMR (300 MHz, DMSO): δ(ppm) 12.72 (s, 1H), 12.04 (s, 1H), 8.41 (dd, *J*¹=8.0 Hz, *J*²=1.3 Hz, 1H), 8.31 (dd, *J*¹=4.7 Hz, *J*²=1.3 Hz, 1H), 8.04 (d, *J*=2.5 Hz, 1H), 7.89 (d, *J*=8.2 Hz, 2H), 7.78-7.77 (m, 2H), 7.56 (d, *J*=8.2 Hz, 2H), 7.20 (dd, *J*¹=8.0 Hz, *J*²=4.7 Hz, 1H), 6.63 (dd, *J*¹=4.1 Hz, *J*²=0.9 Hz, 2H), 6.46 (dd, *J*¹=4.1 Hz, *J*²=1.3 Hz, 2H).

¹³C NMR (75 MHz, DMSO): δ(ppm) 149.6, 144.7, 143.5, 142.1, 140.3, 136.6, 134.4, 131.8, 128.9, 128.1, 125.8, 125.0, 118.2, 117.6, 116.7, 114.0.

UV-VIS, (CH₂Cl₂) λ_{max}(nm), ε(mol⁻¹ L cm⁻¹): 228 (33000), 267 (22000), 395 (18000), 437 (28000).

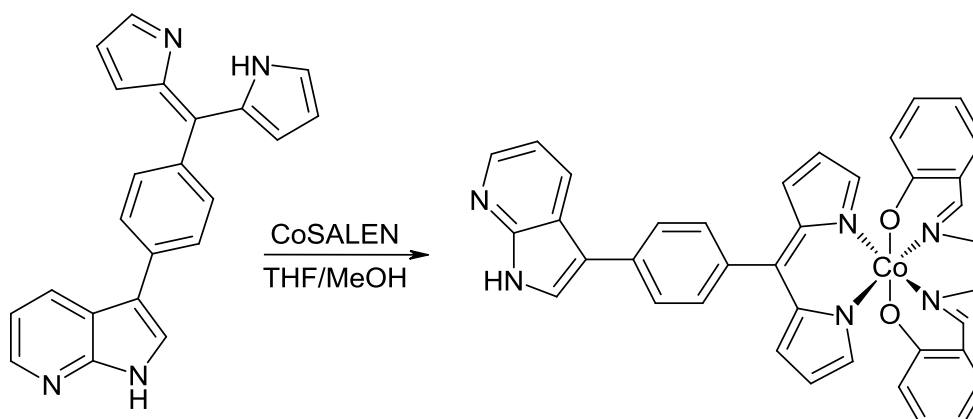
HRMS (ESI), *m/z*: [M + H]⁺ calcd for C₂₂H₁₇N₄: 337.145, found 337.141.

Compound 71**Complex [(5-(4-(7-azaindol-3-yl)phenyl)-dipyrriino)acac]Cu(II)]**

A THF solution (10 mL) of 5-(4-(7-azaindol-3-yl)phenyl)-dipyrriin (20 mg, 0.059 mmol) was added to a THF solution (10 mL) of $\text{Cu}(\text{acac})_2$ (15.5 mg, 0.059 mmol). The mixture turned red and was stirred at RT for 45 min. The solvent was removed under vacuum and the residue was purified by chromatography (SiO_2 , $\text{CH}_2\text{Cl}_2/\text{MeOH}$: 99/1) to afford the product as a red solid (22 mg, 74 %). Two types of green crystals were obtained by slow vapour diffusion of pentane into a solution of the complex.

UV-VIS, (CH_2Cl_2) λ_{max} (nm), ϵ ($\text{mol}^{-1} \text{ L cm}^{-1}$): 229 (68000), 270 (41000), 369 (16000), 475 (32000), 492 (44000).

HRMS (ESI), m/z : $[\text{M} + \text{H}]^+$ calcd for $\text{C}_{27}\text{H}_{23}\text{CuN}_4\text{O}_2$: 498.111, found 498.104

Compound 72**Complex [Salen-(5-(4-(7-azaindol-3-yl)phenyl)-dipyrriino)Co(III)]**

A solution of 5-(4-(7-azaindol-3-yl)phenyl)-dipyrriin (20 mg, 0.059 mmol) in THF (5 mL) was mixed with MeOH solution (7mL) of $\text{Co}(\text{salen})\cdot(\text{H}_2\text{O})$ (19.34 mg, 0.059mmol). The mixture was stirred for 2h at RT and then solvent was removed under vacuum. The resulting solid was purified by chromatography (SiO_2 , EtOAc , $R_f=0.51$) to afford the product as a red solid (21 mg, 53.5 %). Dark-red crystals were grown by slow diffusion of ether in to a DIOX solution of complex.

^1H NMR (300 MHz, CDCl_3): δ (ppm) 9.81 (s, 1H), 8.40 (dd, $J^1=4.6$ Hz, $J^2=1.1$ Hz, 1H), 8.30 (dd, $J^1=8.1$ Hz, $J^2=1.4$ Hz, 1H), 8.21 (s, 1H), 7.90 (t, $J=1.3$ Hz, 1H), 7.68 (d, $J=8.0$ Hz, 2H), 7.54-7.49 (m, 3H), 7.35-7.32 (m, 1H), 7.29 (dd, $J^1=4.1$ Hz, $J^2=1.0$ Hz, 2H), 7.22-7.20 (m, 1H), 7.18 (d, $J=1.4$ Hz, 2H), 7.09-6.98 (m, 2H), 6.91-6.87 (m, 2H), 6.81 (dd, $J^1=4.5$ Hz, $J^2=1.4$ Hz, 1H), 6.59 (m, $J=3.9$ Hz, 1H), 6.43-6.38 (m, 1H), 6.31 (dd, $J^1=4.1$ Hz, $J^2=1.7$ Hz, 1H), 6.20 (dd, $J^1=4.4$ Hz, $J^2=1.5$ Hz, 1H), 3.97 (dd, $J^1=13.3$ Hz, $J^2=6.3$ Hz, 1H), 3.80 (td, $J^1=11.9$ Hz, $J^2=6.4$ Hz, 1H), 3.17 (dd, $J^1=10.3$ Hz, $J^2=5.9$ Hz, 1H), 2.65 (td, $J^1=10.7$ Hz, $J^2=6.7$ Hz, 1H).

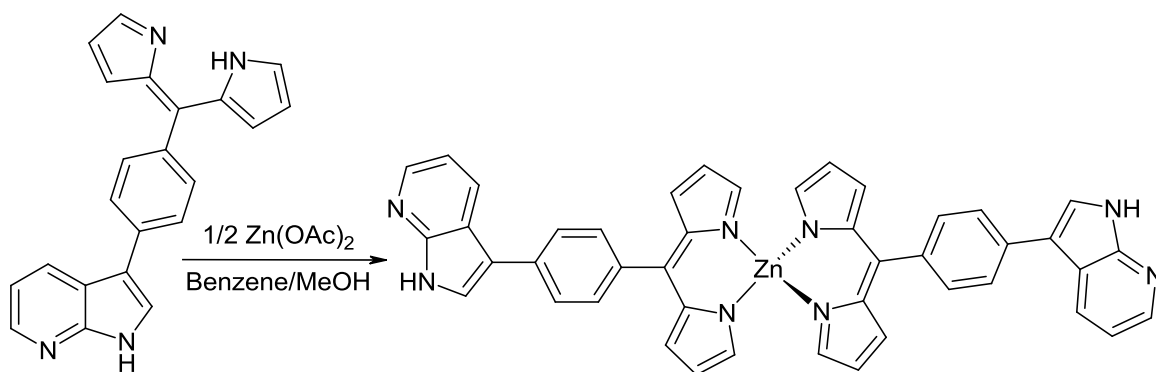
^{13}C NMR (75 MHz, CDCl_3): δ (ppm) 168.0, 166.9, 165.9, 163.8, 159.2, 152.4, 143.5, 139.1, 137.0, 135.6, 135.3, 134.9, 134.6, 134.00, 133.97, 131.9, 131., 131.2, 128.9, 128.3, 126.1, 125.9, 124.6, 124.4, 123.7, 122.4, 119.1, 118.3, 118.2, 116.8, 116.6, 115.9, 114.9, 114.0, 60.7, 60.4

UV-VIS, (CH_2Cl_2) λ_{max} (nm), ϵ (mol^{-1} L cm^{-1}): 229 (63000), 257 (52000), 369 (12000), 487 (12000), 507 (12000).

HRMS (ESI), m/z : $[\text{M} + \text{H}]^+$ calcd for $\text{C}_{38}\text{H}_{29}\text{CoN}_6\text{O}_2$: 661.173, found 661.176.

Compound 73

Complex [Bis(5-(4-(7-azaindol-3-yl)phenyl)-dipyrri-no)Zn(II)]



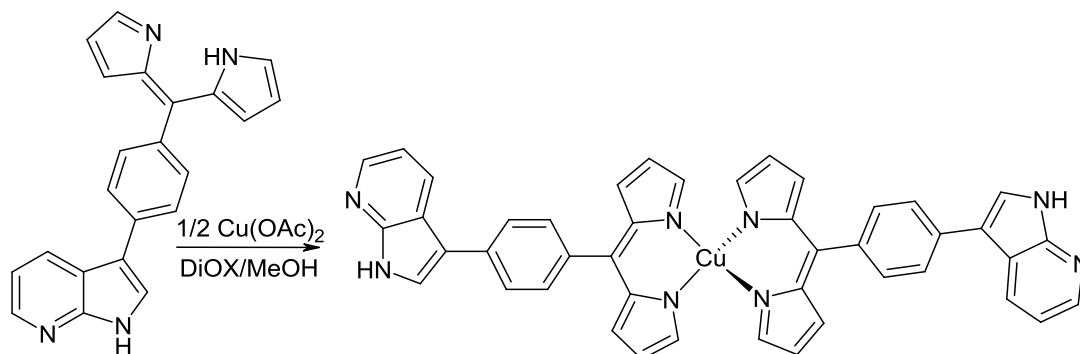
The solution of 5-(4-(7-azaindol-3-yl)phenyl)-dipyrri-no (20 mg, 0.059mmol) in benzene (3 mL) was mixed with a MeOH (5 mL) solution of $\text{Zn}(\text{OAc})_2 \cdot 2(\text{H}_2\text{O})$ (6.5 mg, 0.030 mmol). The reaction mixture was stirred for 5 min and the solvent was removed under vacuum. The resulting solid was washed with MeOH to afford the product as a yellow solid (18.3 mg, 83.6 %). Yellow crystals were grown in a tube by slow diffusion of a benzene solution of the ligand into a MeOH solution of $\text{Zn}(\text{OAc})_2$.

^1H NMR (300 MHz, DMSO-d_6): δ (ppm) 12.05 (s, 2H), 8.44 (d, $J=8.0$ Hz, 2H), 8.32 (dd, $J^1=4.7$ Hz, $J^2=1.4$ Hz, 2H), 8.08 (d, $J=2.5$ Hz, 2H), 7.92 (d, $J=8.0$ Hz, 4H), 7.64 (d, $J=8.0$ Hz, 4H), 7.59 (t, $J=1.3$ Hz, 4H), 7.21 (dd, $J^1=8.0$ Hz, $J^2=4.6$ Hz, 2H), 6.77(d, $J=4.2$ Hz, 4H), 6.49 (dd, $J^1=4.2$ Hz, $J^2=1.0$ Hz, 4H).

^{13}C NMR (75 MHz, DMSO-d_6): δ (ppm) 150.0, 149.7, 149.1, 143.5, 140.4, 136.3, 136.0, 133.1, 131.7, 128.2, 125.4, 125.0, 118.1, 117.7, 116.7, 114.0.

UV-VIS, (DMSO) λ_{max} (nm), ϵ (mol^{-1} L cm^{-1}): 276 (62000), 383 (24000), 466 (92000), 485 (157000).

HRMS (ESI), m/z : $[\text{M} + \text{H}]^+$ calcd for $\text{C}_{44}\text{H}_{31}\text{N}_8\text{Zn}$: 735.196, found 735.193.

Compound 74**Complex [Bis(5-(4-(7-azaindol-3-yl)phenyl)-dipyrriino)Cu(II)]**

The solution of 5-(4-(7-azaindol-3-yl)phenyl)-dipyrriin (10 mg, 0.030 mmol) in DiOX (5 mL) was mixed with MeOH (7 mL) solution of $\text{Cu}(\text{OAc})_2 \cdot (\text{H}_2\text{O})$ (3.0 mg, 0.015 mmol). The reaction mixture was stirred for 5 min and the solvent was removed under vacuum. The resulting solid was washed with MeOH to afford the product as a red solid (8.9 mg, 81.5 %). Red crystals were grown in a tube by slow diffusion of a DiOX solution of the ligand into a MeOH solution of $\text{Cu}(\text{OAc})_2$.

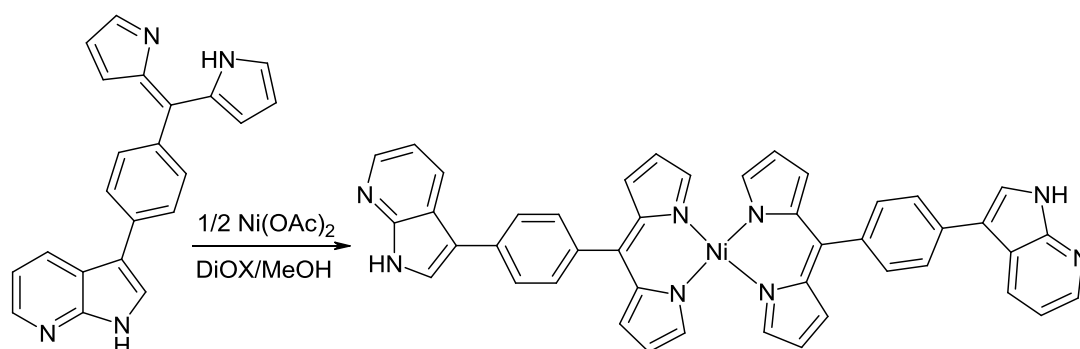
UV-VIS, (DMSO) $\lambda_{\text{max}}(\text{nm})$, $\epsilon(\text{mol}^{-1} \text{L cm}^{-1})$: 276 (34000), 391 (18000), 468 (45000), 510 (17000).

HRMS (ESI), m/z : $[\text{M} + \text{H}]^+$ calcd for $\text{C}_{44}\text{H}_{31}\text{CuN}_8$: 734.196, found 734.203.

Elemental Analysis: $\text{C}_{44}\text{H}_{30}\text{CuN}_8$ (Mw: **734.31** g/mole)

Calculated: C 71.97 %, H 4.12 %, N 15.26 %.

Found: C 71.28 %, H 4.87 %, N 14.59 %.

Compound 75**Complex [Bis(5-(4-(7-azaindol-3-yl)phenyl)-dipyrriino)Ni(II)]**

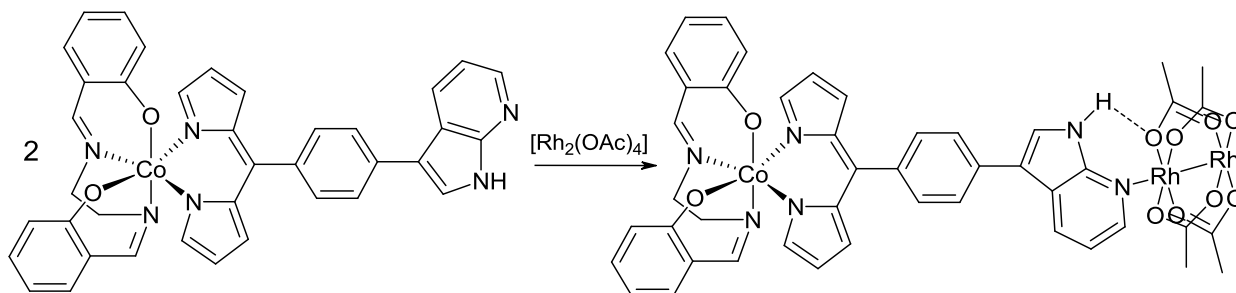
The solution of 5-(4-(7-azaindol-3-yl)phenyl)-dipyrriin (20 mg, 0.059 mmol) in DiOX (5 mL) was mixed with MeOH solution (7 mL) of $\text{Ni}(\text{OAc})_2 \cdot 4(\text{H}_2\text{O})$ (7.4 mg, 0.030 mmol). Reaction mixture was stirred for 5 min and then solvent was removed under vacuum. The resulting solid was washed with MeOH to afford the product as a green solid (18.4 mg, 84.8 %). Green-orange crystals were grown in tube by slow diffusion of a DiOX solution of the ligand into a MeOH solution of $\text{Ni}(\text{OAc})_2$.

UV-VIS, (DMSO) $\lambda_{\text{max}}(\text{nm})$, $\epsilon(\text{mol}^{-1} \text{L cm}^{-1})$: 275 (64000), 368 (28000), 465 (105000), 508 (42000).

HRMS (ESI), m/z : $[M + H]^+$ calcd for $C_{44}H_{31}N_8Ni$: 729.202, found 729.195.

Compound 76

Heterobimetallic complex: $[Rh_2(OAc)_4((Aza-Ph-Dpm)Co(SALEN))]$

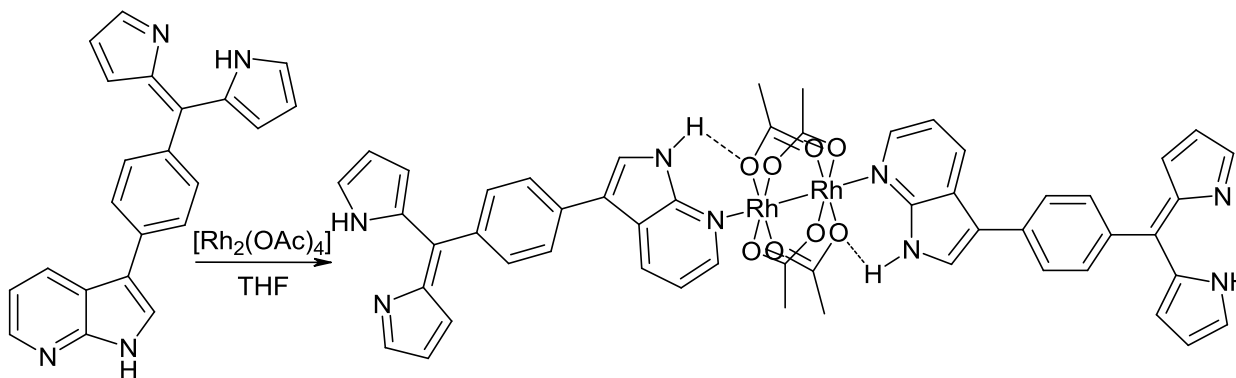


A solution of $[Co(salen)(Aza-Ph-Dpm)]$ (3.7 mg, 0.0056 mmol) in THF (2 mL) was mixed with THF (2 mL) solution of rhodium acetate (1.2 mg, 0.0028 mmol). The reaction mixture was stirred for 5 min and the solvent was removed under vacuum. The resulting red powder was partially dissolved in chloroform and after removal of the insoluble residue by filtration solution was analyzed by 1H NMR.

1H NMR (300 MHz, $CDCl_3$): δ (ppm) 10.53 (br, 1H), 9.00 (br, 1H), 8.60 (d, $J=8.0$ Hz, 1H), 8.23 (s, 1H), 7.91 (t, $J=1.4$ Hz, 1H), 7.81-7.78 (m, 2H), 7.71-7.69 (m, 1H), 7.60-7.57 (m, 3H), 7.36-7.29 (m, 3H), 7.20 (s, 2H), 7.10-7.01 (m, 2H), 6.93-6.90 (m, 2H), 6.87 (d, $J=4.1$ Hz, 1H), 6.63-6.57 (m, 1H), 6.44-6.39 (m, 1H), 6.33 (dd, $J^1=4.1$ Hz, $J^2=1.4$ Hz, 1H), 6.25 (dd, $J^1=4.5$ Hz, $J^2=1.5$ Hz, 1H), 3.97 (m, 1H), 3.80 (m, 1H), 3.19 (m, 1H), 2.66 (m, 1H), 2.00 (s, 12H).

Compound 77

Complex $[Bis(5-(4-(7-azaindol-3-yl)phenyl)-dipyririn)(Rh_2(OAc)_4)]$



A solution of 5-(4-(7-azaindol-3-yl)phenyl)-dipyririn (50 mg, 0.149 mmol) in THF (30 mL) was mixed with a THF (20 mL) solution of $[Rh_2(OAc)_4]$ (32.85 mg, 0.074 mmol). The reaction mixture was stirred for 5 min and the solvent was removed under vacuum. Red crystals were grown by slow diffusion of *n*-pentane into a Diox solution of the complex (71 mg, 65.1 %).

¹H NMR (300 MHz, CDCl₃): δ(ppm) 10.56 (s, 2H), 9.07 (d, J=4.3 Hz, 2H), 8.62 (dd, J¹=7.9 Hz, J²=1.0 Hz, 2H), 7.84-7.81 (m, 4H), 7.71(d, J=2.4 Hz, 2H), 7.68 (t, J=1.1 Hz, 4H), 7.65-7.62 (m, 4H), 7.57 (dd, J¹=7.9 Hz, J²=5.1 Hz, 2H), 6.77(dd, J¹=4.2 Hz, J²=1.0 Hz, 4H), 6.44 (dd, J¹=4.2 Hz, J²=1.4 Hz, 4H), 2.00 (s, 12H).

¹³C NMR (75 MHz, CDCl₃): δ(ppm) 192.3, 148.7, 144.9, 143.6, 140.8, 135.3, 131.8, 129.6, 129.1, 126.2, 122.9, 121.0, 120.3, 117.6, 117.4, 116.2, 113.8, 24.2.

UV-VIS, (CH₂Cl₂) λ_{max}(nm), ε(mol⁻¹ L cm⁻¹): 228 (94000), 269 (52000), 437 (40000), 458 (34000).

IR: ν 1412(COO⁻), 1592 (COO⁻) cm⁻¹.

Elemental Analysis: C₅₂H₄₄N₈O₈Rh₂•4(DiOX) (Mw: **1467.21** g/mole)

Calculated: C 55.66 %, N 7.63 %, H 5.22 %.

Found: C 55.33 %, N 7.99 %, H 4.82 %.

¹ Robinson M.M., Robinson B.L., *J. Am. Chem. Soc.* **1956**, *78*, 1247.

² Alvarez, M., Fernandez, D., Joule, A., *Synthesis* **1999**, *4*, 615.

³ Wang, S., *Organic Letters*, **2002**, *4*, 4049.

⁴ Verbiscar, A. J., *J. Med. Chem.* **1972**, *15*, 149.

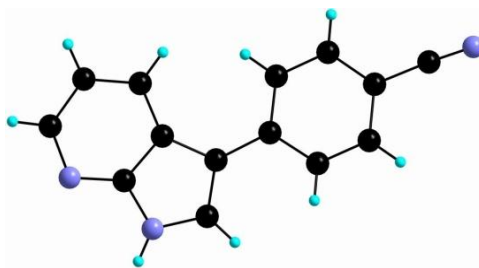
⁵ Inspired from Noland, W. E., Kuryla, W. C., Lange, R. F., *J. Am. Chem. Soc.* **1959**, *81*, 6010.

⁶ Sreedhar, B., *Journal of Molecular Catalysis A: Chemical* **2007**, *265*, 183.

VII. Appendix

1. Compound 7

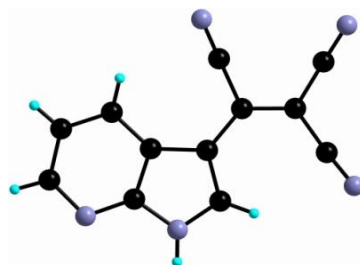
3-(4-benzonitrilyl)-7-azaindole



Empirical formula	C ₁₄ H ₉ N ₃
Formula weight	219.24
Temperature	173(2) K
Wavelength	0.71073 Å
Crystal system	Monoclinic
Space group	P2(1)/c
Unit cell dimensions:	
a = 10.4831(15) Å	α = 90°
b = 14.485(2) Å	β = 104.049(4)°
c = 7.2366(11) Å	γ = 90°
Volume	1066.0(3) Å ³
Z	4
Density (calculated)	1.366 mg/m ³
Absorption coefficient	0.085 mm ⁻¹
F(000)	456
Crystal size	0.18 x 0.15 x 0.13 mm ³
Theta range for data collection	2.81 to 30.07°
Index ranges	-13 ≤ h ≤ 14, -20 ≤ k ≤ 20, -
9 ≤ l ≤ 10	
Reflections collected	9130
Independent reflections	3027 [R(int) = 0.0451]
Completeness to theta = 30.07°	96.9 %
Absorption correction	None
Refinement method	Full-matrix least-squares on F ²
Data / restraints / parameters	3027 / 0 / 154
Goodness-of-fit on F ²	0.932
Final R indices [I > 2σ(I)]	R ₁ = 0.0567, wR ₂ = 0.1340
R indices (all data)	R ₁ = 0.1243, wR ₂ = 0.1641
Largest diff. peak and hole	0.268 and -0.242 e.Å ⁻³

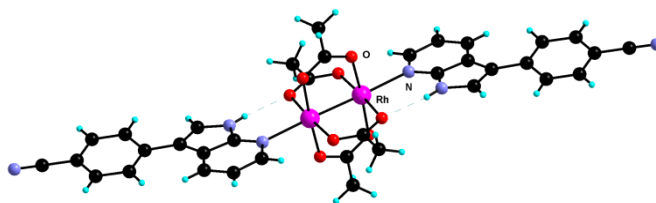
2. Compound 12

3-Tricyanovinylene-7-azaindole



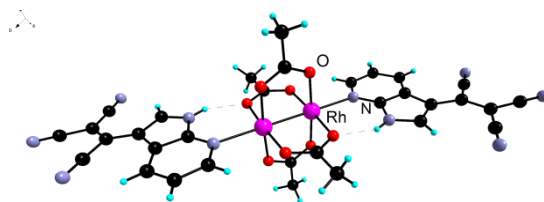
Empirical formula	C ₁₂ H ₅ N ₅
Formula weight	219.21
Temperature	173(2) K
Wavelength	0.71073 Å
Crystal system	Monoclinic
Space group	P2(1)/c
Unit cell dimensions:	
a = 8.9962(4) Å	α = 90°.
b = 5.4962(3) Å	β = 99.713(2)°.
c = 20.0699(8) Å	γ = 90°.
Volume	978.13(8) Å ³
Z	4
Density (calculated)	1.489 mg/m ³
Absorption coefficient	0.098 mm ⁻¹
F(000)	448
Crystal size	0.44 x 0.12 x 0.03 mm ³
Theta range for data collection	2.06 to 27.45°.
Index ranges	-11 ≤ h ≤ 11, -6 ≤ k ≤ 7, -
19 ≤ l ≤ 25	
Reflections collected	6991
Independent reflections	2212 [R(int) = 0.0307]
Completeness to theta = 27.45°	99.0 %
Absorption correction	Semi-empirical from
equivalents	
Max. and min. transmission	0.9971 and 0.9582
Refinement method	Full-matrix least-squares on F ²
Data / restraints / parameters	2212 / 0 / 154
Goodness-of-fit on F ²	1.126
Final R indices [I > 2σ(I)]	R1 = 0.0382, wR2 = 0.1032
R indices (all data)	R1 = 0.0555, wR2 = 0.1219
Largest diff. peak and hole	0.239 and -0.246 e.Å ⁻³

3. Compound 13

Complex [Bis(3-(4-benzonitrilyl)-7-azaindole)(Rh₂(OAc)₄)]

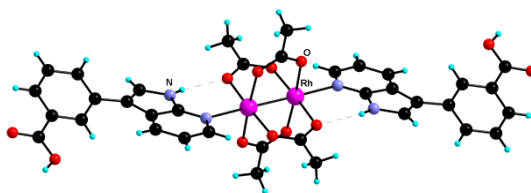
Empirical formula	C ₄₂ H ₄₄ N ₈ O ₁₀ Rh ₂
Formula weight	1026.67
Temperature	173(2) K
Wavelength	0.71073 Å
Crystal system	Triclinic
Space group	P-1
Unit cell dimensions:	
a = 8.0638(2) Å	$\alpha = 78.2360(10)^\circ$
b = 11.2180(3) Å	$\beta = 84.2670(10)^\circ$
c = 12.0060(3) Å	$\gamma = 85.0210(10)^\circ$
Volume	1055.47(5) Å ³
Z	1
Density (calculated)	1.615 mg/m ³
Absorption coefficient	0.850 mm ⁻¹
F(000)	522
Crystal size	0.23 x 0.21 x 0.09 mm ³
Theta range for data collection	1.74 to 27.60°
Index ranges	-10 ≤ h ≤ 10, -14 ≤ k ≤ 14, -
13 ≤ l ≤ 15	
Reflections collected	13745
Independent reflections	4812 [R(int) = 0.0376]
Completeness to theta = 27.60°	98.0 %
Absorption correction	Semi-empirical from
equivalents	
Max. and min. transmission	0.9274 and 0.8285
Refinement method	Full-matrix least-squares on F ²
Data / restraints / parameters	4812 / 0 / 278
Goodness-of-fit on F ²	1.165
Final R indices [I > 2σ(I)]	R1 = 0.0344, wR2 = 0.0848
R indices (all data)	R1 = 0.0434, wR2 = 0.1064
Largest diff. peak and hole	0.836 and -1.150 e. Å ⁻³

4. Compound 14

Complex [Bis(3-Tricyanovinylene-7-azaindole))(Rh₂(OAc)₄)]

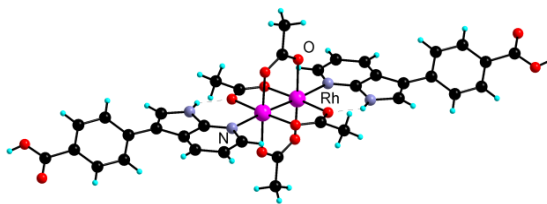
Empirical formula	C ₄₈ H ₅₄ N ₁₀ O ₁₆ Rh ₂
Formula weight	1232.83
Temperature	173(2) K
Wavelength	0.71073 Å
Crystal system	Triclinic
Space group	P-1
Unit cell dimensions: :	
a = 8.8730(2) Å	$\alpha = 107.5620(10)^\circ$.
b = 10.5971(2) Å	$\beta = 90.5040(10)^\circ$.
c = 14.7313(3) Å	$\gamma = 101.4450(10)^\circ$.
Volume	1290.84(5) Å ³
Z	1
Density (calculated)	1.586 mg/m ³
Absorption coefficient	0.719 mm ⁻¹
F(000)	630
Crystal size	0.26 x 0.26 x 0.09 mm ³
Theta range for data collection	1.45 to 30.14°.
Index ranges	-12 ≤ h ≤ 12, -14 ≤ k ≤ 14, -
20 ≤ l ≤ 20	
Reflections collected	28199
Independent reflections	7590 [R(int) = 0.0353]
Completeness to theta = 30.14°	99.3 %
Absorption correction	Semi-empirical from
equivalents	
Max. and min. transmission	0.9381 and 0.8351
Refinement method	Full-matrix least-squares on F ²
Data / restraints / parameters	7590 / 0 / 327
Goodness-of-fit on F ²	1.102
Final R indices [I > 2σ(I)]	R1 = 0.0492, wR2 = 0.1363
R indices (all data)	R1 = 0.0592, wR2 = 0.1533
Largest diff. peak and hole	2.008 and -1.163 e.Å ⁻³

5. Compound 15

Complex [Bis(3-(7-azaindol-3-yl) benzoic acid))(Rh₂(OAc)₄)]

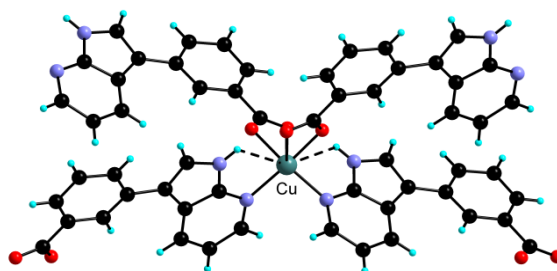
Empirical formula	C ₃₆ H ₃₂ N ₄ O ₁₂ Rh ₂
Formula weight	918.48
Temperature	173(2) K
Wavelength	0.71073 Å
Crystal system	Triclinic
Space group	P-1
Unit cell dimensions:	
a = 7.7872(2) Å	α = 110.5140(10)°.
b = 11.7497(3) Å	β = 96.1150(10)°.
c = 13.7757(4) Å	γ = 96.0720(10)°.
Volume	1159.85(5) Å ³
Z	1
Density (calculated)	1.315 mg/m ³
Absorption coefficient	0.766 mm ⁻¹
F(000)	462
Crystal size	0.10 x 0.08 x 0.06 mm ³
Theta range for data collection	1.60 to 27.50°.
Index ranges	-8 ≤ h ≤ 10, -15 ≤ k ≤ 12, -
17 ≤ l ≤ 17	
Reflections collected	18223
Independent reflections	5262 [R(int) = 0.0290]
Completeness to theta = 27.50°	98.9 %
Absorption correction	Semi-empirical from
equivalents	
Max. and min. transmission	0.9555 and 0.9273
Refinement method	Full-matrix least-squares on F ²
Data / restraints / parameters	5262 / 0 / 247
Goodness-of-fit on F ²	1.035
Final R indices [I > 2σ(I)]	R1 = 0.0323, wR2 = 0.0904
R indices (all data)	R1 = 0.0393, wR2 = 0.0933
Largest diff. peak and hole	1.410 and -0.395 e. Å ⁻³

6. Compound 16

Complex [Bis(4-(7-azaindol-3-yl) benzoic acid))(Rh₂(OAc)₄)]

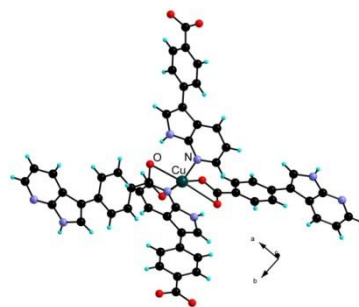
Empirical formula	C ₄₆ H ₅₄ N ₆ O ₁₄ Rh ₂
Formula weight	1120.78
Temperature	173(2) K
Wavelength	0.71073 Å
Crystal system	Triclinic
Space group	P-1
Unit cell dimensions:	
a = 8.4005(2) Å	α = 77.8610(10)°
b = 10.4754(3) Å	β = 88.822(2)°
c = 13.6491(4) Å	γ = 88.1780(10)°
Volume	1173.53(6) Å ³
Z	1
Density (calculated)	1.586 mg/m ³
Absorption coefficient	0.777 mm ⁻¹
F(000)	574
Crystal size	0.21 x 0.08 x 0.02 mm ³
Theta range for data collection	1.53 to 27.52°
Index ranges	-10 ≤ h ≤ 10, -13 ≤ k ≤ 9, -
17 ≤ l ≤ 17	
Reflections collected	17206
Independent reflections	5351 [R(int) = 0.0364]
Completeness to theta = 27.52°	99.1 %
Absorption correction	Semi-empirical from
equivalents	
Max. and min. transmission	0.9846 and 0.8539
Refinement method	Full-matrix least-squares on F ²
Data / restraints / parameters	5351 / 0 / 322
Goodness-of-fit on F ²	1.190
Final R indices [I > 2σ(I)]	R ₁ = 0.0309, wR ₂ = 0.0768
R indices (all data)	R ₁ = 0.0389, wR ₂ = 0.0906
Largest diff. peak and hole	0.579 and -0.639 e.Å ⁻³

7. Compound 17

Network {[Bis(4-(7-azaindol-3-yl) benzoic acid))Cu(II)]}_∞

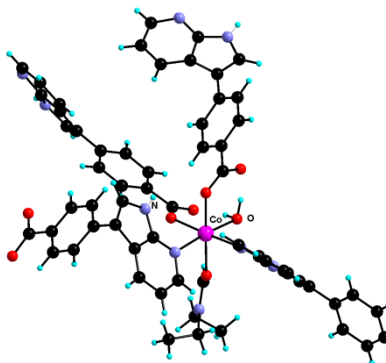
Empirical formula	C ₂₈ H ₁₈ Cu N ₄ O ₄
Formula weight	538.00
Temperature	173(2) K
Wavelength	0.71073 Å
Crystal system	Monoclinic
Space group	C2/c
Unit cell dimensions:	
a = 19.9952(4) Å	α = 90°
b = 9.6168(2) Å	β = 90.024(2)°
c = 11.4677(3) Å	γ = 90°
Volume	2205.12(9) Å ³
Z	4
Density (calculated)	1.621 mg/m ³
Absorption coefficient	1.038 mm ⁻¹
F(000)	1100
Crystal size	0.16 x 0.08 x 0.03 mm ³
Theta range for data collection	2.04 to 27.51°
Index ranges	-25 ≤ h ≤ 25, -12 ≤ k ≤ 12, -
14 ≤ l ≤ 14	
Reflections collected	20049
Independent reflections	2536 [R(int) = 0.0291]
Completeness to theta = 27.51°	99.9 %
Absorption correction	Semi-empirical from
equivalents	
Max. and min. transmission	0.9695 and 0.8515
Refinement method	Full-matrix least-squares on F ²
Data / restraints / parameters	2536 / 0 / 168
Goodness-of-fit on F ²	1.136
Final R indices [I > 2σ(I)]	R1 = 0.0411, wR2 = 0.1244
R indices (all data)	R1 = 0.0450, wR2 = 0.1265
Largest diff. peak and hole	0.757 and -0.424 e.Å ⁻³

8. Compound 18

Network {[Bis(4-(7-azaindol-3-yl) benzoic acid))Cu(II)]_∞ (Solvent)}

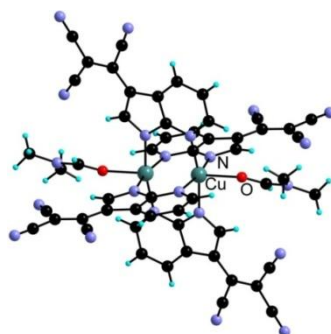
Empirical formula	C ₂₈ H ₁₈ Cu N ₄ O ₄
Formula weight	538.00
Temperature	173(2) K
Wavelength	0.71073 Å
Crystal system	Monoclinic
Space group	P2(1)/n
Unit cell dimensions:	
a = 14.8344(8) Å	α = 90°.
b = 15.7351(8) Å	β = 91.289(2)°.
c = 15.7728(9) Å	γ = 90°.
Volume	3680.8(3) Å ³
Z	4
Density (calculated)	0.971 mg/m ³
Absorption coefficient	0.622 mm ⁻¹
F(000)	1100
Crystal size	0.21 x 0.15 x 0.15 mm ³
Theta range for data collection	1.86 to 27.67°.
Index ranges	-19 ≤ h ≤ 15, -20 ≤ k ≤ 20, -
20 ≤ l ≤ 16	
Reflections collected	25583
Independent reflections	8352 [R(int) = 0.0636]
Completeness to theta = 27.67°	97.0 %
Absorption correction equivalents	Semi-empirical from
Max. and min. transmission	0.9125 and 0.8805
Refinement method	Full-matrix least-squares on F ²
Data / restraints / parameters	8352 / 0 / 335
Goodness-of-fit on F ²	0.879
Final R indices [I > 2σ(I)]	R1 = 0.0534, wR2 = 0.1445
R indices (all data)	R1 = 0.0850, wR2 = 0.1557
Extinction coefficient	0.0014(2)
Largest diff. peak and hole	0.360 and -0.432 e.Å ⁻³

9. Compound 19

Network {[Bis(4-(7-azaindol-3-yl) benzoic acid))(DEF)(H₂O))Co(II)]_∞}

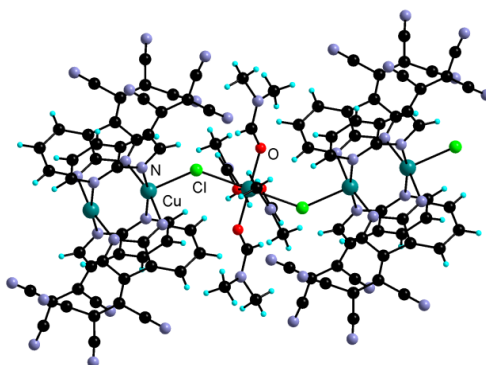
Empirical formula	C ₃₈ H ₄₂ Co N ₆ O ₇
Formula weight	753.72
Temperature	173(2) K
Wavelength	0.71073 Å
Crystal system	Monoclinic
Space group	P2(1)/c
Unit cell dimensions:	
a = 11.2590(3) Å	α = 90°
b = 16.2389(5) Å	β = 101.6720(10)°
c = 20.4134(6) Å	γ = 90°
Volume	3655.08(18) Å ³
Z	4
Density (calculated)	1.370 mg/m ³
Absorption coefficient	0.527 mm ⁻¹
F(000)	1580
Crystal size	0.10 x 0.05 x 0.05 mm ³
Theta range for data collection	1.62 to 27.52°
Index ranges	-7 ≤ h ≤ 14, -21 ≤ k ≤ 21, -
26 ≤ l ≤ 24	
Reflections collected	25495
Independent reflections	8337 [R(int) = 0.0337]
Completeness to theta = 27.52°	99.1 %
Absorption correction equivalents	Semi-empirical from
Max. and min. transmission	0.9741 and 0.9492
Refinement method	Full-matrix least-squares on F ²
Data / restraints / parameters	8337 / 0 / 455
Goodness-of-fit on F ²	1.128
Final R indices [I > 2σ(I)]	R1 = 0.0595, wR2 = 0.1469
R indices (all data)	R1 = 0.0728, wR2 = 0.1627
Largest diff. peak and hole	1.378 and -1.190 e.Å ⁻³

10. Compound 20

Complex $[\text{Cu}_2(\text{3-Tricyanovinylene-7-azaindoly})_4(\text{DMF})_2]$ 

Empirical formula	C ₅₄ H ₃₀ Cu ₂ N ₂₂ O ₂
Formula weight	1146.08
Temperature	173(2) K
Wavelength	0.71073 Å
Crystal system	Triclinic
Space group	P-1
Unit cell dimensions: :	
a = 10.2298(5) Å	$\alpha = 80.0930(10)^\circ$.
b = 11.7962(5) Å	$\beta = 69.9460(10)^\circ$.
c = 12.5120(5) Å	$\gamma = 66.1380(10)^\circ$.
Volume	1296.10(10) Å ³
Z	1
Density (calculated)	1.468 mg/m ³
Absorption coefficient	0.887 mm ⁻¹
F(000)	582
Crystal size	0.15 x 0.09 x 0.04 mm ³
Theta range for data collection	1.73 to 27.54°.
Index ranges	-13 ≤ h ≤ 13, -15 ≤ k ≤ 15, -
11 ≤ l ≤ 16	
Reflections collected	16282
Independent reflections	5896 [R(int) = 0.0429]
Completeness to theta = 27.54°	98.6 %
Absorption correction	Semi-empirical from
equivalents	
Max. and min. transmission	0.9654 and 0.8785
Refinement method	Full-matrix least-squares on F ²
Data / restraints / parameters	5896 / 0 / 351
Goodness-of-fit on F ²	1.092
Final R indices [I > 2σ(I)]	R1 = 0.0609, wR2 = 0.1560
R indices (all data)	R1 = 0.0891, wR2 = 0.1834
Largest diff. peak and hole	1.032 and -0.776 e.Å ⁻³

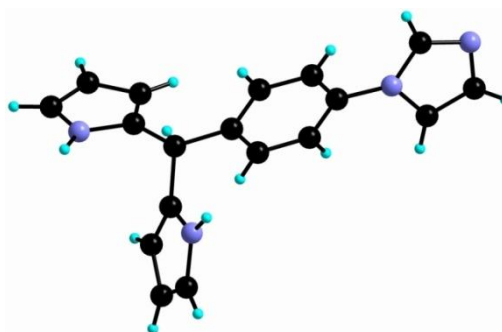
11. Compound 21

Network $\{[(\text{Cu}_2(3\text{-Tricyanovinylene-7-azaindoly})_4)(\text{CuCl}_2)(\text{DMF})_2](\text{DMF})_2\}_\infty$ 

Empirical formula	C ₆₃ H ₅₁ Cl ₂ Cu ₃ N ₂₅ O ₅
Formula weight	1499.81
Temperature	173(2) K
Wavelength	0.71073 Å
Crystal system	Triclinic
Space group	P-1
Unit cell dimensions:	
a = 11.3821(3) Å	$\alpha = 80.5490(10)^\circ$
b = 12.3377(3) Å	$\beta = 89.7350(10)^\circ$
c = 12.5248(3) Å	$\gamma = 85.5500(10)^\circ$
Volume	1729.68(7) Å ³
Z	1
Density (calculated)	1.440 mg/m ³
Absorption coefficient	1.058 mm ⁻¹
F(000)	765
Crystal size	0.16 x 0.12 x 0.09 mm ³
Theta range for data collection	1.65 to 27.61°
Index ranges	-14 ≤ h ≤ 14, -16 ≤ k ≤ 15, -
16 ≤ l ≤ 16	
Reflections collected	43626
Independent reflections	7907 [R(int) = 0.0561]
Completeness to theta = 27.61°	98.6 %
Absorption correction equivalents	Semi-empirical from
Max. and min. transmission	0.9108 and 0.8489
Refinement method	Full-matrix least-squares on F ²
Data / restraints / parameters	7907 / 0 / 460
Goodness-of-fit on F ²	1.078
Final R indices [I > 2σ(I)]	R1 = 0.0653, wR2 = 0.1749
R indices (all data)	R1 = 0.1059, wR2 = 0.2091
Largest diff. peak and hole	1.335 and -1.718 e.Å ⁻³

12. Compound 27

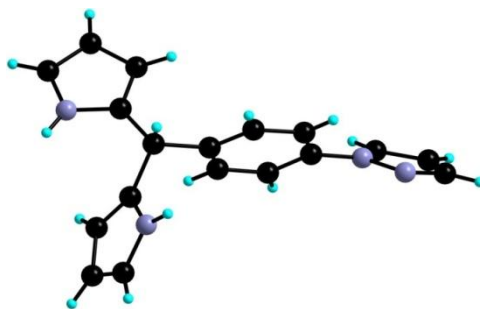
5-(4'-(1H-imidazol-1-yl)phenyl)-dipyrromethane



Empirical formula	C ₁₈ H ₁₆ N ₄
Formula weight	288.35
Temperature	173(2) K
Wavelength	0.71073 Å
Crystal system	Triclinic
Space group	P-1
Unit cell dimensions:	
a = 8.5724(10) Å	a = 62.616(4)°
b = 9.7289(10) Å	b = 80.140(4)°
c = 10.4170(11) Å	g = 83.840(4)°
Volume	759.63(14) Å ³
Z	2
Density (calculated)	1.261 mg/m ³
Absorption coefficient	0.078 mm ⁻¹
F(000)	304
Crystal size	0.12 x 0.10 x 0.05 mm ³
Theta range for data collection	2.22 to 27.11°
Index ranges	-9 ≤ h ≤ 11, -12 ≤ k ≤ 11, -
12 ≤ l ≤ 13	
Reflections collected	6871
Independent reflections	3260 (R(int) = 0.0395)
Completeness to theta = 27.11°	97.2 %
Absorption correction	Semi-empirical from
equivalents	
Max. and min. transmission	0.9961 and 0.9907
Refinement method	Full-matrix least-squares on F ²
Data / restraints / parameters	3260 / 0 / 199
Goodness-of-fit on F ²	1.146
Final R indices (I > 2σ(I))	R ₁ = 0.0758, wR ₂ = 0.1639
R indices (all data)	R ₁ = 0.1038, wR ₂ = 0.1774
Largest diff. peak and hole	0.448 and -0.286 e.Å ⁻³

13. Compound 28

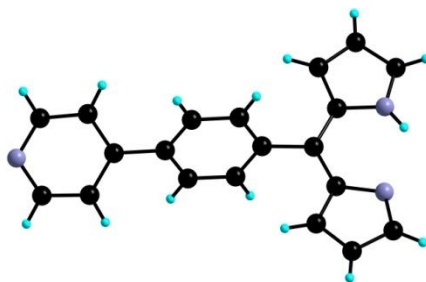
5-(4'-(1H-pyrazol-1-yl)phenyl)-dipyrromethane



Empirical formula	C ₁₈ H ₁₆ N ₄
Formula weight	288.35
Temperature	173(2) K
Wavelength	0.71073 Å
Crystal system	Monoclinic
Space group	P2(1)/n
Unit cell dimensions:	
a = 9.2680(3) Å	$\alpha = 90^\circ$.
b = 17.7535(5) Å	$\beta = 109.2900(10)^\circ$.
c = 9.3468(3) Å	$\gamma = 90^\circ$.
Volume	1451.58(8) Å ³
Z	4
Density (calculated)	1.319 mg/m ³
Absorption coefficient	0.081 mm ⁻¹
F(000)	608
Crystal size	0.12 x 0.09 x 0.06 mm ³
Theta range for data collection	2.29 to 27.49°.
Index ranges	-11 ≤ h ≤ 12, -19 ≤ k ≤ 23, -
12 ≤ l ≤ 11	
Reflections collected	15557
Independent reflections	3298 (R(int) = 0.0255)
Completeness to theta = 27.49°	99.8 %
Absorption correction equivalents	Semi-empirical from
Max. and min. transmission	0.9951 and 0.9903
Refinement method	Full-matrix least-squares on F ²
Data / restraints / parameters	3298 / 0 / 199
Goodness-of-fit on F ²	1.067
Final R indices (I > 2σ(I))	R1 = 0.0415, wR2 = 0.0947
R indices (all data)	R1 = 0.0508, wR2 = 0.1016
Largest diff. peak and hole	0.215 and -0.206 e.Å ⁻³

14. Compound 31

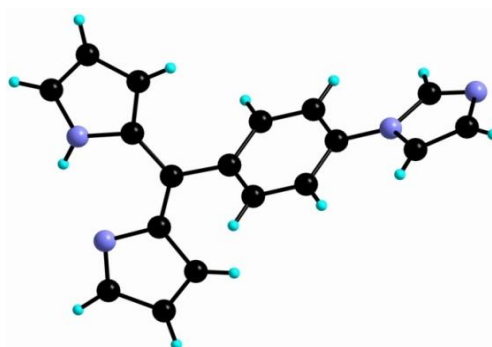
5-(4'-(4-pyridin-1-yl)phenyl)-dipyrrin



Empirical formula	C ₂₀ H ₁₅ N ₃
Formula weight	297.35
Temperature	173(2) K
Wavelength	0.71073 Å
Crystal system	Monoclinic
Space group	P2(1)/n
Unit cell dimensions:	
a = 11.1131(3)Å	α = 90°.
b = 7.2051(2)Å	β = 105.5270(10)°.
c = 19.4251(5)Å	γ = 90°.
Volume	1498.62(7)Å ³
Z	4
Density (calculated)	1.318 mg/m ³
Absorption coefficient	0.080 mm ⁻¹
F(000)	624
Crystal size	0.20 x 0.20 x 0.10 mm ³
Theta range for data collection	1.92 to 27.74°.
Index ranges	-14 ≤ h ≤ 14, -9 ≤ k ≤ 6, -
25 ≤ l ≤ 16	
Reflections collected	11268
Independent reflections	3465 (R(int) = 0.0204)
Completeness to theta = 27.74°	97.9 %
Absorption correction	Semi-empirical from
equivalents	
Max. and min. transmission	0.9921 and 0.9843
Refinement method	Full-matrix least-squares on F ²
Data / restraints / parameters	3465 / 0 / 208
Goodness-of-fit on F ²	1.049
Final R indices [I > 2σ(I)]	R ₁ = 0.0444, wR ₂ = 0.1167
R indices (all data)	R ₁ = 0.0523, wR ₂ = 0.1227
Largest diff. peak and hole	0.372 and -0.341 e.Å ⁻³

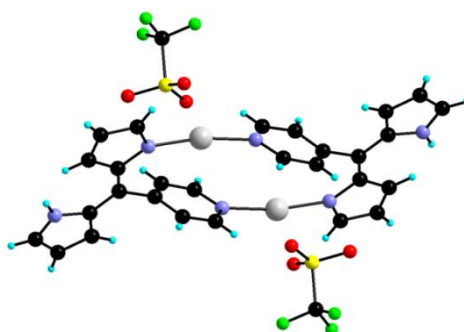
15. Compound 32

5-(4'-(1H-imidazol-1-yl)phenyl)-dipyrrin



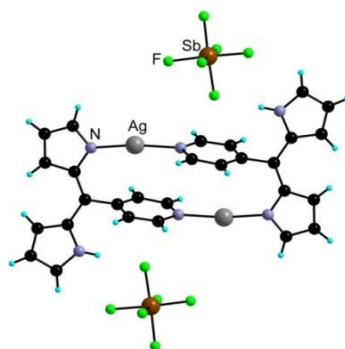
Empirical formula	C ₁₈ H ₁₄ N ₄
Formula weight	286.33
Temperature	173(2) K
Wavelength	0.71073 Å
Crystal system	Monoclinic
Space group	C2/c
Unit cell dimensions:	
a = 12.8270(6) Å	$\alpha = 90^\circ$.
b = 12.5383(5) Å	$\beta = 108.777(2)^\circ$.
c = 18.6260(8) Å	$\gamma = 90^\circ$.
Volume	2836.2(2) Å ³
Z	8
Density (calculated)	1.341 mg/m ³
Absorption coefficient	0.083 mm ⁻¹
F(000)	1200
Crystal size	0.20 x 0.13 x 0.08 mm ³
Theta range for data collection	2.33 to 27.49°.
Index ranges	-16 ≤ h ≤ 16, -14 ≤ k ≤ 16, -
23 ≤ l ≤ 24	
Reflections collected	8513
Independent reflections	3261 (R(int) = 0.0197)
Completeness to theta = 27.49°	99.6 %
Absorption correction	Semi-empirical from
equivalents	
Max. and min. transmission	0.9934 and 0.9836
Refinement method	Full-matrix least-squares on F ²
Data / restraints / parameters	3261 / 0 / 199
Goodness-of-fit on F ²	1.027
Final R indices (I > 2σ(I))	R1 = 0.0435, wR2 = 0.1080
R indices (all data)	R1 = 0.0552, wR2 = 0.1154
Largest diff. peak and hole	0.255 and -0.292 e.Å ⁻³

16. Compound 34

Complex $[(5-(4\text{-pyridin-1-yl})\text{-dipyrroin})_2\text{Ag}_2](\text{OTf})_2$ 

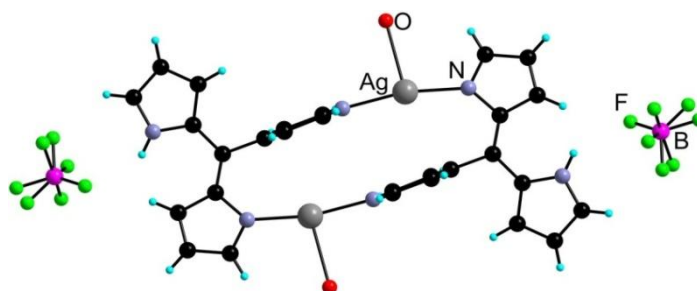
Empirical formula	C ₄₈ H ₄₀ Ag ₂ F ₆ N ₆ O ₆ S ₂
Formula weight	1190.74
Temperature	173(2) K
Wavelength	0.71073 Å
Crystal system	Triclinic
Space group	P-1
Unit cell dimensions:	
a = 9.2123(4) Å	$\alpha = 102.508(3)^\circ$
b = 10.0695(5) Å	$\beta = 93.810(3)^\circ$
c = 13.2746(6) Å	$\gamma = 97.941(3)^\circ$
Volume	1184.71(10) Å ³
Z	1
Density (calculated)	1.669 mg/m ³
Absorption coefficient	0.995 mm ⁻¹
F(000)	598
Crystal size	0.19 x 0.04 x 0.03 mm ³
Theta range for data collection	1.58 to 27.06°
Index ranges	-11 ≤ h ≤ 11, -13 ≤ k ≤ 13, -
17 ≤ l ≤ 16	
Reflections collected	9920
Independent reflections	5061 (R(int) = 0.0574)
Completeness to theta = 27.06°	97.5 %
Absorption correction	Semi-empirical from
equivalents	
Max. and min. transmission	0.9708 and 0.8335
Refinement method	Full-matrix least-squares on F ²
Data / restraints / parameters	5061 / 0 / 316
Goodness-of-fit on F ²	1.170
Final R indices [I > 2σ(I)]	R1 = 0.0691, wR2 = 0.1682
R indices (all data)	R1 = 0.1111, wR2 = 0.2092
Largest diff. peak and hole	0.756 and -1.181 e.Å ⁻³

17. Compound 35

Complex [(5-(4-pyridin-1-yl)-dipyrin)₂Ag₂](SbF₆)₂

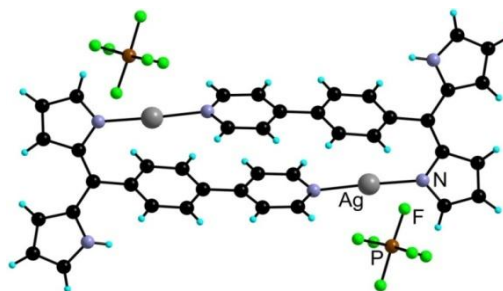
Empirical formula	C ₂₈ H ₂₂ Ag ₂ F ₁₂ N ₆ Sb ₂
Formula weight	1129.76
Temperature	173(2) K
Wavelength	0.71073 Å
Crystal system	Monoclinic
Space group	C2/c
Unit cell dimensions:	
a = 17.3749(9)Å	α = 90°.
b = 12.6487(6)Å	β = 118.616(2)°.
c = 17.0711(8)Å	γ = 90°.
Volume	3293.4(3)Å ³
Z	4
Density (calculated)	2.278 mg/m ³
Absorption coefficient	2.894 mm ⁻¹
F(000)	2144
Crystal size	0.03 x 0.02 x 0.02 mm ³
Theta range for data collection	2.09 to 27.54°.
Index ranges	-22 ≤ h ≤ 19, -14 ≤ k ≤ 16, -
22 ≤ l ≤ 19	
Reflections collected	13212
Independent reflections	3756 (R(int) = 0.0321)
Completeness to theta = 27.54°	98.7 %
Absorption correction	Semi-empirical from
equivalents	
Max. and min. transmission	0.9444 and 0.9182
Refinement method	Full-matrix least-squares on F ²
Data / restraints / parameters	3756 / 0 / 226
Goodness-of-fit on F ²	1.219
Final R indices [I > 2σ(I)]	R ₁ = 0.0698, wR ₂ = 0.1206
R indices (all data)	R ₁ = 0.0947, wR ₂ = 0.1289
Largest diff. peak and hole	1.487 and -2.135 e.Å ⁻³

18. Compound 36

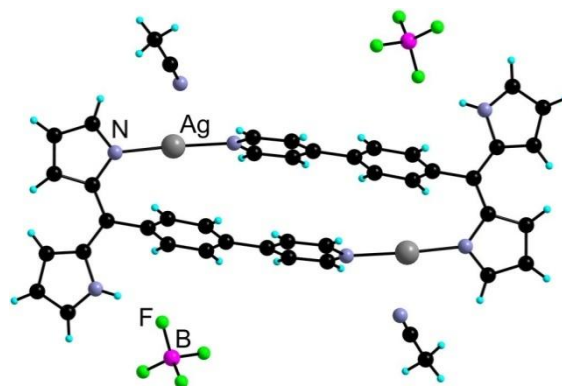
Complex $[(5-(4\text{-pyridin-1-yl})\text{-dipyrin})_2\text{Ag}_2](\text{BF}_4)_2$ 

Empirical formula	C ₂₈ H ₂₆ Ag ₂ B ₂ F ₈ N ₆ O ₂
Formula weight	867.91
Temperature	173(2) K
Wavelength	0.71073 Å
Crystal system	Monoclinic
Space group	P2(1)/n
Unit cell dimensions:	
a = 10.1379(2)Å	$\alpha = 90^\circ$.
b = 9.5859(2)Å	$\beta = 103.4170(10)^\circ$.
c = 15.9091(4)Å	$\gamma = 90^\circ$.
Volume	1503.86(6)Å ³
Z	2
Density (calculated)	1.917 mg/m ³
Absorption coefficient	1.392 mm ⁻¹
F(000)	856
Crystal size	0.12 x 0.11 x 0.04 mm ³
Theta range for data collection	2.50 to 27.48°.
Index ranges	-13 ≤ h ≤ 10, -12 ≤ k ≤ 12, -
20 ≤ l ≤ 20	
Reflections collected	25736
Independent reflections	3415 (R(int) = 0.0237)
Completeness to theta = 27.48°	99.2 %
Absorption correction	Semi-empirical from
equivalents	
Max. and min. transmission	0.9464 and 0.8508
Refinement method	Full-matrix least-squares on F ²
Data / restraints / parameters	3415 / 0 / 245
Goodness-of-fit on F ²	1.124
Final R indices [I > 2σ(I)]	R1 = 0.0308, wR2 = 0.0674
R indices (all data)	R1 = 0.0335, wR2 = 0.0690
Largest diff. peak and hole	0.619 and -0.871 e.Å ⁻³

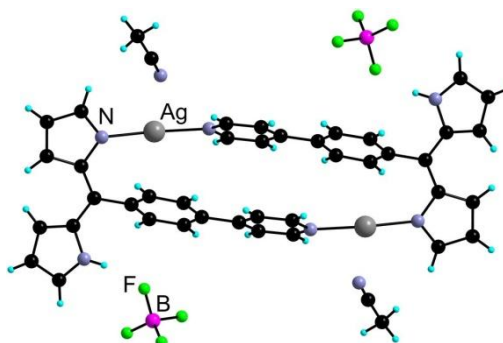
19. Compound 37

Complex $[(5-(4'-(4\text{-pyridin-1-yl})\text{phenyl})\text{-dipyrrin})_2\text{Ag}_2](\text{PF}_6)_2$ 

Empirical formula	C ₄₀ H ₃₀ Ag ₂ F ₁₂ N ₆ P ₂
Formula weight	1100.38
Temperature	173(2) K
Wavelength	0.71073 Å
Crystal system	Monoclinic
Space group	P2(1)/n
Unit cell dimensions:	
a = 10.3668(3) Å	$\alpha = 90^\circ$
b = 13.6996(4) Å	$\beta = 95.6260(10)^\circ$
c = 13.8058(4) Å	$\gamma = 90^\circ$
Volume	1951.27(10) Å ³
Z	2
Density (calculated)	1.873 mg/m ³
Absorption coefficient	1.184 mm ⁻¹
F(000)	1088
Crystal size	0.11 x 0.07 x 0.02 mm ³
Theta range for data collection	2.10 to 27.53°
Index ranges	-12 ≤ h ≤ 13, -17 ≤ k ≤ 12, -
17 ≤ l ≤ 17	
Reflections collected	22705
Independent reflections	4497 (R(int) = 0.0292)
Completeness to theta = 27.53°	99.9 %
Absorption correction	Semi-empirical from
equivalents	
Max. and min. transmission	0.9767 and 0.8808
Refinement method	Full-matrix least-squares on F ²
Data / restraints / parameters	4497 / 0 / 280
Goodness-of-fit on F ²	1.034
Final R indices [I > 2σ(I)]	R1 = 0.0405, wR2 = 0.1057
R indices (all data)	R1 = 0.0531, wR2 = 0.1137
Largest diff. peak and hole	1.267 and -0.657 e.Å ⁻³

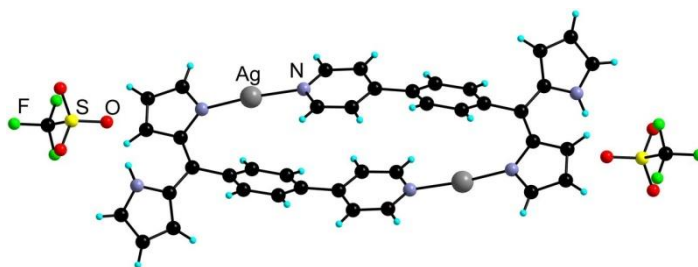
20. Compound $\alpha 38$:Complex $[(5-(4'-(4\text{-pyridin-1-yl})\text{phenyl})\text{-dipyrrin})_2\text{Ag}_2](\text{BF}_4)_2$ 

Empirical formula	C ₄₄ H ₃₆ Ag ₂ B ₂ F ₈ N ₈
Formula weight	1066.17
Temperature	173(2) K
Wavelength	0.71073 Å
Crystal system	Triclinic
Space group	P-1
Unit cell dimensions:	
a = 9.3120(3)Å	$\alpha = 112.286(2)^\circ$.
b = 10.4615(3)Å	$\beta = 94.953(2)^\circ$.
c = 12.4452(4)Å	$\gamma = 101.894(2)^\circ$.
Volume	1079.46(6)Å ³
Z	1
Density (calculated)	1.640 mg/m ³
Absorption coefficient	0.985 mm ⁻¹
F(000)	532
Crystal size	0.09 x 0.09 x 0.04 mm ³
Theta range for data collection	1.80 to 27.55°.
Index ranges	-12 ≤ h ≤ 12, -13 ≤ k ≤ 13, -
15 ≤ l ≤ 16	
Reflections collected	16820
Independent reflections	4916 (R(int) = 0.0269)
Completeness to theta = 27.55°	98.9 %
Absorption correction	Semi-empirical from
equivalents	
Max. and min. transmission	0.9617 and 0.9166
Refinement method	Full-matrix least-squares on F ²
Data / restraints / parameters	4916 / 0 / 284
Goodness-of-fit on F ²	1.091
Final R indices [I > 2σ(I)]	R1 = 0.0449, wR2 = 0.1076
R indices (all data)	R1 = 0.0496, wR2 = 0.1105
Largest diff. peak and hole	1.137 and -0.966 e.Å ⁻³

21. Compound β 38Complex $[(5-(4'-(4\text{-pyridin-1-yl})\text{phenyl})\text{-dipyrin})_2\text{Ag}_2](\text{BF}_4)_2$ 

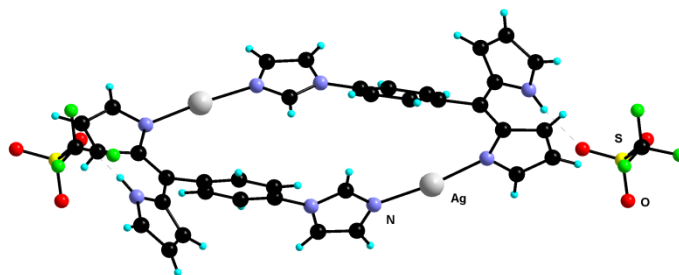
Empirical formula	C ₄₄ H ₃₆ Ag ₂ B ₂ F ₈ N ₈
Formula weight	1066.17
Temperature	173(2) K
Wavelength	0.71073 Å
Crystal system	Monoclinic
Space group	P2(1)/n
Unit cell dimensions:	
a = 10.5431(4)Å	$\alpha = 90^\circ$
b = 7.2584(3)Å	$\beta = 93.822(2)^\circ$
c = 27.3348(11)Å	$\gamma = 90^\circ$
Volume	2087.17(14)Å ³
Z	2
Density (calculated)	1.696 mg/m ³
Absorption coefficient	1.019 mm ⁻¹
F(000)	1064
Crystal size	0.12 x 0.07 x 0.07 mm ³
Theta range for data collection	2.03 to 27.51°
Index ranges	-13 ≤ h ≤ 10, -8 ≤ k ≤ 9, -
35 ≤ l ≤ 33	
Reflections collected	15348
Independent reflections	4798 (R(int) = 0.0267)
Completeness to theta = 27.51°	99.8 %
Absorption correction	Semi-empirical from
equivalents	
Max. and min. transmission	0.9321 and 0.8875
Refinement method	Full-matrix least-squares on F ²
Data / restraints / parameters	4798 / 0 / 290
Goodness-of-fit on F ²	1.044
Final R indices [I > 2σ(I)]	R1 = 0.0366, wR2 = 0.0888
R indices (all data)	R1 = 0.0533, wR2 = 0.0970
Largest diff. peak and hole	1.116 and -0.602 e.Å ⁻³

22. Compound 39

Complex $[(5-(4'-(4\text{-pyridin-1-yl})\text{phenyl})\text{-dipyrin})_2\text{Ag}_2](\text{OTf})_2$ 

Empirical formula	C ₄₂ H ₃₀ Ag ₂ F ₆ N ₆ O ₆ S ₂
Formula weight	1108.58
Temperature	173(2) K
Wavelength	0.71073 Å
Crystal system	Triclinic
Space group	P-1
Unit cell dimensions:	
a = 9.8577(4) Å	$\alpha = 118.0560(10)^\circ$.
b = 11.1300(4) Å	$\beta = 92.695(2)^\circ$.
c = 11.5098(5) Å	$\gamma = 107.9120(10)^\circ$.
Volume	1032.41(7) Å ³
Z	1
Density (calculated)	1.783 mg/m ³
Absorption coefficient	1.134 mm ⁻¹
F(000)	552
Crystal size	0.16 x 0.09 x 0.04 mm ³
Theta range for data collection	2.13 to 27.51°.
Index ranges	-12 ≤ h ≤ 8, -13 ≤ k ≤ 14, -
14 ≤ l ≤ 14	
Reflections collected	12472
Independent reflections	4690 (R(int) = 0.0281)
Completeness to theta = 27.51°	99.0 %
Absorption correction	Semi-empirical from
equivalents	
Max. and min. transmission	0.9560 and 0.8394
Refinement method	Full-matrix least-squares on F ²
Data / restraints / parameters	4690 / 0 / 289
Goodness-of-fit on F ²	1.069
Final R indices [I > 2σ(I)]	R1 = 0.0336, wR2 = 0.0688
R indices (all data)	R1 = 0.0430, wR2 = 0.0749
Largest diff. peak and hole	0.995 and -0.519 e.Å ⁻³

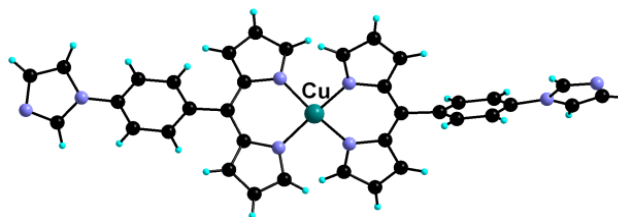
23. Compound 40

Complex $[(5-(4'-(1H\text{-imidazol-1-yl})\text{phenyl})\text{-dipyrrin})_2\text{Ag}_2](\text{OTf})_2$ 

Empirical formula	C ₄₄ H ₃₇ Ag ₂ F ₆ N ₁₁ O ₆ S ₂
Formula weight	1209.71
Temperature	173(2) K
Wavelength	0.71073 Å
Crystal system	Monoclinic
Space group	P2(1)/c
Unit cell dimensions:	
a = 12.7000(3) Å	$\alpha = 90^\circ$.
b = 20.4863(5) Å	$\beta = 103.8480(10)^\circ$.
c = 18.5461(5) Å	$\gamma = 90^\circ$.
Volume	4685.0(2) Å ³
Z	4
Density (calculated)	1.715 mg/m ³
Absorption coefficient	1.010 mm ⁻¹
F(000)	2424
Crystal size	0.09 x 0.07 x 0.03 mm ³
Theta range for data collection	1.93 to 27.54°.
Index ranges	-16 ≤ h ≤ 16, -22 ≤ k ≤ 26, -
24 ≤ l ≤ 19	
Reflections collected	49682
Independent reflections	10775 (R(int) = 0.0327)
Completeness to theta = 27.54°	99.7 %
Absorption correction	Semi-empirical from
equivalents	
Max. and min. transmission	0.9703 and 0.9146
Refinement method	Full-matrix least-squares on F ²
Data / restraints / parameters	10775 / 29 / 724
Goodness-of-fit on F ²	1.180
Final R indices [I > 2σ(I)]	R1 = 0.0386, wR2 = 0.0821
R indices (all data)	R1 = 0.0485, wR2 = 0.0875
Largest diff. peak and hole	0.641 and -0.519 e.Å ⁻³

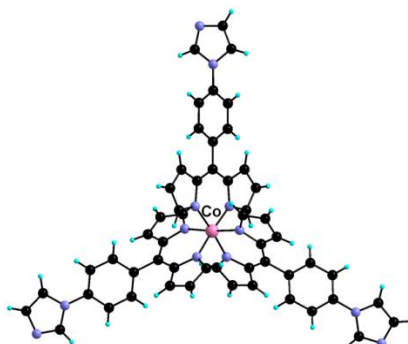
24. Compound 41

Complex [Bis(5-(4'-(1H-imidazol-1-yl)phenyl)-dipyrinato)Cu(II)]



Empirical formula	C ₇₅ H ₅₅ Cl ₉ Cu ₂ N ₁₆
Formula weight	1626.55
Temperature	173(2) K
Wavelength	0.71073 Å
Crystal system	Monoclinic
Space group	C2/c
Unit cell dimensions:	
a = 37.4262(12) Å	α = 90°.
b = 8.9610(3) Å	β = 130.2960(10)°.
c = 28.2529(16) Å	γ = 90°.
Volume	7227.0(5) Å ³
Z	4
Density (calculated)	1.495 mg/m ³
Absorption coefficient	0.978 mm ⁻¹
F(000)	3311
Crystal size	0.12 x 0.10 x 0.04 mm ³
Theta range for data collection	1.43 to 27.51°.
Index ranges	-38 ≤ h ≤ 48, -8 ≤ k ≤ 11, -
36 ≤ l ≤ 31	
Reflections collected	21262
Independent reflections	8279 (R(int) = 0.0320)
Completeness to theta = 27.51°	99.6 %
Absorption correction	Semi-empirical from
equivalents	
Max. and min. transmission	0.9619 and 0.8916
Refinement method	Full-matrix least-squares on F ²
Data / restraints / parameters	8279 / 0 / 487
Goodness-of-fit on F ²	1.031
Final R indices (I > 2σ(I))	R1 = 0.0618, wR2 = 0.1464
R indices (all data)	R1 = 0.0835, wR2 = 0.1668
Largest diff. peak and hole	1.477 and -1.485 e.Å ⁻³

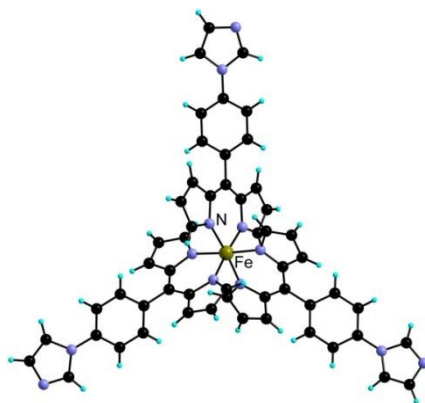
25. Compound 43

Complex [Tris(5-(4'-(1H-imidazol-1-yl)phenyl)-dipyrrinato)Co(III)]

Empirical formula	C ₆₃ H ₆₃ Co N ₁₂ O ₃
Formula weight	1095.18
Temperature	173(2) K
Wavelength	0.71073 Å
Crystal system	Triclinic
Space group	P-1
Unit cell dimensions:	
a = 13.0039(5) Å	$\alpha = 99.0420(10)^\circ$.
b = 13.1505(5) Å	$\beta = 104.7310(10)^\circ$.
c = 18.1471(6) Å	$\gamma = 105.1440(10)^\circ$.
Volume	2812.74(18) Å ³
Z	2
Density (calculated)	1.293 mg/m ³
Absorption coefficient	0.363 mm ⁻¹
F(000)	1152
Crystal size	0.12 x 0.10 x 0.08 mm ³
Theta range for data collection	1.71 to 27.56°.
Index ranges	-16 ≤ h ≤ 16, -17 ≤ k ≤ 17, -
23 ≤ l ≤ 21	
Reflections collected	33649
Independent reflections	12624 (R(int) = 0.0410)
Completeness to theta = 27.56°	97.2 %
Absorption correction	Semi-empirical from
equivalents	
Max. and min. transmission	0.9715 and 0.9577
Refinement method	Full-matrix least-squares on F ²
Data / restraints / parameters	12624 / 2 / 707
Goodness-of-fit on F ²	1.181
Final R indices (I > 2σ(I))	R1 = 0.0877, wR2 = 0.2156
R indices (all data)	R1 = 0.1175, wR2 = 0.2343
Largest diff. peak and hole	1.026 and -0.636 e. Å ⁻³

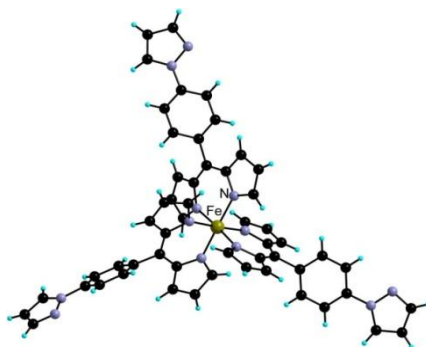
26. Compound 44

Complex [Tris(5-(4'-(1H-imidazol-1-yl)phenyl)-dipyrrinato)Fe(III)]



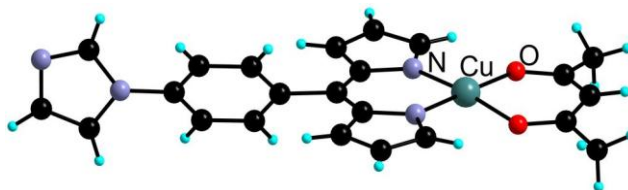
Empirical formula	C ₅₄ H ₃₉ Fe N ₁₂
Formula weight	911.84
Temperature	173(2) K
Wavelength	0.71073 Å
Crystal system	Triclinic
Space group	P-1
Unit cell dimensions:	
a = 12.6205(6) Å	$\alpha = 102.0340(10)^\circ$.
b = 12.9679(5) Å	$\beta = 104.3460(10)^\circ$.
c = 18.6156(8) Å	$\gamma = 109.4160(10)^\circ$.
Volume	2639.0(2) Å ³
Z	2
Density (calculated)	1.148 mg/m ³
Absorption coefficient	0.331 mm ⁻¹
F(000)	946
Crystal size	0.10 x 0.08 x 0.05 mm ³
Theta range for data collection	1.82 to 27.55°.
Index ranges	-16 ≤ h ≤ 15, -16 ≤ k ≤ 16, -
24 ≤ l ≤ 24	
Reflections collected	28454
Independent reflections	11849 [R(int) = 0.0295]
Completeness to theta = 27.55°	97.1 %
Absorption correction	Semi-empirical from
equivalents	
Max. and min. transmission	0.9836 and 0.9676
Refinement method	Full-matrix least-squares on F ²
Data / restraints / parameters	11849 / 0 / 605
Goodness-of-fit on F ²	1.120
Final R indices [I > 2σ(I)]	R1 = 0.0540, wR2 = 0.1619
R indices (all data)	R1 = 0.0752, wR2 = 0.1703
Largest diff. peak and hole	0.541 and -0.415 e.Å ⁻³

27. Compound 45

Complex [Tris(5-(4'-(1H-pyrazol-1-yl)phenyl)-dipyrrinato)Fe(III)]

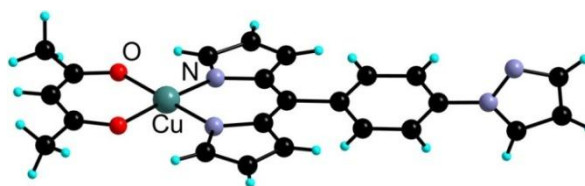
Empirical formula	C ₅₄ H ₃₉ Fe N ₁₂
Formula weight	911.84
Temperature	173(2) K
Wavelength	0.71073 Å
Crystal system	Monoclinic
Space group	P2(1)/n
Unit cell dimensions:	
a = 15.6390(5) Å	$\alpha = 90^\circ$.
b = 9.7211(3) Å	$\beta = 92.1960(10)^\circ$.
c = 28.7144(12) Å	$\gamma = 90^\circ$.
Volume	4362.2(3) Å ³
Z	4
Density (calculated)	1.388 mg/m ³
Absorption coefficient	0.401 mm ⁻¹
F(000)	1892
Crystal size	0.15 x 0.07 x 0.07 mm ³
Theta range for data collection	1.42 to 27.50°.
Index ranges	-15 ≤ h ≤ 20, -12 ≤ k ≤ 8, -
37 ≤ l ≤ 35	
Reflections collected	24034
Independent reflections	10008 (R(int) = 0.0389)
Completeness to theta = 27.50°	99.8 %
Absorption correction	Semi-empirical from
equivalents	
Max. and min. transmission	0.9725 and 0.9423
Refinement method	Full-matrix least-squares on F ²
Data / restraints / parameters	10008 / 0 / 604
Goodness-of-fit on F ²	1.076
Final R indices (I > 2σ(I))	R1 = 0.0505, wR2 = 0.1209
R indices (all data)	R1 = 0.0836, wR2 = 0.1536
Largest diff. peak and hole	0.373 and -0.523 e.Å ⁻³

28. Compound 46

Complex $[(5-(4'-(1H-imidazol-1-yl)phenyl)-dipyrinato)acac]Cu(II)$ 

Empirical formula	C ₂₃ H ₂₀ Cu N ₄ O ₂
Formula weight	447.99
Temperature	173(2) K
Wavelength	0.71073 Å
Crystal system	Triclinic
Space group	P-1
Unit cell dimensions:	
a = 8.6097(2) Å	$\alpha = 82.1660(10)^\circ$.
b = 10.6165(3) Å	$\beta = 87.9790(10)^\circ$.
c = 11.0140(3) Å	$\gamma = 88.6640(10)^\circ$.
Volume	996.54(5) Å ³
Z	2
Density (calculated)	1.493 mg/m ³
Absorption coefficient	1.124 mm ⁻¹
F(000)	462
Crystal size	0.15 x 0.12 x 0.06 mm ³
Theta range for data collection	1.94 to 27.54°.
Index ranges	-11 ≤ h ≤ 11, -13 ≤ k ≤ 13, -
11 ≤ l ≤ 14	
Reflections collected	12188
Independent reflections	4525 (R(int) = 0.0249)
Completeness to theta = 27.54°	98.3 %
Absorption correction	Semi-empirical from
equivalents	
Max. and min. transmission	0.9356 and 0.8495
Refinement method	Full-matrix least-squares on F ²
Data / restraints / parameters	4525 / 0 / 273
Goodness-of-fit on F ²	1.072
Final R indices (I > 2σ(I))	R1 = 0.0339, wR2 = 0.0914
R indices (all data)	R1 = 0.0392, wR2 = 0.0970
Largest diff. peak and hole	0.629 and -0.309 e.Å ⁻³

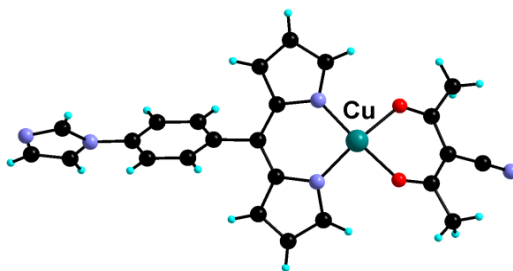
29. Compound 47

Complex [((5-(4'-(1H-imidazol-1-yl)phenyl)-dipyrrinato)acac)Cu(II)]

Empirical formula	C ₂₃ H ₂₀ Cu N ₄ O ₂
Formula weight	447.97
Temperature	173(2) K
Wavelength	0.71073 Å
Crystal system	Monoclinic
Space group	P2(1)/c
Unit cell dimensions:	
a = 14.0618(6) Å	$\alpha = 90^\circ$
b = 17.0890(8) Å	$\beta = 107.739(2)^\circ$
c = 8.8153(4) Å	$\gamma = 90^\circ$
Volume	2017.62(16) Å ³
Z	4
Density (calculated)	1.475 mg/m ³
Absorption coefficient	1.110 mm ⁻¹
F(000)	924
Crystal size	0.20 x 0.18 x 0.03 mm ³
Theta range for data collection	1.52 to 27.52°
Index ranges	-18 ≤ h ≤ 17, -17 ≤ k ≤ 22, -
11 ≤ l ≤ 8	
Reflections collected	13780
Independent reflections	4593 (R(int) = 0.0309)
Completeness to theta = 27.52°	99.1 %
Absorption correction equivalents	Semi-empirical from 0.9675 and 0.8085
Max. and min. transmission	
Refinement method	Full-matrix least-squares on F ²
Data / restraints / parameters	4593 / 0 / 273
Goodness-of-fit on F ²	1.100
Final R indices (I > 2σ(I))	R1 = 0.0403, wR2 = 0.0975
R indices (all data)	R1 = 0.0528, wR2 = 0.1163
Largest diff. peak and hole	0.447 and -0.415 e. Å ⁻³

30. Compound 48

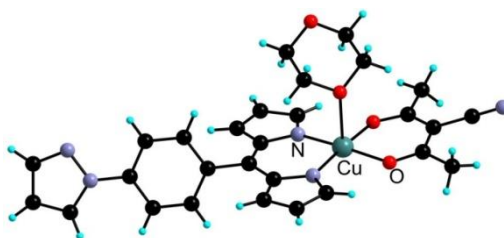
Complex [[(5-(4'-(1H-imidazol-1-yl)-phenyl)-dipyrrinato)acacnitrillo)Cu(II)]



Empirical formula	C ₂₄ H ₁₉ Cu N ₅ O ₂
Formula weight	472.98
Temperature	173(2) K
Wavelength	0.71073 Å
Crystal system	Monoclinic
Space group	P2(1)/c
Unit cell dimensions:	
a = 9.0755(3) Å	$\alpha = 90^\circ$
b = 21.5983(6) Å	$\beta = 94.0810(10)^\circ$
c = 21.3201(6) Å	$\gamma = 90^\circ$
Volume	4168.5(2) Å ³
Z	8
Density (calculated)	1.507 mg/m ³
Absorption coefficient	1.081 mm ⁻¹
F(000)	1944
Crystal size	0.11 x 0.09 x 0.02 mm ³
Theta range for data collection	1.34 to 27.52°
Index ranges	-11 ≤ h ≤ 10, -28 ≤ k ≤ 28, -
27 ≤ l ≤ 27	
Reflections collected	39063
Independent reflections	9592 (R(int) = 0.0398)
Completeness to theta = 27.52°	99.9 %
Absorption correction	Semi-empirical from
equivalents	
Max. and min. transmission	0.9787 and 0.8904
Refinement method	Full-matrix least-squares on F ²
Data / restraints / parameters	9592 / 0 / 581
Goodness-of-fit on F ²	1.082
Final R indices (I > 2σ(I))	R1 = 0.0385, wR2 = 0.0998
R indices (all data)	R1 = 0.0623, wR2 = 0.1161
Largest diff. peak and hole	0.808 and -0.498 e. Å ⁻³

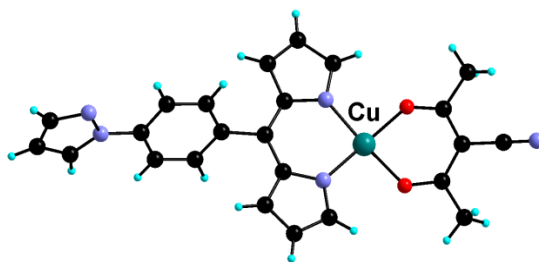
31. Compound 49a

Complex [((5-(4'-(1H-pyrazol-1-yl)-phenyl)-dipyrinato)acacnitrillo)Cu(II)]



Empirical formula	C ₂₈ H ₂₇ Cu N ₅ O ₄
Formula weight	561.10
Temperature	173(2) K
Wavelength	0.71073 Å
Crystal system	Triclinic
Space group	P-1
Unit cell dimensions:	
a = 7.7529(2) Å	$\alpha = 84.4710(10)^\circ$
b = 11.9322(2) Å	$\beta = 74.8250(10)^\circ$
c = 14.8002(4) Å	$\gamma = 72.3840(10)^\circ$
Volume	1259.23(5) Å ³
Z	2
Density (calculated)	1.480 mg/m ³
Absorption coefficient	0.913 mm ⁻¹
F(000)	582
Crystal size	0.18 x 0.11 x 0.11 mm ³
Theta range for data collection	2.27 to 30.09°
Index ranges	-10 ≤ h ≤ 10, -16 ≤ k ≤ 16, -
20 ≤ l ≤ 20	
Reflections collected	26130
Independent reflections	7313 (R(int) = 0.0261)
Completeness to theta = 30.09°	99.1 %
Absorption correction	Semi-empirical from
equivalents	
Max. and min. transmission	0.9063 and 0.8529
Refinement method	Full-matrix least-squares on F ²
Data / restraints / parameters	7313 / 0 / 345
Goodness-of-fit on F ²	1.085
Final R indices (I > 2σ(I))	R1 = 0.0353, wR2 = 0.0857
R indices (all data)	R1 = 0.0409, wR2 = 0.0897
Largest diff. peak and hole	0.507 and -0.300 e.Å ⁻³

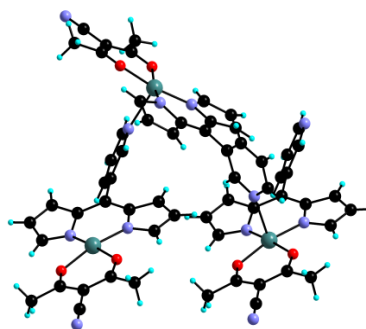
32. Compound 49b

Complex **[[((5-(4'-(1H-pyrazol-1-yl)-phenyl)-dipyrinato)acacnitrillo)Cu(II)]**

Empirical formula	C ₂₄ H ₁₉ Cu N ₅ O ₂
Formula weight	472.98
Temperature	173(2) K
Wavelength	0.71073 Å
Crystal system	Monoclinic
Space group	P2(1)
Unit cell dimensions:	
a = 7.0712(3) Å	α = 90°
b = 15.8916(7) Å	β = 105.4930(10)°
c = 9.4970(4) Å	γ = 90°
Volume	1028.42(8) Å ³
Z	2
Density (calculated)	1.527 mg/m ³
Absorption coefficient	1.095 mm ⁻¹
F(000)	486
Crystal size	0.15 x 0.08 x 0.02 mm ³
Theta range for data collection	2.56 to 27.46°
Index ranges	-9 ≤ h ≤ 8, -20 ≤ k ≤ 16, -
9 ≤ l ≤ 12	
Reflections collected	11992
Independent reflections	4294 (R(int) = 0.0280)
Completeness to theta = 27.46°	99.6 %
Absorption correction	Semi-empirical from
equivalents	
Max. and min. transmission	0.9784 and 0.8530
Refinement method	Full-matrix least-squares on F ²
Data / restraints / parameters	4294 / 1 / 291
Goodness-of-fit on F ²	1.096
Final R indices (I > 2σ(I))	R ₁ = 0.0272, wR ₂ = 0.0661
R indices (all data)	R ₁ = 0.0290, wR ₂ = 0.0678
Absolute structure parameter	0.010(9)
Largest diff. peak and hole	0.255 and -0.219 e.Å ⁻³

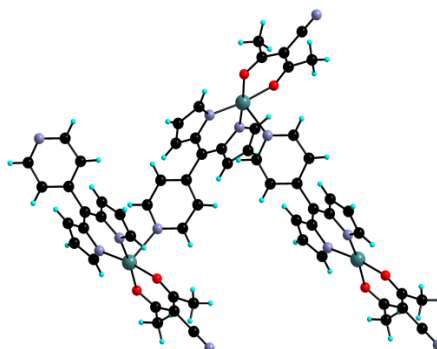
33. Compound 50

Complex [((5-pyridin-3-yl-dipyrinato)acacnitrillo)Cu(II)]



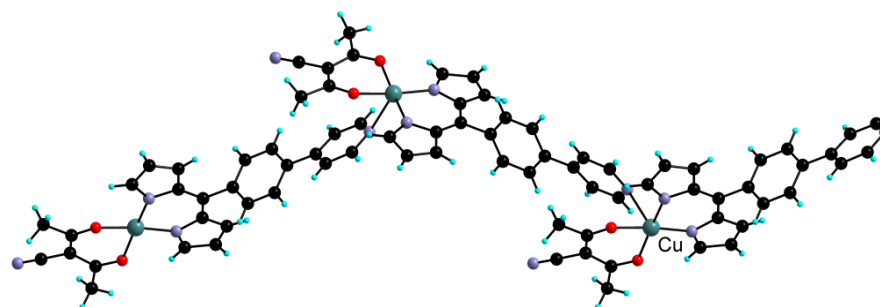
Empirical formula	C ₂₀ H ₁₆ Cu N ₄ O ₂
Formula weight	407.91
Temperature	173(2) K
Wavelength	0.71073 Å
Crystal system	Monoclinic
Space group	P2(1)/c
Unit cell dimensions:	
a = 20.4333(10) Å	$\alpha = 90^\circ$
b = 8.5181(4) Å	$\beta = 99.825(2)^\circ$
c = 21.5238(10) Å	$\gamma = 90^\circ$
Volume	3691.3(3) Å ³
Z	8
Density (calculated)	1.468 mg/m ³
Absorption coefficient	1.206 mm ⁻¹
F(000)	1672
Crystal size	0.13 x 0.10 x 0.06 mm ³
Theta range for data collection	1.92 to 27.53°
Index ranges	-26 ≤ h ≤ 25, -11 ≤ k ≤ 10, -
27 ≤ l ≤ 24	
Reflections collected	29635
Independent reflections	8451 [R(int) = 0.0349]
Completeness to theta = 27.53°	99.5 %
Absorption correction	Semi-empirical from
equivalents	
Max. and min. transmission	0.9312 and 0.8590
Refinement method	Full-matrix least-squares on F ²
Data / restraints / parameters	8451 / 0 / 485
Goodness-of-fit on F ²	1.093
Final R indices [I > 2σ(I)]	R1 = 0.0537, wR2 = 0.1378
R indices (all data)	R1 = 0.0741, wR2 = 0.1464
Largest diff. peak and hole	0.797 and -0.677 e.Å ⁻³

34. Compound 51

Complex **[[((5-pyridin-4-yl-dipyrinato)acacnitrillo)Cu(II)]**

Empirical formula	C ₂₀ H ₁₆ Cu N ₄ O ₂
Formula weight	407.92
Temperature	173(2) K
Wavelength	0.71073 Å
Crystal system	Monoclinic
Space group	C2/c
Unit cell dimensions:	
a = 22.1808(8) Å	α = 90°
b = 11.7623(5) Å	β = 108.2100(10)°
c = 15.1987(6) Å	γ = 90°
Volume	3766.7(3) Å ³
Z	8
Density (calculated)	1.439 mg/m ³
Absorption coefficient	1.182 mm ⁻¹
F(000)	1672
Crystal size	0.12 x 0.09 x 0.08 mm ³
Theta range for data collection	2.60 to 27.50°
Index ranges	-18 ≤ h ≤ 28, -15 ≤ k ≤ 13, -
18 ≤ l ≤ 19	
Reflections collected	12133
Independent reflections	4314 [R(int) = 0.0353]
Completeness to theta = 27.50°	99.7 %
Absorption correction	Semi-empirical from
equivalents	
Max. and min. transmission	0.9114 and 0.8712
Refinement method	Full-matrix least-squares on F ²
Data / restraints / parameters	4314 / 0 / 246
Goodness-of-fit on F ²	1.086
Final R indices [I > 2σ(I)]	R1 = 0.0424, wR2 = 0.0921
R indices (all data)	R1 = 0.0539, wR2 = 0.0977
Largest diff. peak and hole	0.399 and -0.316 e.Å ⁻³

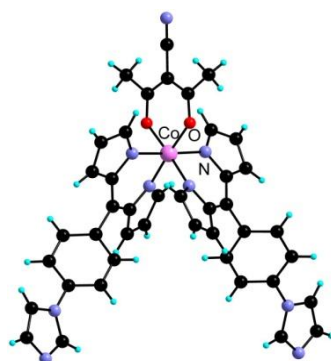
35. Compound 52

Complex **[[5-(4'-(pyridin-4-yl)-phenyl)-dipyrrinato)acacnitrillo]Cu(II)]**

Empirical formula	C ₂₆ H ₂₀ Cu N ₄ O ₂
Formula weight	484.00
Temperature	173(2) K
Wavelength	0.71073 Å
Crystal system	Monoclinic
Space group	P2(1)/c
Unit cell dimensions:	
a = 12.6114(2) Å	$\alpha = 90^\circ$.
b = 15.2947(3) Å	$\beta = 100.9400(10)^\circ$.
c = 11.4970(2) Å	$\gamma = 90^\circ$.
Volume	2177.33(7) Å ³
Z	4
Density (calculated)	1.476 mg/m ³
Absorption coefficient	1.035 mm ⁻¹
F(000)	996
Crystal size	0.10 x 0.05 x 0.03 mm ³
Theta range for data collection	2.12 to 27.53°.
Index ranges	-16 ≤ h ≤ 16, -19 ≤ k ≤ 19, -
13 ≤ l ≤ 14	
Reflections collected	22005
Independent reflections	4929 [R(int) = 0.0277]
Completeness to theta = 27.53°	98.3 %
Absorption correction	Semi-empirical from
equivalents	
Max. and min. transmission	0.9696 and 0.9036
Refinement method	Full-matrix least-squares on F ²
Data / restraints / parameters	4929 / 0 / 300
Goodness-of-fit on F ²	1.054
Final R indices [I > 2σ(I)]	R1 = 0.0315, wR2 = 0.0815
R indices (all data)	R1 = 0.0366, wR2 = 0.0860
Largest diff. peak and hole	0.364 and -0.298 e.Å ⁻³

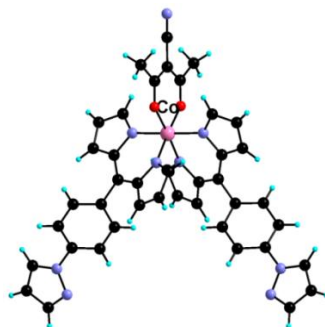
36. Compound 53

Complex [(bis(5-(4'-(1H-imidazol-1-yl)phenyl)-dipyrrinato)acacnitrillo)Co(III)]



Empirical formula	C ₄₆ H ₄₀ Co N ₉ O ₄
Formula weight	841.80
Temperature	173(2) K
Wavelength	0.71073 Å
Crystal system	Orthorhombic
Space group	Pbcn
Unit cell dimensions:	
a = 17.5711(19) Å	α = 90°
b = 28.246(3) Å	β = 90°
c = 8.0465(10) Å	γ = 90°
Volume	3993.6(8) Å ³
Z	4
Density (calculated)	1.400 mg/m ³
Absorption coefficient	0.488 mm ⁻¹
F(000)	1752
Crystal size	0.10 x 0.05 x 0.01 mm ³
Theta range for data collection	1.36 to 27.54°
Index ranges	-17 ≤ h ≤ 22, -36 ≤ k ≤ 36, -
10 ≤ l ≤ 9	
Reflections collected	20627
Independent reflections	4592 (R(int) = 0.0601)
Completeness to theta = 27.54°	99.4 %
Absorption correction	Semi-empirical from
equivalents	
Max. and min. transmission	0.9951 and 0.9528
Refinement method	Full-matrix least-squares on F ²
Data / restraints / parameters	4592 / 3 / 278
Goodness-of-fit on F ²	1.199
Final R indices (I > 2σ(I))	R ₁ = 0.0727, wR ₂ = 0.1694
R indices (all data)	R ₁ = 0.1129, wR ₂ = 0.1971
Largest diff. peak and hole	1.019 and -0.693 e.Å ⁻³

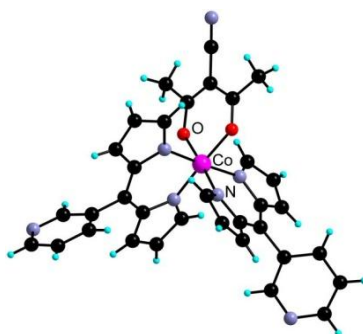
37. Compound 54

Complex [(bis(5-(4'-(1H-pyrazol-1-yl)phenyl)-dipyrinato)acacnitrillo)Co(III)]

Empirical formula	C ₄₆ H ₄₀ Co N ₉ O ₃
Formula weight	825.80
Temperature	173(2) K
Wavelength	0.71073 Å
Crystal system	Orthorhombic
Space group	Pbcn
Unit cell dimensions:	
a = 17.4672(5) Å	$\alpha = 90^\circ$
b = 27.9203(9) Å	$\beta = 90^\circ$
c = 8.1112(3) Å	$\gamma = 90^\circ$
Volume	3955.7(2) Å ³
Z	4
Density (calculated)	1.387 mg/m ³
Absorption coefficient	0.489 mm ⁻¹
F(000)	1720
Crystal size	0.12 x 0.07 x 0.04 mm ³
Theta range for data collection	1.38 to 27.50°
Index ranges	-22 ≤ h ≤ 19, -36 ≤ k ≤ 35, -
10 ≤ l ≤ 9	
Reflections collected	72913
Independent reflections	4514 (R(int) = 0.0508)
Completeness to theta = 27.50°	99.1 %
Absorption correction	Semi-empirical from
equivalents	
Max. and min. transmission	0.9807 and 0.9436
Refinement method	Full-matrix least-squares on F ²
Data / restraints / parameters	4514 / 2 / 260
Goodness-of-fit on F ²	1.136
Final R indices (I > 2σ(I))	R1 = 0.0514, wR2 = 0.1431
R indices (all data)	R1 = 0.0793, wR2 = 0.1708
Largest diff. peak and hole	1.491 and -0.779 e.Å ⁻³

38. Compound 55

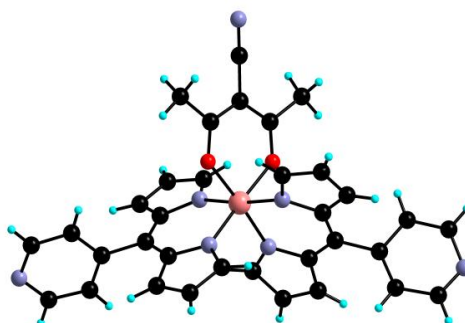
Complex [(bis(5-(pyridin-3-yl)phenyl)-dipyrinato)acacnitrilo)Co(III)]



Empirical formula	C ₆₉ H ₅₃ Cl ₃ Co ₂ N ₁₄ O ₄
Formula weight	1366.46
Temperature	173(2) K
Wavelength	0.71073 Å
Crystal system	Triclinic
Space group	P-1
Unit cell dimensions:	
a = 8.0265(2) Å	$\alpha = 99.6540(10)^\circ$
b = 9.5883(2) Å	$\beta = 90.6380(10)^\circ$
c = 20.0801(5) Å	$\gamma = 96.9870(10)^\circ$
Volume	1511.39(6) Å ³
Z	1
Density (calculated)	1.501 mg/m ³
Absorption coefficient	0.747 mm ⁻¹
F(000)	702
Crystal size	0.16 x 0.10 x 0.04 mm ³
Theta range for data collection	2.06 to 27.70°
Index ranges	-10 ≤ h ≤ 10, -12 ≤ k ≤ 12, -
25 ≤ l ≤ 26	
Reflections collected	18888
Independent reflections	6968 [R(int) = 0.0260]
Completeness to theta = 27.70°	98.0 %
Absorption correction	Semi-empirical from
equivalents	
Max. and min. transmission	0.9707 and 0.8899
Refinement method	Full-matrix least-squares on F ²
Data / restraints / parameters	6968 / 2 / 423
Goodness-of-fit on F ²	1.044
Final R indices [I > 2σ(I)]	R1 = 0.0486, wR2 = 0.1327
R indices (all data)	R1 = 0.0544, wR2 = 0.1368
Largest diff. peak and hole	1.565 and -1.393 e.Å ⁻³

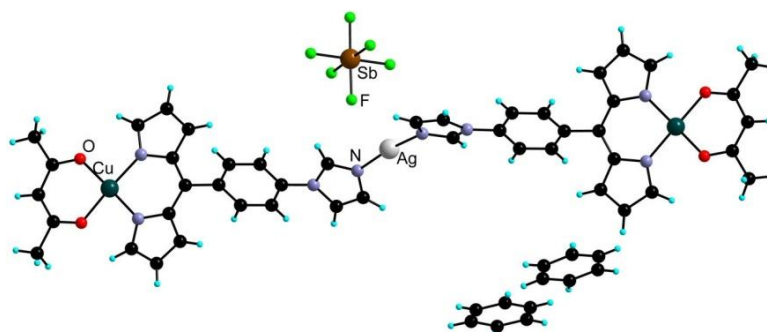
39. Compound 56

Complex [(bis(5-(pyridin-4-yl)phenyl)-dipyrinato)acacnitrillo)Co(III)]



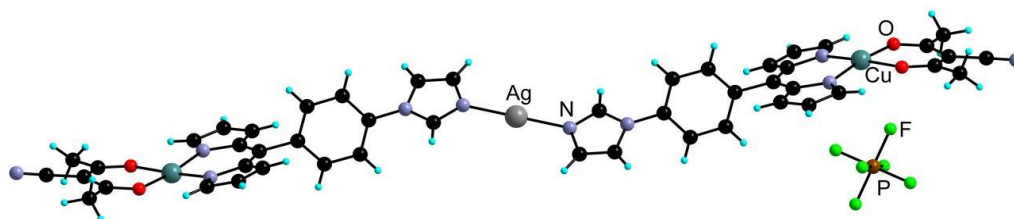
Empirical formula	C70 H58 Co2 N14 O6
Formula weight	1309.16
Temperature	173(2) K
Wavelength	0.71073 Å
Crystal system	Triclinic
Space group	P-1
Unit cell dimensions:	
a = 13.9897(4) Å	$\alpha = 102.396(2)^\circ$
b = 14.8513(5) Å	$\beta = 100.227(2)^\circ$
c = 16.8446(9) Å	$\gamma = 108.7790(10)^\circ$
Volume	3118.9(2) Å ³
Z	2
Density (calculated)	1.394 mg/m ³
Absorption coefficient	0.598 mm ⁻¹
F(000)	1356
Crystal size	0.15 x 0.04 x 0.01 mm ³
Theta range for data collection	1.28 to 27.62°
Index ranges	-18 ≤ h ≤ 18, -19 ≤ k ≤ 18, -
15 ≤ l ≤ 21	
Reflections collected	37451
Independent reflections	14235 [R(int) = 0.0355]
Completeness to theta = 27.62°	98.3 %
Absorption correction	Semi-empirical from
equivalents	
Max. and min. transmission	0.9940 and 0.9156
Refinement method	Full-matrix least-squares on F ²
Data / restraints / parameters	14235 / 2 / 803
Goodness-of-fit on F ²	1.086
Final R indices [I > 2σ(I)]	R1 = 0.0590, wR2 = 0.1495
R indices (all data)	R1 = 0.0756, wR2 = 0.1698
Largest diff. peak and hole	1.564 and -0.693 e.Å ⁻³

40. Compound 57

Heterometallic complex: [(Ag((acac)Cu(Im-Ph-DPM))₂)(SbF₆)](C₆H₆)₂

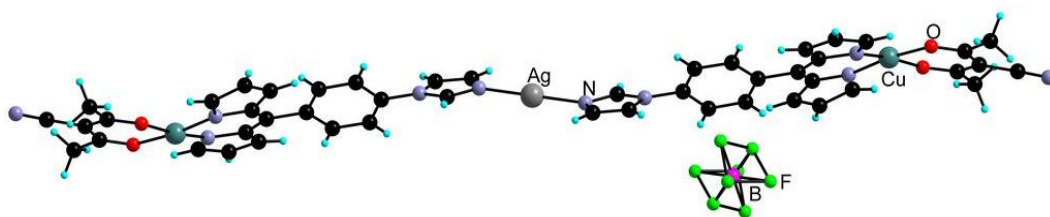
Empirical formula	C ₅₈ H ₅₂ Ag Cu ₂ F ₆ N ₈ O ₄ Sb
Formula weight	1395.78
Temperature	173(2) K
Wavelength	0.71073 Å
Crystal system	Triclinic
Space group	P-1
Unit cell dimensions:	
a = 10.2596(2) Å	α = 110.1590(10)°
b = 15.4490(3) Å	β = 97.3400(10)°
c = 19.2748(4) Å	γ = 95.1390(10)°
Volume	2814.97(10) Å ³
Z	2
Density (calculated)	1.647 mg/m ³
Absorption coefficient	1.637 mm ⁻¹
F(000)	1396
Crystal size	0.14 x 0.08 x 0.07 mm ³
Theta range for data collection	1.14 to 27.58°
Index ranges	-13 ≤ h ≤ 13, -20 ≤ k ≤ 20, -
24 ≤ l ≤ 25	
Reflections collected	33360
Independent reflections	12742 (R(int) = 0.0342)
Completeness to theta = 27.58°	97.9 %
Absorption correction	Semi-empirical from
equivalents	
Max. and min. transmission	0.8940 and 0.8033
Refinement method	Full-matrix least-squares on F ²
Data / restraints / parameters	12742 / 0 / 725
Goodness-of-fit on F ²	1.129
Final R indices (I > 2σ(I))	R ₁ = 0.0452, wR ₂ = 0.1070
R indices (all data)	R ₁ = 0.0649, wR ₂ = 0.1332
Largest diff. peak and hole	1.371 and -0.928 e.Å ⁻³

41. Compound 58

Heterobimetallic network: $\{[(Ag((acacCN)Cu(Im-Ph-DPM))_2)](PF_6)\}_\infty$ (THF)

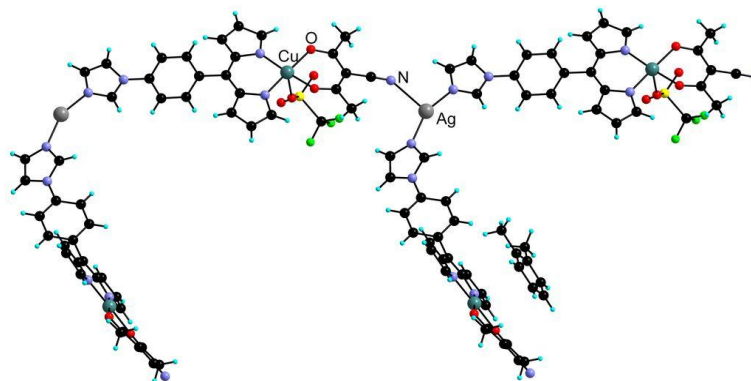
Empirical formula	C ₅₂ H ₄₆ Ag Cu ₂ F ₆ N ₁₀ O ₅ P
Formula weight	1270.91
Temperature	173(2) K
Wavelength	0.71073 Å
Crystal system	Triclinic
Space group	P-1
Unit cell dimensions:	
a = 6.8023(7) Å	$\alpha = 82.210(4)^\circ$.
b = 8.5991(10) Å	$\beta = 81.502(4)^\circ$.
c = 22.727(3) Å	$\gamma = 79.614(4)^\circ$.
Volume	1285.1(2) Å ³
Z	1
Density (calculated)	1.642 mg/m ³
Absorption coefficient	1.309 mm ⁻¹
F(000)	642
Crystal size	0.15 x 0.06 x 0.02 mm ³
Theta range for data collection	1.82 to 27.58°.
Index ranges	-8 ≤ h ≤ 6, -11 ≤ k ≤ 11, -
29 ≤ l ≤ 29	
Reflections collected	12020
Independent reflections	5716 (R(int) = 0.0318)
Completeness to theta = 27.58°	96.0 %
Absorption correction	Semi-empirical from
equivalents	
Max. and min. transmission	0.9743 and 0.8278
Refinement method	Full-matrix least-squares on F ²
Data / restraints / parameters	5716 / 5 / 354
Goodness-of-fit on F ²	1.016
Final R indices (I > 2σ(I))	R1 = 0.0456, wR2 = 0.0991
R indices (all data)	R1 = 0.0772, wR2 = 0.1099
Largest diff. peak and hole	0.729 and -0.594 e.Å ⁻³

42. Compound 59

Heterobimetallic network: $\{[(Ag((acacCN)Cu(Im-Ph-DPM))_2)](BF_4)\}_\infty(Benzene)$ 

Empirical formula	C ₅₄ H ₄₄ Ag B Cu ₂ F ₄ N ₁₀ O ₄
Formula weight	1218.78
Temperature	173(2) K
Wavelength	0.71073 Å
Crystal system	Triclinic
Space group	P-1
Unit cell dimensions:	
a = 6.8931(3) Å	$\alpha = 79.907(2)^\circ$
b = 8.5345(4) Å	$\beta = 83.993(2)^\circ$
c = 22.8014(10) Å	$\gamma = 78.969(2)^\circ$
Volume	1292.71(10) Å ³
Z	1
Density (calculated)	1.566 mg/m ³
Absorption coefficient	1.261 mm ⁻¹
F(000)	616
Crystal size	0.11 x 0.11 x 0.03 mm ³
Theta range for data collection	1.82 to 27.45°
Index ranges	-8 ≤ h ≤ 8, -10 ≤ k ≤ 11, -
21 ≤ l ≤ 29	
Reflections collected	23641
Independent reflections	5824 (R(int) = 0.0267)
Completeness to theta = 27.45°	98.8 %
Absorption correction	Semi-empirical from
equivalents	
Max. and min. transmission	0.9631 and 0.8737
Refinement method	Full-matrix least-squares on F ²
Data / restraints / parameters	5824 / 0 / 366
Goodness-of-fit on F ²	1.033
Final R indices (I > 2σ(I))	R1 = 0.0302, wR2 = 0.0723
R indices (all data)	R1 = 0.0384, wR2 = 0.0755
Largest diff. peak and hole	0.408 and -0.340 e. Å ⁻³

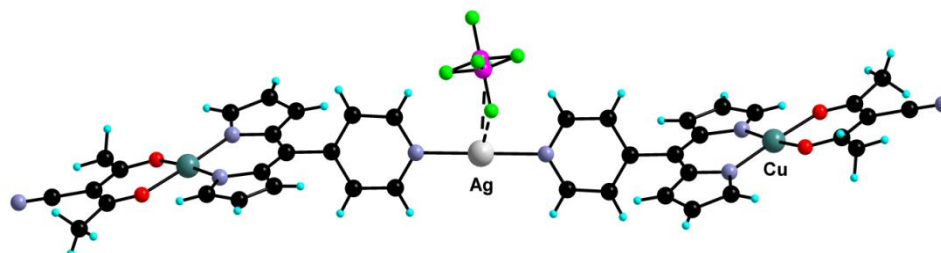
43. Compound 60

Heterobimetallic network: $\{[(Ag((acacCN)Cu(Im-Ph-DPM))_2)](OTf)\}_\infty(o\text{-xylene})$ 

Empirical formula	C ₅₇ H ₄₈ Ag Cu ₂ F ₃ N ₁₀ O ₇ S
Formula weight	1309.09
Temperature	173(2) K
Wavelength	0.71073 Å
Crystal system	Triclinic
Space group	P-1
Unit cell dimensions:	
a = 11.9313(2) Å	$\alpha = 74.9010(10)^\circ$
b = 12.1710(3) Å	$\beta = 82.2040(10)^\circ$
c = 21.7466(5) Å	$\gamma = 64.6080(10)^\circ$
Volume	2753.35(10) Å ³
Z	2
Density (calculated)	1.579 mg/m ³
Absorption coefficient	1.229 mm ⁻¹
F(000)	1328
Crystal size	0.10 x 0.10 x 0.07 mm ³
Theta range for data collection	1.90 to 27.50°
Index ranges	-15 ≤ h ≤ 15, -15 ≤ k ≤ 15, -
26 ≤ l ≤ 28	
Reflections collected	31895
Independent reflections	12394 (R(int) = 0.0280)
Completeness to theta = 27.50°	97.9 %
Absorption correction	Semi-empirical from
equivalents	
Max. and min. transmission	0.9189 and 0.8870
Refinement method	Full-matrix least-squares on F ²
Data / restraints / parameters	12394 / 0 / 730
Goodness-of-fit on F ²	1.172
Final R indices (I > 2σ(I))	R1 = 0.0464, wR2 = 0.1131
R indices (all data)	R1 = 0.0552, wR2 = 0.1191
Largest diff. peak and hole	0.875 and -1.187 e. Å ⁻³

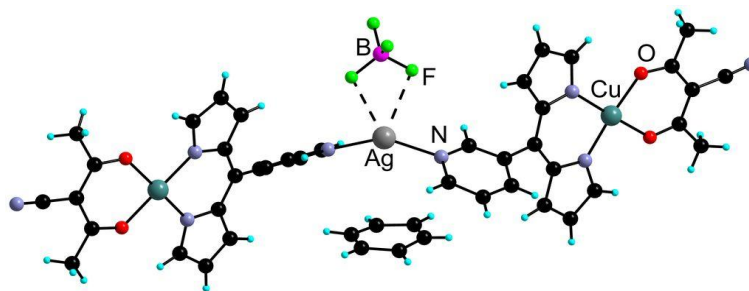
44. Compound 61

Heterobimetallic network: $\{[(\text{Ag}((\text{acacCN})\text{Cu}(4\text{-Py-DPM}))_2)](\text{BF}_4)\}_\infty$



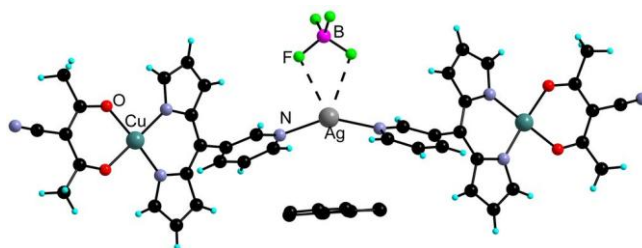
Empirical formula	C ₄₀ H ₃₂ Ag B Cu ₂ F ₄ N ₈ O ₄
Formula weight	1010.50
Temperature	173(2) K
Wavelength	0.71073 Å
Crystal system	Monoclinic
Space group	P2(1)/n
Unit cell dimensions:	
a = 7.2622(2) Å	α = 90°
b = 21.5157(6) Å	β = 91.519(2)°
c = 12.3601(4) Å	γ = 90°
Volume	1930.60(10) Å ³
Z	2
Density (calculated)	1.738 mg/m ³
Absorption coefficient	1.668 mm ⁻¹
F(000)	1012
Crystal size	0.12 x 0.10 x 0.07 mm ³
Theta range for data collection	1.90 to 27.52°
Index ranges	-9 ≤ h ≤ 9, -27 ≤ k ≤ 27, -
16 ≤ l ≤ 16	
Reflections collected	35838
Independent reflections	4413 [R(int) = 0.0279]
Completeness to theta = 27.52°	99.1 %
Absorption correction	Semi-empirical from
equivalents	
Max. and min. transmission	0.8922 and 0.8249
Refinement method	Full-matrix least-squares on F ²
Data / restraints / parameters	4413 / 0 / 288
Goodness-of-fit on F ²	1.114
Final R indices [I > 2σ(I)]	R ₁ = 0.0426, wR ₂ = 0.1085
R indices (all data)	R ₁ = 0.0460, wR ₂ = 0.1114
Largest diff. peak and hole	2.410 and -0.987 e.Å ⁻³

45. Compound 62a

Heterobimetallic network: $\{[(Ag((acacCN)Cu(3-Py-DPM))_2)](BF_4)\}_\infty(\text{Benzene})$ 

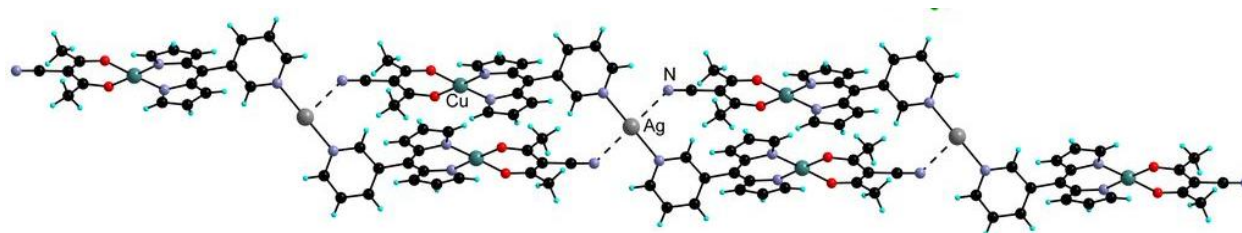
Empirical formula	C ₄₆ H ₃₈ Ag B Cu ₂ F ₄ N ₈ O ₄
Formula weight	1088.63
Temperature	173(2) K
Wavelength	0.71073 Å
Crystal system	Monoclinic
Space group	C2/c
Unit cell dimensions:	
a = 21.0203(7) Å	$\alpha = 90^\circ$.
b = 19.2974(7) Å	$\beta = 131.0430(10)^\circ$.
c = 14.3301(5) Å	$\gamma = 90^\circ$.
Volume	4384.1(3) Å ³
Z	4
Density (calculated)	1.649 mg/m ³
Absorption coefficient	1.476 mm ⁻¹
F(000)	2192
Crystal size	0.20 x 0.07 x 0.06 mm ³
Theta range for data collection	1.66 to 27.52°.
Index ranges	-20 ≤ h ≤ 27, -23 ≤ k ≤ 25, -
18 ≤ l ≤ 18	
Reflections collected	14782
Independent reflections	5021 [R(int) = 0.0293]
Completeness to theta = 27.52°	99.4 %
Absorption correction	Semi-empirical from
equivalents	
Max. and min. transmission	0.9167 and 0.7568
Refinement method	Full-matrix least-squares on F ²
Data / restraints / parameters	5021 / 5 / 301
Goodness-of-fit on F ²	1.125
Final R indices [I > 2σ(I)]	R ₁ = 0.0371, wR ₂ = 0.0992
R indices (all data)	R ₁ = 0.0491, wR ₂ = 0.1231
Largest diff. peak and hole	1.072 and -0.516 e.Å ⁻³

46. Compound 62b

Heterobimetallic network: $\{[(Ag((acacCN)Cu(3-Py-DPM))_2)](BF_4)\}_\infty(o\text{-xylene})$ 

Empirical formula	C ₄₈ H ₄₁ Ag B Cu ₂ F ₄ N ₈ O ₄
Formula weight	1115.65
Temperature	173(2) K
Wavelength	0.71073 Å
Crystal system	Monoclinic
Space group	C2/c
Unit cell dimensions:	
a = 21.0234(5) Å	α = 90°
b = 19.4123(4) Å	β = 130.9340(10)°
c = 14.4511(3) Å	γ = 90°
Volume	4455.48(17) Å ³
Z	4
Density (calculated)	1.663 mg/m ³
Absorption coefficient	1.454 mm ⁻¹
F(000)	2252
Crystal size	0.15 x 0.13 x 0.09 mm ³
Theta range for data collection	1.66 to 27.51°
Index ranges	-27 ≤ h ≤ 27, -25 ≤ k ≤ 21, -
18 ≤ l ≤ 15	
Reflections collected	14442
Independent reflections	5118 [R(int) = 0.0244]
Completeness to theta = 27.51°	99.8 %
Absorption correction	Semi-empirical from
equivalents	
Max. and min. transmission	0.8803 and 0.8114
Refinement method	Full-matrix least-squares on F ²
Data / restraints / parameters	5118 / 0 / 319
Goodness-of-fit on F ²	1.104
Final R indices [I > 2σ(I)]	R1 = 0.0322, wR2 = 0.0901
R indices (all data)	R1 = 0.0399, wR2 = 0.0968
Largest diff. peak and hole	0.602 and -0.383 e.Å ⁻³

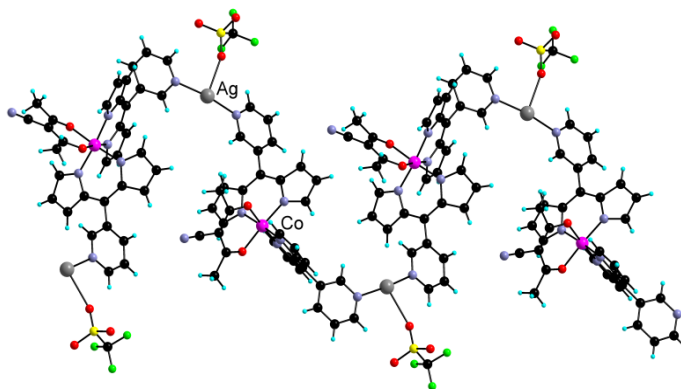
47. Compound 63

Heterobimetallic network: $\{[(Ag((acacCN)Cu(3-Py-DPM))_2)](OTf)\}_\infty(\text{Benzene})$ 

Empirical formula	C ₄₁ H ₃₂ Ag Cu ₂ F ₃ N ₈ O ₇ S
Formula weight	1072.76
Temperature	173(2) K
Wavelength	0.71073 Å
Crystal system	Triclinic
Space group	P-1
Unit cell dimensions:	
a = 7.9711(2) Å	$\alpha = 101.2980(10)^\circ$
b = 9.1922(2) Å	$\beta = 93.9740(10)^\circ$
c = 14.6259(4) Å	$\gamma = 102.1420(10)^\circ$
Volume	1020.54(4) Å ³
Z	1
Density (calculated)	1.745 mg/m ³
Absorption coefficient	1.635 mm ⁻¹
F(000)	538
Crystal size	0.12 x 0.12 x 0.10 mm ³
Theta range for data collection	1.43 to 27.55°
Index ranges	-10 ≤ h ≤ 9, -11 ≤ k ≤ 11, -
18 ≤ l ≤ 18	
Reflections collected	15337
Independent reflections	4624 [R(int) = 0.0256]
Completeness to theta = 27.55°	98.3 %
Absorption correction	Semi-empirical from
equivalents	
Max. and min. transmission	0.8536 and 0.8280
Refinement method	Full-matrix least-squares on F ²
Data / restraints / parameters	4624 / 6 / 292
Goodness-of-fit on F ²	1.263
Final R indices [I > 2σ(I)]	R ₁ = 0.0844, wR ₂ = 0.1884
R indices (all data)	R ₁ = 0.0854, wR ₂ = 0.1890
Largest diff. peak and hole	3.126 and -3.885 e.Å ⁻³

48. Compound 64

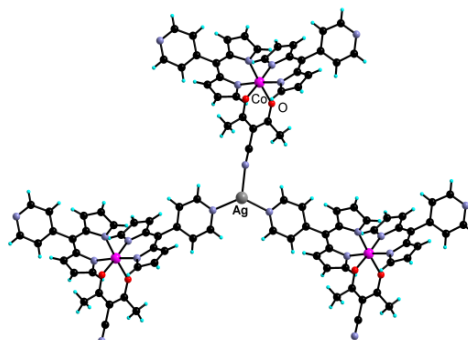
Heterobimetallic network: $\{[(Ag((acacCN)Co(3-Py-DPM))_2)_2](OTf)_\infty(CH_3CN)_3\}$



Empirical formula	C ₃₇ H ₂₉ Ag Co F ₃ N ₈ O ₅ S
Formula weight	921.54
Temperature	173(2) K
Wavelength	0.71073 Å
Crystal system	Monoclinic
Space group	P2(1)/n
Unit cell dimensions:	
a = 11.4601(2) Å	α = 90°
b = 25.0292(6) Å	β = 109.0160(10)°
c = 13.8946(3) Å	γ = 90°
Volume	3767.99(14) Å ³
Z	4
Density (calculated)	1.624 mg/m ³
Absorption coefficient	1.085 mm ⁻¹
F(000)	1856
Crystal size	0.12 x 0.07 x 0.05 mm ³
Theta range for data collection	1.63 to 27.53°
Index ranges	-10 ≤ h ≤ 14, -32 ≤ k ≤ 31, -
17 ≤ l ≤ 18	
Reflections collected	27714
Independent reflections	8608 [R(int) = 0.0352]
Completeness to theta = 27.53°	99.1 %
Absorption correction	Semi-empirical from
equivalents	
Max. and min. transmission	0.9478 and 0.8808
Refinement method	Full-matrix least-squares on F ²
Data / restraints / parameters	8608 / 0 / 508
Goodness-of-fit on F ²	1.111
Final R indices [I > 2σ(I)]	R1 = 0.0579, wR2 = 0.1453
R indices (all data)	R1 = 0.0736, wR2 = 0.1630
Largest diff. peak and hole	2.220 and -1.056 e.Å ⁻³

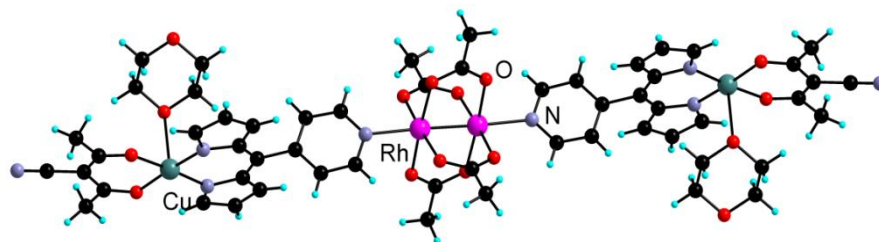
49. Compound 65

Heterobimetallic network: $\{[(Ag((acacCN)Co(4-Py-DPM))_2)_2](BF_4)\}_\infty(Benzene)_{0.5}(CH_3CN)_3$



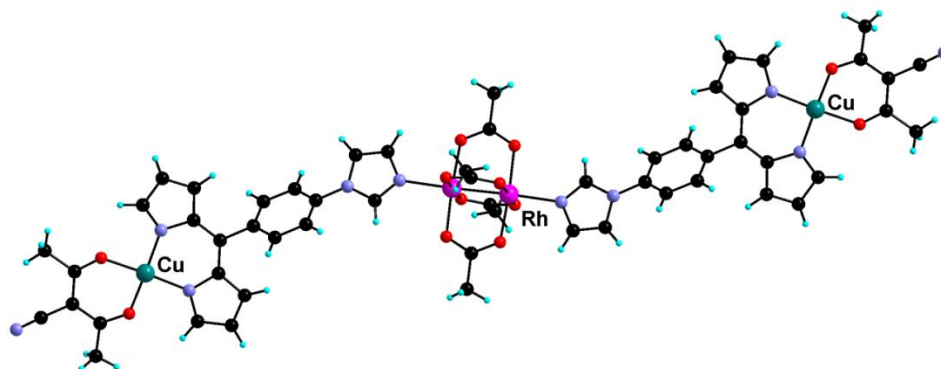
Empirical formula	C ₄₃ H ₃₈ Ag B Co F ₄ N ₁₀ O ₂
Formula weight	980.44
Temperature	173(2) K
Wavelength	0.71073 Å
Crystal system	Triclinic
Space group	P-1
Unit cell dimensions:	
a = 9.9369(3) Å	α = 73.8980(10)°
b = 14.1115(3) Å	β = 86.2550(10)°
c = 15.8223(4) Å	γ = 89.2360(10)°
Volume	2127.06(10) Å ³
Z	2
Density (calculated)	1.531 mg/m ³
Absorption coefficient	0.918 mm ⁻¹
F(000)	994
Crystal size	0.11 x 0.09 x 0.03 mm ³
Theta range for data collection	1.34 to 27.55°
Index ranges	-12 ≤ h ≤ 12, -18 ≤ k ≤ 18, -
20 ≤ l ≤ 20	
Reflections collected	30834
Independent reflections	9685 [R(int) = 0.0313]
Completeness to theta = 27.55°	98.6 %
Absorption correction	Semi-empirical from
equivalents	
Max. and min. transmission	0.9730 and 0.9058
Refinement method	Full-matrix least-squares on F ²
Data / restraints / parameters	9685 / 2 / 564
Goodness-of-fit on F ²	1.121
Final R indices [I > 2σ(I)]	R1 = 0.0486, wR2 = 0.1168
R indices (all data)	R1 = 0.0610, wR2 = 0.1289
Largest diff. peak and hole	0.894 and -0.690 e.Å ⁻³

50. Compound 66

Heterobimetallic complex: $[\text{Rh}_2(\text{OAc})_4((\text{acacCN})\text{Cu}(\text{Dpm-4-Py}))_2](\text{DiOX})_4$ 

Empirical formula	C ₈₀ H ₁₀₈ Cu ₂ N ₈ O ₂₈ Rh ₂
Formula weight	1962.68
Temperature	173(2) K
Wavelength	0.71073 Å
Crystal system	Triclinic
Space group	P-1
Unit cell dimensions:	
a = 13.1331(6) Å	$\alpha = 116.4400(10)^\circ$
b = 13.9427(3) Å	$\beta = 109.4340(10)^\circ$
c = 14.9120(3) Å	$\gamma = 96.4360(10)^\circ$
Volume	2193.40(12) Å ³
Z	1
Density (calculated)	1.486 mg/m ³
Absorption coefficient	0.930 mm ⁻¹
F(000)	1016
Crystal size	0.08 x 0.06 x 0.03 mm ³
Theta range for data collection	1.69 to 27.29°
Index ranges	-17 ≤ h ≤ 17, -17 ≤ k ≤ 17, -
16 ≤ l ≤ 19	
Reflections collected	38690
Independent reflections	9691 [R(int) = 0.0378]
Completeness to theta = 27.29°	98.4 %
Absorption correction	Semi-empirical from
equivalents	
Max. and min. transmission	0.9726 and 0.9293
Refinement method	Full-matrix least-squares on F ²
Data / restraints / parameters	9691 / 0 / 545
Goodness-of-fit on F ²	1.064
Final R indices [I > 2σ(I)]	R1 = 0.0381, wR2 = 0.0804
R indices (all data)	R1 = 0.0583, wR2 = 0.0930
Largest diff. peak and hole	0.581 and -0.543 e.Å ⁻³

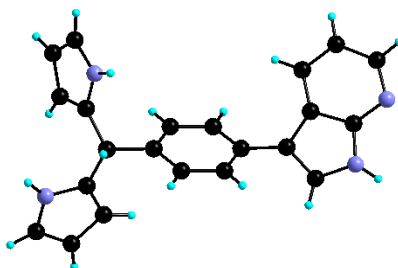
51. Compound 67

Heterobimetallic complex (II): $[\text{Rh}_2(\text{OAc})_4((\text{acacCN})\text{Cu}(\text{Dpm-Ph-Im}))_2](\text{CHCl}_3)_3$ 

Empirical formula	C ₅₉ H ₅₃ Cl ₉ Cu ₂ N ₁₀ O ₁₂ Rh ₂
Formula weight	1746.06
Temperature	173(2) K
Wavelength	0.71073 Å
Crystal system	Monoclinic
Space group	P2(1)/c
Unit cell dimensions:	
a = 20.5149(6) Å	α = 90°
b = 13.5029(4) Å	β = 97.7920(10)°
c = 12.3993(4) Å	γ = 90°
Volume	3403.02(18) Å ³
Z	2
Density (calculated)	1.704 mg/m ³
Absorption coefficient	1.513 mm ⁻¹
F(000)	1748
Crystal size	0.12 x 0.04 x 0.04 mm ³
Theta range for data collection	2.24 to 27.69°
Index ranges	-26 ≤ h ≤ 26, -17 ≤ k ≤ 17, -
16 ≤ l ≤ 16	
Reflections collected	39581
Independent reflections	7844 (R(int) = 0.0378)
Completeness to theta = 27.69°	98.6 %
Absorption correction equivalents	Semi-empirical from
Max. and min. transmission	0.9420 and 0.8393
Refinement method	Full-matrix least-squares on F ²
Data / restraints / parameters	7844 / 3 / 428
Goodness-of-fit on F ²	1.044
Final R indices (I > 2σ(I))	R1 = 0.0494, wR2 = 0.1259
R indices (all data)	R1 = 0.0661, wR2 = 0.1372
Largest diff. peak and hole	2.157 and -1.217 e. Å ⁻³

52. Compound 69

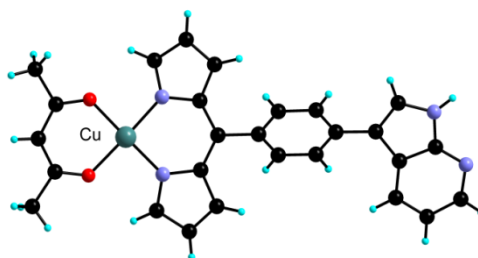
5-(4-(7-azaindol-3-yl)phenyl)-dipyrromethane



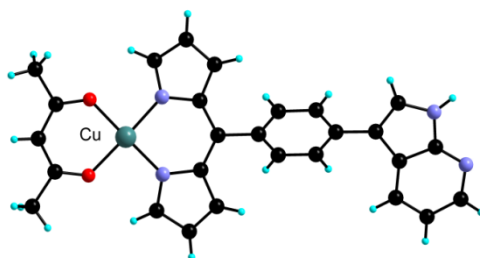
Empirical formula	C ₂₆ H ₂₆ N ₄ O ₂
Formula weight	426.51
Temperature	173(2) K
Wavelength	0.71073 Å
Crystal system	Triclinic
Space group	P-1
Unit cell dimensions:	
a = 8.5597(3) Å	$\alpha = 100.454(2)^\circ$.
b = 9.3106(2) Å	$\beta = 97.8740(10)^\circ$.
c = 15.2765(4) Å	$\gamma = 109.0960(10)^\circ$.
Volume	1105.84(5) Å ³
Z	2
Density (calculated)	1.281 mg/m ³
Absorption coefficient	0.083 mm ⁻¹
F(000)	452
Crystal size	0.15 x 0.11 x 0.03 mm ³
Theta range for data collection	1.39 to 27.69°.
Index ranges	-11 ≤ h ≤ 11, -12 ≤ k ≤ 11, -
15 ≤ l ≤ 19	
Reflections collected	12267
Independent reflections	5012 [R(int) = 0.0270]
Completeness to theta = 27.69°	96.7 %
Absorption correction	Semi-empirical from
equivalents	
Max. and min. transmission	0.9975 and 0.9877
Refinement method	Full-matrix least-squares on F ²
Data / restraints / parameters	5012 / 0 / 289
Goodness-of-fit on F ²	1.061
Final R indices [I > 2σ(I)]	R1 = 0.0566, wR2 = 0.1521
R indices (all data)	R1 = 0.0807, wR2 = 0.1695
Largest diff. peak and hole	0.659 and -0.380 e. Å ⁻³

53. Compound 71a

Complex [((5-(4-(7-azaindol-3-yl)phenyl)-dipyrri-no)acac)Cu(II)]

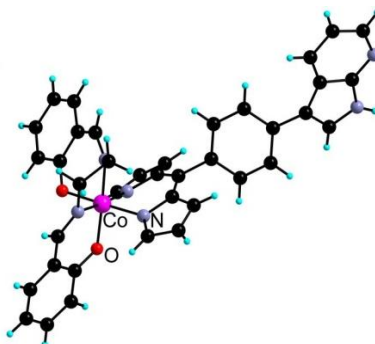


Empirical formula	C ₂₇ H ₂₂ Cu N ₄ O ₂
Formula weight	498.03
Temperature	173(2) K
Wavelength	0.71073 Å
Crystal system	Monoclinic
Space group	P2(1)/c
Unit cell dimensions:	
a = 15.8296(5) Å	$\alpha = 90^\circ$
b = 16.3701(6) Å	$\beta = 94.6270(10)^\circ$
c = 8.7589(3) Å	$\gamma = 90^\circ$
Volume	2262.32(13) Å ³
Z	4
Density (calculated)	1.462 mg/m ³
Absorption coefficient	0.999 mm ⁻¹
F(000)	1028
Crystal size	0.15 x 0.10 x 0.03 mm ³
Theta range for data collection	2.49 to 27.64°
Index ranges	-20 ≤ h ≤ 18, -20 ≤ k ≤ 20, -
11 ≤ l ≤ 11	
Reflections collected	18401
Independent reflections	5168 [R(int) = 0.0319]
Completeness to theta = 27.64°	97.8 %
Absorption correction equivalents	Semi-empirical from 0.9707 and 0.8647
Max. and min. transmission	
Refinement method	Full-matrix least-squares on F ²
Data / restraints / parameters	5168 / 0 / 309
Goodness-of-fit on F ²	1.084
Final R indices [I > 2σ(I)]	R1 = 0.0433, wR2 = 0.1007
R indices (all data)	R1 = 0.0558, wR2 = 0.1076
Largest diff. peak and hole	0.427 and -0.300 e. Å ⁻³

54. *Compound 71b***Complex [(5-(4-(7-azaindol-3-yl)phenyl)-dipyrriino)acac]Cu(II)]**

Empirical formula	C ₂₇ H ₂₂ Cu N ₄ O ₂
Formula weight	498.03
Temperature	173(2) K
Wavelength	0.71073 Å
Crystal system	Monoclinic
Space group	P2(1)/n
Unit cell dimensions	
a = 10.7498(2) Å	$\alpha = 90^\circ$
b = 16.8606(3) Å	$\beta = 99.3050(10)^\circ$
c = 24.8963(6) Å	$\gamma = 90^\circ$
Volume	4453.03(16) Å ³
Z	8
Density (calculated)	1.486 Mg/m ³
Absorption coefficient	1.015 mm ⁻¹
F(000)	2056
Crystal size	0.12 x 0.12 x 0.03 mm ³
Theta range for data collection	1.46 to 27.53°
Index ranges	-13 ≤ h ≤ 13, -21 ≤ k ≤ 15, -
32 ≤ l ≤ 32	
Reflections collected	44695
Independent reflections	10208 [R(int) = 0.0323]
Completeness to theta = 27.53°	99.6 %
Absorption correction equivalents	Semi-empirical from
Max. and min. transmission	0.9702 and 0.8879
Refinement method	Full-matrix least-squares on F ²
Data / restraints / parameters	10208 / 0 / 617
Goodness-of-fit on F ²	1.038
Final R indices [I > 2σ(I)]	R1 = 0.0402, wR2 = 0.0978
R indices (all data)	R1 = 0.0584, wR2 = 0.1070
Largest diff. peak and hole	0.496 and -0.427 e. Å ⁻³

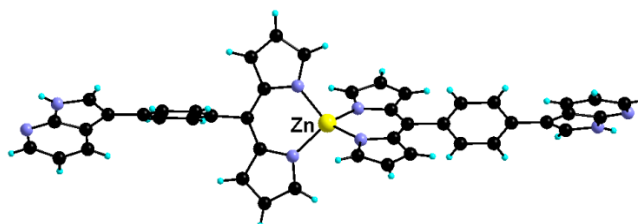
55. Compound 72

Complex [Salen-(5-(4-(7-azaindol-3-yl)phenyl)-dipyrri-no)-Co(III)]

Empirical formula	C ₄₈ H ₄₉ Co N ₆ O ₇
Formula weight	880.86
Temperature	173(2) K
Wavelength	0.71073 Å
Crystal system	Triclinic
Space group	P-1
Unit cell dimensions:	
a = 10.1522(2) Å	$\alpha = 84.7710(10)^\circ$
b = 11.1044(2) Å	$\beta = 86.2170(10)^\circ$
c = 20.8685(4) Å	$\gamma = 67.1980(10)^\circ$
Volume	2158.51(7) Å ³
Z	2
Density (calculated)	1.355 mg/m ³
Absorption coefficient	0.458 mm ⁻¹
F(000)	924
Crystal size	0.15 x 0.12 x 0.05 mm ³
Theta range for data collection	1.99 to 27.54°
Index ranges	-13 ≤ h ≤ 12, -14 ≤ k ≤ 14, -
26 ≤ l ≤ 27	
Reflections collected	27973
Independent reflections	9623 [R(int) = 0.0331]
Completeness to theta = 27.54°	96.7 %
Absorption correction	Semi-empirical from
equivalents	
Max. and min. transmission	0.9775 and 0.9345
Refinement method	Full-matrix least-squares on F ²
Data / restraints / parameters	9623 / 0 / 535
Goodness-of-fit on F ²	1.040
Final R indices [I > 2σ(I)]	R ₁ = 0.0581, wR ₂ = 0.1508
R indices (all data)	R ₁ = 0.0782, wR ₂ = 0.1643
Largest diff. peak and hole	1.723 and -1.204 e.Å ⁻³

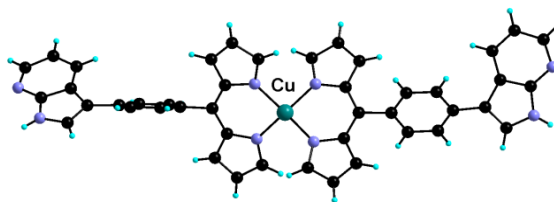
56. Compound 73

Complex [Bis(5-(4-(7-azaindol-3-yl)phenyl)-dipyrriino)Zn(II)]



Empirical formula	C ₆₂ H ₄₈ N ₈ Zn
Formula weight	970.45
Temperature	173(2) K
Wavelength	0.71073 Å
Crystal system	Triclinic
Space group	P-1
Unit cell dimensions:	
a = 13.7544(3) Å	$\alpha = 100.0140(10)^\circ$
b = 14.2777(3) Å	$\beta = 92.7050(10)^\circ$
c = 14.5027(6) Å	$\gamma = 117.2820(10)^\circ$
Volume	2466.34(13) Å ³
Z	2
Density (calculated)	1.307 mg/m ³
Absorption coefficient	0.548 mm ⁻¹
F(000)	1012
Crystal size	0.12 x 0.12 x 0.11 mm ³
Theta range for data collection	1.68 to 27.50°
Index ranges	-17 ≤ h ≤ 17, -18 ≤ k ≤ 17, -
18 ≤ l ≤ 18	
Reflections collected	27798
Independent reflections	11038 [R(int) = 0.0256]
Completeness to theta = 27.50°	97.4 %
Absorption correction	Semi-empirical from
equivalents	
Max. and min. transmission	0.9422 and 0.9371
Refinement method	Full-matrix least-squares on F ²
Data / restraints / parameters	11038 / 0 / 640
Goodness-of-fit on F ²	1.023
Final R indices [I > 2σ(I)]	R1 = 0.0363, wR2 = 0.0849
R indices (all data)	R1 = 0.0464, wR2 = 0.0906
Largest diff. peak and hole	0.365 and -0.316 e.Å ⁻³

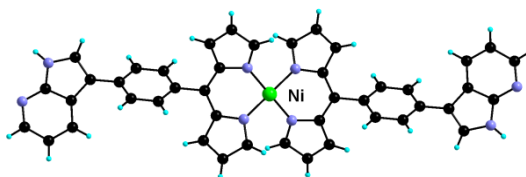
57. Compound 74

Complex [Bis(5-(4-(7-azaindol-3-yl)phenyl)-dipyrriino)Cu(II)]

Empirical formula	C ₄₄ H ₃₀ Cu N ₈
Formula weight	734.30
Temperature	173(2) K
Wavelength	0.71073 Å
Crystal system	Monoclinic
Space group	P2(1)/n
Unit cell dimensions:	
a = 9.4224(3) Å	$\alpha = 90^\circ$.
b = 14.6230(4) Å	$\beta = 92.2260(10)^\circ$.
c = 24.5401(7) Å	$\gamma = 90^\circ$.
Volume	3378.68(17) Å ³
Z	4
Density (calculated)	1.444 mg/m ³
Absorption coefficient	0.694 mm ⁻¹
F(000)	1516
Crystal size	0.14 x 0.13 x 0.05 mm ³
Theta range for data collection	2.17 to 27.63°.
Index ranges	-11 ≤ h ≤ 12, -18 ≤ k ≤ 18, -
31 ≤ l ≤ 18	
Reflections collected	30628
Independent reflections	7655 [R(int) = 0.0373]
Completeness to theta = 27.63°	97.4 %
Absorption correction equivalents	Semi-empirical from
Max. and min. transmission	0.9661 and 0.9091
Refinement method	Full-matrix least-squares on F ²
Data / restraints / parameters	7655 / 0 / 478
Goodness-of-fit on F ²	1.055
Final R indices [I > 2σ(I)]	R1 = 0.0511, wR2 = 0.1240
R indices (all data)	R1 = 0.0695, wR2 = 0.1330
Largest diff. peak and hole	0.473 and -0.745 e.Å ⁻³

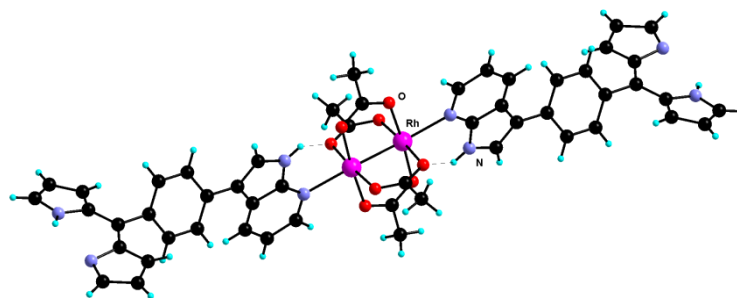
58. Compound 75

Complex [Bis(5-(4-(7-azaindol-3-yl)phenyl)-dipyrri-no)Ni(II)]



Empirical formula	C ₄₄ H ₃₀ N ₈ Ni
Formula weight	729.47
Temperature	173(2) K
Wavelength	0.71073 Å
Crystal system	Monoclinic
Space group	P2(1)/c
Unit cell dimensions:	
a = 12.7240(6) Å	$\alpha = 90^\circ$
b = 14.9607(7) Å	$\beta = 109.720(2)^\circ$
c = 9.1463(4) Å	$\gamma = 90^\circ$
Volume	1638.98(13) Å ³
Z	2
Density (calculated)	1.478 mg/m ³
Absorption coefficient	0.641 mm ⁻¹
F(000)	756
Crystal size	0.15 x 0.10 x 0.08 mm ³
Theta range for data collection	2.18 to 27.60°
Index ranges	-16 ≤ h ≤ 14, -19 ≤ k ≤ 19, -
11 ≤ l ≤ 11	
Reflections collected	22537
Independent reflections	3782 [R(int) = 0.0585]
Completeness to theta = 27.60°	99.6 %
Absorption correction equivalents	Semi-empirical from
Max. and min. transmission	0.9505 and 0.9100
Refinement method	Full-matrix least-squares on F ²
Data / restraints / parameters	3782 / 0 / 241
Goodness-of-fit on F ²	1.052
Final R indices [I > 2σ(I)]	R1 = 0.0601, wR2 = 0.1930
R indices (all data)	R1 = 0.0717, wR2 = 0.2059
Largest diff. peak and hole	0.687 and -1.229 e. Å ⁻³

59. Compound 77

[Bis(5-(4-(7-azaindol-3-yl)phenyl)-dipyrrin)(Rh₂(OAc)₄)] Complex

Empirical formula	C ₆₈ H ₇₆ N ₈ O ₁₆ Rh ₂
Formula weight	1467.21
Temperature	173(2) K
Wavelength	0.71073 Å
Crystal system	Monoclinic
Space group	P2(1)/n
Unit cell dimensions:	
a = 8.7968(4) Å	α = 90°
b = 36.9943(15) Å	β = 100.402(2)°
c = 10.2665(4) Å	γ = 90°
Volume	3286.1(2) Å ³
Z	2
Density (calculated)	1.483 mg/m ³
Absorption coefficient	0.577 mm ⁻¹
F(000)	1516
Crystal size	0.22 x 0.13 x 0.02 mm ³
Theta range for data collection	2.30 to 27.52°
Index ranges	-10 ≤ h ≤ 11, -47 ≤ k ≤ 45, -
13 ≤ l ≤ 12	
Reflections collected	18888
Independent reflections	7311 [R(int) = 0.0501]
Completeness to theta = 27.52°	96.6 %
Absorption correction equivalents	Semi-empirical from
Max. and min. transmission	0.9885 and 0.8835
Refinement method	Full-matrix least-squares on F ²
Data / restraints / parameters	7311 / 0 / 424
Goodness-of-fit on F ²	1.159
Final R indices [I > 2σ(I)]	R1 = 0.0605, wR2 = 0.1074
R indices (all data)	R1 = 0.0885, wR2 = 0.1199
Largest diff. peak and hole	0.771 and -1.060 e.Å ⁻³

Abstract

Coordination polymers have attracted considerable interest over the past few years owing to their potential application in gas storage or catalysis, for example. While the vast majority of these compounds are homometallic systems, the synthesis of heterometallic architectures remains challenging. Indeed, a one-pot synthetic approach in principle leads to a statistical mixture of homo- and hetero-metallic assemblies. To circumvent this synthetic issue, a sequential approach has been developed. The latter relies on the use of ligands bearing differentiated coordination sites hence allowing the stepwise elaboration of heterometallic architectures. Reaction of such a ligand with a first metal center leads to the formation of a metal complex bearing peripheral coordinating sites available for ligation to other metal centers. This approach has been explored by ligands based on the 7-azaindole and dipyrin moieties.

In a first part, functionalized 7-azaindole derivatives have been synthesized and employed as ligands for the preparation of Cu(II) discrete complexes and networks. In a second part of the work, novel dipyrin appended with imidazolyl, pyrazolyl or pyridyl groups have been prepared and used as ligands for the synthesis of heteroleptic Cu(II) and Co(III) complexes. These species form mono- and bi-dimensional networks upon assembly with silver salts, AgX. The solid state arrangement of these species is influenced by the nature of the X^- anion. In a third and final part, a ligand incorporating both a dipyrin and a 7-azaindole has been conceived and prepared. The latter shows a recurrent hydrogen bonding motif that leads to the formation of one-dimensional networks upon coordination of divalent metals such as Ni(II), Zn(II) and Cu(II) by the dipyrin, regardless of the nature of the metal centre.

Keywords

Supramolecular chemistry, molecular tectonics, self-assembly, coordination networks, heterometallic architectures, dipyrin, azaindole

Résumé

Les polymères de coordination revêtent un grand intérêt de par leurs applications potentielles dans les domaines de la catalyse ou du stockage de gaz, par exemple. Alors que la majorité des architectures décrites sont homométalliques, l'obtention de leurs analogues hétérométalliques représente un défi synthétique. En effet, une approche « one-pot », par principe, peut mener à un mélange statistique de composés homo- et hétérométalliques. Afin de résoudre ce problème, une stratégie séquentielle a été mise au point. Elle repose sur l'utilisation de ligands portant des pôles de coordination différenciés. Ainsi, par réaction avec un premier centre métallique, un complexe portant des sites de coordination périphériques disponibles pour la coordination d'autres centres métalliques est formé. Cette voie a été développée à partir de ligands dérivés du 7-azaindole et de la dipyrine.

Dans une première partie, des dérivés fonctionnalisés du 7-azaindole ont été synthétisés et utilisés comme ligands pour la préparation de complexes et de réseaux à base de Cu(II). Dans une deuxième partie, des dérivés de la dipyrine portant un groupement imidazole, pyrazole ou pyridyle périphérique ont été préparés ainsi que leurs complexes hétéroleptiques de Cu(II) et Co(III). Ces composés forment par auto-assemblage avec des sels d'argent, AgX, des architectures hétérométalliques mono- et bi-dimensionnelles. L'organisation de ces réseaux est influencée la nature de l'anion X^- . Dans une troisième et dernière partie, un ligand comprenant à la fois les noyaux dipyrine et 7-azaindole a été synthétisé. Ce dernier groupement montre une récurrence d'un motif auto-complémentaire de liaison hydrogène. Ainsi, les complexes obtenus par coordination de la fonction dipyrine à des métaux divalents tels que Ni(II), Cu(II) et Zn(II) forment des réseaux unidimensionnels, indépendamment de la géométrie autour du centre métallique.

Mots clés

Chimie supramoléculaire, tectonique moléculaire, auto-assemblage, réseaux de coordination, architectures hétérométalliques, dipyrine, azaindole.